ELECTRONIC PROPERTIES OF SEMICONDUCTORS

BY

STEPHEN.P.NAJDA

A Thesis submitted for the degree of

Doctor of Philosophy

at the

University of St.Andrews

St Salvator college

St.Andrews

Candlemas term

1985

TO MY PARENTS

DECLARATION

I hereby certify that this thesis has been composed by myself and is a record of work done over three years in the Physical Sciences Laboratory of the University of St.Andrews, under the supervision of Professor R.A.Stradling.

S.P NAJDA

I hereby certify that Stephen.P.Najda has spent nine terms of research work in the Laboratories of the School of Physical Sciences, University of St.Andrews, under my direction, and that he has fulfilled the conditions of the resolution of the University court, 1967, No 1 and that he is qualified to submit the accompanying thesis in application for the degree of Doctor of Philosophy.

R.A STRADLING

Research supervisor.

ACKNOWLEDGEMENTS

I am grateful to Professor R.A.Stradling for his support and patient help throughout this project. I would like to express my thanks to Mr R.H.Mitchell and the technical staff for their assistance. Many useful and interesting discussions occurred with the 'group', consisting of; Chris Armistead, Murray Davidson, Clivia Sotomayor-Torres, Zbnignew Wasilewski, Carol Trager, Izabela Gorczyca, David Marks, David Cowan and Antony Thorley. Finally, I would like to extend my gratitude to all my friends in St.Andrews.

ABSTRACT

The extreme sensitivity of far-infrared photoconductivity (FIRPC) techniques in combination with a large magnetic field are exploited to resolve very small central-cell corrections, which identify the residual shallow substitutional donors in ultra-high purity GaAs and InP epitaxial layers. Undoped VPE, LPE or MOCVD material usually contains the same combination of donors irrespective of the source of the sample, but different growth techniques produce a different set of donors. Most of the likely donors are tentatively identified in GaAs by using back-doped and neutron transmutated doped samples, but only four out of a possible twelve central-cell peaks are identified in InP. Not all the central-cell components can be accounted for by simple substitutional donor impurities. Hydrostatic pressure is used as an additional experimental parameter to improve the spectral resolution, both by increasing the central-cell splitting and by sharpening lines.

D^- states (a neutral donor D^o binding an extra electron), D^o interexcited state transitions and the cyclotron resonance are all observed simultaneously in GaAs and InP. This observation constitutes the first unambiguous identification of D^- states in any semiconductor. In addition a tentative identification of D^- states in n-InSb is made. D^- states are studied under a variety of experimental conditions such as magnetic field, intrinsic illumination, hydrostatic pressure, temperature and electric field bias. The magnitude of the D^- transition increases markedly with increasing electric field bias and the intensity of D^- can become an order of magnitude greater than the D^0 'interexcited state' and cyclotron resonance lines. Divergence

between theory and experiment is evident when the dimensionless magnetic field parameter δ, exceeds unity, indicating the inadequacy of existing variational calculations in this regime. Hydrostatic pressure is found to strongly enhance D^- in InP, but not in VPE GaAs. Effects attributable to the formation of D^- complexes occur in GaAs when the temperature is reduced from 4.2 to 2.0K.

CONTENTS

INTRODUCTION TO CENTRAL CELL IDENTIFICATION

Advances in semiconductor technology make it essential to develop new methods for monitoring and controlling the quality of ultra-pure crystals. Contamination introduced during growth severely limits material quality and consequently inhibits device performance. Characterisation of the crystal provides valuable information for improvements in purification technology, enabling better quality crystals to be grown. Furthermore, identification, with the hope of eliminating or at worst regulating the introduction of various residual contaminants, would obviously be a great asset in growth diagnostics.

Many types of impurities are inadvertently introduced into the crystal during growth. However, this thesis considers in particular shallow substitutional donor impurities, which by their chemical nature and concentration can dramatically influence the electrical and optical properties of the crystal. Shallow donor impurities in the elemental semiconductors, Ge and Si, have been studied spectroscopically for many years with the result that their behaviour and chemical identity are now well understood. In contrast, much less is known about the contaminating impurities in III-V compound semiconductors. This is due to far greater quality control available in the elemental semiconductors, for example, residual donor concentrations in Ge, can be as low as $10^{9}cm^{-3}$, compared with typical residual concentrations of $10^{14}cm^{-3}$ impurities in the best quality III-V material.

This thesis is conveniently divided into two parts. The first part discusses donor identification of shallow substitutional impurities in GaAs and InP. In the latter part, D^- states (where a neutral donor impurity binds a second electron) are identified for the first time in GaAs and InP. An introduction to D^- states is considered in the latter part of the thesis.

Two III-V compound semiconductors are studied, GaAs and InP. Both of these materials and their corresponding ternary and quaternary alloys (not considered in this thesis) are technologically very important. The former material is probably the highest purity, and most characterised III-V semiconductor available. InP is rather less studied, which perhaps reflects the difficulty of growing high quality crystals of this material.

GaAs and InP are comparable in many respects. For example, the conduction band minimum is located at the centre of the Brillouin zone i.e $k=0$, is isotropic and non-parabolicity is small. In this case, the shallow donors are regarded as solid-state analogous of the hydrogen atom but contained in a dielectric medium and an 'effective-mass' of the donor electron is introduced to take into account the periodicity of the lattice. Since the 'hydrogen-like' donors are associated with a single spherical energy surface, they have a particularly simple form to interpret. However, there are small corrections to the 'hydrogen-model' arising from the deviation of the donor Coulombic potential due to the different chemical contaminants. These corrections are most significant for the ground state because of the appreciable amplitude of the 1S ground state wavefunction close to the origin. The observation of central-cell

structure permits the identification of chemical contaminants. Also, in both materials the combination of small effective mass and relatively large dielectric constant ensures that the donor binding energies are small ~5meV, with a corresponding 'effective' Bohr radius of ~100A. The chemical shifts of the individual donors are only of the order of 50ueV ($<1cm^{-3}$). This is compared to differences of several meV for the binding energies of shallow donors in the elemental semiconductors. Thus the resolution of such small energy differences is a difficult problem. Most direct chemical identification techniques are insensitive to the number of residual contaminants in state-of-the-art high purity III-V compound semiconductors. The complementary techniques of photoluminescence and photothermal ionisation spectroscopy provide the only method for evaluating the chemical nature of shallow donor impurities in high quality material by resolving the central-cell structure. The extreme high sensitivity of far-infrared photoconductivity (FIRPC) in combination with a large magnetic field is exploited to identify the residual dopants in high purity epitaxial GaAs and InP. Large Zeeman splittings are easily obtained on the 1S-2P transition and the regime where the zero-point cyclotron energy is comparable or exceeds the Coulomb binding energy can be reached. Central-cell features are resolved on each of the Zeeman split transitions. The technique has several advantages over existing detection methods.

i) the very high sensitivity enables contaminating impurities to be detected with a sensitivity far superior to other techniques. For example, 10^7 impurities cm^{-3} (Skolnick 1974) in high purity Ge have been established.

ii) relative concentrations of different donor species are obtained from the amplitudes of the corresponding spectral peaks.

iii) Spectra are observed from ultra-pure and very thin epitaxial

films that would otherwise be unobtainable from absorption/transmission experiments.

The experiments in this thesis are carried out using a far infrared (FIR) laser as the source of radiation. The laser offers greater resolution and signal-to-noise ratios than the standard Fourier transform spectrometer, thus enabling weak structure to be resolved. Since the laser operates at fixed frequency, the magnetic field must be swept in order to obtain a spectrum. However, this method has the disadvantage that the lineshapes can become distorted.

The chemical shifts on the Zeeman split 1S-2P transitions are studied in high purity GaAs and InP. Unfortunately, the problem of resolving central-cell structure is compounded by broadened transition lines. Several different techniques are used to reduce the linewidth and in some cases the results can be quite dramatic.

i) As the dominant broadening is from ionised impurities further narrowing can be achieved by neutralising these impurities with intrinsic illumination, since the band-gap radiation creates electrons and holes which are selectively trapped by a proportion of the ionised donors and acceptors respectively.

ii) A reduction in the temperature from 4.2K to 1.5K can frequently narrow transition lines even though the total number of ionised sites does not change significantly in this temperature range.

iii) Hydrostatic pressure is used as an additional new technique to further reduce broadening. The application of pressure increases both the band gap and the chemical shifts in a similar manner to a magnetic field.

The broadening of some lines can be reduced quite dramatically in some cases, especially if the above methods are used in combination.

Various methods are employed in an attempt to identify each of the central-cell peaks with their corresponding residual contaminating impurities.

i) Carefully controlled back doped crystals are grown, by introducing a very small quantity of known dopant into the system and the photothermal ionisation spectra are compared to spectra of undoped material. Unfortunately, such crystals are difficult to grow because of the small donor concentration range between the purest material which can be grown, and that for which impurity-impurity interactions degrade the spectra by broadening and distorting the lineshapes thus making the analysis more difficult to interpret.

ii) Following bombardment of GaAs samples with a flux of thermal neutrons a small proportion of Ga atoms are captured and decay into Ge atoms. Similarly As transmutes into Se , and for InP, In goes to Sn and P goes to S. However, only two dopants can be identified using this method.

iii) Correlation with different crystal growing conditions also enables the identification of certain contaminants.

A comparison of central-cell identification by other groups around the world is made.

CHAPTER 1

THEORY OF NEUTRAL DONOR IMPURITIES

The following chapter considers the theoretical models required to describe shallow substitutional donor impurities in III-V compound semiconductors under the influence of various external parameters such as a magnetic field. Although, the mathematical treatment of the theories involved are kept to a minimum for brevity , the relevant points are highlighted to help interpret the experimental results, which follow in chapters three and four. Since GaAs is well characterised, any reference for comparison with theory is made with consideration to this material. However, implicit in this description is a similar argument for InP; any differences are described where appropriate.

1.1 Band structure of GaAs and InP

Both GaAs and InP crystallise in the zincblende structure which can be regarded as two interpenetrating face-centred-cubic sub-lattices with each unit cell containing two different atoms, similar to the diamond structure of the elemental semiconductors Si and Ge but lacking inversion symmetry (figure 1.1). The associated Brillouin zone is a truncated octahedron with high symmetry points at the centre of the zone ie k=0 (Γ),along the (111) axis at the zone edge (L) and along the (100) axis at point (X) (figure 1.2). The conduction band (CB) is composed of several subband`s. The lowest minimum on a band structure diagram is located at the zone centre, Γ , i.e k=0, and subsidiary minima appear at the L and X zone edges (figure 1.3). The constant energy surface is spherical at the Γ extremum , and near the L and X extrema the energy surfaces are ellipsoids of revolution with symmetry axis along the (111) and (100) axis respectively. The relative order of the GaAs conduction band

minima has been a controversial problem. However, a recent and conclusive electroreflectance experiment by Aspnes (1976) confirmed the theoretical prediction of Chelikowsky and Cohen (1976) by demonstrating that the order is Γ-L-X. The X minima are probably at the edges of the Brillouin zone at about 0.4eV above the Γ minimum, and a set of four degenerate L equivalent minima, are several tenths of millielectron volts lower in energy. Thus $E(\Gamma-X)=0.467\pm0.005$eV, Onton et al (1972), measured by infrared absorption at 2K; and $E(\Gamma-L)=0.29\pm0.05$eV, Aspnes (1976), using electroreflectance at 110K. Similarly with InP the relative order of the conduction band minima are believed to be Γ-L-X with energy separations $E(\Gamma-X)=0.960+0.005$eV, Onton et al (1972), determined by infrared absorption studies at 8K; and $E(\Gamma-L)=0.8$eV, Brust (1971), calculated at 0K using a self consistent pseudopotential theory. The conduction band is separated from the valence band by 1.5177 ± 0.0001eV, Aspnes (1973); and 1.423 ± 0.005eV Rochen (1975) in GaAs and InP respectively. The valence band is composed of three subbands (neglecting spin), two of the three are degenerate at k=0 and form the upper edge of the band. For $k\neq 0$ the 4-fold degenerate band (including spin) is split into a 2-fold degenerate V1 (heavy hole) and a 2-fold degenerate V2 (light hole) band. Furthermore, the spin-orbit interaction causes a splitting of the bands at k=0 giving rise to the 2-fold degenerate split-off band (V3), defined by an energy Δ (see figure 1.3).

To a first approximation the conduction band at the centre of the Brillouin zone is parabolic ie

$$E(k) = \hbar^2 k^2 / 2m^* \qquad (1.1)$$

where $\hbar = h/2\pi$, h - is Plank's constant

k - is the wavevector

m^* - the conduction band effective mass.

In reality, the conduction band of GaAs has a small but significant nonparabolicity component together with very slight anisotropy for the minimum. A more realistic approach using Kane's $\underline{k}.\underline{p}$ theory (1957), very accurately takes into account the nonparabolicity in the vicinity of an extremum. The Hamiltonian for the problem is

$$[\underline{p}^2/2m + \hbar/m\ \underline{k}.\underline{p} + \hbar/4m^2c^2\ (\nabla V \times \underline{p}).\underline{\sigma}]; \qquad (1.2)$$

where the third and fourth terms are the $\underline{k}.\underline{p}$ and spin-orbit perturbations respectively. By solving the Schrodinger equation an 8*8 secular determinant is obtained. The solution of the determinant results in the equation

$$E\{E(E - E_G)(E + \Delta) - k^2P^2(E + 2/3\Delta)\} = 0;$$

where P is the matrix element connecting the conduction band to the light hole and spin orbit split-off valence band, and the spin-orbit splitting Δ, are defined as

$$P = -i(\hbar/m) < S \mid p_z \mid Z >$$

$$\text{and } \Delta = 3\hbar i/4mc < X \mid \nabla V \times \underline{p} \mid Y >$$

E_G - energy gap.

For small values of k^2 the solution for the conduction band is;

$$E_c = E_G + \hbar^2k^2/2m + P^2k^2/3\ (2/E_G + 1/(E_G + \Delta)). \qquad (1.3)$$

The conduction band is parabolic near its Γ minimum. However, with increasing k (or energy) the curvature increases but less rapidly, and consequently the effective mass of the conduction electron increases. Equation (1.1) is valid up to values of about 0.1eV above the minimum which is adequate to describe the contribution of the minimum towards the entire conduction band system. In this approximation the bands are isotropic and spin degenerate. Due to non-parabolicity of the conduction band, the concept of effective mass must be used with care, since different definitions of the effective mass produce different effective mass values m^*. However, all the various definitions of the effective mass converge near to the band edge . The band edge effective mass has been determined very accurately for GaAs as $m^*=0.06650\pm0.00007m$ by Stillman et al (1971), using donor magneto-spectroscopy at 4.2K and by Chamberlain et al (1972) by the cyclotron resonance. Similarly, with InP, the band edge effective mass $m^*=0.0803\pm0.0003m$ was determined by Chamberlain et al (1972), where m is the free electron mass.

In a magnetic field the conduction band is split into a series of magnetic sub-bands, called Landau levels, each with a continuous energy distribution in the direction of the magnetic field. The E(k), variation for a parabolic conduction band is described by equation (1.4), with a magnetic field (B), in the z direction (B_z).

$$E(k_z) = (N + 1/2) \hbar w_c + \hbar^2 k^2_z / 2m^* \qquad (1.4)$$

In this expression, N is the quantum number of the magnetic field subbands or Landau levels.

1.2 EFFECTIVE MASS THEORY OF IMPURITIES

Consider a perfect periodic crystal lattice in which one foreign neutral atom (constituting an extra valence electron and one extra positive ion charge) is introduced substitutionally by replacing a lattice ion e.g phosphorus, in silicon or sulphur replacing As in GaAs. The extra free electron, donated by the impurity to the lattice, can be described as an independent free particle moving in the lattice periodic potential V(r). Hence, the name 'donor' is attributed to these impurities and 'acceptors' are impurities which accept an electron or donate a positive 'hole'. The electron or hole associated with the impurity is described by an 'effective mass' which is related intimately to the curvature of the band structure and subject to screening by the dielectric function of the host crystal. Effective mass theory (E.M.T) is appropriate for materials with a small effective mass and a large dielectric constant, so the bound impurity state wavefunction extends over many lattice cells. Over these large distances, the positive ion is assumed to have a simple Coulombic potential. The Hamiltonian for a carrier in a periodic potential V(r), and bound to an impurity with a smoothly varying potential U(r), takes the form

$$H = [p^2/2m + V(r) + U(r)]. \qquad (1.5)$$

The perturbing potential for large distances, r, compared to the lattice spacing, a, is

$$U(r) = - e^2/4\pi\varepsilon\varepsilon_o r; \qquad (1.6)$$

where ε is the static dielectric constant

e - charge of the electron

ε_o - permittivity of free space.

Bloch functions in the reduced zone scheme are of the form

$$\psi_{n,\underline{k}} = u_{n,\underline{k}}(\underline{r}) \exp(i\underline{k}.\underline{r}); \qquad (1.7)$$

where n is the band index, and $u_{n,\underline{k}}(\underline{r})$ is the lattice periodic function.

The impurity wavefunction is expanded in terms of $\psi_{n,\underline{k}}$;

$$\psi = \sum_{n',\underline{k}'} A(n',\underline{k}')\psi_{n',\underline{k}'}. \qquad (1.8)$$

If we multiply by $\psi^*_{n,\underline{k}}$ and integrate over all space, the Schrödinger equation becomes;

$$(E_{n,\underline{k}}-E)A(n,\underline{k}) + \sum_{n} \int < n\underline{k} \mid U(r) \mid n'\underline{k}' > A(n',\underline{k}')d\underline{k}' = 0 \qquad (1.9)$$

where $$<n\underline{k} \mid U(r) \mid n'\underline{k}'> = \mathcal{V}(\underline{k}'-\underline{k}) \qquad (1.10)$$

is the Fourier transform of the potential.

Due to the localised character of $A(n,\underline{k})$, the $d\underline{k}'$ integration can be extended to the whole of $\underline{k}$-space without loss of accuracy.

1.3 Hydrogen model of impurity donors

The simplest solution to equation (1.5), assumes a non-degenerate, parabolic and isotropic conduction band, with a single valley located at k=0. This case often occurs for shallow donor impurities in cubic crystals, and is typical of direct-gap III-V and II-VI semiconductor compounds . This means that the strength of the impurity potential is small compared to the energy gaps so that there will be negligible mixing of different bands in the impurity state. It is therefore possible to include only one band in equation (1.9) (Kohn 1957).

Substitute (1.10) into (1.9) and (1.1) i.e $E=\hbar^2\underline{k}^2/2m^*$ into (1.9), gives

$$(\hbar^2\underline{k}^2/2m^* - E)\, A(\underline{k}') + A(\underline{k}')\,\mathcal{V}(\underline{k}'-\underline{k}) = 0 \qquad (1.11)$$

Transform the Schrodinger equation from momentum to real space using

$$F(\underline{r}) = \sum_{\underline{k}} A(\underline{k})\, \exp(i\underline{k}.\underline{r}) \qquad (1.12)$$

thus equation (1.11) reduces to a 'hydrogen-like' Schrodinger equation

$$[-\hbar^2\underline{k}^2/2m^* + U(\underline{r})]\, F(\underline{r}) = E\, F(\underline{r}) \qquad (1.13)$$

where $$F(\underline{r}) = (\pi a^{*3})^{-1/2} \exp(-r/a^*) \qquad (1.14)$$

is a slowly varying 'hydrogen-like' envelope function. Equation (1.13) has eigenenergies similar to the hydrogen atom, with a corresponding

'effective' Bohr radius and 'effective' Rydberg.

$$E_n = - e^4 m^*/2\hbar^2 \varepsilon^2(0)\ n^2 = - R^*/n^2,\ n=1,2,3.. \qquad (1.15)$$

where $$R^* = (m^*/m).1/\varepsilon^2.R_H \qquad (1.16)$$

is the effective Rydberg and R_H is the hydrogen atom Rydberg.

$$a^*_B = \hbar^2/e^2.\ \varepsilon/m^*.\ n^2 = \varepsilon.\ 1/(m^*/m).\ a_o \qquad (1.17)$$

is the effective Bohr radius and a_o is the Bohr radius of a hydrogen atom.

Substituting in the appropriate effective mass and static dielectric constant values for GaAs, $m^* = 0.0665m_o$ and $\varepsilon(0) = 12.84$ (Stillman 1977) respectively, gives a ground state binding energy of 5.5meV and an effective Bohr radius of 99Å. Thus a large Bohr radius i.e $a_B >> a$, where a is the lattice constant and a slowly varying Coulomb impurity potential U(r), justify the approximations made in the effective mass approximation for GaAs. Only 'shallow' donors with a small binding energy compared to the energy gap, E_g, will satisfy the above conditions.

The electron bound to the impurity, according to equation (1.8) is a superposition of Bloch waves and is localised at the impurity centre. Assuming that $A_n=0$ for $n \neq 0$ and that k is small, using equation (1.14), the coefficients $A_o(k)$ have the form (Kohn 1957)

$$A_o(k) = 1 / (1 + (k^2 a^*)^2)^2 \qquad (1.18)$$

so that $A_o(\underline{k})$ extends appreciably in momentum space to values of k less than or equal to $\underline{k}=1/a^*$. Since the donor impurity wavefunction in GaAs extends in real space over many lattice cells and therefore varies little over each cell, in k-space the wavefunction $A(\underline{k})$ is confined to within 1% of the Γ extremum centre and beyond this value falls of rapidly as $\sim 1/k^4$. Thus the substitution of the dispersion relationship for a parabolic band is justified. The envelope function is centred about critical points in $\underline{k}$-space where $\nabla_k E(\underline{k}) = 0$. There will be impurity states associated with other critical points in $\underline{k}$-space i.e maximum, minimum and saddle points in the band structure. Corresponding to solutions other than n=0, the wavefunctions of the hydrogenic states are constructed from an admixture of all bound states which $k < 1/a^*$. The coefficients $A_n(k)$ for $n \neq 0$ were estimated by Kohn (1957), giving

$$A_n \sim E_o/\Delta E . a/a^* . A_o \qquad (1.19)$$

where E_o - ionisation energy

ΔE - band gap energy

a - lattice constant

Consequently, A_n/A_o is very small for a shallow donor associated with a simple band. In general, impurity states contain contributions from more than one critical point, but the effect is small if the separation between the extrema is large. The extension in $\underline{k}$-space of the excited states is obviously much smaller and hence is expected to be even better described by effective mass theory.

1.4 Donor levels associated with subsidiary minima

Effective mass theory can be extended to take into account the equivalent higher order minima in GaAs and InP. According to effective mass theory, resonant states exist under each secondary minima, degenerate with the lowest principal band. Also, resonant states can occur at saddle points of the band structure. Many of the conclusions from donor levels associated with equivalent minima e.g Si and Ge, apply to the effects connected with degenerate subsidiary minima. In this case, take linear combinations of impurity wavefunctions from each equivalent extrema i.e consider donor wavefunctions associated with the L minima.

$$\Psi(r) = \sum_{i=1}^{\nu} a^i F^i(r) \psi^i(r)$$

where a^i - numerical coefficients which describe the relative contribution from the different minima.

As the energy difference between the subsidiary minima and the absolute minimum is reduced e.g with pressure, a superposition of Bloch waves from states associated with the principal minimum occurs (see section 3.5). A schematic representation of the conduction band minima, with their associated impurity states of three common donors X_1, X_2, and X_3 are shown in figure (1.4).

1.5 CENTRAL-CELL CORRECTIONS

The effective mass treatment is particularly successful for shallow donors in GaAs and InP, disregarding the central-cell potential, because both have 'simple' bands, and the conditions of small effective mass and large dielectric constant are readily satisfied. Consequently, the simple hydrogenic model suggests optical

transitions similar to the Lyman, Balmer etc.. series of the hydrogen atom and is expected to predict their shallow donor transition energies reasonably well. However, effective mass theory predicts the same energy for all donors irrespective of their chemical nature, and hence fails to include the true potential of the impurity. The potential of the impurity ion is not a simple Coulombic potential close to the ion core and depends strongly upon the chemical nature of the impurity present. In addition the local distortion of the lattice around the impurity, can contribute to the 'central-cell' effects. Thus the 'central-cell' potential contains corrective terms from the short range impurity component of the 'bare' Coulomb potential as well as the dispersion of the dielectric function. These effects extend over a volume of the size of the unit cell, and can produce a significant perturbation of the 'bare' Coulomb potential in this region. These effects are accentuated by a non-vanishing wavefunction at the donor centre. It has been shown experimentally (Fetterman et al 1971) that the central-cell corrections are described by

$$E_i = K_i \left| \psi_{1s}(0) \right|^2 \qquad (1.20)$$

where K_i is a field independent parameter characteristic of a particular donor species.

The energy differences between the different central-cell components are extremely small in GaAs and InP, corresponding to the order of 1% of the donor binding energy. Resolving such small energy differences of the 1S ground state provides the only method of identifying the various shallow donors in high purity material. Unfortunately, broadening even in the highest purity crystals obscures the fine central-cell structure. A magnetic field is used to reduce the broadening.

1.6 Shallow donor impurities in a magnetic field

Hydrogen-like donors in a magnetic field have been extensively studied . There is also a similar problem in astrophysics, since the scaling due to the differences in the effective mass compared to the free mass, provides a terrestrial way to study the effect of extremely large magnetic fields generated from, for example, white dwarfs (10^5 - 10^6T) acting on a free hydrogen atom.

Consider the simplest case, a Coulombic donor in a uniform magnetic field applied parallel to the z-axis, associated with a parabolic, isotropic and non-degenerate (except for spin) band. The Hamiltonian takes the form

$$H = (\underline{p} - e\underline{A})^2/2m^* - e^2/4\pi\varepsilon\varepsilon_o r; \qquad (1.21)$$

where $\underline{p} = -ih\nabla$, and $\underline{A} = 1/2\ \underline{r} \times \underline{B}$ is the vector potential. In the symmetric gauge using cylindrical coordinates $(\rho,\emptyset,z)$;

$$A = B/2\ (y,-x,0).$$

The Hamiltonian for an impurity in a magnetic field is

$$H/R^*_y = -\nabla^2 + \gamma L_z + \gamma^2/4(x^2 + y^2) - 2/r; \qquad (1.22)$$

where $\gamma = \hbar w_c/2R^*_y$ is the dimensionless magnetic field parameter , and $r = (x^2 + y^2 + z^2)^{1/2}$.

The second term in equation (1.22) contains the effect of the magnetic field and describes the Lorentz force on the electron, this term both distorts and shrinks the wavefunction. The units used are

$$R_y^* = m^* e^4/2h^2\varepsilon^2 \quad \text{for energy}$$

$$\text{and} \quad a_B^* = h^2\varepsilon/m^* e^4 \quad \text{for length.}$$

At a field of 1T, $\gamma \sim 5 \times 10^{-6}$, for a hydrogen atom, $\gamma \sim 0.2$, for a donor in GaAs, and in InSb $\gamma \sim 6$. For large γ, the charge distribution assumes a cigar-like shape oriented along the field direction e.g a donor in InSb at 10T, gives $\gamma = 69$, the transverse axis is compressed to ~81Å and its longitudinal dimension reduced to ~200Å compared to its zero field value of 673Å. The Schrodinger equation (1.22) has to be solved. However the Coulomb term is inseparable in cylindrical coordinates. Various approximations have been developed depending on the value of γ.

Three distinct limits are obtained, depending on the validity of the approximations made in equation (1.22).

i) <u>low field limit ($\gamma \ll 1$)</u>, shallow donors are well described in this regime. The effect of the magnetic field is treated as a perturbation of the Coulomb potential, and gives rise to Zeeman splitting in a similar manner to the free hydrogen atom.

ii)<u>intermediate field ($\gamma \sim 1$)</u>, this regime is of particular interest since the donor states of GaAs and InP lie in a region of experimentally obtainable magnetic fields. Unfortunately, this regime is difficult to mathematically model since the eigenfunctions have to be flexible enough to accurately describe both the low field limit, where states are mainly hydrogenic in character, and the high field limit where they begin to resemble Landau states. Possibly, the most successful treatment of the problem was achieved by Aldrich and Greene (1979) and later extended by Makado (1984). They calculated accurate

variational energies for the first four excited state transitions for a hydrogen atom in this magnetic field regime. Relatively simple trial wavefunctions of the type below were used

$$\psi_i = \rho^{|m|} e^{im\phi}\, z^q \exp(-a_i \rho^2) \exp(-b_i z^2) \qquad (1.23)$$

The variational wavefunctions are expanded in terms of a set of basis functions.

$$\Psi = c_i \psi_i \qquad (1.24)$$

For a given set of a_i and b_i, the coefficients c_i in the expansion (1.24) are determined by a variational procedure by minimising the energy. Figure (1.5) plots the variational energies as calculated by Makado (1984) for the ground and some excited states of the neutral donor atom in a magnetic field.

iii)<u>High field limit ($\gamma >> 1$)</u>, the adiabatic approximation is appropriate i.e regard the impurity potential as a perturbation (Yafet, Keyes and Adams 1956) . Hence equation (1.22) becomes approximately separable in cylindrical coordinates ,and the eigenfunction becomes

$$\psi_{NMB}(\rho,\phi,z) = F_{NM}(\rho,\phi) f_{NMB}(z) \qquad (1.25)$$

For large γ. the Coulomb potential in the direction perpendicular to the field is neglected, but the potential along the field is still important, and is described by an effective potential

$$V_{NM}(z) = -2 \iint |F_{NM}(\rho,\phi)|^2 / \sqrt{\rho^2 + z^2}\, dxdy \qquad (1.26)$$

At extremely large fields the impurity potential can be neglected completely, and the Schrodinger equation can be solved exactly, giving eigenenergies, with the inclusion of spin,

$$E_N(k_z) = (N + 1/2)\, \hbar w_c + \hbar^2 k_z^2 / 2m^* + 1/2 g^* \beta B, \quad N=1,2,3... \qquad (1.27)$$

where $w_c = eB/m^*$ is the cyclotron frequency of the orbiting electrons;

g^* - effective g value,

β = eh/2mc - Bohr magneton.

The effective g value for GaAs is small and its effect is negligible at low magnetic fields. In contrast, InSb has a large g^* value, consequently spin-splitting effects are much more important.

A magnetic field has the following effects.

i) Increased Coulomb binding energy, the effective Rydberg of the ground state energy as a function of magnetic field is calculated very approximately in the high field regime i.e $\delta >> 1$, by combining (1.14) and (1.16)

$$R_y^*(B) \sim 1/[\ 2\ \varepsilon\ (a_o^*\ r_B)^{1/3} = 1/[\ 2\ \varepsilon\ (a_o^*\ B^{-1})^{1/3}] \sim B^{1/3}.$$

where r_B is the radius of cyclotron motion in field B

$$r_B = (eh/B)^{1/2}$$

The Coulomb binding energy increases as $B^{1/3}$, and can contribute to carrier 'freeze-out' at low temperatures.

ii) Reduction of overlap of donor wavefunctions, for example in InSb with donor concentration $\sim 10^{14} cm^{-3}$, the wavefunction overlap is reduced by the application of a magnetic field, leading to a metal-insulator transition at low temperatures i.e carrier localisation at donor ions with increasing field.

iii) Increased central-cell effects , the chemical shifts due to central-cell interactions increase approximately linearly with field (Cabib 1971).

iv) Decrease in linebroadening, due to a change of the quadrupole interaction and a reduction in the quadratic Stark shift caused by ionised impurities.

v) <u>Δg splitting</u> Non-parabolicity of the conduction band becomes important at high magnetic fields in GaAs i.e above 7T. Each donor peak in the $1S\text{-}2P_{+1}$ impurity state transition splits due to the spin-conserving transitions between the spin-up and spin-down states having different energies. This splitting in energy is attributed to different spin g-factors because of non-parabolicity between the lowest N=0 and N=1 Landau levels. The effective Δg value difference between the two levels is proportional to B^2 (Simmonds 1973).

Figure(1.1)

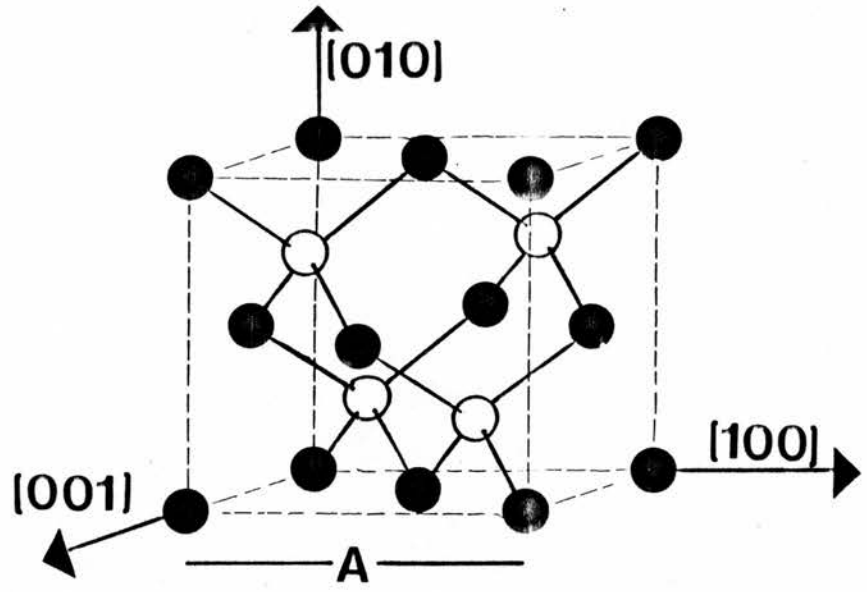

figure(1.1) Shows the zinc-blende lattice with unit cube of volume A^3, A is the edge length of the elementary cube of the face-centre-cubic lattice. Another face-centre-cubic lattice, but of different atoms, is oriented parallel but displaced by the vector t = (A/4, A/4, A/4) from each other.

● - atoms X

○ - atoms Y

Figure(1.2)

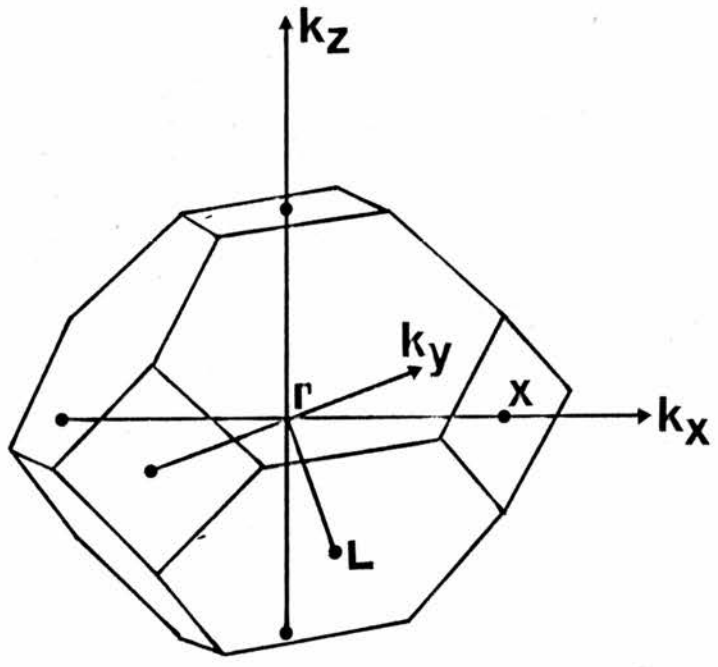

Figure (1.2) The associated Brillouin zone of the zinc-blende crystal structure is a truncated octahedron, with the most important symmetry points shown.

Figure (1·3)

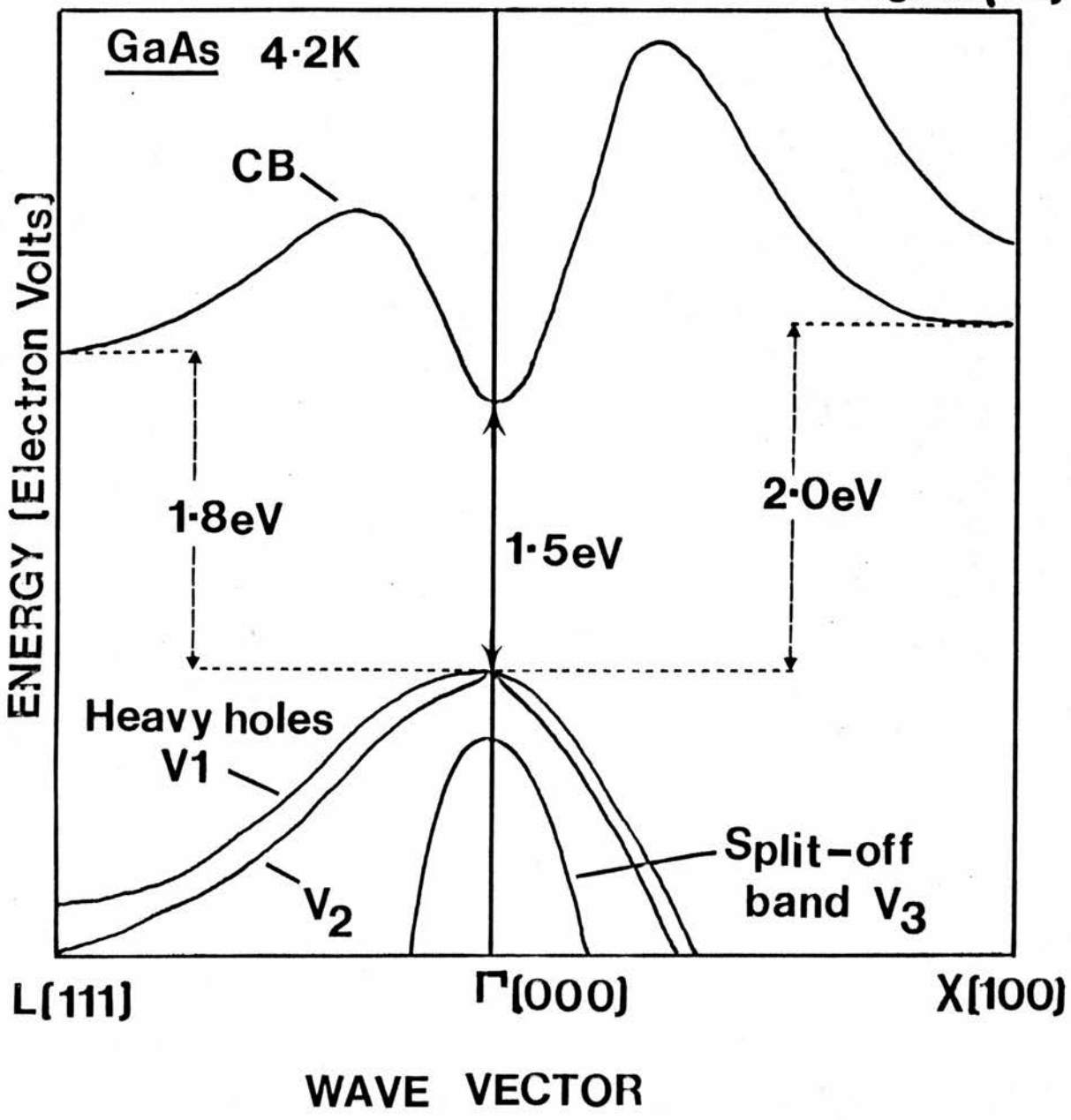

Figure (1.3) Variation of energy versus wave vector for GaAs in the vicinity of the forbidden gap is displayed in this figure. The energy gaps are shown as appropriate for 4.2°K.

CB - conduction band

V1 - heavy hole valence band

V2 - light hole valence band

V3 - split off valence band

Figure (1·4)

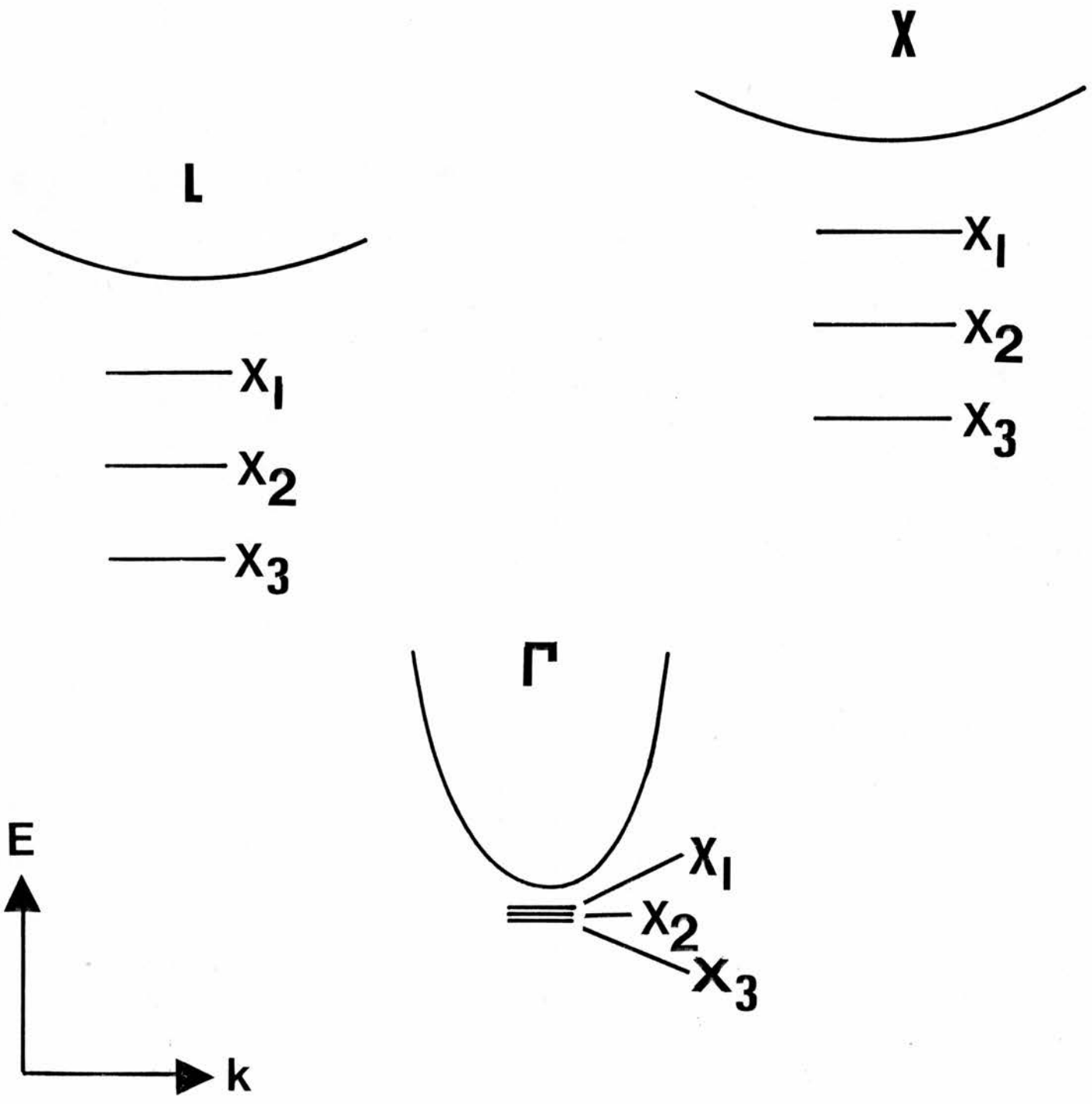

Figure (1.4) Displays a schematic diagram of the conduction band minima of GaAs with associated impurity states (not drawn to scale).

Figure (1·5)

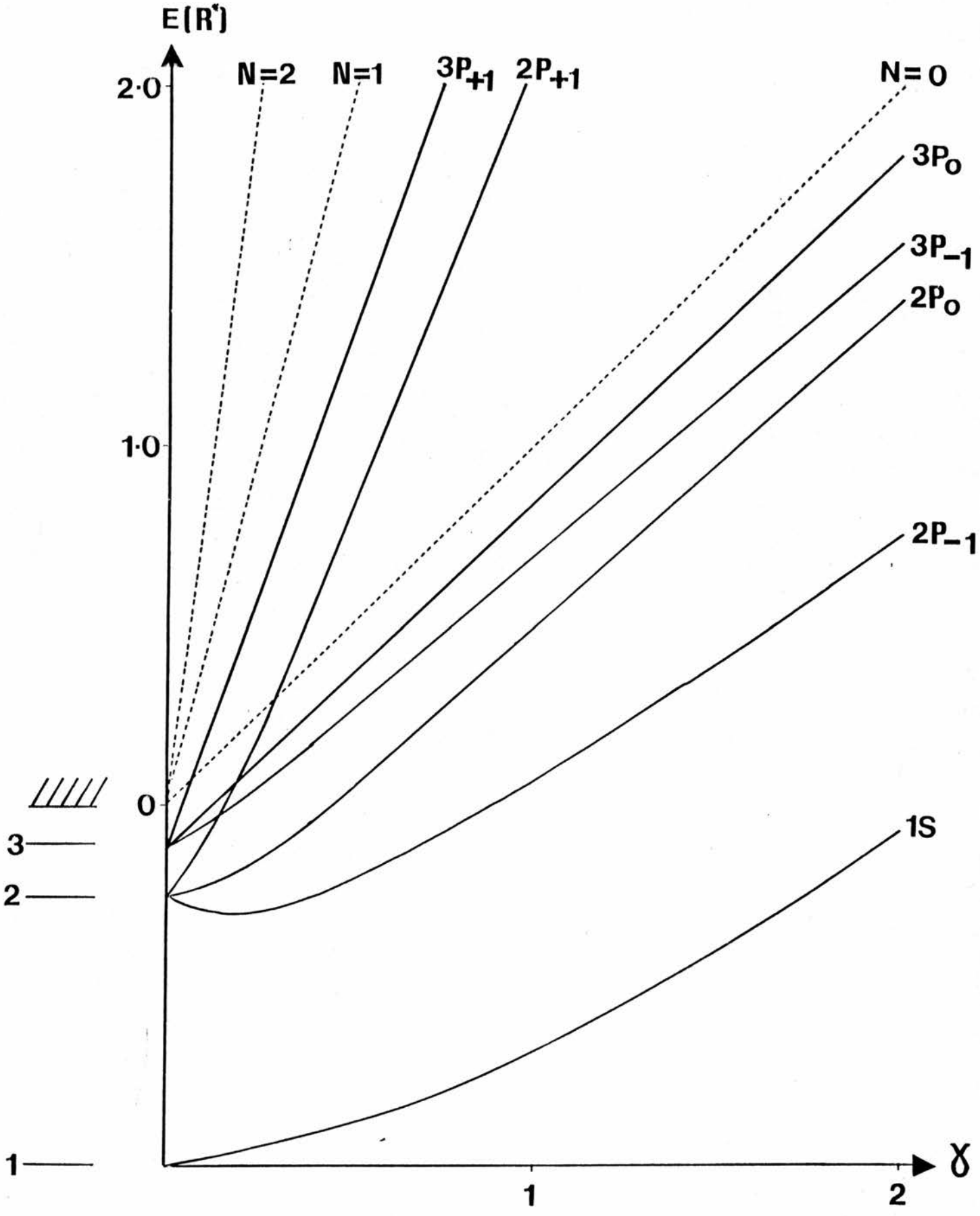

Figure (1.5) The dimensionless magnetic field parameter γ is plotted against energy for several donor transitions and Landau levels. On the bottom left hand corner a zero magnetic field

CHAPTER 2

EXPERIMENTAL PROCEDURE AND PHOTOCONDUCTIVITY MECHANISMS

Far-Infrared (FIR) spectroscopy is an extremely powerful tool for the study of shallow donor impurities in semiconductors. However, the technique is limited by the availability of good FIR sources. Two important sources of FIR radiation are molecular gas lasers and Fourier transform spectrometers. These sources are to a considerable degree complementary, with each possessing particular advantages. The laser has much greater power levels, with high resolution and better signal-to-noise ratios, is superior for observing fine central-cell structure or weak interexcited state transitions. However, since these measurements are taken at fixed wavelengths, the magnetic field must be swept through the various spectroscopic transitions in order to obtain a spectrum, this can lead to distorted lineshapes. The impurity population may alter by sweeping the field so that the relative intensities of different lines may give a misleading impression of the different concentrations of residual impurities. Furthermore, the photoconductivity spectra may be also distorted as the sample resistance and hence the sensitivity of detection changes with magnetic field. On the other hand, the broadband blackbody spectrum available within the Fourier transform spectrometer enables a complete frequency sweep to be made at constant field. Consequently the population of the impurity levels and the photoconductivity sensitivity are constant over the range of frequencies. Although much smaller powers are available, transitions may be observed which are not seen by the laser due to the lack of a suitable wavelength. Tuneable FIR radiation is also available from a cyclotron emission spectrometer, but this is still at the development stage.

2.1 Experimental apparatus and system

This thesis describes experiments performed by a FIR laser system together with a 13T Oxford Instruments superconducting magnet. This magnet is particularly suited for central-cell identification since it has a high homogeneity , calibrated to 1 part in 10^5. The laser system is chosen for its particular advantages of high power and high resolution, and consists of two lasers, an Edinburgh Instruments (EI) PL4 step-tuneable cw CO_2 infrared gas laser which can give output powers in excess of 50W in the 9-11μm region, optically pumping an EI Model 195 FIR molecular gas laser which has a tuning range from 40-1200μm, with up to 100mW of FIR radiation on the most powerful lines. A selection of FIR wavelengths are available from various organic gases. One of the most useful and powerful lines is 118μm with CH_3OH which is optically pumped by 9P36 CO_2 radiation. This line is chosen for its ease of operation, stability and suitability for looking at the $1S-2P_{+1}$ transition. The transition is observed on the photoconductivity spectra at approximately 3.5T and 3.6T in InP and GaAs respectively.

CO_2 radiation is directed into the FIR cavity by a system of mirrors. Inside the cavity, the CO_2 radiation is absorbed and excites an appropriate organic gas eg methanol. Lasing action is induced in the FIR. The FIR radiation is then guided by brass pipes and mirrors down into the magnet, and then focused onto the sample. Figure (2.1) shows a schematic representation of the experimental lay-out. The sample can be orientated either in the Faraday or Voigt configuration ie with the magnetic field parallel to the radiation propagation direction or at right angles to it. The two orientations exhibit

different quantum mechanically allowed transitions because of the different selection rules that apply. However, experimentally the selection rules are broken for various reasons, e.g radiation rarely propagates in an exactly parallel beam or the admixtures of states are brought about by the Stark interaction, and theoretically forbidden transitions are often observed. For example, the $1S-2P_o$ transition is parity forbidden in the Faraday geometry, but it can generally be observed in the spectra. All of the spectra recorded in this thesis are observed in the Faraday geometry.

Pure Indium contacts are alloyed to a clean sample surface in a reducing atmosphere of hydrogen/nitrogen gas at a temperature of $300^{o}C$. A constant voltage supply is connected across the sample, with a typical bias voltage in the range $0.1-0.3 Vcm^{-1}$, well below any tunnelling or impact ionisation effects. The resulting voltage signal is fed through an a.c. amplifier and into a phase sensitive detector (p.s.d). A reference signal for the p.s.d. is taken from the chopper in the CO_2 beam. The p.s.d. output ie photoconductive response, is recorded on the Y-scale of a chart recorder. The X-scale is a linear function of magnetic field. The magnet is swept on a stabilised current mode. Both the up sweep and the down sweep are recorded so that any lag between the voltage across the magnet shunt resistance and the actual field across the sample can be averaged out. Also, two sweeps should clarify any spurious laser drift or noise which can sometimes complicate the spectra.

Hydrostatic pressure can be used as an additional experimental parameter. Large hydrostatic pressures are generated by a Be-Cu or Ni-Cr piston which is tightened inside a non-magnetic Be-Cu cell, containing petrol as the hydrostatic medium. An exploded diagram of

the pressure cell is displayed in figure (2.2). It is possible to achieve any pressure up to 15kBar and this can be measured to a precision of approximately 100bar (i.e 1% accuracy), by measuring the change in resistance of a heavily doped InSb manometer. The cell has a sapphire window at one end allowing FIR access, together with 12 electrical leads from the manometer and sample which run through the centre of the piston at the other end. The cell is then sealed and cooled to operating temperatures as low as ~2K at magnetic fields up to 12.7T, with the resulting pressure homogeneous to 1 part in 1000.

2.2 PHOTOCONDUCTIVITY MECHANISMS

There are three types of photoconductive process to consider.

i) absorption of radiation by free carriers - at low temperatures the coupling between the lattice and electrons can be very weak. Free electrons can therefore be 'heated' out of their energy equilibrium with respect to the lattice by the interaction of sufficient incident radiation and/or applied electric field. A change in the electron mobility can occur, and hence the conductivity of the sample changes.

ii) intrinsic photoconductivity - involves the excitation of electrons from the valence band to the conduction band. The conductivity of the sample is increased as both free electrons and free holes are created. This condition is obtained when band gap radiation is applied to the sample, for example, from a white light source.

iii) extrinsic photoconductivity - occurs at low temperatures i.e $4.2^{o}K$ so that most of the uncompensated donors are neutral. Photoconductivity results from the excitation into the conduction band of an electron bound to a neutral donor by FIR radiation, this can occur as a direct process or involve an intermediate state. Either process only involves one type of free carrier in contrast to intrinsic photoconductivity.

The second extrinsic photoconductivity mechanism involves the transfer of an electron from a ground state into an intermediate excited state by the absorption of a FIR photon. Further excitation into the conduction band is possible by the following means;

i) electric field tunnelling from the excited state to the conduction band.

ii) impact ionisation of the electrons in the excited states by energetic free electrons.

iii) photoionisation by the absorption of a second photon.

iv) hopping between excited states.

v) thermal ionisation by the absorption of one or more phonons.

The final process is called 'photothermal ionisation', and can be observed in many semiconductors if the temperature is chosen correctly (Kogan and Lifshits 1977). The optically excited electron absorbs and emits single phonons as it wanders through the bound excited states until it is either finally captured in the ground state or released into the conduction band where it contributes to the conductivity (see figure 2.3). Figure (2.4) is a schematic diagram of donors A, B, C; illustrating the different ground state binding energies of each particular impurity. The probability of thermal ionisation can be almost 100% . The photoconductivity signal can be regarded as a convolution of three processes, absorption, energy relaxation, and recombination.

For 'photothermal ionisation' to occur, the conditions are chosen such that

i) the temperature should be high enough to provide thermal ionisation from the excited states, but

ii) the temperature should not be so high to produce thermal ionisation of ground state impurities.

Thus at the working temperature of 4.2K for GaAs and InP, most of the electrons are frozen out onto the ground states. In GaAs the energy gap between the first excited level n=2 and the ground state n=1 is E=4.3meV and is much larger than kT at T=4.2K . The temperature dependence of the photoconductivity due to photothermal ionisation is obtained by the dependence of the probability of thermal ionisation of the 2P level.

Extrinsic far-infrared photoconductivity is one of the most powerful techniques for investigating the chemical nature of shallow impurity electronic states in semiconductors. Extremely high sensitivity and resolution can be achieved with high purity, thin film samples. The extreme sensitivity is a consequence of the fact that the total photo-response is effectively independent of the impurity concentration, hence the photoconductivity response continues to improve with sample quality (Kogan and Lifshits 1977). This is in contrast to absorption/transmission measurements, where the signal becomes poorer with increasing crystal quality. The increase in the free carrier concentration Vn resulting from illumination is given by

$$Vn = G\ T_{recomb}$$

where the generation rate, G is proportional to the intensity, I, and T_{recomb} is the recombination time. The intensity after passing through a thickness x of material whose absorption length, L, is

$$I = I_o \exp(-x/L)$$

An expansion of the exponential to first order gives, $VI \sim I_o x/L$, for $x \ll L$.

Thus $\Delta n \sim I_o . (x/L) . T_{recomb} / \hbar w$

Since $L \sim 1/N$, therefore $\Delta n \sim N$, where N is the number of donors.

Here

n - is the total carrier concentration without illumination.

Δn - is the change in carrier concentration with illumination.

The change in conductivity $\Delta\sigma$, is determined by the electron generation and recombination rate in the conduction band and is measured experimentally as a change in signal voltage Δv by,

$$\Delta V/V_o = \Delta\rho/\rho = -\Delta\sigma/\sigma = -\Delta n/n \sim I_o . T_{recomb} / \hbar w$$

provided that $\Delta\sigma << \sigma$, where V_o is the bias voltage and ρ is the resistivity.

Thus, to first order, the signal is indepenedent of the purity. However, the peak intensity of the photoconductivity lines improves as the impurity concentration decreases since the lines narrow as the electric field effects from neighbouring ionised impurities are reduced. Also, T_{recomb} increases as N decreases. Thus the photoconductivity signal improves with increasing purity. The relative proportions of different impurities can be found from the ratios of the corresponding spectral line amplitudes. The absolute value of the impurity concentration is then obtained by means of Hall measurements.

Another advantage of using the 'photothermal ionisation' technique is that interexcited state transitions can be observed. Optical excitation from the 2P state allows transitions to higher S and D states for which an electric dipole transition from the ground state is parity forbidden. For S-like excited states the central-cell corrections are much less important than for the ground 1S state and are described by EMT to better than 1% e.g $1/8^{th}$ on 2S at B=0.

Various methods are employed in an attempt to identify each of the central-cell peaks with their corresponding residual contaminating impurities.

i) Carefully controlled back-doped doped crystals are grown by introducing a very small quantity of known dopant into the system. The back-doped photoconductivity spectra is compared to the various photothermal ionisation peaks from undoped samples in an attempt to locate exactly where the dopants are in energy. Unfortunately, the spectra of such doped material is difficult to analyse because of the very small donor concentration range between the purest material which can be grown, and that where impurity interactions degrade the spectra by broadening and distorting the spectral lines.

ii) Bombardment of the crystal with a flux of thermal neutrons can transmute a small proportion of Ga atoms into Ge donors and As atoms into Se donors, similarly with InP; In goes to Sn and P goes to S. Neutron transmutation doping (NTD) of the sample in this way, in principle should decrease the compensation ratio by introducing new donors without the accompanying increase in compensating acceptors as would be introduced during the melt. Unfortunately, neutron bombardment introduces many crystalline defects and the sample must be thermally annealed before its conductivity can be recovered. In reality, although thermal annealing repairs most of the neutron damage, deeper lying traps are not annealed out, consequently the effective compensation ratio increases. Besides the disadvantage of thermally annealing, NTD is limited for central-cell identification since only two dopants are identified.

iii) A comparison of the growth parameters can help the identification of donors. e.g a reduction in the Ga to As ratio will assist the incorporation of group IV elements on the Ga site.

FIRPC is an extremely sensitive method for resolving very small central-cell energy differences between the residual shallow donor impurities in high purity GaAs and InP. The problem of identifying the contaminants is compounded by inhomogeneous Stark broadening and the accompanying shift of the line position. Only neutral donors can absorb FIR photons. Ionised impurities make their presence known by their perturbing effects on the lineshapes of the FIR optical transitions or the neutrals. The extraneous inhomogeneous broadening is several orders of magnitude greater than the intrinsic 'phonon' linewidths, this is due to electric field and electric field gradients arising from charged impurities in the host crystal. An understanding of the mechanisms involved in the broadening processes is given in the next section. Obviously, a reduction of the inhomogeneous broadening would be advantageous in resolving central-cell spectra. Various methods are employed to reduce the effect of inhomogeneous broadening and there are described in the following chapter.

2.3 INHOMOGENEOUS BROADENING

An electron bound to a donor will experience not only the Coulomb potential of the central donor ion, but also the sum of Coulomb potentials from all other charged impurity ions in the lattice. However, nearest-neighbour charges are expected to be the most effective in shifting the donor transition energy. The neutral donor centre and ion-impurity can be regarded as the analogue of the hydrogen molecule H_2^+. For large separations R between the neutral atom and ion ie R>>a (a-Bohr radius), the ion Coulomb field can be very accurately treated in second-order perturbation theory (Larsen 1973). A pair of neutral donors can similarly be treated as a neutral hydrogen molecule.

Consider an electron bound to a shallow donor impurity. The Hamiltonian, of a single hydrogenic donor perturbed by surrounding ionised impurities is given by

$$H = H_o - eV_{ext}(\underline{r});$$

where $H_o = p^2/2m^* - e^2/4\pi\varepsilon\varepsilon_o r$ is the unperturbed Hamiltonian.
The potential energy due to the interaction of the neutral donor centre with all ionised impurities is

$$V_{ext}(\underline{r}) = e_i/4\pi\varepsilon\varepsilon_o|R_i - r|;$$

where the ith ion has charge e_i and is located at R_i;
$\underline{r}$ - is the displacement of the electron, assume $R_i >> r$.

Expand $V_{ext}(\underline{r})$ in a Taylor series about r=0.

$$V(\underline{r}) = V(0) + \underline{r}.\nabla V(0) + 1/2(x^2\, d^2/dx^2 + y^2\, d^2/dy^2 + z^2\, d^2/dz^2)V(0) + \ldots$$

The first term in the expansion shifts all the levels by the same amount and hence leaves the system unchanged. Terms proportional to r^2 give potentials of the various field gradients. The second term gives rise to the linear Stark effect

$$\underline{r}.\nabla V(0) = -\underline{E}.\underline{r};$$

the third term becomes

$$-1/2(z^2 - 1/2\rho^2)\, dE_z(0)/dz;$$

and is the source of the quadrupole term.

The lowest order energy shift of the state is , in first order perturbation theory,

$$\Delta E_i = e\langle \phi_i |\, V(\underline{r})\, | \phi_i \rangle = eV(0) - 1/4Q_i\, dE_z/dz;$$

where $Q_i = e\langle \phi_i |(2z^2 - \rho^2)| \phi_i \rangle$ is the quadrupole moment, which varies with magnetic field. The quadrupole moment tends to zero with increasing magnetic field for the $1S\text{-}2P_{\pm 1}$ transition. In contrast, the quadrupole broadening term of the $1S\text{-}2P_0$ transition is still important at high fields (Larsen 1973).

The change in donor transition energy is

$$\Delta T = \Delta E_j - \Delta E_i = -1/4(Q_j - Q_i)dE_z(0)/dz$$

The magnetic field direction is chosen as the axis of symmetry, parallel to the z-axis. The line-shape and width due to transition energy shifts are obtained by calculating the statistical distribution of the electric fields and field gradients dE_z/dz, of a random spatial distribution of ionised impurities located throughout the crystal. This is described by a Holtsmark distribution function. Thus the net transition spectrum is a superposition of a large number of sharp lines centred at different frequencies. The $1S\text{-}2P_o$ transition distribution is well described by a Lorentzian, and gives a symmetric

line-shape.

To describe the asymmetry observed on the $1S\text{-}2P_{-1}$ transition, one needs to treat the Stark term $\underline{r}.\nabla V(0)$ by second order perturbation theory. The quadratic Stark effect is the most important source of inhomogeneous broadening for both the $1S\text{-}2P_{+1}$ and $1S\text{-}2P_{-1}$ transition. Most of the inhomogeneous lineshape is due to nearest neighbour impurities within the sphere of influence of the neutral donor. On the $1S\text{-}2P_{-1}$ line the effect displaces the peak position to lower energy as well as producing an asymmetric tail towards lower energy. The $1S\text{-}2P_{+1}$ line is more symmetric and there is the same peak displacement to higher energy.

$$\Delta E_i = e^2 \lesssim_j |\langle \phi_j | V(r) | \phi_i \rangle|^2 / (E_i - E_j)$$
$$= A_i(B)\, E_\perp^2(0) + C_i(B)\, E_\parallel^2(0)$$

where $\underline{E}.\underline{B} = E_\parallel B$ and $E_\perp = \underline{E} - E_\parallel \underline{B}/B$

A_i and C_i are polarisabilities which depend on the magnetic field strength. The total energy shift is

$$\Delta T = -1/4(Q_j - Q_i)\, dE_z(0)/dz + (A_j - A_i)\, E_\perp^2(0) + (C_j - C_i)\, E_\parallel^2(0)$$

The quadratic Stark effect dominates the field gradient or quadrupole shift, so the first term can be neglected. The statistical distribution of $(aE_\perp^2 + cE_\parallel^2)$, where $a = A_j - A_i$ and $c = C_j - C_i$, is computed with a random impurity model.

The $1S\text{-}2P_{+1}$ lineshape is dominated by the quadratic Stark effect. However, the $1S\text{-}2P_{+1}$ is broader than expected compared to theory. This is because the $2P_{+1}$ level crosses the n=0 Landau level at 2.0T in GaAs so the $2P_{+1}$ level is always degenerate with the continuum in the lowest Landau level. Electric fields perpendicular to the applied magnetic field can induce interactions between bound $2P_{+1}$ state and the continuum states. The broadening from this process is

proportional to $E_{\perp}$(Larsen 1977).

As a magnetic field is applied, the Stark broadening is expected to decrease with increasing magnetic field because the energy levels have a tendency to spread out and the wavefunctions are compressed as the field increases. Consequently, the energy denominator is enlarged and the interactions are reduced.

Instead of a random ion impurity distribution throughout the crystal, at low temperatures i.e $4.2^{o}K$, correlation effects can occur because the thermal energy (~kT) is much less than <E>, (Golka et al 1977) where

$$\langle E \rangle = e^2/\epsilon r$$

is the mean Coulomb binding energy of an ionised donor bound to a near-by ionised acceptor, and

$$r = (4/3\pi N_d)^{-1/3}$$

is the radius of sphere containing on average one donor
Thus at low temperatures, the nearest donor to an ionised acceptor tends also to be ionised, and the spatial distribution of charged donors and acceptors are strongly correlated. Hence a neutral donor experiences an electric field produced by a set of randomly distributed dipoles. The electric fields generated by the paired ionised impurities are much weaker than those produced by uncorrelated , randomly distributed point charges. The relatively weak dipole fields still give rise to some inhomogeneous linewidth, but much less compared to an uncorrelated distribution.

2.4 CONCENTRATION BROADENING

As the impurity concentration increases, the perturbation approach used to describe Stark broadening breaks down. The resultant overlap of the donor wavefunctions gives rise to broadening of the transitions. Broadening of the 'hydrogenic' donor lines become very large when,

$$r_S \lesssim 6na_B$$

n - principal quantum number.

a_B - effective Bohr radius of the bound carrier.

r_s is defined by

$$4\pi r_s^3/3 = 1/N_i$$

N_i - impurity concentration.

2.5 LINE NARROWING

Several techniques are introduced to narrow lines and improve the resolution of the spectra.

i) as mentioned before a magnetic field compresses the donor wavefunction and enlarges the central-cell splittings. Also, as indicated in the previous section, the $1S\text{-}2P_{-1}$ transitions has the narrowest linewidth compared to the other two Zeeman split transitions. A peculiarity of the $1S\text{-}2P_{-1}$ transition is that it varies little in energy with increasing magnetic field. If a suitable laser line is used, the central-cell components are spread over a very large magnetic field range. For example, 302μm radiation crosses all but the deepest of the shallow donor transitions in GaAs and the

components are spread over about 3T (figure 2.5). The resulting lineshapes can be rather misleading. However further central-cell structure can be resolved. Unfortunately, there is no available FIR laser line to look at the $1S-2P_{-1}$ transition in InP. Although, the $1S-2P_{o}$ transition can be observed in Faraday geometry, it is usually weak and is not studied as a matter of course. The $1S-2P_{+1}$ transition has the advantage that many good FIR laser lines are accessible to the transition. This transition is routinely studied in GaAs and InP.

ii) In principle, Stark broadening due to the electric fields and field gradients from neighbouring charged impurities can be reduced by band-gap radiation. Illumination of the sample with a white light band-gap source, excites electrons and holes into the conduction and valence bands respectively, from where they are selectively captured and neutralise a proportion of the ionised donor and acceptor sites, thereby reducing the random electric fields which broaden lines. The photo-narrowing achieved for a high purity sample of GaAs is demonstrated in figure (3.1). Unfortunately, the effect of intrinsic illumination is much less pronounced with less pure samples, i.e $>10^{15}cm^{-3}$, where the narrowing would be more beneficial. The decrease in efficiency of the neutralising light is thought to result from the rapid increase in direct donor acceptor recombination with increasing concentration. Nevertheless, the effect of intrinsic illumination is studied as a matter of course with all samples.

iii) A reduction of the temperature from 4.2 to 2.0K can frequently narrow the lines even though the total number of ionised sites does not change significantly over this temperature range. This is thought to occur from an enhancement of the correlation effects mentioned in section (2.3). With decreasing temperature, phonon assisted hopping

of donor electrons from neutral to ionised sites, and the average separation within the donor-acceptor dipoles both decrease. Thus the intensity of the electric dipole fields decrease correspondingly, and hence the linewidth is reduced with temperature (Golka 1977 and Larsen 1975).

iv) The addition of hydrostatic pressure provides a new technique for further resolving central-cell structure. Pressure acts in a similar way to a magnetic field by increasing the band-gap and also the effective mass, thus deepening the donor states. The donor wavefunctions are compressed and the chemical shifts increase with increasing pressure, although the increases are not due entirely to an increase of the effective mass but the dielectric constant decreases correspondingly (Wasilewski 1984). Stark broadening is expected to decrease due to the compression of the donor wavefunctions and also due to increased correlation. Furthermore, the sample resistance increases, thereby improving the sensitivity of photoconductivity detection. As the pressure increases, the Ge donor in GaAs anomalously deepens as hybridisation from other similar states of the same symmetry but associated with a subsidiary minima occurs. The Γ associated components of the state thus disappear completely from the spectrum (Armistead et al 1984).

Most of the above line narrowing techniques are used in combination with each other and occasionally all four are used together. The resultant narrowing can be dramatic. Unfortunately, mounting of samples in pressure cells can be very time consuming and therefore the technique is only used on a limited number of samples. Complications in the analysis of the spectra arise and have to be taken into account;

i) The line position observed in photoconductivity compared to absorption may differ by up to half a linewidth when tunnelling between adjacent impurity sites rather than the normal photothermal mechanism is responsible for the generation of the photoconductivity signal (Carter 1977).

ii) Intrinsic illumination, while being beneficial in reducing the number of ionised impurity sites and hence the linewidth, introduces a further complication . The current paths will be altered by the presence of photoexcited carriers and can lead to spurious effects. A new equilibrium situation is achieved in the distribution of electrons and holes, and hence the current paths will be altered by the presence of photoexcited carriers. With band-gap illumination impurities from the surface regions of the sample will increase their contribution to the photoconductivity signal. This will change the relative central-cell peak heights in an inhomogeneous sample.

iii) A 'notch' effect occasionally appears in the central-cell structure of the photoconductivity response with high purity GaAs and InP. This effect has previously been observed by Stillman (1982) and Gershenzon (1977). The occurrence of a 'notch' can be very misleading since it gives the impression that two central-cell components have been resolved. Peak inversion seems to affect some of the larger amplitude central-cell peaks i.e higher donor concentration, and the effect appears to be enhanced by band-gap illumination. Stillman et al (1985) have developed a model for the dielectric response of the crystal to account for central-cell peak inversion which is occasionally observed in the photoconductivity spectra of GaAs and InP. They calculated that the dielectric susceptibility near a donor

transition can be very large, this can cause the real part of the dielectric function $E_1(w)$ to be negative over a short range of frequency, w, just above the transition. Consequently, the strong behaviour of $E_1(w)$ has a pronounced effect on the complex refractive index N(w), and the real part n(w) almost disappears over the narrow range of frequency where $E_1(w)$ is negative. In this regime the reflectance approaches unity, hence both the transmittance and absorbance nearly vanish, in a high purity sample of sufficient thickness. When $E_1(w)$ becomes positive again, the complex refractive index approaches a real value. The reflectance goes through zero before reaching a value less than unity, and hence the absorbance assumes a finite value. The result of an abrupt change in the absorbance giving rise to a sharp 'cross-over' peak. This effect can be extremely confusing and great care is required in order not to misidentify a 'notch' as two individual central-cell components.

iv) As the inhomogeneous broadening theory of donor transitions involves a perturbation approach it is likely to breakdown for impurity separations less than about 10 Bohr radii for the donors concerned. Additional weak and broad lines are frequently observed due to molecular (Bajaj 1975),(Berman 1975,1976,1980) or charge transfer states (Thomas 1981) and to possible complex formation (Fedders 1982). A complex would have local symmetry which would give rise to a splitting on the observed transitions for particular directions of magnetic field with respect to the crystal axis. In addition the overlap with adjacent incompletely resolved lines can shift the line positions by an appreciable fraction of the observed linewidth.

v) There exists the possibility that standing wave resonances can occur within the sample, this can give rise to irregular lineshapes.

vi) Polarisation phenomena inadvertently produced by the various optical components and by the sample itself, can occur.

vii) There can be unresolved structure due to non-parabolicity effects which can act to shift line positions.

viii) It is possible that the laser can emit two FIR wavelengths simultaneously.

xi) The strongest FIR lines can give rise to carrier heating.

Most of the above considerations can be taken into account in the final analysis. However, the 'notch' effect can sometimes be very deceptive. The only possible way to eliminate this effect is by comparing the reproducibility of the effect to other samples, vary experimental conditions, compare the spectra with different Zeeman transitions or by using a different laser wavelength. In this way, any 'peak inversion' is excluded.

Figure(2·1)

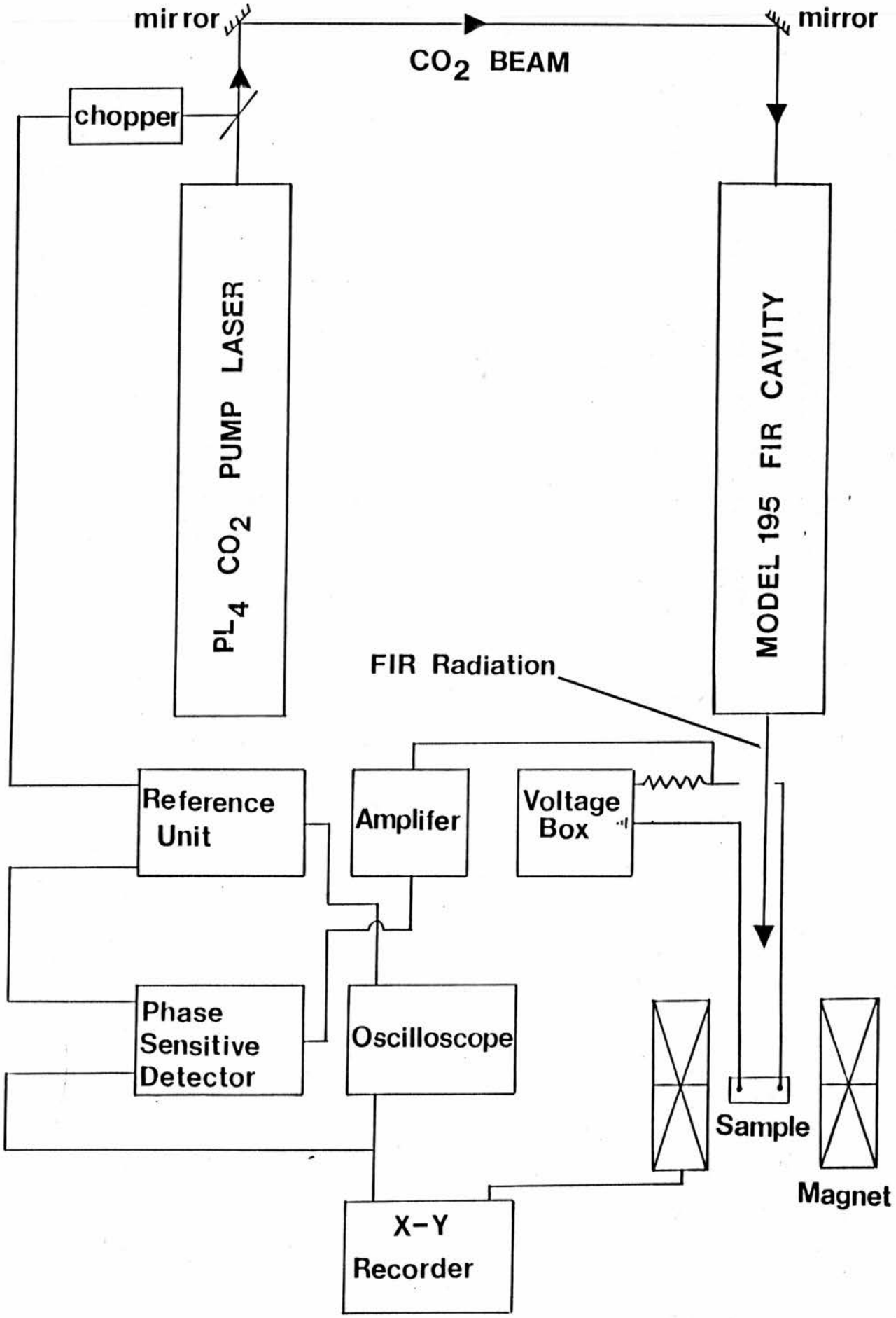

Figure (2.1) Displays the experimental layout.

Figure(2·2)

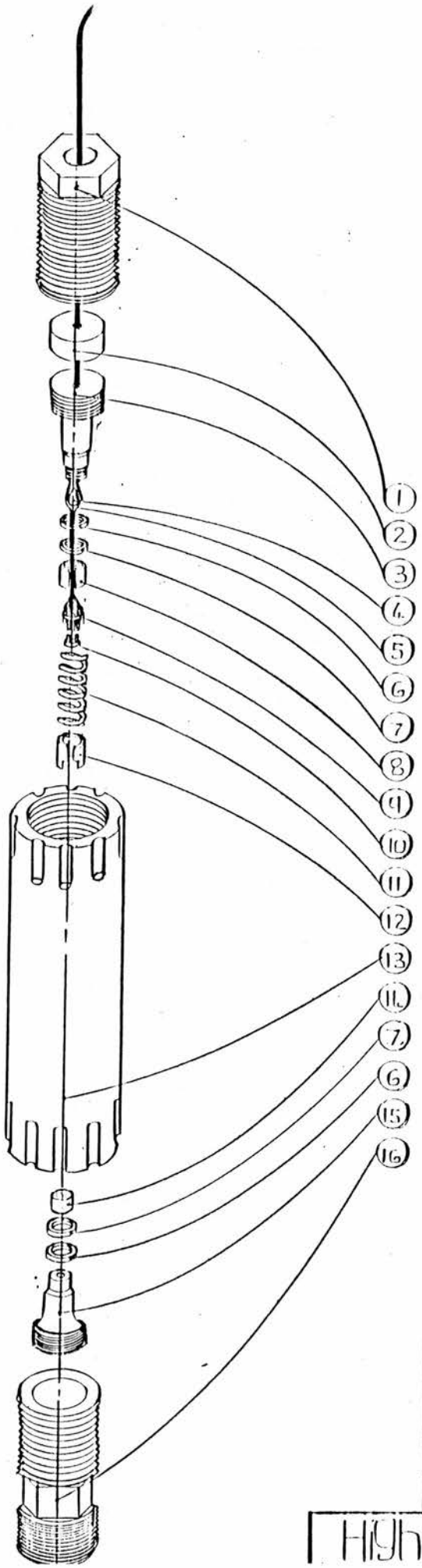

PART No	PART NAME	No OFF	MATERIAL
16	LOCKING NUT	1	Be Cu
15	FIXED PISTON	1	Be Cu
14	SAPPHIRE WINDOW	1	IND. SAPPHIRE
13	CELL BODY	1	Be Cu
12	PROTECTIVE CAP	1	Be Cu
11	COIL SPRING	1	Be Cu
10	SAMPLE TABLE	1	Be Cu
9	SAMPLE STAGE	1	Be Cu
8	RETAINING NUT	1	Be Cu
7	GASKET	2	RUBBER/P.T.F.E
6	GASKET	2	BRASS
5	ENAMEL COATED WIRE	10	Cu
4	TAPERED PLUG	1	Be Cu
3	SLIDING PISTON	1	Be Cu
2	SPACER	1	Be Cu
1	LOCKING NUT	1	Be Cu

High Pressure Cell

Figure (2.2) Exploded diagram of the pressure cell (courtesy of D. Irons).

Figure(2·3)

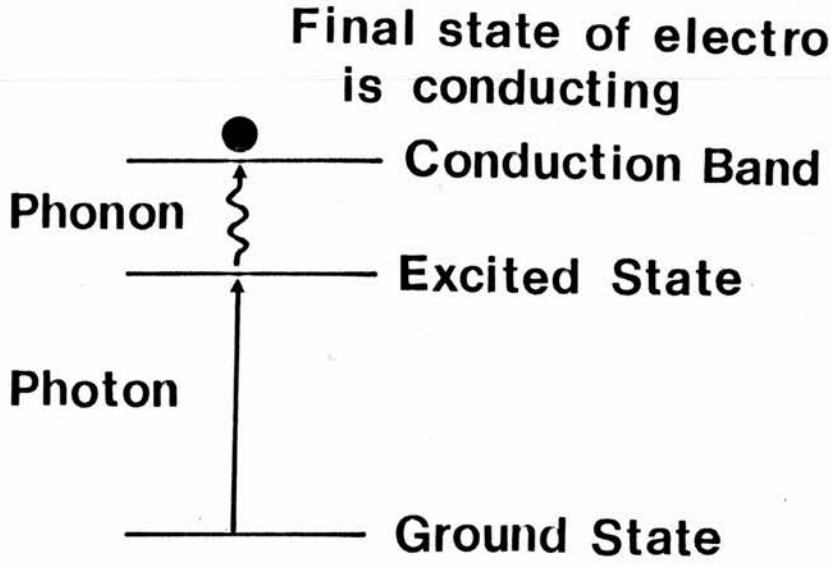

Figure (2.3) Schematic representation of the photothermal ionisation process.

Figure(2·4)

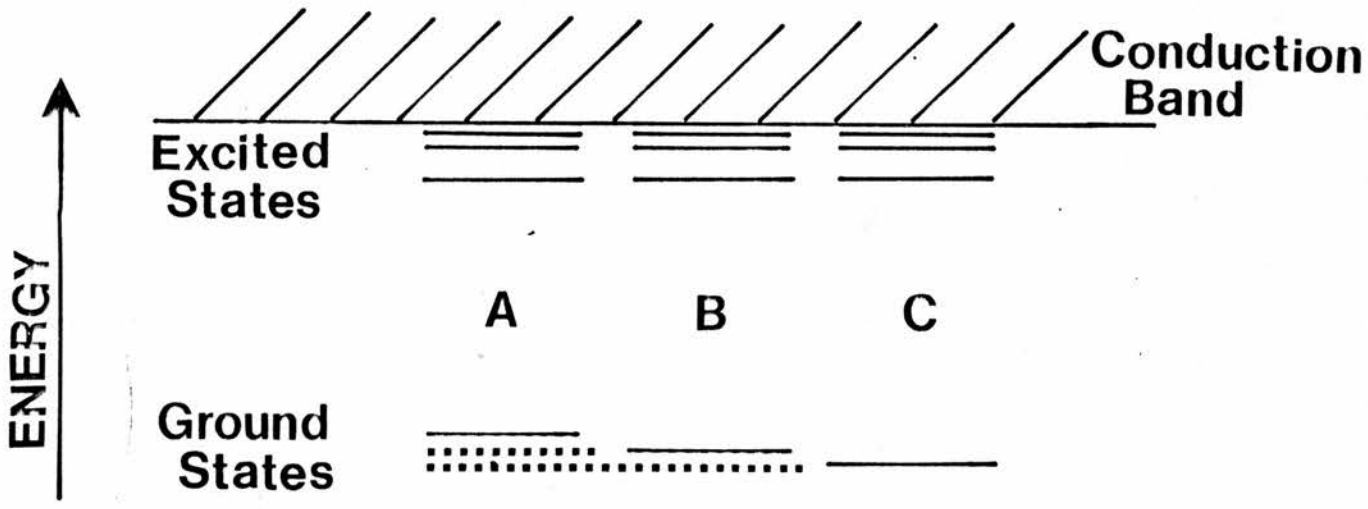

Figure (2.4) Schematic diagram of the slightly different ground state energies of different donor impurities A, B, and C.

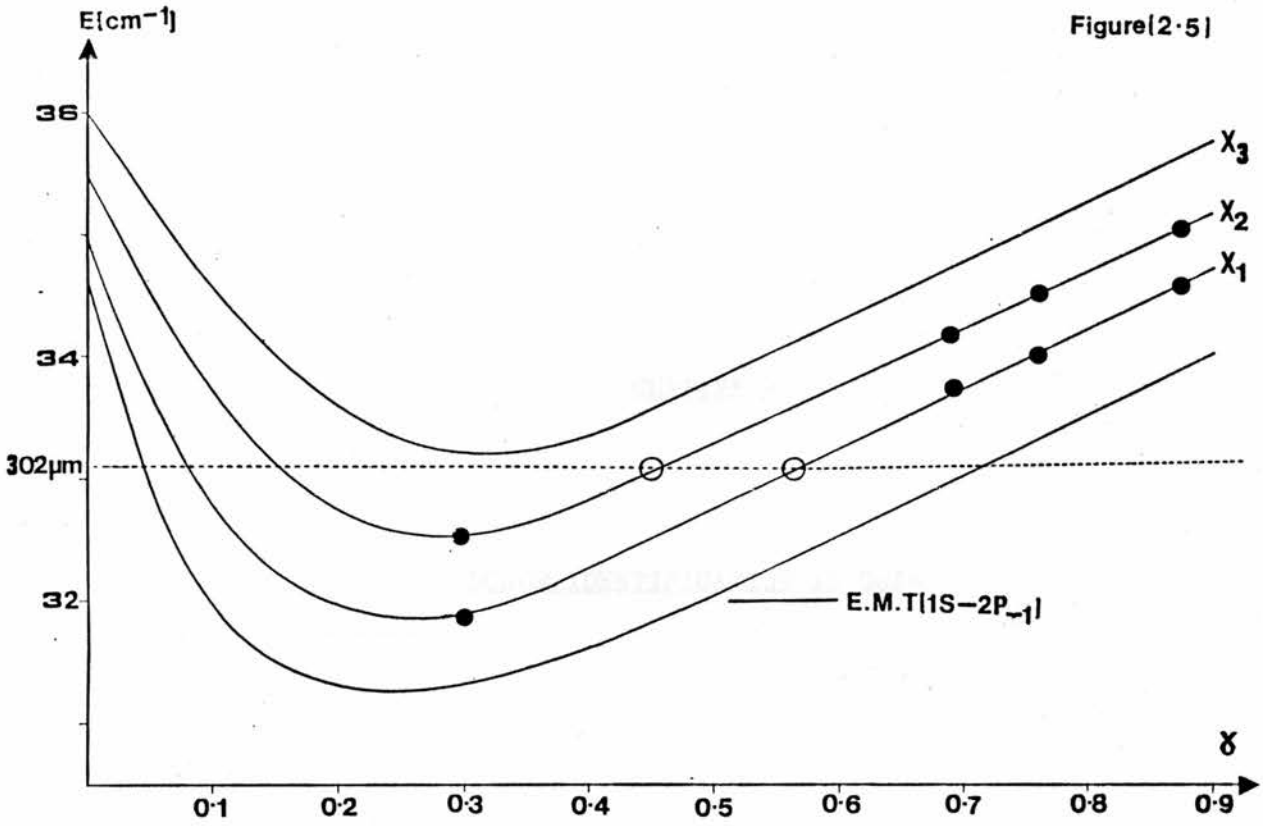

Figure (2.5) The dimensionless magnetic field parameter $\gamma=\hbar\omega/2R^*$ is plotted against energy (cm^{-1}) for the $1S-2P_{-1}$ transition. Central-cell corrections to the effective mass theory (E.M.T) of donors X_1, X_2, and X_3 are shown. Fourier transform and laser data are plotted. This diagram illustrates how the 302μm laser wavelength does not cross the deepest donor X_3, and thus is not observed on the spectra. An estimate of the field variation is drawn, since no data was available for this donor.

Over the past ten years there have been confusing and conflicting reports from various groups around the world, working on the problem of identifying central-cell structure in GaAs. This perhaps gives an indication of the difficulty in resolving and identifying each individual central-cell component. A magnetic field dramatically improves the resolution of the spectra, revealing fine central-cell structure on each of the Zeeman split transitions. This improvement in resolution is partly due to the wavefunction shrinking together with central-cell splittings increasing with magnetic field. Fine structure observed on, for example, the $1S-2P_{+1}$ transition is due to each different impurity species having a slightly different chemical shift of the ground state 1S energy. The various components of the fine structure identify different chemical species and their amplitudes reflect the relative concentration of each dopant. Three large peaks on the 1S-2P Zeeman split transition, corresponding to the three main residual dopants, labelled X_1, X_2, and X_3 by Low et al (1982) or b, c, and h by Cooke et al (1978), consistently appear in the central-cell structure of VPE GaAs. In LPE grown material X_2 frequently appears, together with two other shallower donors. Two donors, sulphur (S) and silicon (Si) are expected to be incorporated into the GaAs crystal during growth, since they commonly appear in most other III-V semiconductor compounds e.g GaP, GaSb etc. Most of the conflicting evidence centres around the relative assignment of the positions of S and Si. Peak X_2 was originally associated with Si by Wolfe et al (1976), but subsequent doping experiments by Ozeki et al (1977) and Stillman (1982) have indicated that X_1 belongs to the Si donor. Stillman (1982) using S doped MOCVD GaAs, showed sulphur to be responsible for the appearance of X_2. This identification confirms that of Ozeki (1977). Initial experiments resulted in the tentative

identification of X_3 with carbon donors (Wolfe 1972). However, VPE grown GaAs doped with Ge, by adding the dopant into the system Ozeki et al (1977) and also by neutron transmutation doping [Asfar (1980) and Stoelinga (1978)], have indicated that Ge donors contribute a peak at X_3 in energy. There now appears to be general agreement over the chemical identity of the three main residual dopants in ultra-pure VPE GaAs. The consensus of opinion now allocates the Si donor to peak X_1, S to X_2, and Ge to X_3. The present experiments provide strong evidence for the positive identification of several donors in n-GaAs. However, the evidence does not necessarily indicate a simple substitutional donor and possible donor complexes could occur.

Since the FIR laser radiation is constant in frequency, photoconductivity spectra are obtained by sweeping the magnetic field through the various Zeeman split transitions. The $1S\text{-}2P_{+1}$ transition is the most easily accessible with the laser since this transition moves rapidly with magnetic field, but is generally broader than the $1S\text{-}2P_{-1}$ transition. The 302μm formic acid line enables all but the deepest of the shallow donors to be studied on the $1S\text{-}2P_{-1}$ transition (see figure 2.5). The very slow movement of the $1S\text{-}2P_{-1}$ transition with field spreads out the central-cell components over a large span in field. Very high resolution is achieved because of the narrowness in energy of this transition, enabling donors to be observed which were previously undetected on the $1S\text{-}2P_{+1}$ transition. In addition to the use of a magnetic field further improvement in resolution is obtained by reducing the temperature to 1.5K and applying band-gap radiation. The combination of reduced temperature and band-gap radiation can reduce the linewidth by up to 50% in the purest samples.

3.1 CENTRAL-CELL STRUCTURE ON THE $1S-2P_{+1}$ TRANSITION

Figures (3.1 and 3.2) show the characteristic $1S-2P_{+1}$ fine structure 'signature' of high purity VPE GaAs, samples S1 and RR125, with three common residual donors X_1, X_2, X_3, of which X_3 is the deepest. Peaks X_1 and X_2 are thought to be due to Si and S respectively (Stillman 1985) and are usually the most dominant residual donors in VPE GaAs. X_3/Ge is usually a small, but conspicuous peak relatively isolated from the main 'group' of structure. Two FIR laser wavelenghts, 118.8μm and 70.6μm are used to observe the $1S-2P_{+1}$ transition, and cross the transition at approximately 3.6T and 7.7T respectively. The benefit of intrinsic illumination is illustrated on this diagram, the upper set of recordings at each wavelength are with band-gap illumination, the lower set without. Band-gap radiation enhances and narrows X_2 and X_3, resolves the higher field shoulder of X_1 into a separate donor, X_0, and also intensifies a very shallow donor 'a' in RR125 at 118μm (figure 3.1). Donor 'a' corresponds to the shallowest common residual donor in LPE material, labelled A by Stradling et al (1972) and Cooke et al (1978), and was tentatively identified as lead (Pb). Intrinsic illumination has a similar effect on sample S1, except in addition to donor 'a', two other donors shallower than X_1 are resolved. One of the donors appears between X_1 and X_0 and is believed to be due to selenium (Se) (see section 3.3), the other is named 'b' and is even shallower than donor 'a'. The change in central-cell intensity with band-gap illumination gives an indication of how inhomogeneous the impurity concentrations are with depth and suggests that there is a considerable accumulation of donors X_2 and X_3 near the surface. At first sight, donor X_0 could be interpreted as peak inversion, but

after many experiments with various VPE samples, under different experimental conditions and the observation of similar structure by other groups (for example Ivanov and Lifshits 1983), it is believed that X_0 is a single independent donor. The problem of resolving structure in this region around X_1 is further complicated because several other donors appear with very similar energy. Hence 'peak-pulling' is expected to be significant in this region. However, it can be said with some confidence that there are three other donors very close to X_1 i.e Se, X_o, and Sn (not observed on the $1S-2P_+$ transition with these samples, except under pressure). Even shallower structure is apparent beyond the X_1 peak in the purest samples. The Sn donor has been identified by Fetterman et al (1972). 3LE165 a Sn doped GaAs sample confirms this assignment (see figure 3.13).

At short wavelengths (70.6μm) i.e higher magnetic field (~7.7T), each of the central-cell peaks splits due to the slightly different transition energies arising from non-parabolicity because of the two different spin orientations. This effect is proportional to B^2 and is usually only observed on the $1S-2P_{+1}$ line at fields greater than ~7T or wavelengths less than 90μm. This 'double-structure' complicates the spectra especially if there are two or more donors with similar energy. A very weak feature at higher fields than X_1 is resolved in S1 (figure 3.2) with band-gap radiation i.e donor 'b'. At 70.6μm impurity 'b' is $0.55cm^{-1}$ shallower than the shallowest common residual donor in LPE material i.e donor 'a'. This gives an estimated absolute chemical-shift of $-0.35cm^{-1}$ and is the first positive identification of a negative central-cell shift in GaAs.

Figure (3.3) shows the $1S\text{-}2P_{+1}$ transition at 118μm for a selection of samples grown by P.Colter at the Wright-Patterson avionics laboratory on a VPE ($AsCl_3/Ga/H_2$) machine. The samples displayed have liquid nitrogen mobilities ranging from 60,000 to 160,000cm^2/Vs and carrier concentrations of the order of $10^{14}cm^{-3}$. The spectra displayed are taken under similar experimental conditions i.e temperature 4.2K, low electric field bias and band-gap illumination. All the spectra show very similar structure, with characteristic X_1, X_2, and X_3 donors, typical of VPE material, except for the poorest quality samples RR39 and RR17, where X_3 is not resolved. RR17 illustrates a good example of peak inversion. With optical pumping, peak X_2 inverts, appearing to give rise to two peaks, but both peaks do not correspond to any other donor position. The minimum of the inverted peak aligns well with the X_2 peak position on other samples. Without optical pumping, only two peaks are observed, corresponding to X_1 and X_2. It is also noticed that small traces of donor 'a' and 'b' appear in RR125 and donor 'a' in RR96.

The compensation ratio, N_a/N_d, of several of these samples has been improved by pre-baking the Ga source for 24 hours prior to growth, to eradicate undesirable Zn acceptors (Colter 1983). This method has resulted in some of the lowest compensation GaAs material to date. D^- states were observed for the first time with these particular samples of GaAs and give an indication of how low the compensation is (see chapter 6). It is interesting to compare the samples in which the Ga source has been pre-baked i.e show D^-, to the 'reference' samples which have not e.g RR136, (see figure 3.3). The X_1 peaks of all the samples align well together. However, it is noticed that in all the pre-baked samples structure appears between X_1

and X_0 which does not appear in the 'reference' samples. The donor between X_1 and X_2 is believed to be Se (see section 3.3). This suggest that either slight Se contamination has occurred or donor X_0 is reduced during bake-out. P.Colter concludes that the donor concentration is relatively unaffected by the bake-out. Comparing the FIRPC spectra before and after bake-out, this appears to be the case (apart from the small discrepancy mentioned above).

Figure (3.4) displays the photoconductivity recordings for LPE grown GaAs. 118μm radiation is used to observe the $1S-2P_{+1}$ transition. The most striking difference between LPE and VPE spectra, is that there is no detectable quantity of X_3/Ge donors. The LPE central-cell 'signature' consists of sulphur as the dominant residual donor, with Sn and donor 'a' (Pb/Te) appearing in various quantities. Both samples of LPE GaAs have been grown by the same type of machine but at different locations. The sample giving the top trace was grown in the centre of Stuttgart i.e E351, while the sample below i.e R137, was grown at a suburban site. The shallowest donor is believed to be caused by lead contamination and it was suggested by Armistead et al (1982) that this could be due to atmospheric pollution in the city location.

3.2 CENTRAL-CELL EFFECTS ON THE $1S-2P_{-1}$ TRANSITION.

Figure (3.5) displays three VPE GaAs samples RR97, RR98, and RR99. 302μm laser radiation is used to study the $1S-2P_{-1}$ transition. All the spectra are observed under similar experimental conditions, except the bottom recording which shows the effect of reducing the temperature from 4.2K to 2.0K on sample RR98. The photoconductivity spectra can only show X_2 or shallower donors, since there is

insufficient photon energy to excite an electron from the ground state of the deepest donor X_3/Ge into the $2P_{-1}$ level. X_2/S appears as a large asymmetric peak at low fields i.e ~3T. The shape is described by Larsen's (1975) inhomogeneous broadening theory. It is noticed that there is some structure on the high field asymmetric tail of this donor transition . This structure is believed to arise from a 'stepped' variation in the impurity distribution. Larsen's lineshape theory predicts that both the shape and peak position of a FIR magneto-optical donor transition will change as a function of donor concentration. With no band-gap radiation, no structure is observed on the asymmetric donor 'tail'. Applying intrinsic illumination, any concentration inhomogeneity is accentuated, since donor-acceptor recombination is most rapid in the areas of high concentration, whereas in the relatively pure regions a substantial increase in donors occur, giving rise to a 'double-peak'.

It can be clearly seen that four donors are present with comparable energy around 3.5T i.e Sn, X_1, Se, and X_0. A sharp Sn component is resolved in all three VPE samples, which is not observed in the $1S-2P_{+1}$ spectra (but is resolved under pressure see section 3.5). By comparison with the $1S-2P_{+1}$ spectra, it is tentatively suggested, that X_1 is the deepest, then Se, and that X_0 is the shallowest donor in this region. Although, the central-cell components are more spread out in energy, the problem of identifying individual donors in the region around X_1 is again difficult because there appears to be considerable 'peak-pulling' in this area. For example, consider the spectral region around X_1, for sample RR98. At 4.2K, two well resolved peaks are observed (neglecting X_2, Sn and any smaller structure to higher field) , similarly with the $1S-2P_{+1}$ transition (figure 3.6), only X_1 and X_0 are resolved. Reducing the

temperature to 2.0K, a third peak evolves between donors X_1 and X_0, this is also observed on the $1S\text{-}2P_{+1}$ transition on reducing the temperature. It is clear from NTD experiments that this donor is Se, which appears between X_1 and X_0. Any deviation of the other peaks is ascribed to 'peak-pulling'. From back doping experiments Se is known to appear in the region around X_1 (see for example Hoult 1973). However, it is difficult to precisely assign the exact position of this donor because of line broadening and also due to the difficulty in resolving independent donors within this very small region of energy. Donor 'a' appears infrequently in a few high quality samples of VPE crystals, i.e RR99, S1 and RR125, but is more common in LPE material.

There is a certain amount of confusion and conflict over the identification of donor 'a' since this donor has been associated with Pb (Wolfe et al 1978) and Te (Colter 1984). RR99 has been tellurium (Te) doped by placing a highly doped tellurium substrate in the $AsCl_3$ VPE reactor next to the substrate on which the epilayer was grown. Subsequent photoluminescence experiments determined the position of the tellurium donor to be coincident with that of donor 'a' (Colter). However, the FIRPC data does not show any dramatic change in the spectra compared to other similar VPE samples, indicating that tellurium incorporation is slight. Donor 'a' is observed as a minor contaminant in two other VPE samples S1 and RR125, but only with optical excitation, suggesting that it has a relatively higher concentration nearer the surface. Also, this donor commonly appears in larger quantities in LPE grown material, e.g E351.

According to Kang and Greene (1968), the segregation coefficient of Sn increases with temperature, while the segregation coefficient of Te decreases with increasing temperature. Thus in an epitaxial layer containing both Sn and Te donors, the relative concentration of Sn will increase with depth, with respect to Te. The conclusion of the temperature dependence of other impurities, is that group VI donors behave similarly to Te and group IV donors like Sn. Hence, according to this idea, Te donors are expected to occur towards the surface compared to Pb donors. This is in agreement with the photoluminescence data of Colter et al (1984), because the technique only measures the first micron or so of the epitaxial layer and also explains why donor 'a' is more pronounced under band-gap illumination in the FIRPC spectra. Furthermore, both group VI donors sulphur and selenium usually grow with intrinsic illumination. However, X_3/Ge, a group IV impurity behaves similarly to a group VI, in contradiction to the above idea (figures 3.1 and 3.2). The confusion over the correct identification of donor 'a' remains to be resolved.

Figure (3.7) shows the photoconductive response for three LPE samples using 302μm radiation. All three samples clearly show sulphur and tin as common residual dopants. Donor 'a' appears, but only in small quantities in 7LE45 and 3LE165. In E351, lead appears as a major residual dopant, for reasons discussed earlier. With band-gap illumination, doublet structure appears on all of the donor transitions, reminiscent of the inhomogeneous 'stepped' impurity concentration profile as mentioned before for the $1S\text{-}2P_{-1}$ spectrum of RR98. 3LE165 has been lightly back-doped with Sn giving a large donor peak between X_2 and X_1.

3.3 NEUTRON TRANSMUTATION DOPING (NTD) of GaAs

Neutron transmutation doping (NTD) of GaAs by thermal neutrons was first reported by Mirianoshvili and Nanobashvili (1971). Thermal neutrons are captured by the GaAs lattice nuclei, in proportion to the relative abundance of Ga and As isotopes and their different capture cross-sections i.e relative abundance of the stable isotopes are $^{69}Ga(60.2\%)$, $^{71}Ga(39.8\%)$, and $^{75}As(100\%)$. The following nuclear reactions are undergone after a thermal neutron is captured, the atoms decay from an excited state by emitting B^- and δ particles to form a stable donor atom i.e a lattice atom transmutes to a donor impurity.

$$^{69}Ga \longrightarrow {}^{70}Ga \longrightarrow {}^{70}Ge$$
$$^{71}Ga \longrightarrow {}^{72}Ga \longrightarrow {}^{72}Ge$$
$$^{75}As \longrightarrow {}^{76}As \longrightarrow {}^{76}Se$$

All naturally occurring isotopes of Ga and As participate in transmutation doping. 40% of the donors formed are $^{70,72}Ge$ and 60% being ^{76}Se, due to the different thermal neutron capture cross-section of the respective lattice atoms. After the GaAs samples have been irradiated, a considerable amount of defects occur and the samples are found to have very nigh restivities. Subsequent thermal annealing of the radiation damaged crystal is required in order to recover the maximum electrically active shallow donor concentration. This is done by placing the neutron damaged sample together with a small quantity of GaAs powder, to avoid As loss, inside a clean quartz tube. A smaller quartz tube is inserted inside the larger to reduce the volume thus minimising vapour transportation, then the tubes are evacuated and sealed. Two samples RR125 and RR17 were subject to a flux of

thermal neutrons ($10^{12}s^{-1}$) for 16 and 8 minutes respectively at the Scottish university research and reactor centre, East Kilbride. The samples were then thermally annealed at 600C and 625C for 60 minutes, to recover their mobility. After annealing, most transmuted Ge atoms end up on Ga sites and most transmuted Se donor atoms are on As sites, giving rise to shallow donors, without generating additional substitutional acceptors. Hence the compensation ratio is expected to decrease. The effect of thermal neutron bombardment and subsequent annealing on GaAs can clearly be seen on the central-cell structure, figure (3.8). The top and bottom recordings of both samples have been taken at similar bias conditions i.e 4.2K, low electric field bias, and intrinsic illumination. The loss of spectral quality in NTD RR125 is probably due to the sample not being annealed for a sufficient length of time or at too low a temperature to fully repair the neutron damage.

A proportion of Ga and As atoms are transmuted into Ge and Se donors. This is demonstrated on the bottom trace, the Ge/X_3 component of NTD RR125 grows significantly compared to the other central-cell peaks, indicating that Ga atoms have been transmuted into Ge donors. In RR17, the effect is more striking, since before irradiation, no X_3 component is observed, after irradiation, although Se should appear with 50% greater intensity, the X_3/Ge dopant becomes the major peak, larger than any of the other central-cell components. The rather broad X_3/Ge line may give some credence to the involvement of defects. This result confirms the assignment of the Ge donor to X_3 by Low et al (1982) (using a back-doped sample). Stoelinga et al (1978), also performed a similar FIR experiment using a Fourier transform spectrometer with NTD VPE GaAs, and also attributed X_3 to Ge.

Stoelinga et al, could not assign a peak to Se, which should also occur in the spectra, but concluded that the Se donor lies in the vicinity of X_1 and is considerably broader than the Ge line. Using the higher resolution of a FIR laser, a well resolved peak appears in both irradiated samples between X_1 and X_0, this is believed to be due to the Se donor which is incorporated into the lattice during irradiation, figure (3.8). This appears to be consistent with Stoelinga's NTD results and also back-doped data, but the broadening was too great in all previous recordings to positively identify the Se donor position. The Se donor linewidth in both RR17 and RR125 is not as broad as that observed by Stoelinga et al, enabling the donor to be resolved. The reason why Stoelinga's results produced such broadened magneto-optical transitions, is probably much the same reason why there are broad lines in NTD RR125. That is simply due to the sample not having been thermally annealed completely rather than an increase in the neutral donor-neutral donor Van der Waals interaction, as tentatively suggested in their analysis.

From the ratios of the naturally occurring Ga and As isotopes, together with their relative difference of the thermal neutron capture-cross section, it is predicted that ~50% more Se than Ge donors should be present after irradiation with thermal neutrons. In NTD RR17, the contrary is the case, where Ge is ~50% larger than the corresponding Se donor. However, in NTD RR125, the Se donor is about ~50% larger than Ge, in agreement with theory. It could be argued that there is a significant but unresolved proportion of Se donors, which would reduce the above percentage difference. Also, a similar lack of Se donors occurs in Stoelinga's spectra if broadening is not as large as he had postulated. The reason for this discrepancy

remains to be answered. However, none of the above discussion excludes the possibility that X_3 is a complex involving Ge and a radiation induced defect, indeed the RR17 result could be taken as evidence of this.

In addition to neutron irradiation producing donors, the relative peak heights of other impurities change intensity. There are a number of reasons why this can occur.

i) impurities can diffuse from the substrate into the epilayer during thermal annealing.

ii) impurities can be introduced unintentionally during the annealing process from the surrounding environment.

iii) bombardment with thermal neutrons (also a few high energy neutrons present during irradiation) and thermal annealing, can redistribute the residual impurities throughout the crystal.

iv) complex formation can occur.

3.4 COMPARISON OF GaAs GROWTH SYSTEMS

Figure (3.9) compares the photoconductivity response of the $1S\text{-}2P_{+1}$ transition taken with 118μm radiation, for four GaAs samples grown by different techniques. In descending order, the spectra are of GaAs grown by MOCVD, LPE, VPE, and MBE systems respectively. In figure (3.10), four recordings of the $1S\text{-}2P_{-1}$ transition using the 302μm laser line, for three growth kits are compared, again in descending order are VPE, LPE, and MBE respectively. The recordings display typical characteristic central-cell 'signatures' for each individual growth system.

The top trace in figure (3.9) is from a MOCVD grown GaAs sample. This particular sample is not of such good quality, as compared to the LPE and VPE samples shown below on the diagram. Consequently the donor transitions are broader. However, it is clearly seen that the deepest donor, X_3/Ge, is by far the most dominant dopant. This is a typical result for MOCVD grown GaAs, and is confirmed by several other workers, Cooke et al (1978), Low et al (1982) and Stillman et al (1984). X_2/S and X_1/Si are also observed on the MOCVD FIR spectra, but in much lesser quantity compared to X_3/Ge. Stillman et al (1984), using better quality MOCVD material, succeeded in observing very small traces of Sn and donor 'a' (Pb/Te) in addition to S, Si, and the main residual donor, Ge.

The central-cell 'signature' for LPE grown GaAs has quite a striking difference to MOCVD grown material. No detectable amount of Ge is observed on any of the LPE samples. Only one large central-cell component, belonging to S is evident on the $1S\text{-}2P_{+1}$ transition of R137. Sulphur readily incorporates into GaAs epitaxial layers grown by all of the major growth techniques, and usually comprises a substantial fraction of the total residual donor concentration. Kang and Greene (1969) suggested that sulphur is present due to contamination from the graphite boats used in all the mentioned growth techniques. This appears to be in agreement with the FIRPC results, as the sulphur donor commonly appears in all the spectra regardless of the growth method. In all LPE grown samples, Sn and donor 'a' (Pb/Te) can comprise a significant amount of the residual donors impurities present. Surprisingly, silicon does not appear in the spectra with this growth system, since silicon is generally recognised as an ubiquitous contaminant in GaAs due to the reaction of H_2 and HCl with

the silica reactor tube. Ashen (1974) using a boron nitride (BN) furnace liner with a VPE system proved that the primary source of Si contamination is due to HCl attacking the quartz lining. Also, Ozeki et al (1977) managed to reduce the Si contamination in VPE material by using a Ga-$AsCl_3$-N_2 system, rather than a hydrogen system as used by P.Colter who grew the RR series of samples. Furthermore, the introduction of a small quantity of water vapour can reduce the Si contamination [Hicks and Greene (1970)].

Silicon is a major contaminant but is incorporated as an acceptor rather a donor in LPE material, this is due to the number of vacancies introduced during the growth process. Ashen (1974) suggested that LPE material has relatively more As vacancies than VPE grown crystals. Thus, since Si is amphoteric, the Si impurities would be more likely to be acceptors rather than donors. This interpretation appears consistent with the FIRPC results presented here, because Si appears only as a minor donor contaminant (see R137) but readily appears as an acceptor on the photoluminescence spectra of LPE GaAs (Ashen 1975). The converse is true for VPE material, Ashen (1975) predicts that Si acceptors are never present in this growth technique. Consequently Si impurities are more likely to be donors than acceptors in VPE grown material. This argument could also explain why there are no Ge donors in LPE GaAs, but Ge/X_3 is often seen in VPE material, since Ge is also ampnoteric. Both Sn and Pb are in principle amphoteric and are not expected to appear in the photoconductivity spectra of LPE material using the above argument. However, both impurities are observed in the photoconductivity response of LPE GaAs, and Sn also appears as a common acceptor in this material (Schairer et al 1976). Carbon is likely to be incorporated into GaAs, but the electric properties of the impurity are uncertain. It is noted that using the Ga-$AsCl_3$-H_2

VPE growth technique, Ozeki (1977) reported only very small traces of carbon acceptors were present, suggesting carbon donors may be present. This is compared to LPE samples, where carbon acceptors were always present and are generally the dominant shallow acceptor (Kirkman 1978). Whereas Wolfe et al (1977), argued that carbon might be a residual donor impurity, implying a possible amphoteric behaviour like Si (also Lum and Wielder 1977). The carbon donor could explain the appearance of some of the extra shallow central-cell structure on VPE material, but in terms of electro-negativity it would be expected to be deeper. Although oxygen is a possible substitutional donor, it may not be incorporated into the lattice, since N_D-N_A reduces through the addition of water vapour (or O_2), (Hales and Knight 1979). Furthermore, if oxygen is a residual impurity in GaAs, there is evidence that it may occur much deeper in the energy gap (White et al 1978).

GaAs grown by MBE is usually not as pure as the best VPE or LPE material. As a consequence the lineshapes of the $1S\text{-}2P_{-1}$ transition are broadened and asymmetrically distorted due to the Stark effect from neighbouring charged impurities. X_2/S and X_1/Si are observed to be the dominating donor species. However, due to the strong asymmetrical broadening more impurity species cannot be excluded from the interpretation. In a similar experiment using a Fourier spectrometer, but with better quality MBE samples, Stillman (1978) associated Pb, Si, Sn, and S as residual donors present in MBE grown material.

A simple LCAO model describing the relative order of the chemical shifts for particular simple substitutional impurities has been developed by Hjalmerson et al (1980). This model predicts that the central-cell potential is governed by the outermost atomic s states for donors. Thus, the more s electro-negative of two donors has a larger binding energy with respect to the conduction band edge.

The FIRPC spectra of VPE grown sample S1 displays most of the donors incorporated into the GaAs epilayer during growth. In ascending order, the central-cell assignments for each peak are Ge, S, Sn (not observed in this sample), Si, Se, X_0, a(Pb/Te) and with b being the shallowest donor observed. Only oxygen, carbon, lead and tellurium are left as possible substitutional shallow donors. Polonium is not considered since this element is very rare and does not occur naturally. From back-doped experiments and on electro-negative trends Te and Pb are expected in the region around donor 'a', but there is conflicting evidence as to which donor belongs to 'a'. Carbon is expected to be a donor in VPE material and an acceptor in LPE crystals, according to Ashen's vacancy argument. Thus, the only possible peak position not already assigned is X_0. This peak commonly occurs in VPE but not LPE material, suggesting C as a possible candidate.. However, this is contradictory to electro-negative trends and by comparison to the energy ordering of shallow donors in other similar semiconductors such as GaP (Dean et al 1973). Assuming the above central-cell assignments are correct, the central-cell components appear to align themselves in order of increasing electro-negativity. Donors substituting on a Ga site, with increasing electro-negativity are Ge, Sn, Pb and on an As site are S, Se, Te respectively. The exception is silicon which is expected deeper on

electro-negative trends. This illustrates the possibility that not all of the peaks may belong to simple substitutional donors. A possible candidate for explaining the unidentified structure could be a double donor consisting of a deep EL2 donor with a shallow donor state (Walukiewicz et al 1983). The first ionisation energy of the double donor may be comparable to a simple substitutional donor and thus might be closely effective-mass like. Furthermore, the metastability associated with the deepest donor in GaAs and InSb (Armistead et al 1984) suggests that the donor may for a complex with a vacancy, since vacancies generally produce very deep energy states subject to a large lattice relaxation (Pons and Bourgouin 1981).

In summary, there are distinct differences in the residual donor impurities with samples prepared by different growth techniques, and these differences appear to be consistent for samples prepared in different laboratories. Each high purity technique commonly produces epitaxial layers with certain trace residual donor impurities, characteristic of the particular growth technique. Most of the shallow donors are identified, but some of them only tentatively. Sulphur appears as the dominant residual donor in most crystals grown by any technique. The residual donor impurities that substitute on either possible site appear to align in order of increasing electro-negativity. There is evidence that not all the observed central-cell peaks may belong to simple substitutional impurities.

3.5 GAAS UNDER LARGE HYDROSTATIC PRESSURE

FIRPC is proven to be extremely sensitive in detecting very low concentrations of contaminating donor impurities by resolving the small central-cell corrections that occur in most of the III-V compound materials. However the extreme sensitivity of this technique is limited by ionised impurity broadening , which is intrinsic to the crystal. Certain techniques are employed to reduce the influence of ionised impurities and hence line narrowing. Hydrostatic pressure is used in conjunction with the FIR experiments to further improve the spectral resolution.

Effects of hydrostatic pressure on the band structure

The application of hydrostatic pressure does not effect the symmetry of the crystal. Pressure simply causes a small decrease (~2% for GaAs at 10kbar) in the crystal volume and hence a corresponding decrease in the lattice constant, a. The adiabatic elastic response of the solid is described by a tensor stress to strain relation. For cubic crystals such as GaAs and InP, the energy shift of the conduction band edge (dE) caused by a hydrostatic compressive pressure P, is written as

$$dE_c/dp = -3(\Xi_d^c + 1/3\, \Xi_u^c)(S_{11} + 2S_{12}).$$

Where S_{ij} are components of the compliance tensor relating the strain produced to the applied stress.

Ξ_d^c and Ξ_u^c are the dilational and shear deformation potentials

(Herring and Vogt 1956).

As the lattice constant decreases with increasing hydrostatic pressure, the enforced contraction increases the width of the energy gap, Eg.

$E_g = 1.45 + 0.0126P - 3.77\ 10^{-5}P^2$eV (at RT for GaAs), where P is in kbar.

According to effective mass theory, impurity states contain admixtures from many band minima but frequently take their dominant character from one set of minima. Thus in direct gap III-V materials a series of impurity levels appear below each of the Γ, L, and X minima and have pressure coefficients similar to the minima which determine their character. For the case of the subsidiary minima X and L, there are resonant states associated with each minima i.e states degenerate with the Γ conduction band (see figure 1.4). Effective mass theory predicts that for the four equivalent L conduction band minima in GaAs, the ground state will be 4-fold degenerate. The wavefunction of the ground state is constructed by forming linear combinations of wavefunctions from each of the four equivalent valleys. Group theory indicates that due to a perturbation the 4-fold degenerate ground state must split into a singlet and a triplet state of the Td group representation. The singlet state is found to be the lowest in energy. A similar argument describes the splitting of the 3-fold ground state associated with the three equivalent X minima, giving rise to a 1-fold and a 2-fold degenerate levels. The energy between the singlet and triplet (or doublet) is called the valley-orbit splitting.

The subsidiary conduction band minima X and L also move as a function of pressure but at different rates with respect to the Γ conduction band, and the states associated with each minima move linearly in accordance to the pressure dependence of the minima. Consequently, the shifts of the impurity levels can be inferred from the shift of the band extrema i.e the shallow donor levels simply follow the band extrema to which they belong.

Shallow donor impurities in GaAs have binding energies of the order of 5meV with respect to the Γ conduction band, and are generally well described by effective mass theory. Central-cell splittings, of approximately 1% of the donor binding energy are apparent, indicating a significant perturbation by the local donor impurity potential. If a sufficiently large pressure is applied , resonant states associated with subsidiary minima and not of Γ character are introduced into the forbidden gap. The existence of these states can modify the shallow donor spectrum which was previously thought to be well described by simple effective mass theory.

The resonant impurity levels move linearly with pressure coefficients 20mev/kbar and 15mev/kbar for the L and X conduction band minima respectively, the L associated states of donor X_3 can cross into the gap at about 8kbar. As the Γ and higher band states of the same donor attempt to cross each other, an interaction is expected. According to the non-crossing rule for states of the same symmetry, the two states repel each other as they approach one another, and an 'anti-crossing' occurs. In summary, hydrostatic pressure has the following effects.

i) pressure acts in a similar way to a magnetic field by compressing

the donor wavefunctions and consequently the central-cell splittings increase.

ii) the direct band-gap increases, deepening the shallow donor states concerned. Hence the effective mass increases.

iii) when higher band states move into the forbidden band an 'anti-crossing' of the deepest of the shallow donors in GaAs and InSb occurs.

iv) the sample resistance can increase dramatically, thereby improving the sensitivity of photoconductivt y detection.

v) a pronounced narrowing of the donor lines frequently occurs.

vi) some of the states involved with the 'cross-over' can experience a strong lattice relaxation and are metastable.

Magneto-optical evidence for an interaction between Γ and subsidiary minima states

Magneto-optical experiments are performed in order to investigate the interaction between the Γ and states belonging to the subsidiary minima. The experimental recordings are shown in figure (3.11). The top result is a typical spectrum of VPE GaAs at ambient pressure. The three main residual donors X_1, X_2, and X_3 are clearly resolved. With increasing pressure the deepest donor X_3 anomalously deepens and looses it intensity with respect to the other group of donors. The lines narrow substantially with pressure, so that the Sn donor is resolved for the first time on the $1S\text{-}2P_{+1}$ transition for this particular sample (the Sn donor is observed on the $1S\text{-}2P_{-1}$ transition). In addition, another weak donor transition is resolved on the high field shoulder of X_1. The increase in central-cell splitting as a function of pressure is evident with the splitting between X_2 and X_1 increasing by more than a factor of two at the

highest pressure. However, the anomalous deepening of impurity X_3 and the fall-off in signal intensity can be interpreted as due to the interaction between the Γ and L levels and the associated admixture of wavefunctions. As the Γ and higher band states attempt to cross, two branches of the coupled mode interaction can be seen (figure 3.13). As the higher bands move deeper into the forbidden gap, the two branches interchange intensity with increasing pressure. All intensity is lost on the Γ like magneto-optical spectra of the deepest donor as the electrons transfer to levels associated with higher order minima which have moved deep into the forbidden gap. The anomalous behaviour is only observed for the deepest of the shallow donor states at the available pressures, Alteralli (1978), Armistead (1984). At the highest pressure obtained i.e 17kbar, all signal intensity is lost from the deepest donor. The level crossing is usually accompanied by a resistance increase, and an improvement in mobility. In addition a dramatic narrowing of the line can occur.

At the available pressures (up to 17kbar) only the deepest of the common residual donors in InSb or GaAs have states that cross in this manner. In principle, as the pressure range is increased more higher lying states should become accessible. There is some indication in figure (3.12) that donor X_2 is beginning to deepen anomalously in a similar manner to X_3, at the highest pressure. However, the sample can become extremely high resistance when the crossing occurs, if the compensation is high so that the total number of acceptors exceeds the total number of donors besides the deepest. If the samples are sufficiently uncompensated the resistance remains relatively low.

PRESSURE LINE-NARROWING

The line narrowing frequently achieved by applying pressure is extremely useful in central-cell identification experiments. Dramatic line narrowing, by up to an order of magnitude, has been observed with InSb. With high-purity GaAs, the line narrowing achieved so far is not as pronounced, nevertheless a significant improvement can be obtained. The pressure-narrowing may be due to several effects.

i) an enhancement of the correlation effects may occur, thought responsible for line narrowing at pumped He temperatures (section 2.3).

ii) because of the deepening of the donor states, the number of electrons in the conduction band and the number of ionised states will fall. This will be a significant effect in uncompensated InSb at $4.2^{o}K$ and at fields of the order of 2T. However, in GaAs virtually all the electrons are frozen out onto the donors at $4.2^{o}K$, so the percentage change will be very small.

iii) the removal of states from the spectrum will decrease the absorption. Hence line broadening due to over-absorption will be decreased. Again this can be an important effect in InSb when thick samples are employed, but with high purity GaAs samples of thicknesses of the order of 10μm, this effect is likely to be small.

The change of effective mass with pressure is too small to account for the changes in the line width observed. It appears that a redistribution of neutral donors with respect to ionised impurities may be responsible for the line narrowing. On applying pressure, the mean binding energy increases as r decreases , hence the correlated dipole contribution to the broadening is expected to be less (see

section 2.3). A narrowing is observed on figure (3.11), the line width for donor X_1 decreases by more than 30% with the addition of hydrostatic pressure. Due to the application of pressure, the Sn donor is observed for the first time on the $1S\text{-}2P_{+1}$ transition with this particular series of VPE samples, also donor X_o is observed on the high field side of donor X_1.

An interesting experiment with a GaAs VPE sample doped with Ge was performed. The sample impurity concentration is of the order of $10^{15}cm^{-3}$. At this level of doping, concentration broadening becomes more important. Hence, a very broad peak occurred with no central-cell structure resolved. This result is typical of back-doped material, and gives an indication of the difficulty in growing lightly doped samples for the purpose of central-cell identification (top left hand trace of figure 3.13). The broad peak position corresponds approximately to donor X_2, but is very difficult to judge exactly where the peak is. Only at 70.6μm at 2K and with strong band-gap illumination is there a reasonably resolved peak, but with still no central-cell structure.

The effect of hydrostatic pressure on the magneto-optical spectra is quite striking. The bottom right hand trace of figure (3.13), shows peaks X_2 and X_1 corresponding to the characteristic central-cell 'signature' of VPE grown material. In fact the sample under pressure is behaving as if it were not purposely doped. This dramatic narrowing is explained as follows. Level-crossing between the Γ and subsidiary minima of the Ge donor occur at about 8.5kbars, and the Ge central-cell component anomalously deepens. Two modes of the interaction can be seen in this diagram, the lower field component is of L character, while the Γ associated peak tends to remain close to

the other central-cell structure. Most of the intensity from the Ge donor is lost from the Γ minimum and is expected to completely disappear from the spectra at higher pressure, leaving only the 'undoped' spectra. An improvement in the quality of the photoconductivity spectra by applying hydrostatic pressure is demonstrated for another doped GaAs sample in this figure. The top left hand trace displays the $1S\text{-}2P_{-1}$ transition for a purposely Sn doped LPE sample 3LE165. Applying pressure to the sample (bottom left hand trace) the central-cell splitting increases and the donor transitions narrow enabling structure to be observed on the Sn donor.

Field positions of the central-cell peaks in GaAs

Donor species (118μm)	Field position (T)
X_3/Ge	3.580
X_2/S	3.630
Sn	3.648
X_1/Si	3.666
Se	3.675
X_0	3.682
a(Pb/Te)	3.722
b	3.747
302μm	
X_2	2.945
Sn	3.442
X_1/Si	3.560
Se	3.655
X_0	3.720
a	3.930
b	4.166

Figure(3·1)

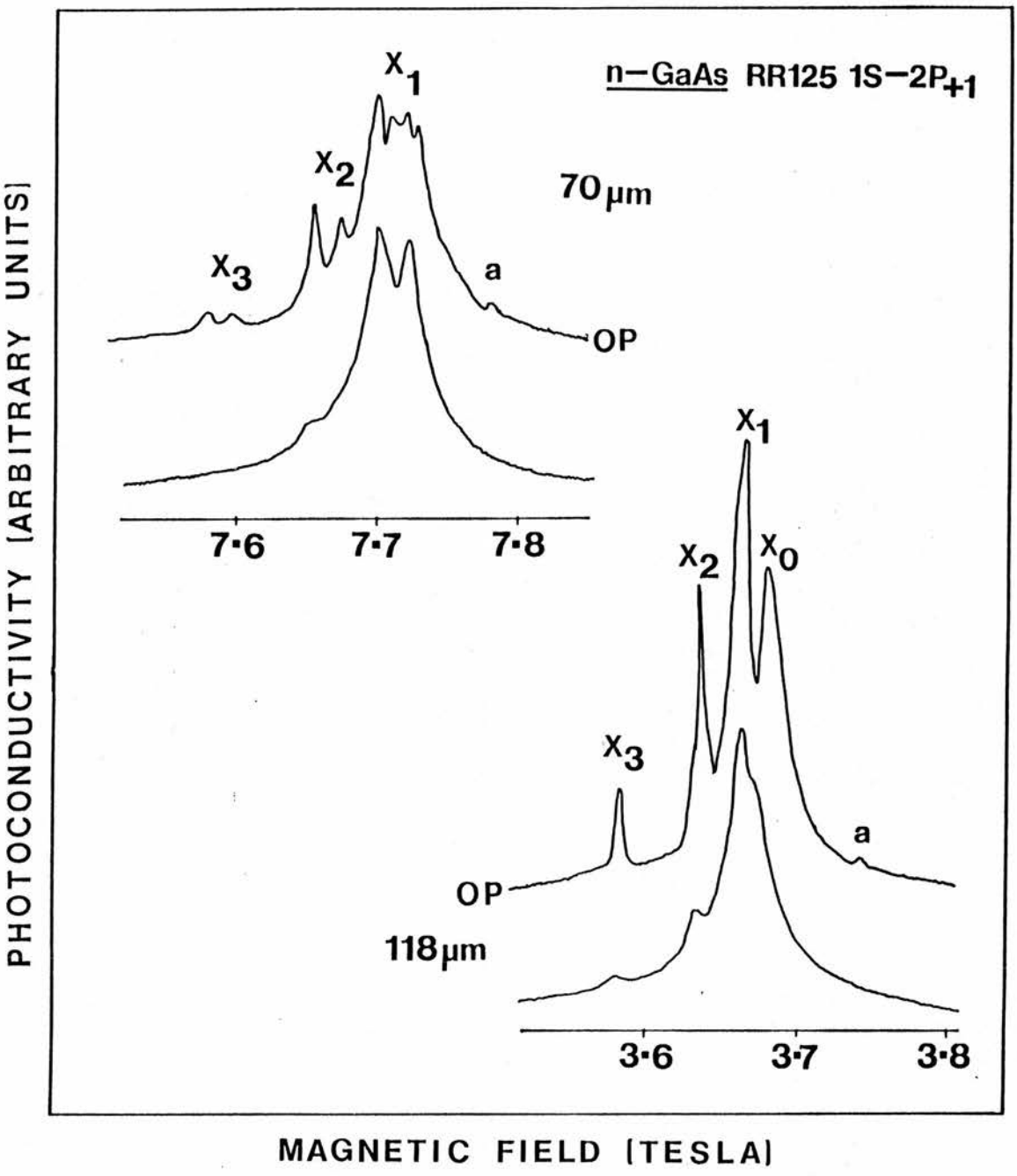

Figure (3.1) The photoconductivity (in arbitrary units) arising from the 1S to $2P_{+1}$ transition in n-GaAs against magnetic field is displayed for two laser wavelengths , the upper two recordings are for 70.6μm and the lower two for 118.8μm FIR radiation. The figure shows the line narrowing and improvement in resolution that can result on illumination with band-gap illumination (the upper of each pair of recordings is taken with band-gap illumination). X_3 is scarcely visible without band-gap radiation which also brings out donor 'a' and donor X_0. The sample is RR125 and the temperature is 4.2K. The doubling of the peaks at 70.6μm wavelength arises from the differing transition energies for the two spin-orientations caused by band non-parabolicity.

Figure(3·2)

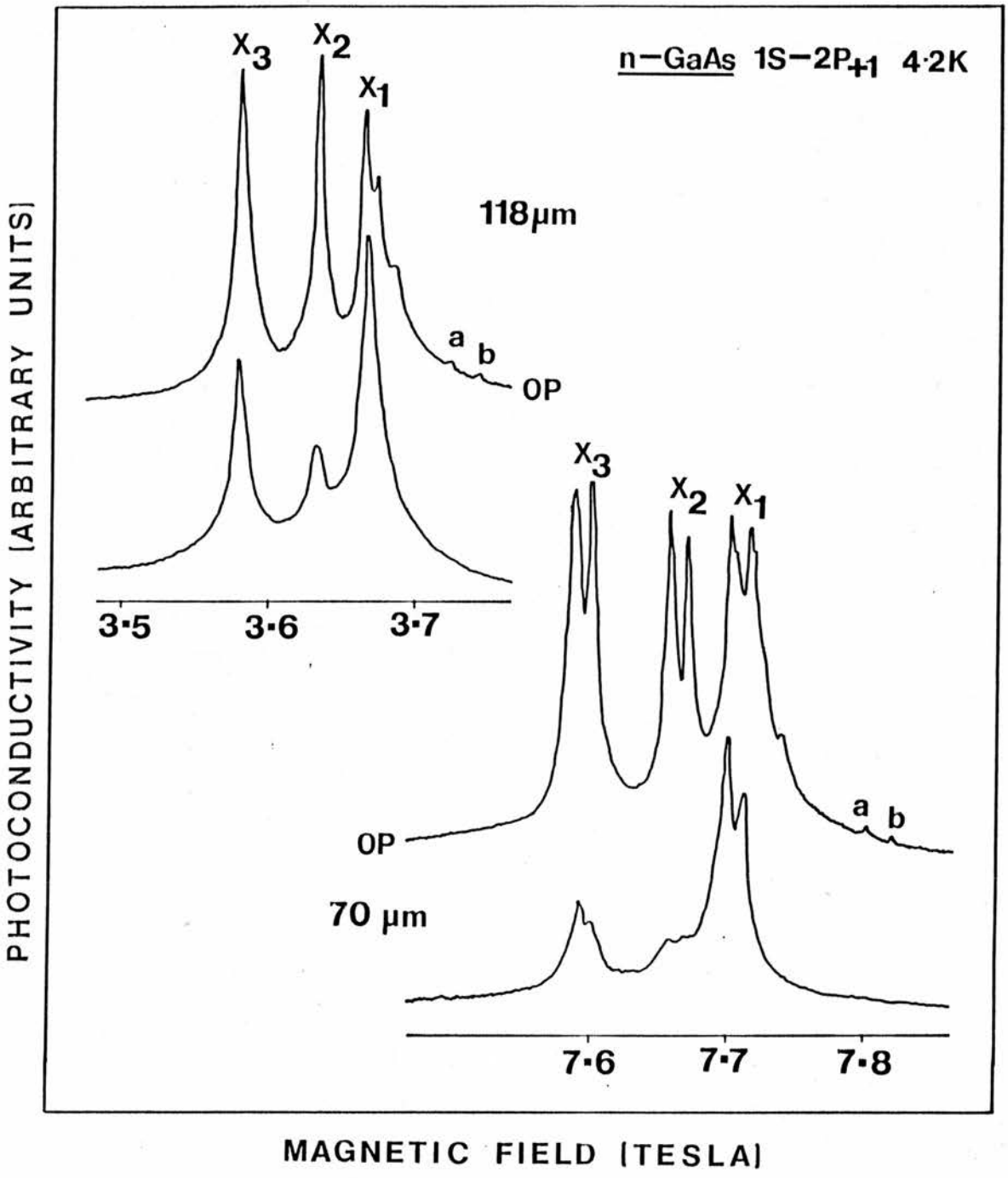

Figure (3.2) The photoconductivity arising from the $1S\text{-}2P_{+1}$ transition in high purity n-GaAs, sample S1, against magnetic field for two laser wavelengths. Line narrowing causes improvement in the resolution of the two spin components observed in 70.6μm and the negative central-cell component (donor 'b') is clearly observed.

OP- intrinsic illumination.

Figure[3·3]

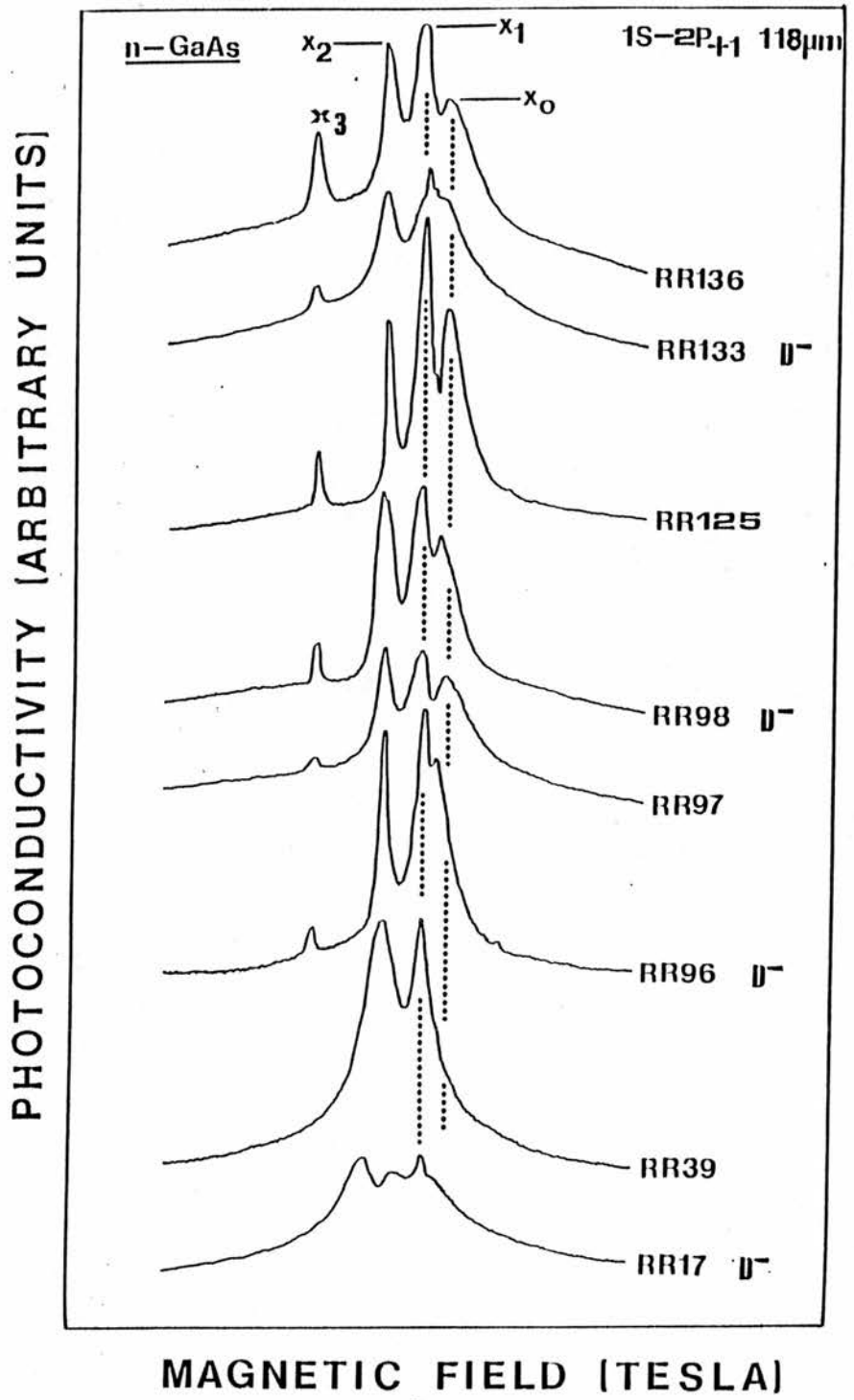

Figure (3.3) Displays a series of recordings of high-purity GaAs grown by the same VPE machine. The 'RR' series of GaAs have mobilities ranging from 50,000 to 160,000 cm^2/VS. D^- states have been observed with the samples marked (D^-), which gives an indication of the low compensation ratio. Low compensation is achieved by pre-baking the Ga source prior to growth, to eradicate undesirable Zn acceptors. This process appears to have slightly changed the central-cell structure between donors X_1 and X_0. Peak inversion of peak X_2 is apparent on the structure of sample RR17 with band-gap illumination (OP).

Figure(3·4)

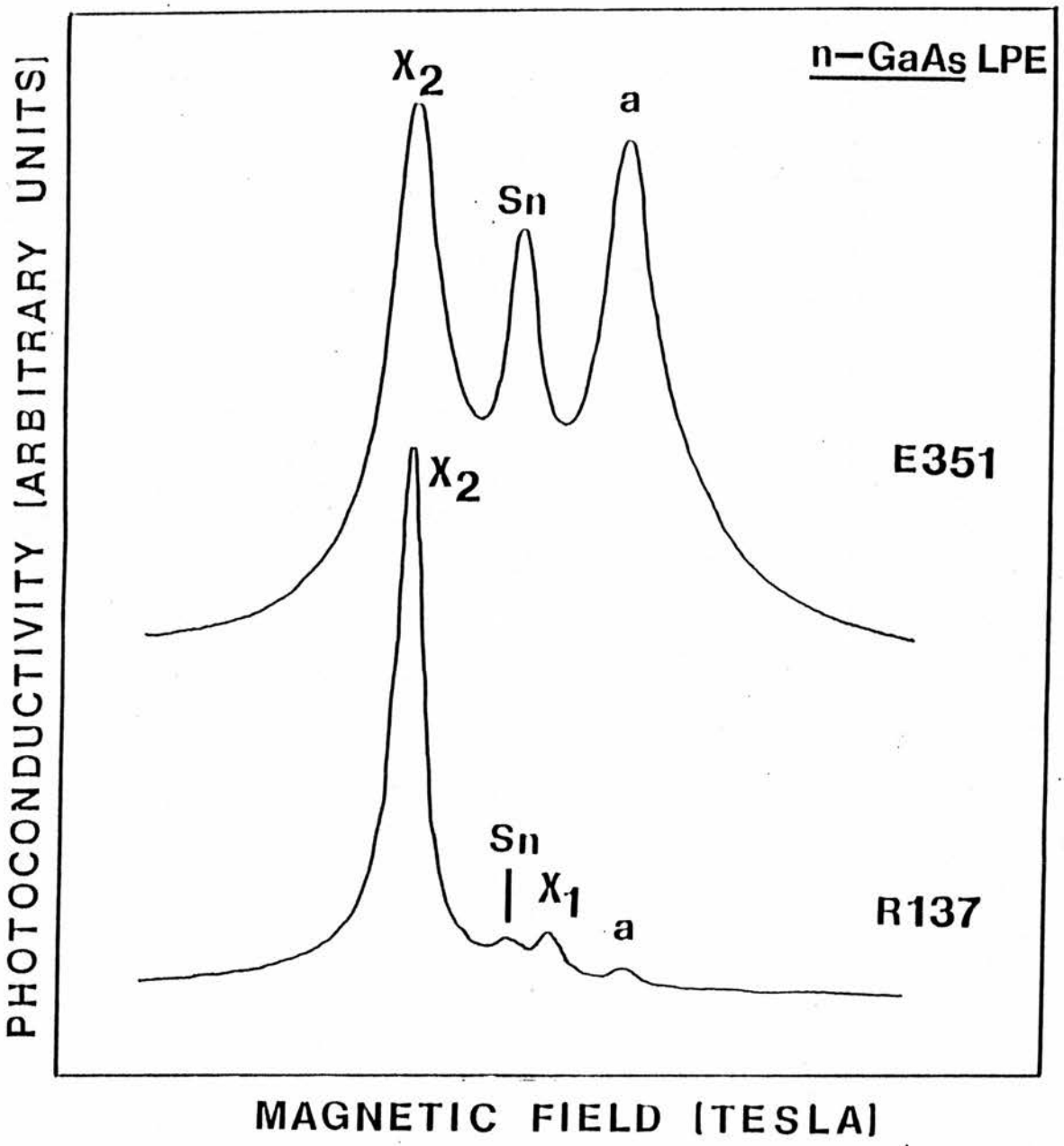

Figure (3.4) Displays the $1S\text{-}2P_{+1}$ transition taken at 118μm wavelength for two high purity LPE GaAs samples grown by Dr E.Bauser of the Max-Plank Institute (photoconductivity against magnetic field). The levels of tin and donor 'a' are much reduced in sample R137, grown at a different location from E351, allowing donor X_1 to be detected for the first time in LPE material.

Figure[3·5]

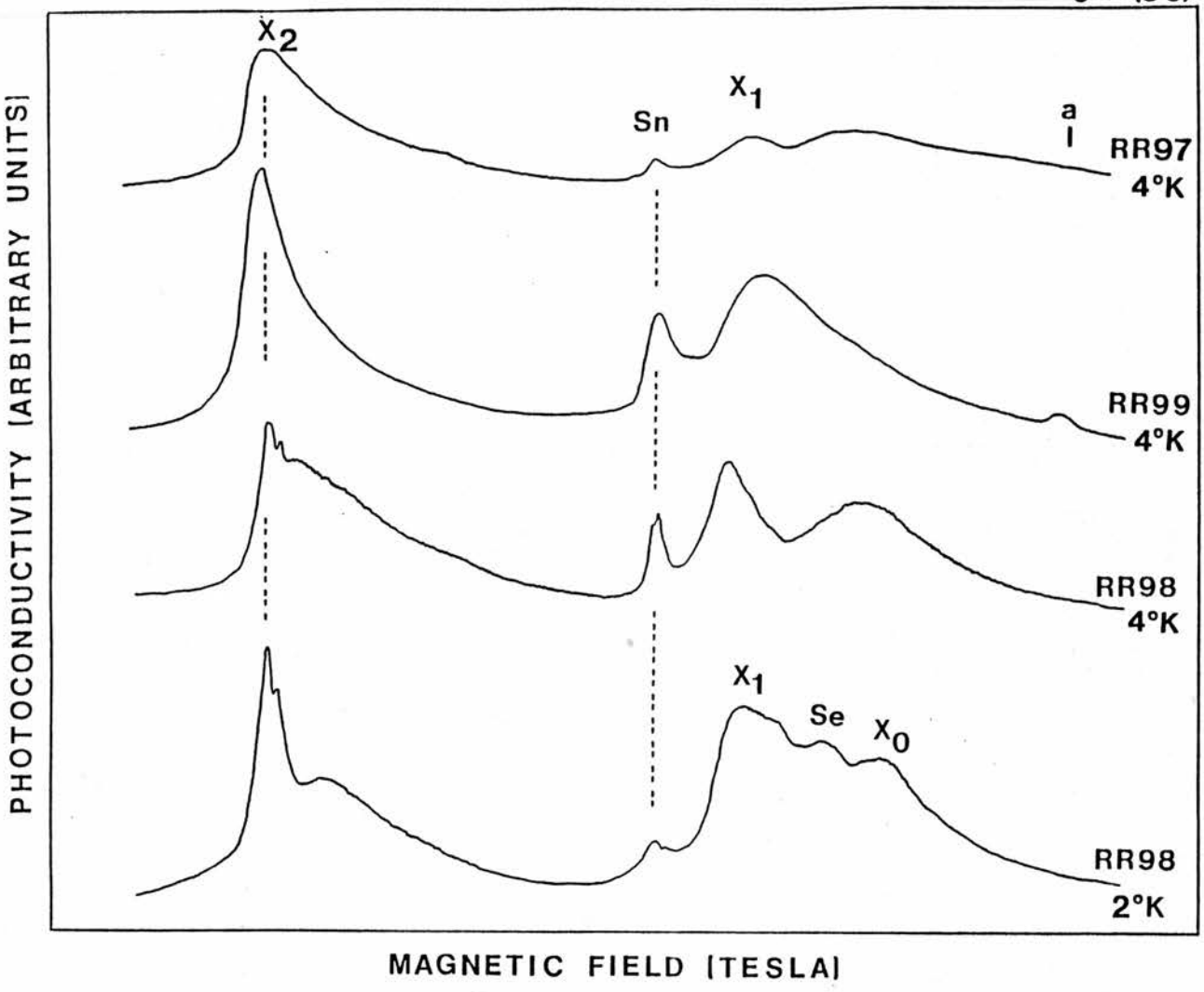

Figure (3.5) The photoconductivity for the $1S-2P_{-1}$ transition against magnetic field for VPE samples RR97, RR98, and RR99 taken with a laser wavelength of 302μm. Shorter wavelength studies of the $1S-2P_{+1}$ line for these samples show the presence of donor X_3 (not seen in the recordings shown because the photon energy is insufficient to excite an electron from the 1S state), X_2/S, and a very broad line in the region of X_1 with some structure. A sharp tin component is observed with all three samples. In the case of RR99 a line is seen in the position of the shallowest donor, found commonly with LPE material (donor 'a' Cooke et al 1978). X_1/Si is observed in all three samples and X_0 appears in RR97 and RR98 at $4^{\circ}K$. Reducing the temperature from $4.2^{\circ}K$ to $2^{\circ}K$, with band-gap illumination a donor is resolved between X_1 and X_0, believed to be selenium (also see figure 3.6).

Figure[3·6]

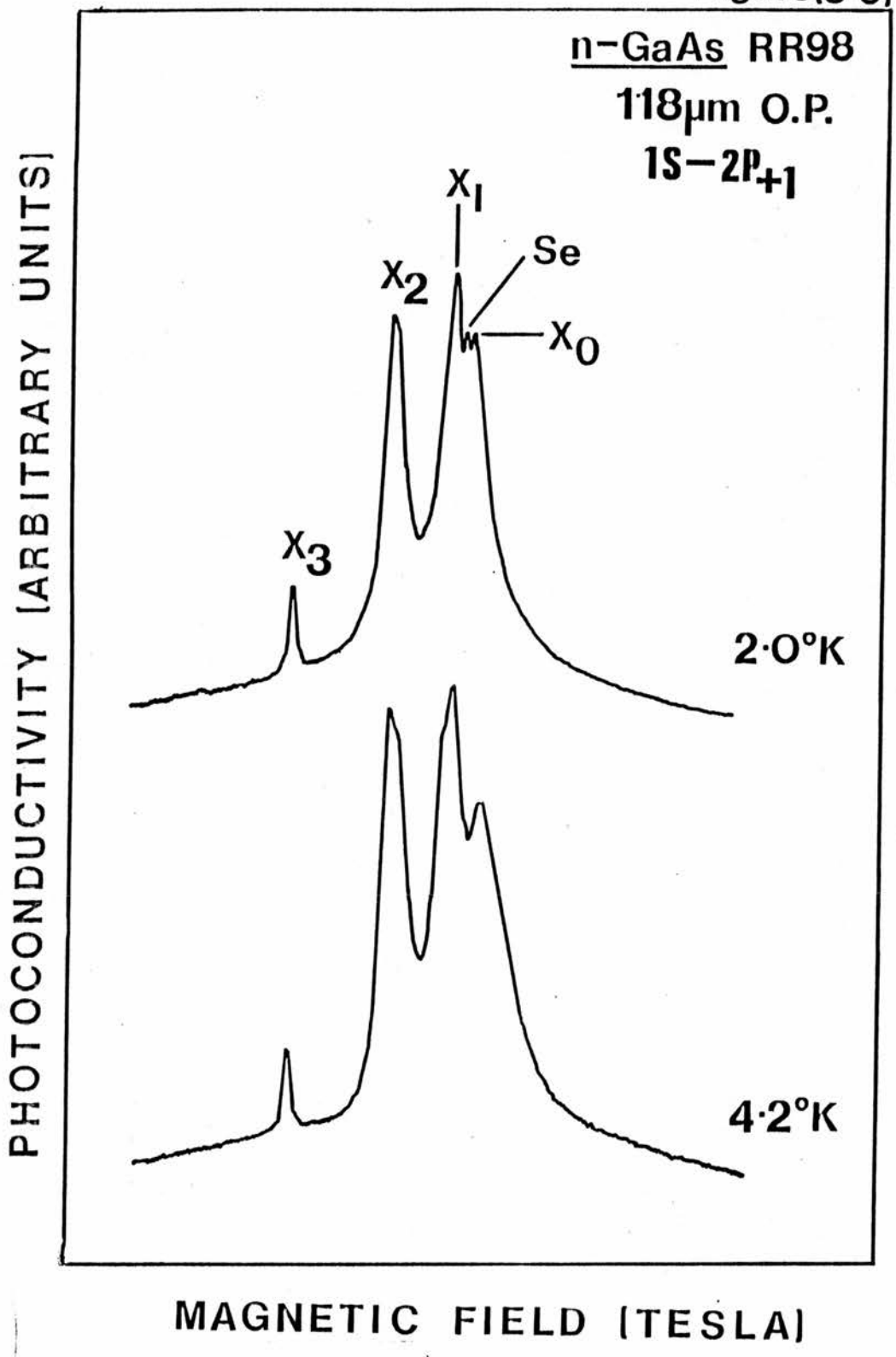

Figure (3.6) Displays the photoconductivity response versus magnetic field for RR98 at 118μm. The Se donor is resolved between X_1 and X_0, by lower the temperature from 4.2K to 2K (figure 3.5 is a recording of the same sample, but the $1S-2P_{+1}$ transition is shown).

OP- optical pumping.

Figure(3·7)

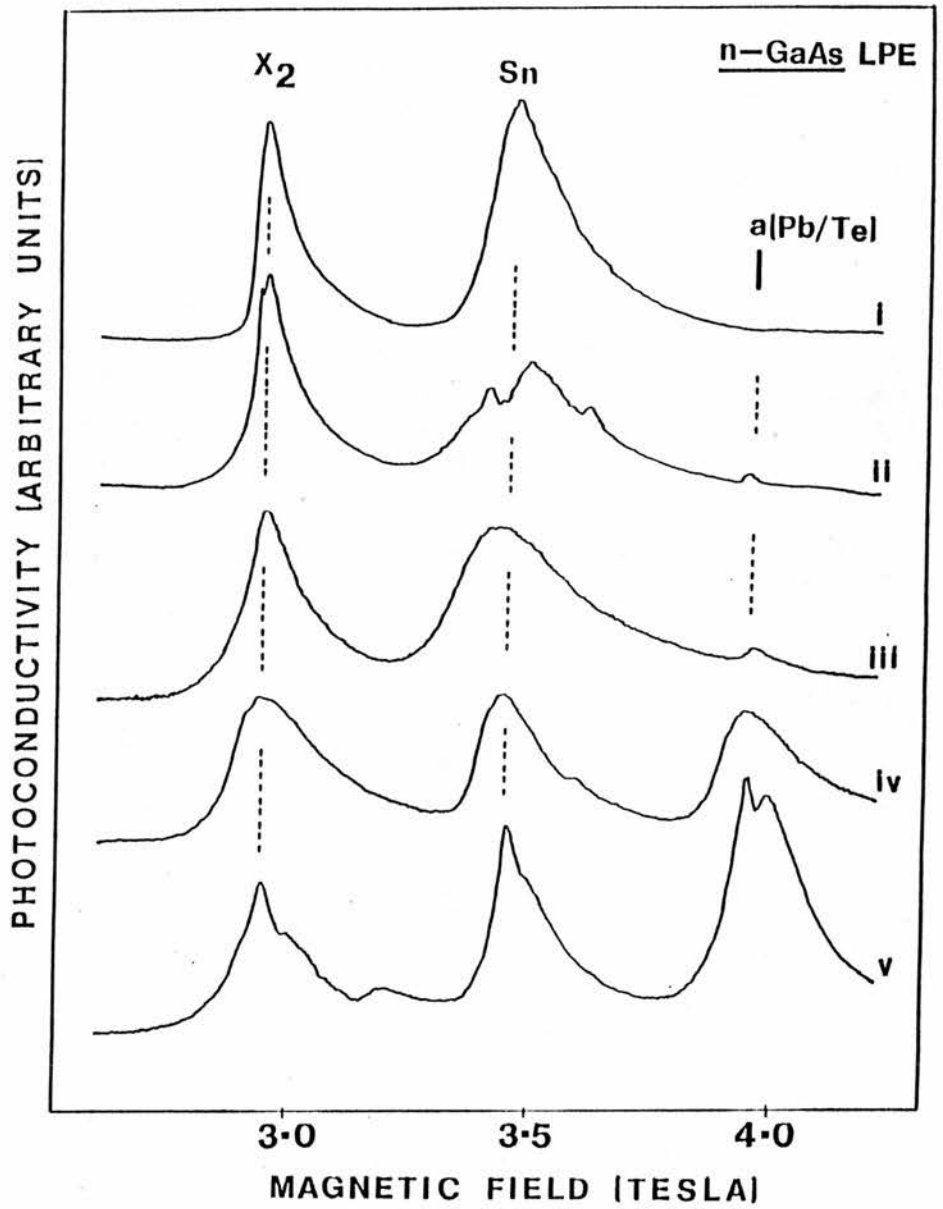

Figure (3.7) Shows the photoconductivity against magnetic field for the $1S\text{-}2P_{-1}$ transition at 302μm wavelength for three GaAs LPE samples. All three show $X_2(S)$, Sn and a third donor 'a' which may be Pb or Te. Donor 'a' can only be seen on illumination with band-gap radiation in 7LE45 but is the most abundant donor in sample E351 (see figure 3.4 also). Band-gap radiation brings out other peaks close to the Sn donor in 7LE45. E351 shows doublet structure on all lines, reminiscent of the structure observed on the $1S\text{-}2P_{+1}$ transition of RR98 (figure 3.5).

i) sample 7LE45, no band-gap illumination.

ii) sample 7LE45, with band-gap illumination.

iii) sample 3LE165, no illumination.

iv) sample E351, no illumination.

v) sample E351, with band-gap illumination.

Figure(3·8)

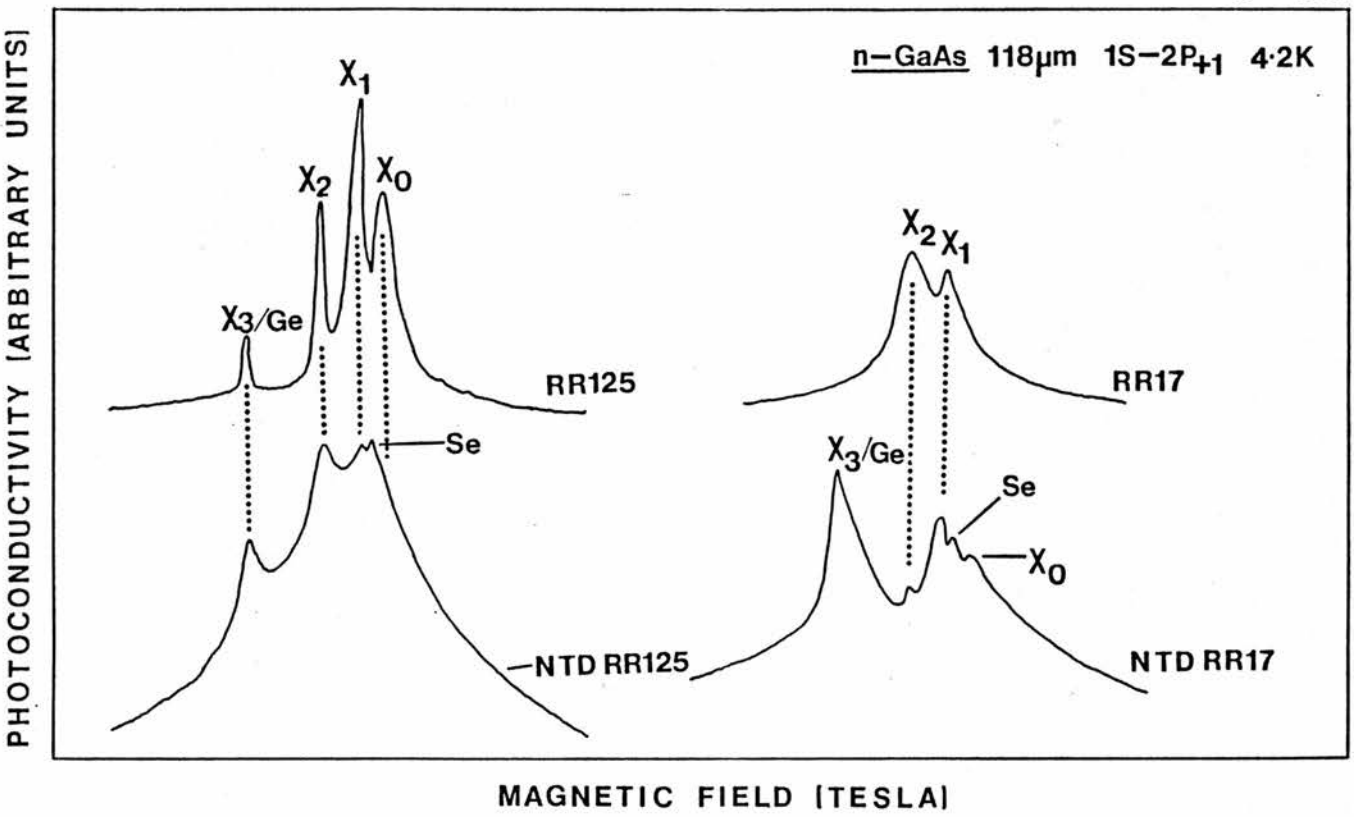

Figure (3.8) The effect of irradiating two high purity GaAs samples RR17 and RR125, with a flux of thermal neutrons is shown. Ga and As lattice atoms transmute into Ge and Se donors respectively. The top two traces are before irradiation and the bottom two after. X_3/Ge grows in both samples, and the Se peak appears between donors X_1 and X_0, enabling the Se donor to be positively identified for the first time. All the recordings are taken with intrinsic illumination (OP), except the top trace of RR17.

Figure(3.9)

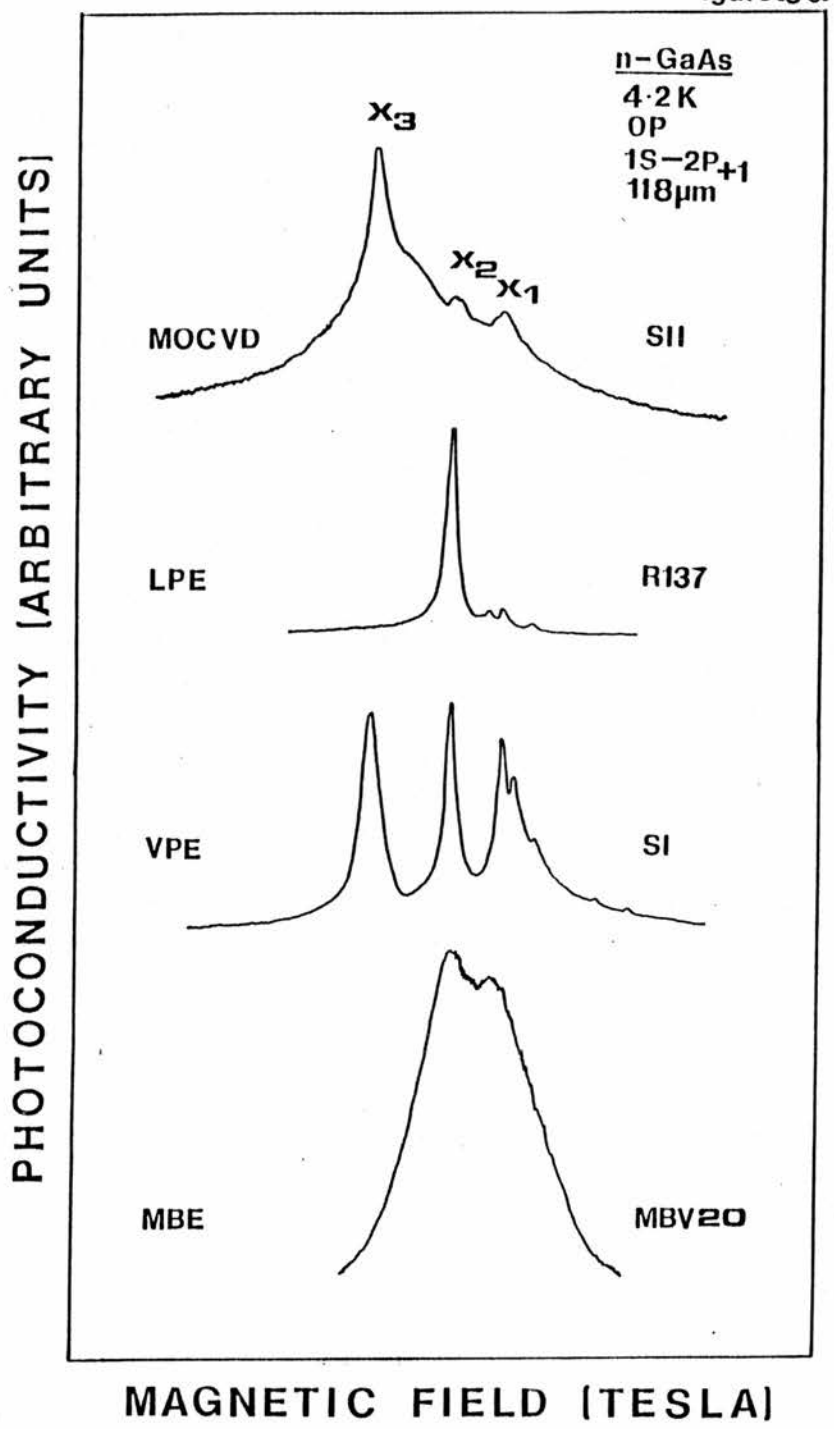

Figure (3.9) Compares the photoconductivity response against magnetic field for different GaAs samples grown by four different techniques. Each growth method has its own characteristic central-cell 'signature'. MOCVD grown GaAS has typically X_3/Ge dominant, with less X_1 and X_2. LPE has X_2 dominant, with no trace of X_3. VPE usually have X_3, X_2, and X_1 as the main dopants, but X_3 does not necessary appear in as large quantities as observed with this sample. MBE material has typically X_2 and X_1 as the main donors.

OP-optical pumping.

Figure(3·10)

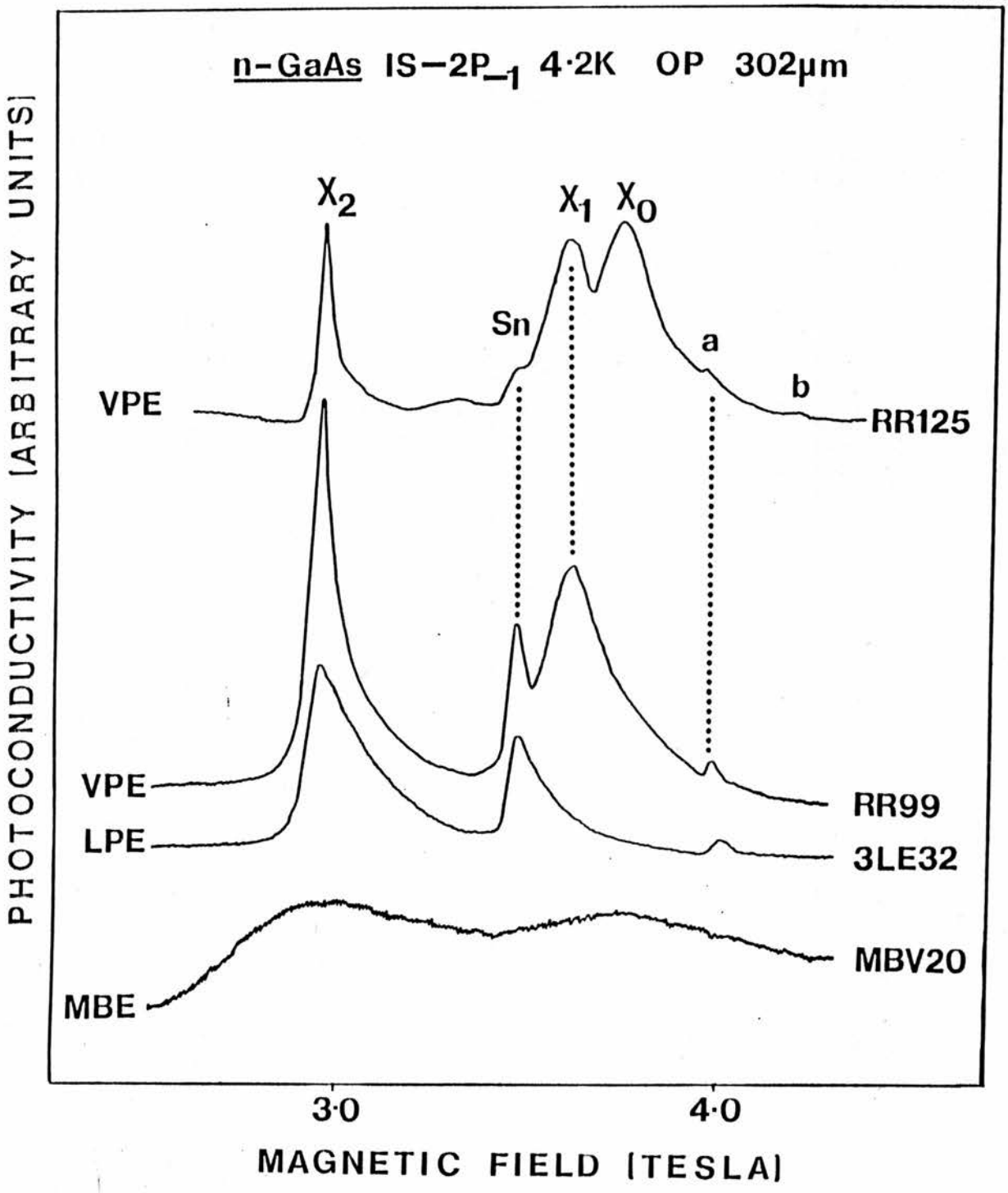

Figure (3.10) A comparison of the results for two VPE samples, RR99 and RR125, a LPE sample 3LE32 and a MBE sample MBV20. X_2 and X_1 appear common to all samples. Donor 'a' occurs in both VPE samples and in the LPE sample, a shallower donor 'b' also is observed in RR125. All recordings are of photoconductivity against magnetic field for a laser wavelength of 302μm.

Figure(3·11)

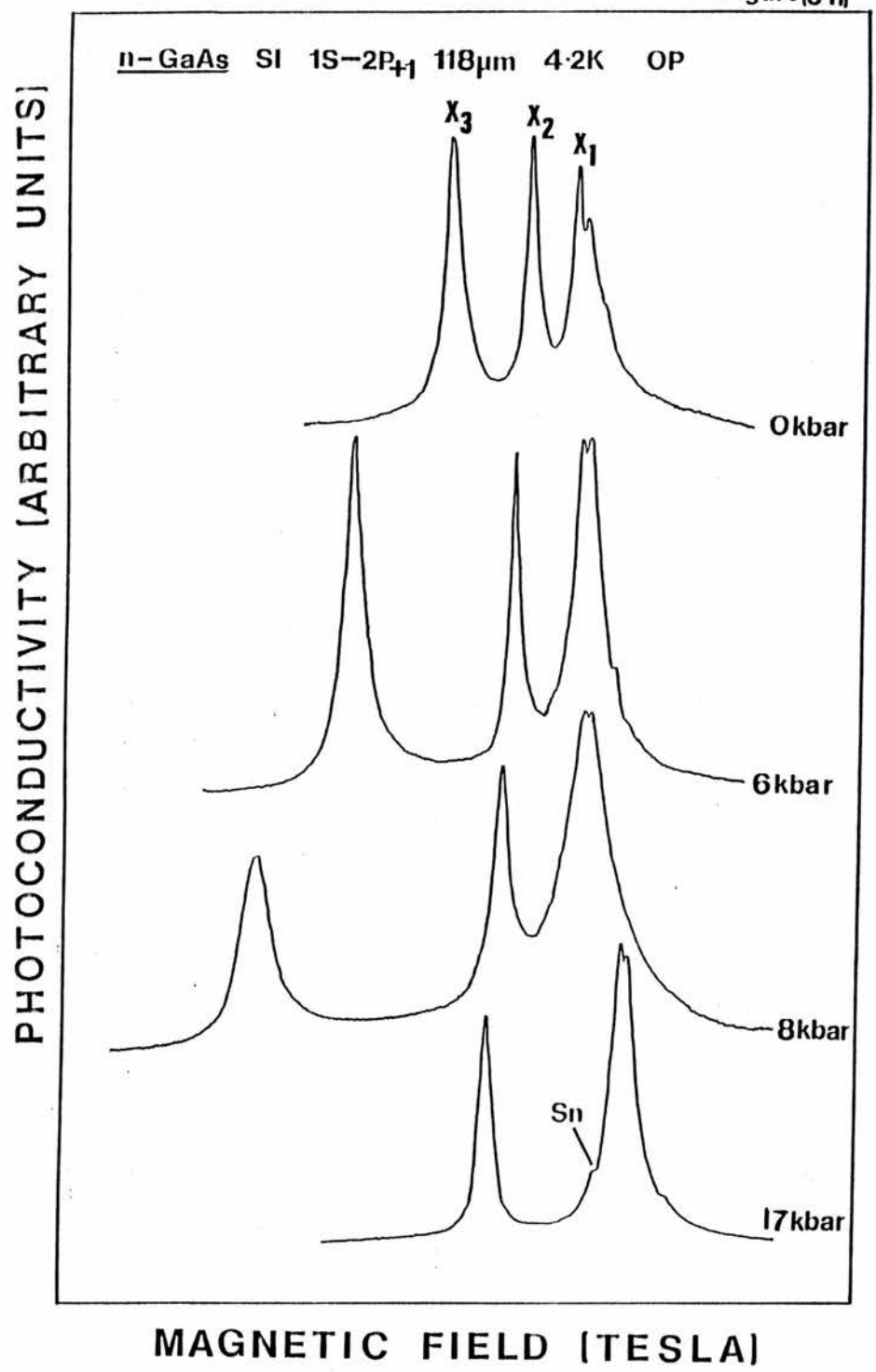

Figure (3.11) Shows the effect of pressure on the central-cell structure of a high quality GaAs sample, S1. The diagram displays the photoconductivity response against magnetic field with increasing pressure. An anomalous deepening, of the deepest donor X_3 is apparent. The increase in central-cell splitting occurs with increasing pressure, enabling the Sn donor to be resolved.

OP- band-gap illumination.

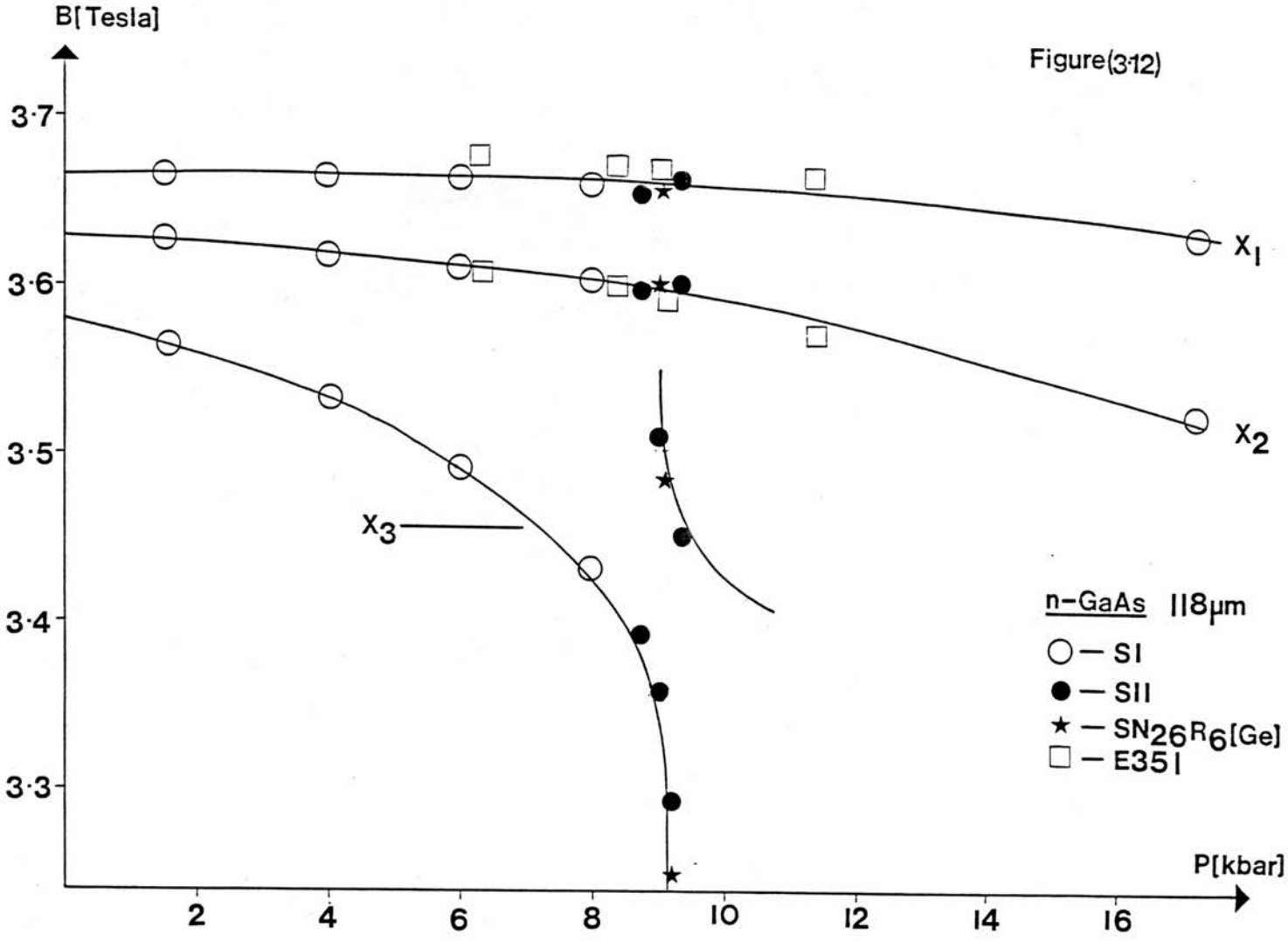

Figure (3.12) A diagram of pressure P(kbar) against magnetic field B(Tesla), is drawn for the $1S\text{-}2P_{+1}$ transition at 118μm for various GaAs samples. An anti-crossing of the deepest donor X_3 is clearly observed.

Figure (3·13)

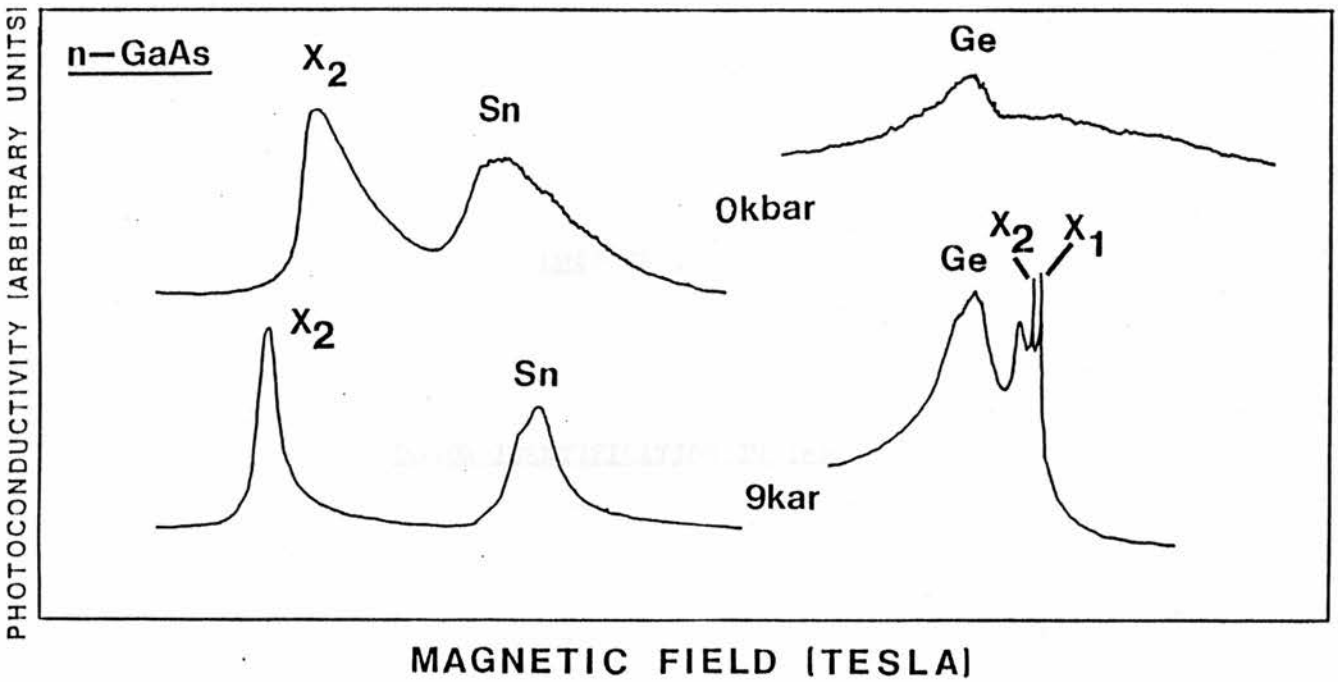

Figure (3.13) The improvement in resolution that can be achieved by the application of pressure is illustrated on this diagram. The upper two recordings are at ambient pressure and the lower two are for a pressure of the order of 9kbar. The left hand pair are for a GaAs sample, 3LE165, at 255μm wavelength and show the $1S\text{-}2P_{-1}$ transition. The right-hand recordings are taken at 118μm and display the $1S\text{-}2P_{+1}$ transition for a germanium doped GaAs sample ($SN_{26}R_6$). The pressure is close to that required for the maximum anti-crossing effect discussed in section (3.6). The two broad lines at low field are believed to be caused by the two branches of Ge impurity (Γ-like and L-like), see figure (3.12). The sharper lines at higher field are X_2 and X_1, and are commonly observed in undoped VPE material. Because pressure causes a large change in binding energy, the fields have been shifted to bring the central-cell components into approximate coincidence.

Low temperature FIR spectroscopy at high magnetic fields is employed to study the residual donor impurities in InP grown by a variety of different techniques including vapour phase epitaxy (VPE), metalorganic chemical vapour deposition (MOCVD) and liquid encapsulated Czochralski (LEC). Although the growth techniques for InP are not as highly developed compared to GaAs, many of the same considerations apply to both materials. However, there are technical difficulties, particular to InP, in consistently producing high quality material. This is reflected in inferior mobilities and higher impurity concentration samples, compared to GaAs.

The first report of central-cell structure in InP was made by Stradling et al (1972). Since then, many samples have been studied, and it is believed that up to twelve independent donors may have been resolved in the highest purity InP available (Stradling 1978). Compared to GaAs, similar problems are encountered in resolving the extremely small chemical shifts, but due to the number of impurities commonly present and poorer spectral resolution, resolving central-cell components in InP is particularly difficult. Experiments with back-doped and neutron transmutated doped samples are performed in an attempt to identify some of the residual donors present. However, only four donor peaks have been identified to date.

The linewidth advantages gained by studying the $1S\text{-}2P_{-1}$ transition are not accessible in InP, since there is no suitable laser line available for studying this transition. However, the narrowing achieved by using a large magnetic field can be fully exploited, since no Δg splitting is observed on the $1S\text{-}2P_{+1}$ line, at any field under

consideration. This is partly because the magnetic field has a proportionally lesser effect on perturbing the donor wavefunction due to the larger effective mass and also because non-parabolicity is smaller in InP than GaAs (Ohyama 1983). The reproducibility of most lines from sample to sample is of the order of 0.005T at 118μm wavelength i.e 0.2%.

4.1 CENTRAL-CELL STRUCTURE OBSERVED ON THE $1S-2P_{+1}$ TRANSITION

To investigate the nature of the residual contaminants in InP, experiments with back-doped samples were performed. Very broad lines are encountered with back-doped InP, similar to GaAs doped crystals. Consider a high quality undoped VPE sample of InP, QM274 (figure 4.1), three well resolved peaks are observed on the $1S-2P_{+1}$ transition with peak X_6 dominant. QM274 is a Plessey VPE undoped sample, grown using the 'Nozaki effect' i.e 6% of the growth PCl_3 is added to the seed zone to suppress the carrier concentration. This undoped sample is used as a reference sample to compare two back-doped crystals grown by the same machine. Two crystals QM273 and QM272 are lightly back-doped with Si and S respectively. Both photoconductivity spectra show only one broad peak, typical of most back-doped samples although QM273 has an unresolved high field shoulder. However, the low and high field peak positions either side of donor X_6 for the undoped crystal correspond to the S and Si peaks on the doped samples. A similar Si back-doped crystal KV348 figure (4.10) displays a distinctly abnormal large peak corresponding to the Si peak in undoped material. Usually, in samples grown by the 'KV' reactor, the Si peak is of much smaller intensity than the S peak, so it can be said with some confidence that slight Si contamination has occurred. Note that donor X_6 in the undoped sample also appears occasionally in VPE material grown by

different reactors.

Dean et al (1984), using the complementary technique of near band-edge photoluminescence, succeeded in resolving spectral features due to two residual donor species. Sulphur and silicon were also identified as the main residual dopants in high purity epitaxial InP, with sulphur deeper and usually dominant. This is in general agreement with the far-infrared photoconductivity (FIRPC) results of Armistead et al (1984). The proportion of the epitaxial layer examined by the two techniques is very different. The photoluminescence method collects information from approximately 2% of the depth of the layer, compared to the FIRPC response, which is on average from the whole contribution of the epitaxial layer. There is good agreement of the S-Si splitting energy between the FIRPC and photoluminescence results. Furthermore, the identification of the S donor is made with consideration that this contaminant commonly occurs in other similar III-V material and occurs deeper than Si e.g GaAs (section 3.3) and GaP (Dean 1968). Also the shallower donor, silicon, has been observed to decrease markedly in the FIRPC spectra when water vapour (or O_2) is deliberately introduced into the reactor (Hales 1979). The effect of the H_2O is to reduce Si contamination from the quartz reactor components.

Figure (4.2) displays the $1S-2P_{+1}$ transition for NAG747, one of the highest mobility InP samples ever grown. Two laser wavelengths are used to study the $1S-2P_{+1}$ transition, 118μm and 70.6μm, and the recordings taken with these wavelengths are shown on the left and right columns of the figure respectively. A comparison is made between the effectiveness of different narrowing techniques. The top left hand trace, is taken without band-gap illumination with 118μm

laser radiation, and at 4.2K. Only two large broad peaks are evident, corresponding to S and Si donor impurities, similar to structure obtained with inferior quality material. Looking at the same transition, but at shorter wavelength (70.6μm) i.e higher magnetic field (approximately 8.5T), a splitting of the S peak occurs. This splitting is reminiscent of the 'notch' effect described in the previous chapter, but is observed without optical pumping in this particular InP sample. An increase in central-cell splitting is apparent on going to higher fields. If intrinsic illumination (OP) is applied to the sample, together with 118μm radiation at 4.2K, structure is resolved on both the low field wing of the S donor and on the high field side of the Si donor. At 70.6μm, little additional structure is resolved with the benefit of a larger magnetic field, except the S peak splitting has been enhanced. On reducing the temperature to 2.0K a further increase in spectral quality is observed. Three well resolved peaks are clearly resolved on the low field side of the S donor. The two lower field features are believed to belong to independent donors, Ge and Sn respectively (see later in this section), while the higher field structure is thought to arise from peak inversion (PI), since peak splitting occurs in this region using 70.6μm radiation, and often occurs here with other high quality InP samples. The magnetic field over the range 3.5T-8.5T, appears to have a lesser narrowing effect compared to band-gap illumination or lowering the temperature, as can be seen on comparison with the top two spectra taken at 4.2K and with no band-gap radiation. Under these conditions the field reduces the S peak by 20% and the Si peak by 25%, but at $2^{o}K$ and with optical pumping the magnetic field has little difference on the linewidth. Well resolved donors, X_4, X_3, and X_1, with very small intensity are observed on the high field side of the Si peak and have also been observed in high quality VPE samples grown

by the KV reactor (see figure 4.10). The Si peak narrows considerably at the reduced temperature and with band-gap illumination; also the relative height of the Si transition increases, becoming comparable to the S donor. This is explained on the assumption that relatively purer Si areas near the surface are being enhanced by the intrinsic illumination, and that these areas contain proportionally less S. This appears inconsistent with the photoluminescence results of Dean et al (1982), who suggest that Si is present at higher concentration towards the layer-substrate interface, and towards the surface, presenting a 'U' shaped impurity profile. The FIRPC result for NAG747 is in agreement with different segregation coefficients of Si and S, according to Kang and Greene (1968), assuming their ideas can be extrapolated to InP. The S peak is narrowed by almost 50% and the Si peak by over 75% just by the application of band-gap light and pumping on the helium to 2K. This narrowing of the Si donor is not necessarily as dramatic in other high quality InP samples e.g NAG762 shows no relative change in the S/Si ratio (figure 4.9), indicating the inhomogeneous impurity concentration profile may vary for different samples.

Figure (4.3) shows the photoconductivity response of the $1S-2P_{+1}$ transition at two wavelengths. The top left hand trace is taken without optical pumping at $2^{o}K$. NAG775 appears the exception of the NAG series of VPE grown InP, with Si being the major donor with almost twice the intensity of S. Applying intrinsic illumination, the S component narrows dramatically, and grows with respect to S. Donor X_3 is also clearly resolved. This recording emphasises the variation of the surface ratio of S/Si from sample to sample, since this recording is almost completely contradictory to the results for NAG747. Presumably, the impurity variation also differs throughout the sample.

An etching experiment was performed to investigate the change in relative intensity of the S and Si donor concentrations which are expected to vary as a function of epitaxial layer depth. Measurements were performed on an InP sample, KV465, before and after about half of the layer was removed. The top left hand side trace of figure (4.4) was taken with 118μm radiation and no optical pumping. S and Si appear with approximately equal concentration. Under similar experimental conditions, but with half of the epilayer removed (trace ii), the relative S/Si ratio changes, as the Si intensity drops with respect to the S peak, i.e relatively more Si donors have been removed during the etching process than S impurities. This suggests that Si donors are in higher concentration towards the surface, in agreement with Dean et al (1982), but in contradiction with the NAG747 result. At higher fields using 70.6μm radiation, the two peaks narrow but the relative intensity of the S/Si ratio remained unchanged compared to the 118μm trace without band-gap illumination (trace iii). Applying intrinsic illumination to the etched sample at 70.6μm, the Si peak grows rapidly and narrows with respect to S; also donor X_6 becomes resolved on the high field shoulder of the S peak (trace iv). The Si concentration appears to fall after etching but Si rapidly grows with respect to S after light excitation. The growth and narrowing of Si under illumination could be understood if the etching had exposed a region of low concentration of Si to the intrinsic light. This is consistent with the 'U' impurity concentration profile described by Dean et al (1982). There is also a significant shift of the Si peak position by about 10mT upon etching. It is not clear if this represents a change in the relative concentration of the Si donor or a shift due to an unresolved second donor or whether surface strains are responsible. The results certainly indicate a variation of Si

concentration with depth but are somewhat inconclusive concerning the exact location of Si from sample to sample.

The effects of band-gap illumination and magnetic field are illustrated in figure (4.5). All the spectra displayed are for a high purity VPE InP sample, NAG780, with a liquid nitrogen mobility of 100,000cm^2/Vs. The spectra in the left column are taken with 118μm and on the right with 70.6μm laser radiation. The spectra at the top are without band-gap illumination and below with; otherwise the experimental parameters are similar. With no optical pumping , only two large broad peaks are resolved. Increasing the magnetic field from approximately 3.5T to 8.5T narrows the donor transitions by only 10-15%. On applying band-gap illumination, more structure is resolved, including a Ge peak which appears characteristically in most of the high mobility InP layers grown by the NAG reactor. There is no obvious change in the S/Si ratio by applying band-gap radiation with this high quality sample, in contrast to NAG747 and NAG775. Both the S and Si donors split and the centre of their respective inverted peaks align well with their peak position in the spectra without band-gap illumination. This effect is more clearly seen at 70.6μm with optical pumping and is believed to be caused by the 'notch' effect described for GaAs. Optical pumping narrows the S line by over 50% and the Si donor transition by over 30%.

Figure (4.6) displays the $1S-2P_{+1}$ transition, again observed with 118μm and 70.6μm on the left and right hand side of the figure. This figure compares five different samples grown by the same VPE NAG growth system , with liquid nitrogen mobilities ranging from 50,000 to 100,000 cm^2/Vs. A surprising feature that is found particularly with InP, is that without optical illumination the quality of spectra does

not improve considerably with increasing mobility, over the above mobility range. In contrast, the linewidths for GaAs can decrease by almost an order of magnitude over the same mobility range, as can be seen for example, by comparing the results for MBV20 and RR99 (figure 3.10) in the last chapter. However, a substantial improvement in the quality of the spectra becomes apparent for $77^{o}K$ mobilities in excess of 100,000 cm^2/Vs, particularly with the use of optical illumination. For example, compare NAG762 to the other samples shown in figure (4.9). All of the displayed spectra are taken under similar experimental conditions at 4.2K and optical pumping. No significant narrowing occurs if the temperature is reduced to 2K. All of the samples show that S and Si are by far the most common residual donors in VPE grown material. A third donor, X_3, becomes completely resolved with optical pumping with the highest mobility sample shown NAG686. This donor also commonly appears in VPE material grown by the CR reactor (figure 4.9). Other features are observed with optical pumping on the wings of both the S and Si donors, but are very weak. A substantial improvement in the quality of the spectra becomes apparent for samples with $77^{o}K$ mobilities in excess of 100,000 cm^2/Vs, but only at pumped helium temperatures and with optical pumping. For example, compare the spectra of NAG747 with a $77^{o}K$ mobility of 120,000cm^2/Vs (figure 4.2) with that for NAG618 with a mobility of 53,000 cm^2/Vs (figure 4.6). At $4.2^{o}K$ there is little difference in structure, the reason why InP does not narrow with increasing mobility without optical pumping in a similar manner to GaAs remains to be answered.

In spite of the initial success in obtaining the chemical identity of two donor species, there remains a total of ten distinct unidentified central-cell components in VPE, LEC, and MOCVD material (see table see table at end of chapter). Two of the peaks, X_5 and X_7, are possibly due to peak inversion and thus can be excluded from the analysis. There remains however, a total of eight remaining unidentified peaks and it seems unlikely that all possible donors will occur, for the same reasons as explained for GaAs. Ge and Sn back-doped crystals were obtained from RSRE, in an attempt to further identify central-cell features in the photoconductivity response of undoped InP.

FIRPC results are shown for the Ge-doped sample are shown in figure (4.7), taken with 70.6μm laser radiation. A large hydrostatic pressure is applied to all the samples displayed in this figure to help resolve the central-cell structure. Near-band gap photoluminescence experiments were also performed on the same InP samples by Skolnick et al (1984), and provide an alternative analysis.

At 118μm, a single broad peak, with no central-cell structure is observed, even at 2K and with strong band-gap illumination (not displayed). This indicates that a significant number of impurity donors have been introduced. Only at higher field with 70.6μm radiation is central-cell structure resolved. The higher field component of the doublet at 8.500T corresponds well to the S donor peak position in undoped material. The lower field peak at 8.440T, is identified as belonging to the Ge donor, since it is not present in as large quantities in any other undoped samples. Also, this peak aligns

well with the deepest residual donor present in high purity undoped VPE InP. The Ge-S separation is in good agreement with photoluminescence results confirming the identification of the Ge donor. Thus a magnetic field rather than band-gap illumination or reducing the temperature provides the best mechanism for line-narrowing, in contrast to high quality undoped material e.g NAG747 (see figure 4.2). This is probably because of a significant increase in the donor-acceptor pair recombination due to the introduction of Ge donors. Hydrostatic pressure improved the quality of the spectra, but did not provide any additional information with this sample.

No additional central-cell structure is introduced by Sn doping with either of the wavelengths. However, the broad single peak is noticeably shifted to slightly lower field from the S donor peak position in undoped material. It is concluded from these results that the Sn donor has a chemical shift close to but deeper than S. Photoluminescence measurements confirm that the chemical shift of the central-cell peak is very close to the S donor (Skolnick et al 1984). A large hydrostatic pressure applied to the sample, with 70.6μm laser wavelength radiation, enables two central-cell components to be resolved. The deepest peak is believed to be due to Sn, since no other peak of comparable intensity occurs in this region and the peak position is significantly lower in field than S. The Sn peak position aligns well with the second deepest donor in undoped material. The shallower peak position corresponds to the Si donor. Neutron transmutation doped InP samples confirm this result (see section 4.5). Hydrostatic pressure was also applied to the silicon doped sample QM274, in an attempt to improve the central-cell structure. Unfortunately, there was no appreciable change. The peak positions

for each of the doped samples are plotted as a function of pressure and compared to undoped InP (see section 4.5). The relative ordering of the chemical shifts of the shallow donors Ge, Sn, S, and Si is different as found for those donors in GaAs i.e Ge, S, Sn, Si.

4.2 CENTRAL-CELL IDENTIFICATION IN BULK INP

The quality of liquid encapsulated Czochralski (LEC) grown bulk InP samples falls substantially short of state-of-the-art epitaxial material. Typical values of net electron concentration and liquid nitrogen mobilities in undoped high purity LEC InP are in the region of $1\times10^{15}cm^{-3}$ and $50,000cm^2/Vs$ respectively. Four LEC samples obtained from RSRE are studied. Silica crucibles were used to contain the melt for all four samples. Thus, Si is expected to be a major contaminant in this material.

The photoconductivity signal versus magnetic field for the four LEC InP samples are displayed in figure (4.8). The spectra were obtained using 118μm radiation at 4.2K, and with intrinsic illumination. Up to four residual donors appear in the central-cell structure. Sulphur is usually a significant impurity except in L816, Silicon is a minor contaminant which is only evident in VIPC 611 and L816, shallow donors X_0 and X_1 are incorporated as the principal donor species. It is surprising that Si is not apparent on the central-cell structure in as large quantities, suggesting that this impurity is introduced into the crystal as an acceptor. The central-cell 'signature' for LEC grown material contrasts strongly with the data for InP epitaxial layers. It was suggested by Dean et al (1984), that the much greater temperatures required for LEC growth could be responsible for the radically different central-cell structure. The

above results were confirmed by photoluminescence measurements by Dean et al (1984), who conclude that shallow donors X_0 and X_1 may not be simple substitutional donors.

4.3 COMPARISON OF GROWTH SYSTEMS

Figure (4.9) compares the photoconductivity spectra of the $1S\text{-}2P_{+1}$ transition at 118μm for samples grown by different techniques. All of the spectra shown are with band-gap illumination except the top trace. A comparison is made first, between the central-cell structure of VPE samples grown from different VPE kits. The top recording is for NAG762, which has the highest liquid nitrogen mobility yet recorded i.e 130,000 cm^2/Vs. At 4.2K and no optical pumping only two peaks are resolved, corresponding to the main residual contaminants, S and Si. However, at the same temperature, but on applying band-gap illumination, fine structure is apparent on the high field and low field wings of Si and S respectively, corresponding to Ge, Sn and X_3 donors. The VPE InP grown by the 'CR' reactor has commonly four shallow residual donors (trace iii) i.e CR276, with approximately equal intensity, two of which are S and Si, the other two X_6 and X_3 are unidentified. This is compared to VPE InP grown by the 'KV' and 'R' reactors, which both produce strong but broad lines attributed to S and Si, with Si usually weaker. The particular KV grown sample displayed in figure (4.10) is very lightly doped with Si, so the Si component is expected to be enhanced, thus confirming the identification of the donor (Knowles et al 1982). Also observed as minor contaminants are donors X_3 and X_2, on the high field shoulder of Si. The sequence of samples shown in figure (4.6) grown by the NAG reactor all show S to be dominant, Si contamination is common but appears more erratic, donor X_6 is present in only two NAG samples.

This series of results indicate that the residual background can fluctuate either through changes in the reactor itself or because of differences in contamination of the chemicals employed. The NAG reactor has consistently produced material with liquid nitrogen mobilities in excess of 100,000 cm^2/Vs. The highest mobility samples generally appear to have a strong Si line , presumably due to a reduction in S contamination.

The 'QM' VPE growth kit introduces three residual donors into the InP epitaxy layer (figure 4.1). This growth kit appears to be the exception, in that S is not the major residual donor, but rather donor X_6 . Donor X_6 also appears as a common residual dopant in VPE material grown by the 'CR' reactor and occasionally appears in the NAG series in small quantities. The 'R' series of VPE produce spectra similar to the 'KV' series, with S dominant (figure 4.10).

The MOCVD sample grown at RSRE (figure 4.9iv) displays two major shallow donors, S and Si. The mobility of this sample is much less than that of NAG762 . The difference in mobility between the two samples is evident by comparing their respective linewidths. Comparing the RSRE MOCVD InP to the Thomson CSF grown MOCVD InP (figure 4.9v), the Thomson CSF sample shows Si as the strongest line with S present at about one third intensity and also a significant amount of a very shallow donor X_0 which is thought to have a negative chemical shift. Dean (1984) also report Si to be strong in MOCVD material and generally found Si to be twice as intense as S. Apart from the bulk material (LEC), all the epitaxial samples have very similar features. However, there are notable exceptions especially in the incorporation of donors X_6 and X_3 in VPE material, even with crystals grown by the same reactor. For example, X_3 appears as a

major dopant in NAG775 and NAG686, but appears little elsewhere in other crystals grown by the same machine. Furthermore, X_3 is evident in some, but not in other crystals grown by the same method but in different laboratories. This 'random' impurity incorporation, perhaps suggests that the contamination is introduced by the quality of the starting materials, which presumably come from different sources.

4.4 NEUTRON TRANSMUTATION DOPING OF INP

An InP sample NAG634 was subject to a flux of thermal neutrons by Professor F.Kuchar of Vienna, in an attempt to transmute a number of In and P lattice sites into Sn and S donors respectively, by the absorption of a neutron and subsequent nuclear decay. By far the most important nuclear reaction concerns ^{115}In which is the most naturally abundant isotope of In i.e 95.8%, with a thermal neutron cross-section of 157 barns (1 barn = $10^{-24}cm^2$). ^{113}In appears naturally in much lesser quantities i.e 4.3% and has a much smaller cross-section of 3.2 barns. Both isotopes decay into Sn after the absorption of a thermal neutron. The thermal neutron cross-section for the only naturally occurring isotope of ^{31}P is several orders of magnitude less than for ^{115}In i.e 190mbarns. Thus during irradiation approximately $10^{14}cm^{-3}$ impurities are introduced onto substitutional donor sites, 99.9% of all the nuclear reactions transmute In into Sn donors and only about 0.01% into S donors. The neutron radiation bombardment creates a considerable number of lattice defects which act as scattering centres. To regain the crystal's previous mobility, the sample is thermally annealed at 525°C for one hour in a similar manner described for GaAs (section 3.3).

The FIRPC spectra for NTD NAG634 is displayed in figure (4.11). All the recordings are of the $1S-2P_{+1}$ transition, observed under similar experimental conditions i.e 4.2°K and optical pumping. The top traces are for the same sample before irradiation, at 118μm and 70.6μm. Sulphur is the dominant donor with Si donor appearing as a shoulder at two-thirds intensity of the main donor. After irradiation and subsequent annealing, a small feature appears on the low field

side of the S peak with 118μm radiation and optical pumping. The line-width of the S donor is comparable before and after irradiation, indicating a successful thermal anneal. However probably deeper traps have not been annealed out; thus the compensation ratio is expected to increase. At shorter wavelenghts i.e 70.6μm and optical pumping, this feature increases into a well resolved peak, separated by almost 20mT from the S peak. This peak does not appear as large on any undoped VPE material and consequently is regarded as belonging to the Sn donor. This corresponds well to the Sn peak resolved under pressure with the back-doped sample NAG854 and relates well to the the second deepest donor in undoped material. There is little change in the size and shape of the S peak, this is in agreement with the above prediction, that few S donors are produced during irradiation.

4.5 InP SUBJECT TO HYDROSTATIC PRESSURE

InP is less compressible than GaAs. The direct energy gap E_g = 1.34eV at ambient pressure, and increases at a rate of dE( )/dp = $+9.5 \times 10^{-6}$eV/bar with hydrostatic pressure (Pitt 1973), calculated from magneto-phonon measurements. The Γ-X interband energy in InP is measured as 960±5meV at 8^{o}K by Onton (1972) and as 900±20meV by Dumke (1970), and as 700±70meV by Pitt (1970). This magnitude is in agreement with the theory of Brust (1971) for 0^{o}K, who calculates the Γ-X separation as 0.95eV using a self consistent pseudo-potential theory and predicts the Γ-L separation to be 0.8eV. The latter value is in reasonable agreement with experiment by Onton (1972) of 610meV. Hence, the L minima in InP lie between the X and Γ extrema in energy. This configuration is similar to GaAs (James et al 1970 and Pitt 1970), but the energy separations are much larger. However, the pressure coefficients for the X and L minima are dE(L)/dp = $+3.4 \pm 1.5\ 10^{-6}$ev/bar (Camphausen 1971) and dE(X)/dp = $-3 \pm 0.4\ 10^{-6}$eV/bar respectively (Muller 1980). Only the X minimum moves down with respect to the Γ conduction band minimum. In GaAs the L and X minima cross into the forbidden gap at approximately 30kbars. A similar crossing effect is expected for the X minima in InP, but at much higher pressure, since the Γ-X energy separation is much larger and the pressure coefficients are less than for GaAs. Crossing between the Γ and X minima occurs at 104±1kbar (Muller 1980).

FIRPC experiments with InP under large hydrostatic pressure are performed in a similar manner to those with GaAs (see section 3.5). As yet no anti-crossing of the deepest shallow donor with states associated with higher order conduction band minima has been observed in InP, at the available pressures i.e 15kbar. This appears to be a reflection on the lower pressure coefficients and the much larger conduction band energy separation. However, the work of Adams et al (1978) with $InAs_{1-x}P_x$ suggests a crossing at about 20kbar which is independent of x over a range from 0.1 to 0.4.

Figure (4.12) demonstrates the improvement in resolution of the different donors with pressure. Pressure both narrows the donor transitions and increases the central-cell splittings. The top trace displays the photoconductivity spectra of NAG747 at 118μm, 2°K, with optical pumping at ambient pressure. The bottom two spectra are examined under the same experimental conditions, but a different piece of the same sample is used . The Si peak is considerably smaller indicating a considerable surface variation in Si contamination of the two pieces. This was also noticed by Dean et al (1984) who scanned a focused beam over the sample surface. Peak-inversion on the S peak disappears under pressure. Otherwise the individual central-cell components track with increasing pressure. For example, both the S-Si and S-Ge separations increase by a factor of 1.55+0.1mT on applying a pressure of 16Kbar. The central-cell splitting would be expected to increase as the cube of the ratio of effective mass to dielectric constant. An indication of the increase in the effective mass is obtained from the cyclotron resonance values taken at 570μm at different pressures (figure 4.14). The effective mass has increased by ~8% at this pressure so the increase in splitting on applying

pressure would require an increase in the dielectric constant of 6.5% or the approach of anti-crossing with resonance states associated with subsidiary minima. By comparing the width at half maximum of the sulphur donor, pressure narrows this line by 25% at the highest pressure obtained. Thus pressure linenarrowing and increased central-cell splitting is very beneficial in resolving very weak structure.

In summary, up to twelve different central-cell peaks have been observed in the FIRPC of high purity VPE InP. Only four peaks have been identified as Ge, Sn, S, and Si; S is usually the dominant, with Si often occurring by in varying quantities. Bulk InP provides a radically different central-cell structure to typical epitaxial growth, with large quantities of shallow donors evident. Large differences in the impurity concentration exist. Difficulty is encountered explaining the trend of the S/Si profile ratio throughout the epitaxial layer, from sample to sample, illustrating the difficulty of growing homogeneous high purity InP samples. Hydrostatic pressure is used as an additional experimental parameter. No level-crossing of the deepest shallow donor is observed, but the central-cell splitting increases and the quality of the spectra improves.

Table of magnetic field position of central-cell peaks in n-InP

	118μm B(T)	70μm B(T)
X_0	3.853	8.755
X_1	3.771	8.659
X_2	3.739	8.648
X_3	3.718	8.579
X_4	3.705	8.566
Si	3.699	8.556
X_5	3.690	8.550
X_6	3.678	8.538
S	3.660	8.514
X_7	3.653	8.503
Sn	3.641	8.490
Ge	3.615	8.460

X_5 and X_7 are probably due to peak inversion.

Figure(4·1)

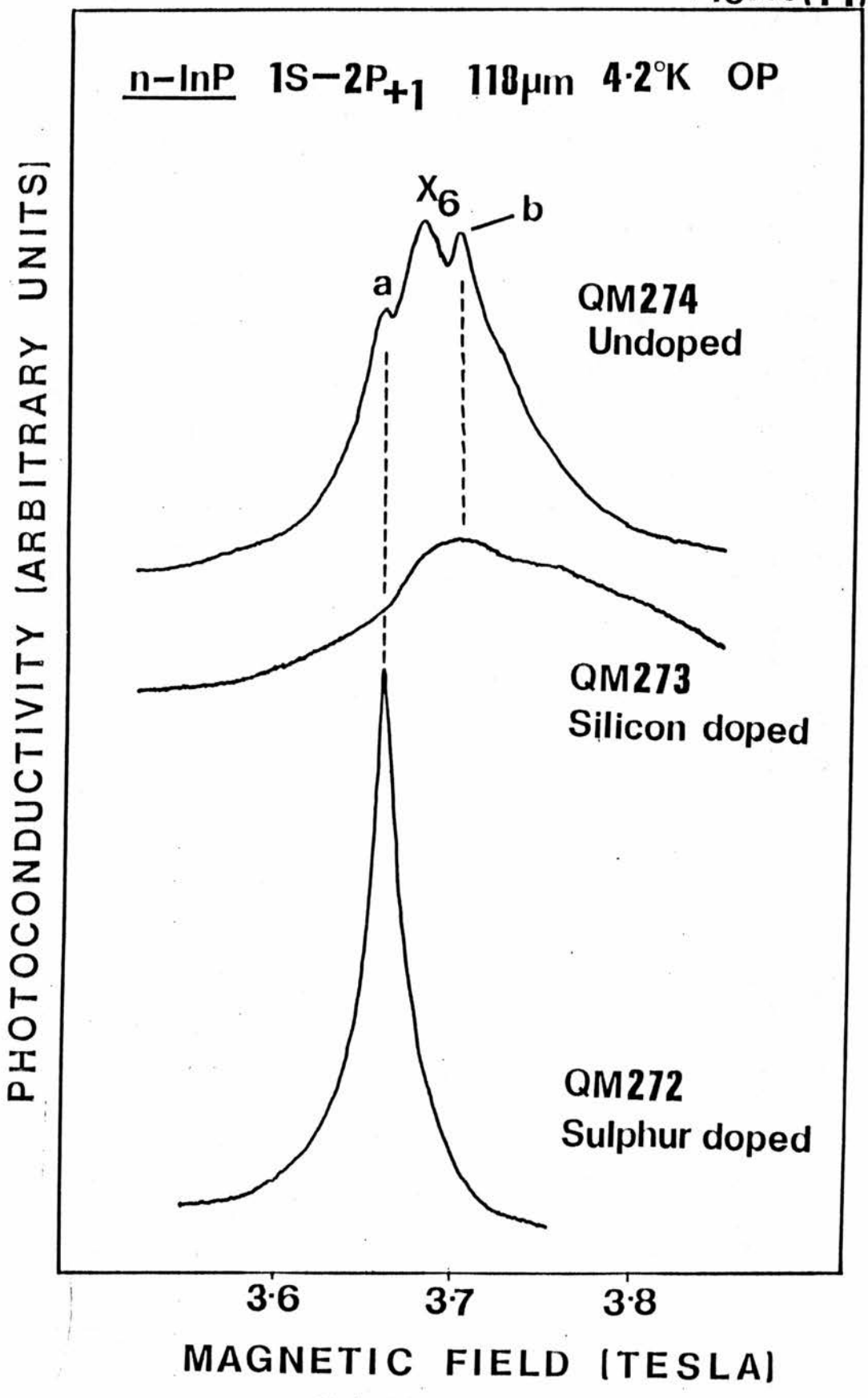

Figure (4.1) Compares the photoconductivity response against magnetic field at 118μm, for an undoped n-InP sample, (QM274), a silicon doped sample (QM273) and a sulphur sample (QM272), grown by the same VPE machine.

OP - intrinsic illumination.

Figure(4·2)

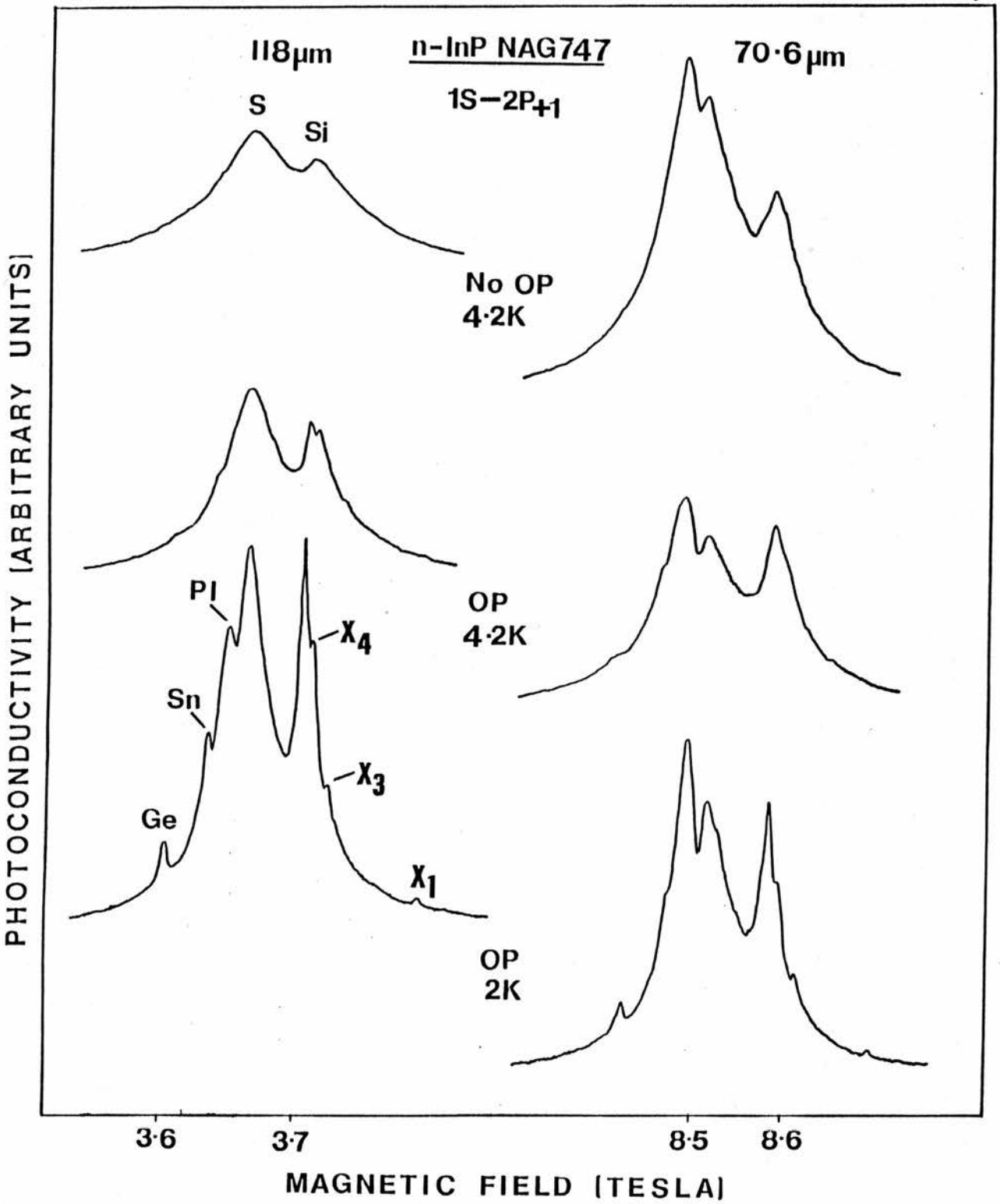

Figure (4.2) Illustrates the benefits of intrinsic illumination, reducing the temperature to 2°K and using a larger magnetic field, to improve the linewidth. The recordings are for photoconductivity versus magnetic field, with a high quality n-InP sample NAG747, using two laser wavelengths 118μm and 70μm. Note a dramatic narrowing of the Si donor occurs.

OP - band-gap illumination.

Figure(4·3)

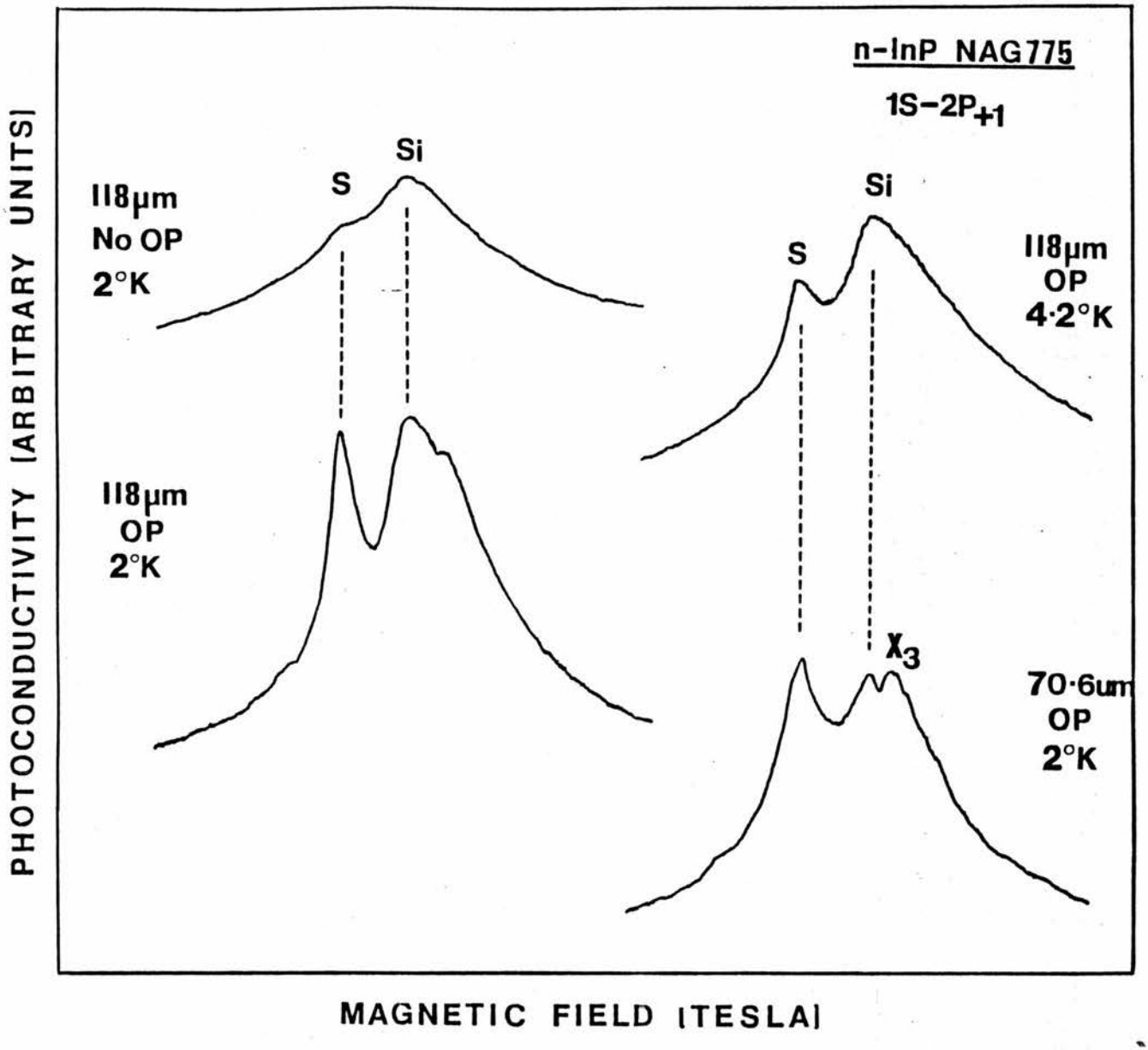

Figure (4.3) Demonstrates the narrowing achieved by reducing the temperature from 4.2K to 2K, by applying intrinsic illumination and increasing the magnetic field, at two laser wavelengths 118μm and 70μm. A dramatic narrowing of the S donor occurs at 2^{o}K with optical pumping (OP), in contrast to NAG747 (figure 4.2).

Figure(4·4)

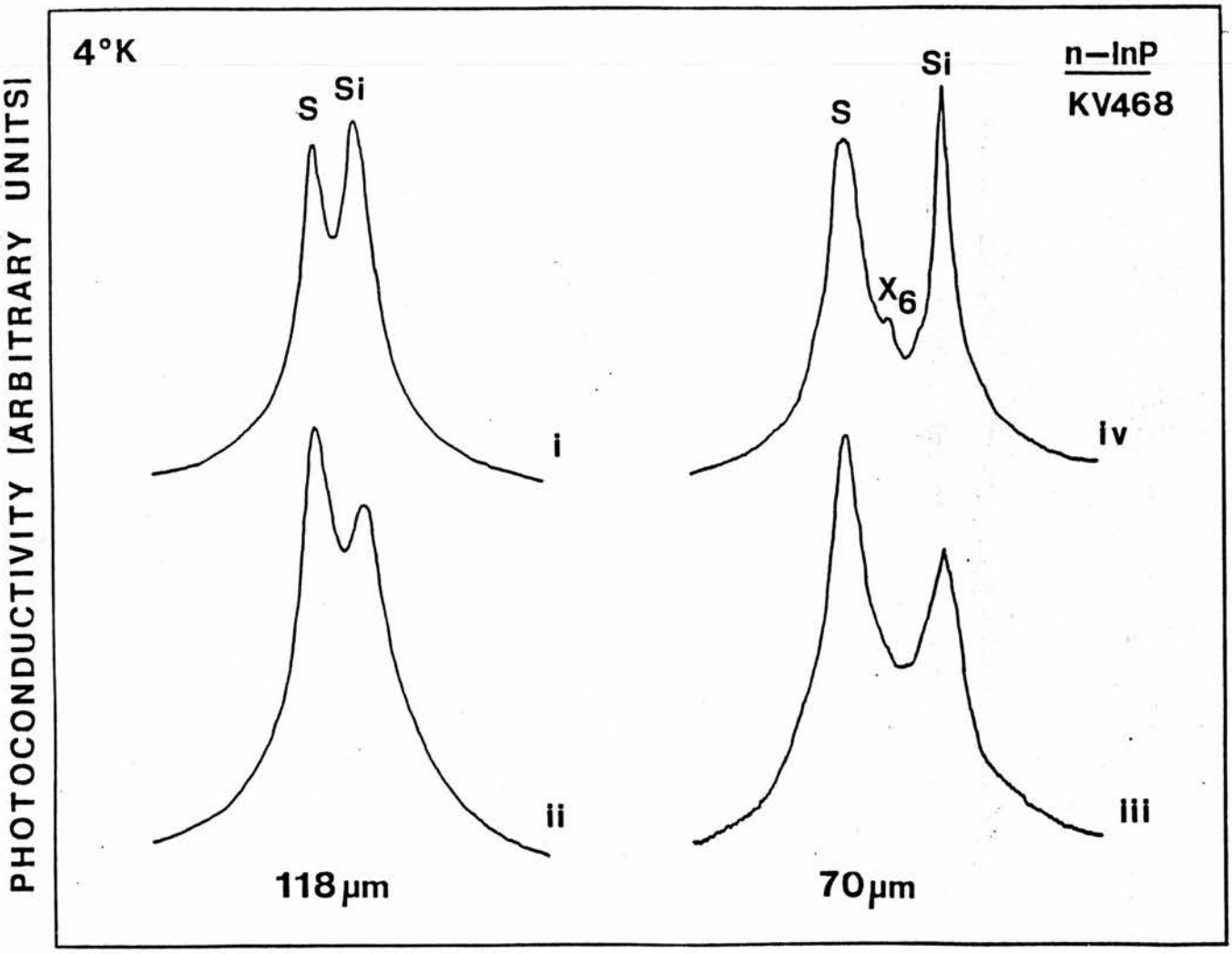

Figure (4.4) The effect of removing about half of the epitaxial layer by etching for a VPE sample (KV468). The recordings are for photoconductivity against magnetic field. (i) and (ii) are taken at a laser wavelength of 118μm without band-gap illumination; (ii) is taken after etching and shows that the Si line has been reduced by almost a factor of two with respect to sulphur; (iii) is identical to (ii) except that a laser wavelength of 70μm is used. The Si line narrows and increases its intensity with respect to (iii) and donor X_6 appears between the Si and S lines.

Figure(4·5)

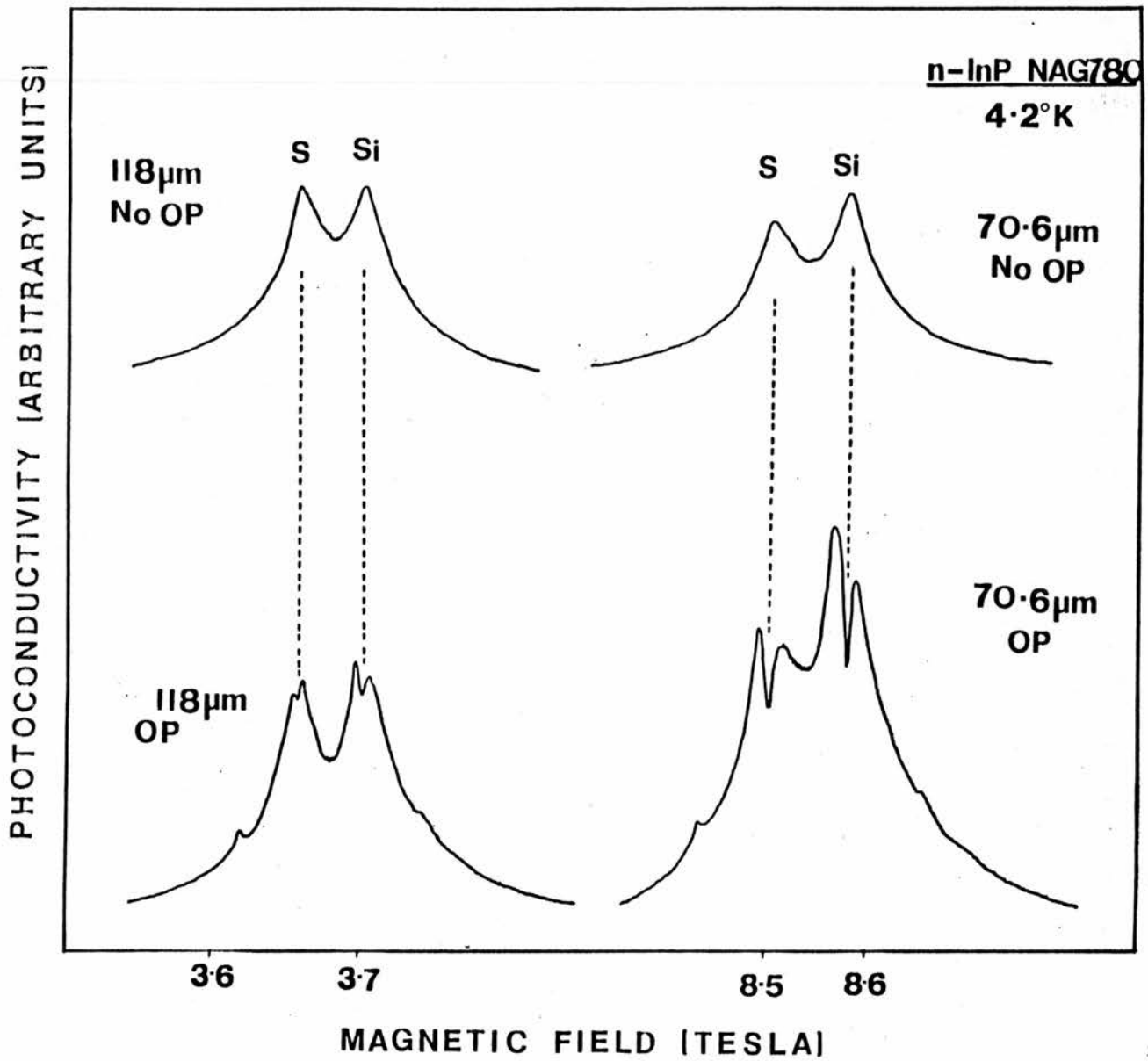

Figure (4.5) Shows the effect of band-gap radiation at two different magnetic fields. The sample is high quality n-InP sample, NAG780, displaying photoconductivity against magnetic field. Peak inversion is clearly illustrated by the splitting of the S and Si peak with the addition of band-gap illumination (OP).

Figure(4·6)

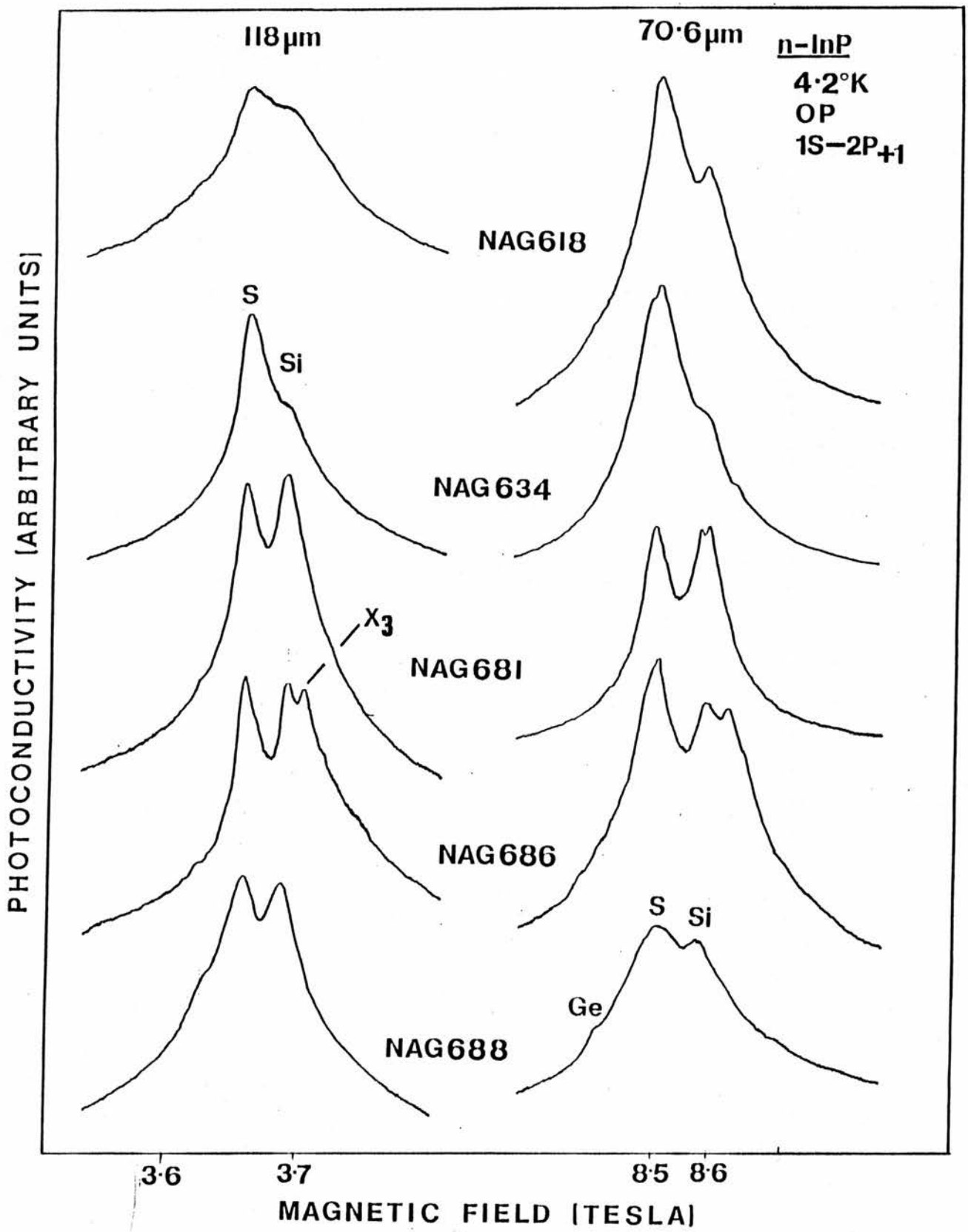

Figure (4.6) Displays a series of recordings for five NAG n-InP samples, with mobilities ranging from 50,000 to 100,000cm^2/VS. Photoconductivity against magnetic field is plotted at two wavelengths 118μm on the left hand side and 70μm on the right hand side of the diagram, at 4.2^{o}K. S and Si commonly appear, donor X_3 is evident on sample NAG686.

OP- intrinsic illumination.

Figure(4·7)

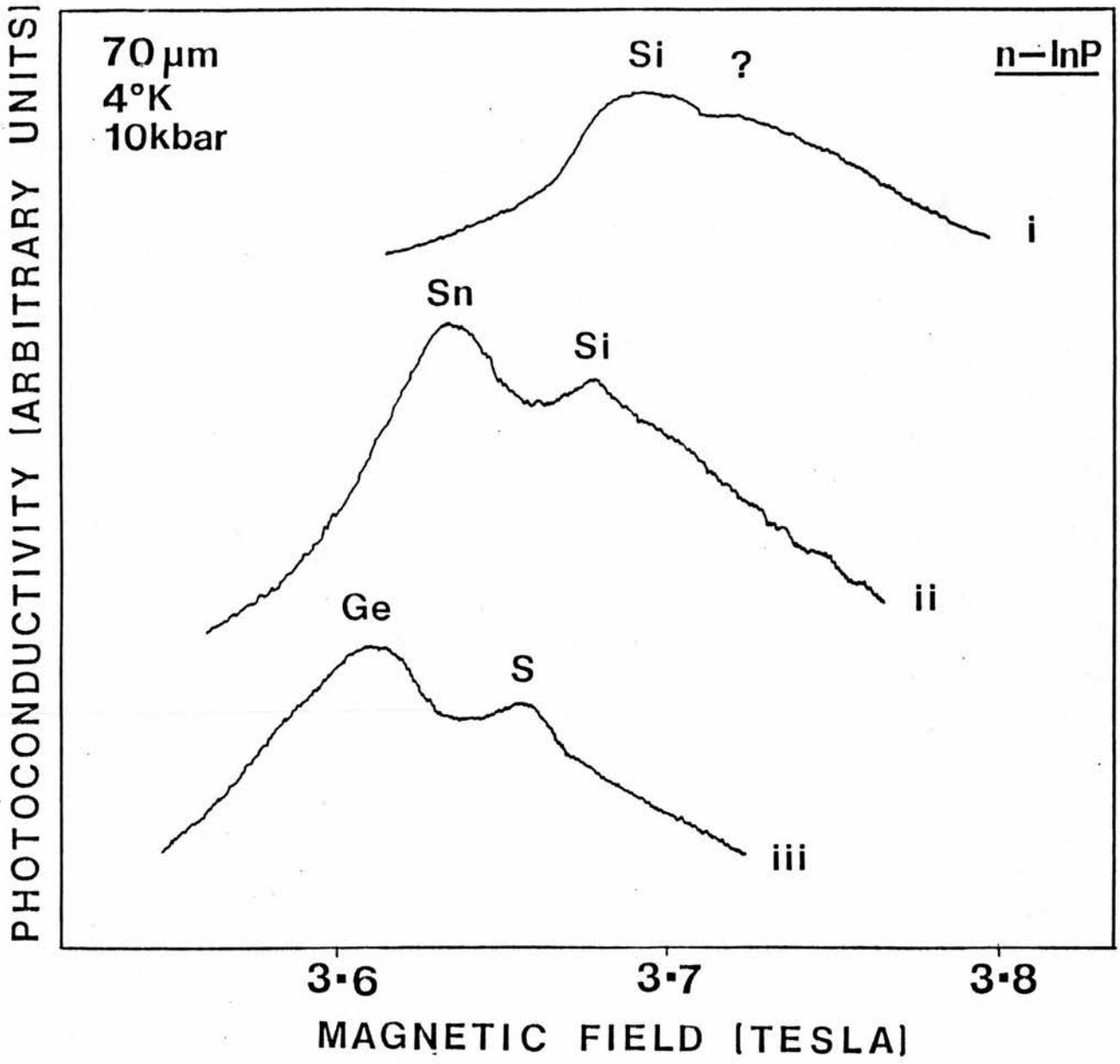

Figure (4.7) Plots the photoconductivity against magnetic field for three doped n-InP samples, with a large hydrostatic pressure applied.

i) a silicon doped sample (QM273)

ii) a Sn-doped sample (NAG852)

iii) a Ge-doped sample (NAG853).

Figure(4·8)

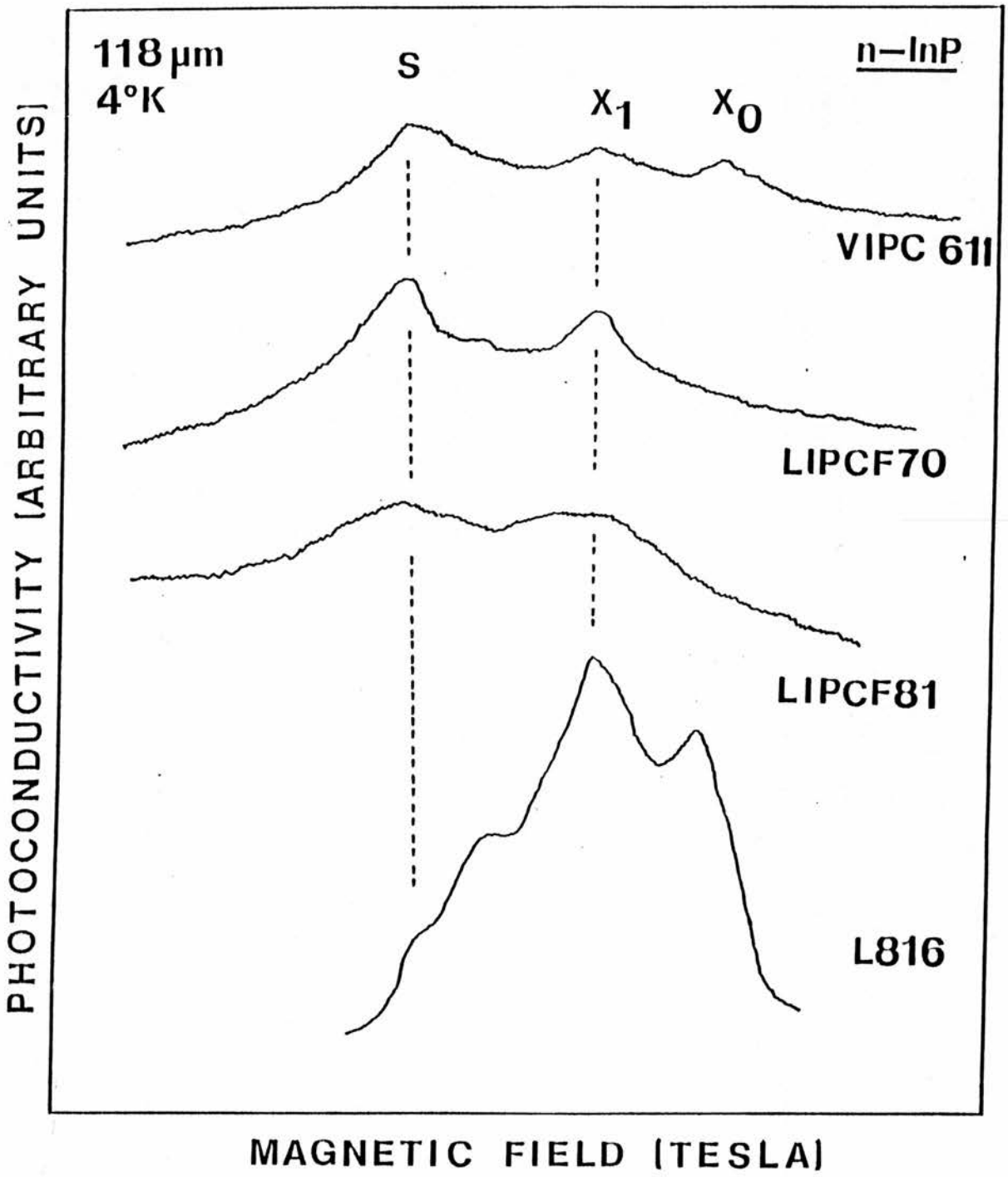

Figure (4.8) The photoconductivity against magnetic field for four bulk grown samples. Apart from sulphur, all the samples contain one or more very shallow donor species.

Figure(4·9)

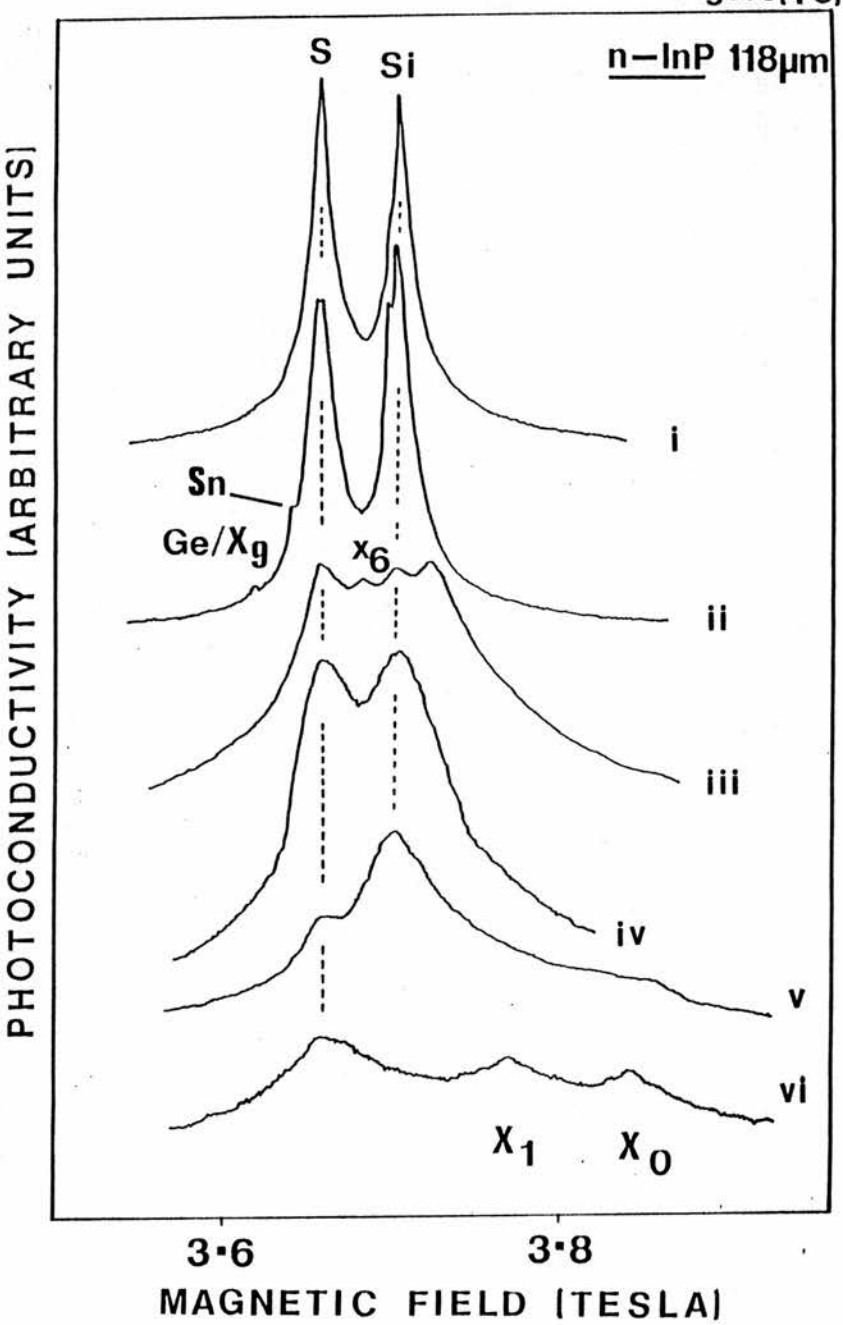

Figure (4.9) Displays the photoconductivity against magnetic field for a variety of n-InP prepared by different growth kits. All the recordings are taken with a laser wavelength of 118um

i) the highest mobility sample NAG762 without band-gap illumination. Only S and Si are observed at 4.2K, without band-gap radiation.

ii) the same sample with band-gap illumination (Ge and Sn donors are observed on the low field wing of the S donor).

iii) a VPE sample (CR276), shows an additional two major donors X_6 and X_3, compared to the VPE sample above.

iv) a MOCVD sample prepared at RSRE Malvern (807A).

v) a MOCVD sample prepared at Thomson-CSF (T127), displaying an additional residual donor X_0, in comparison to the above grown MOCVD material.

vi) a bulk sample grown by LEC (VIPC 611), this sample contains very shallow donors X_1 and X_0

Figure 4.10

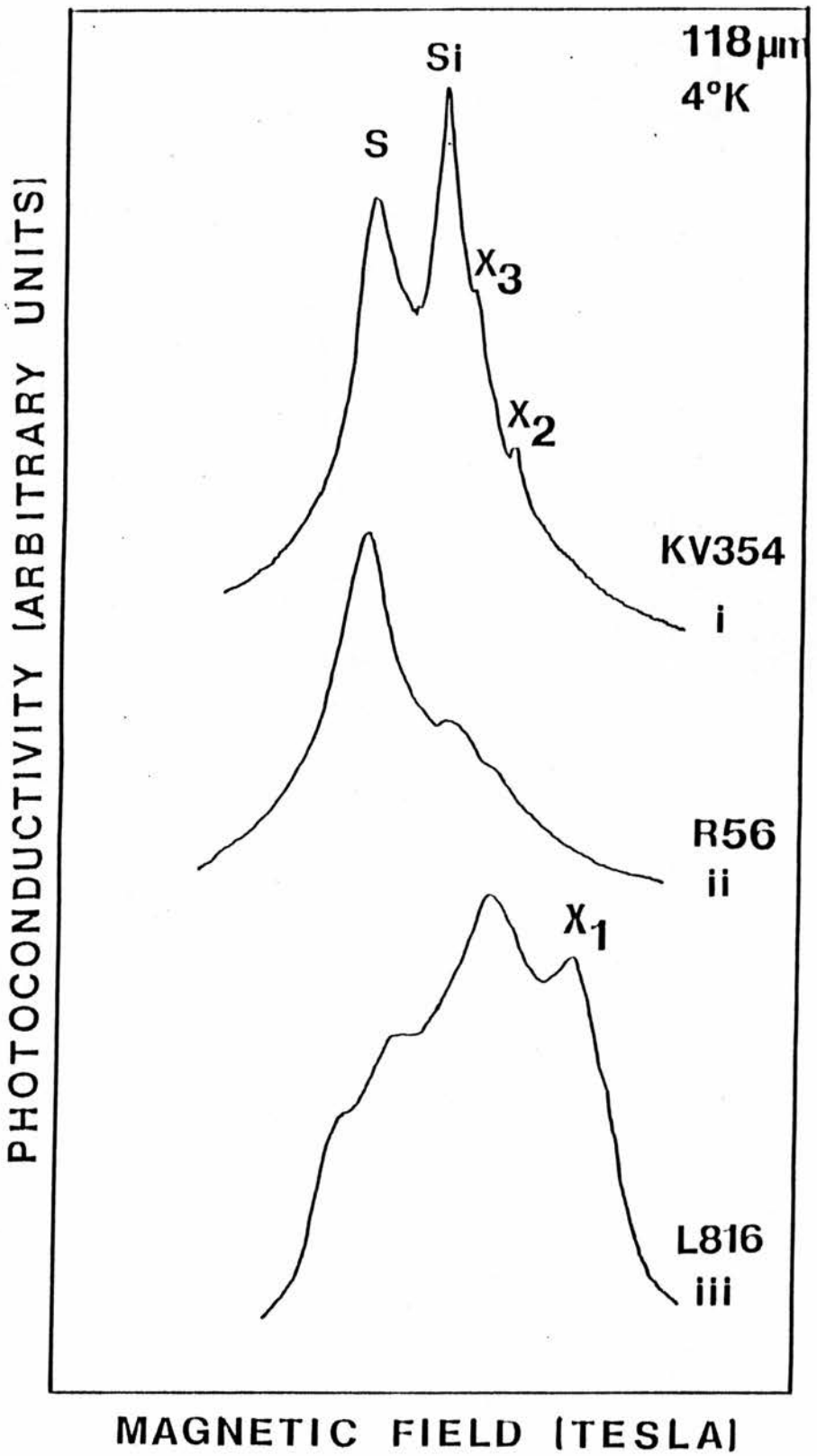

Figure (4.10) Photoconductivity against magnetic field of the $1S-2P_{+1}$ transition at 118μm, for

i) a VPE sample very lightly doped with Si.

ii) an undoped VPE sample grown from a different reactor.

iii) a bulk sample (L816).

Figure 4.11

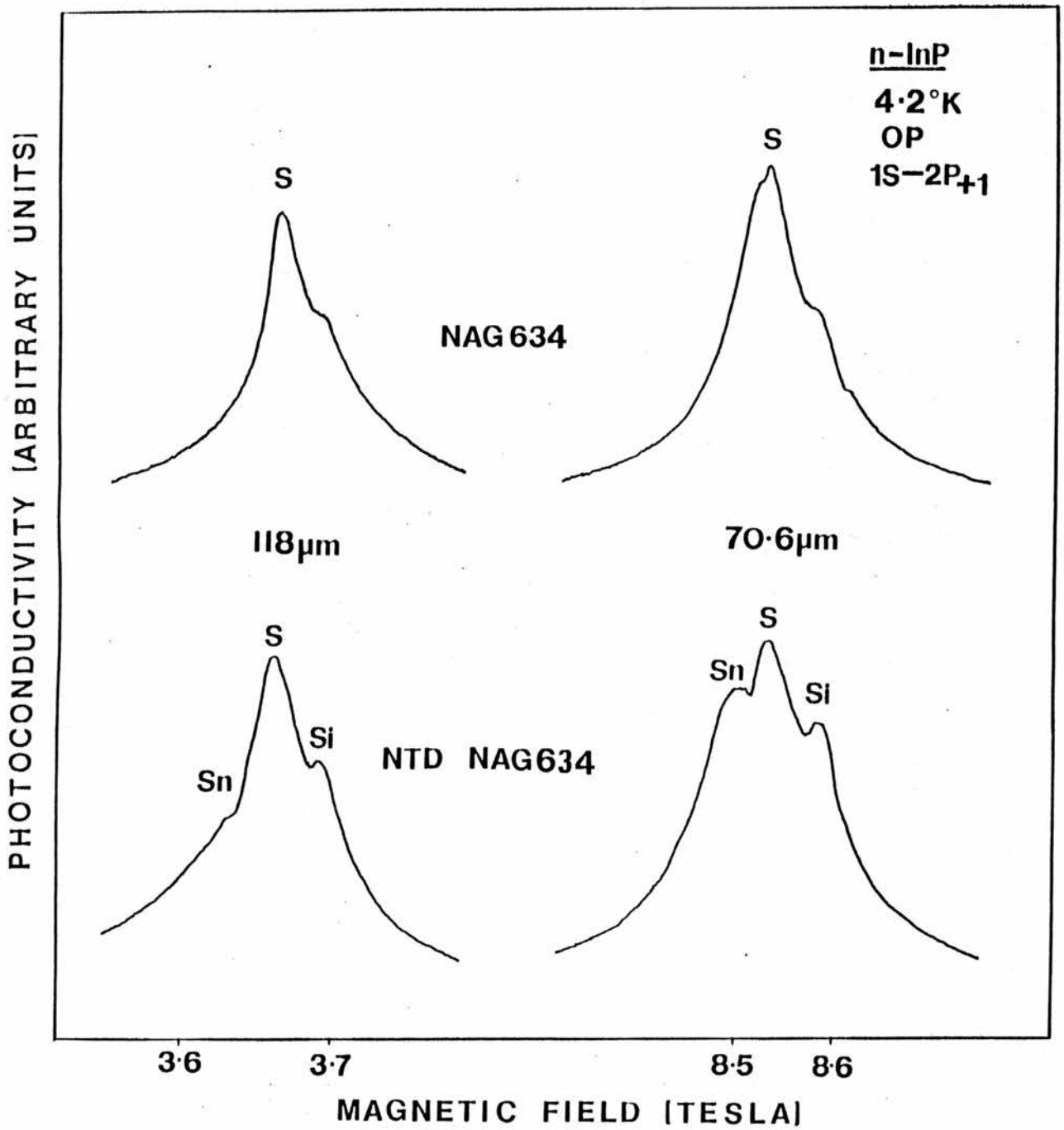

Figure (4.11) n-InP NAG634 was subject to a flux of thermal neutrons. In and P lattice atoms are neutron transmutated into Sn and S donors respectively. Structure due to Sn is apparent on the low field wing of the S peak. There is no change in the S peak intensity, since few additional S donors are produced in the process.

Figure(4·12)

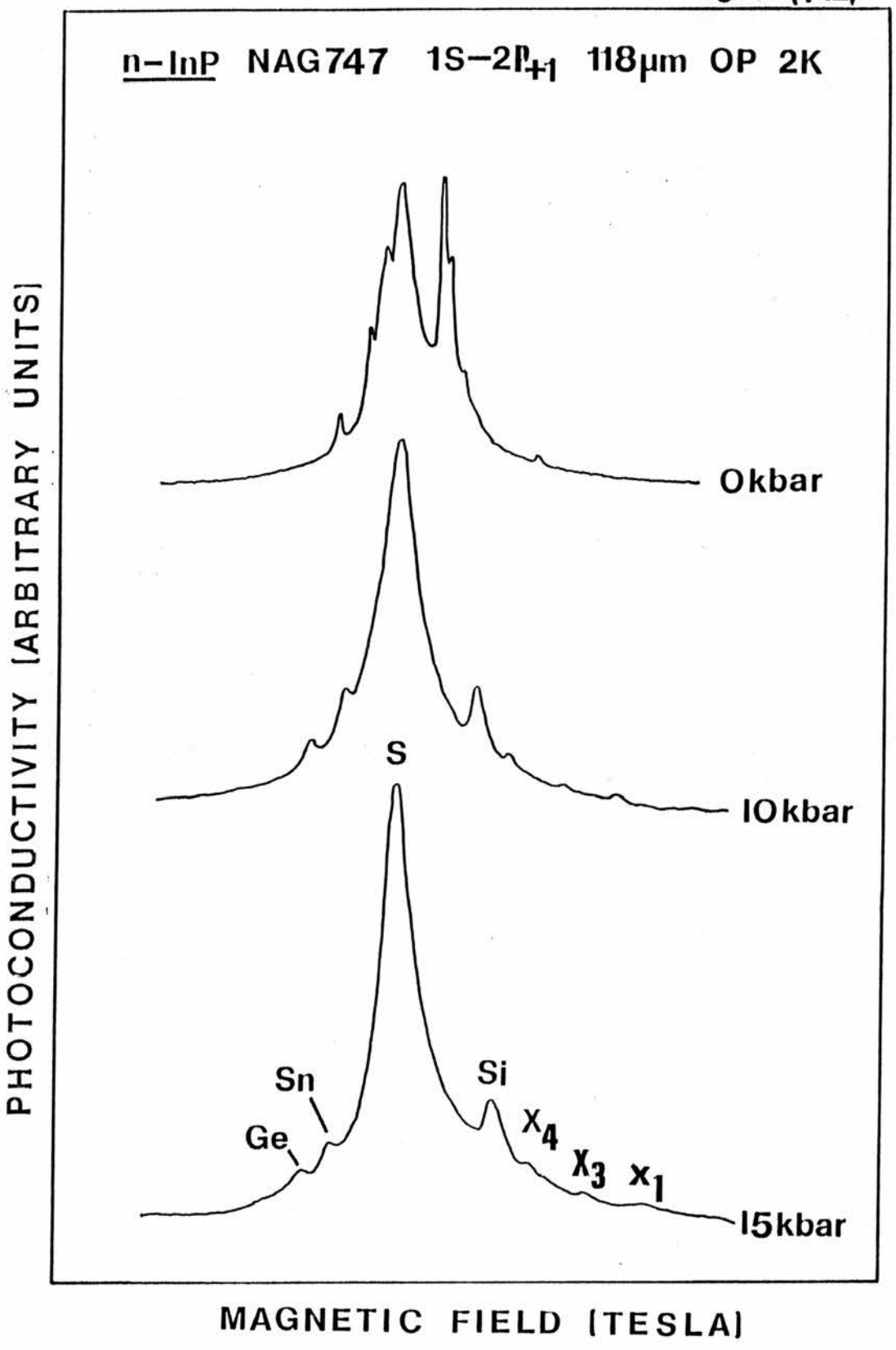

Figure (4.12) displays the effect of pressure on the central-cell structure of a high purity InP sample, NAG747. Considerable narrowing is achieved with increasing pressure as well as increased central-cell splitting. The figure plots photoconductivity against magnetic field for a wavelenght of 118μm at 2K.

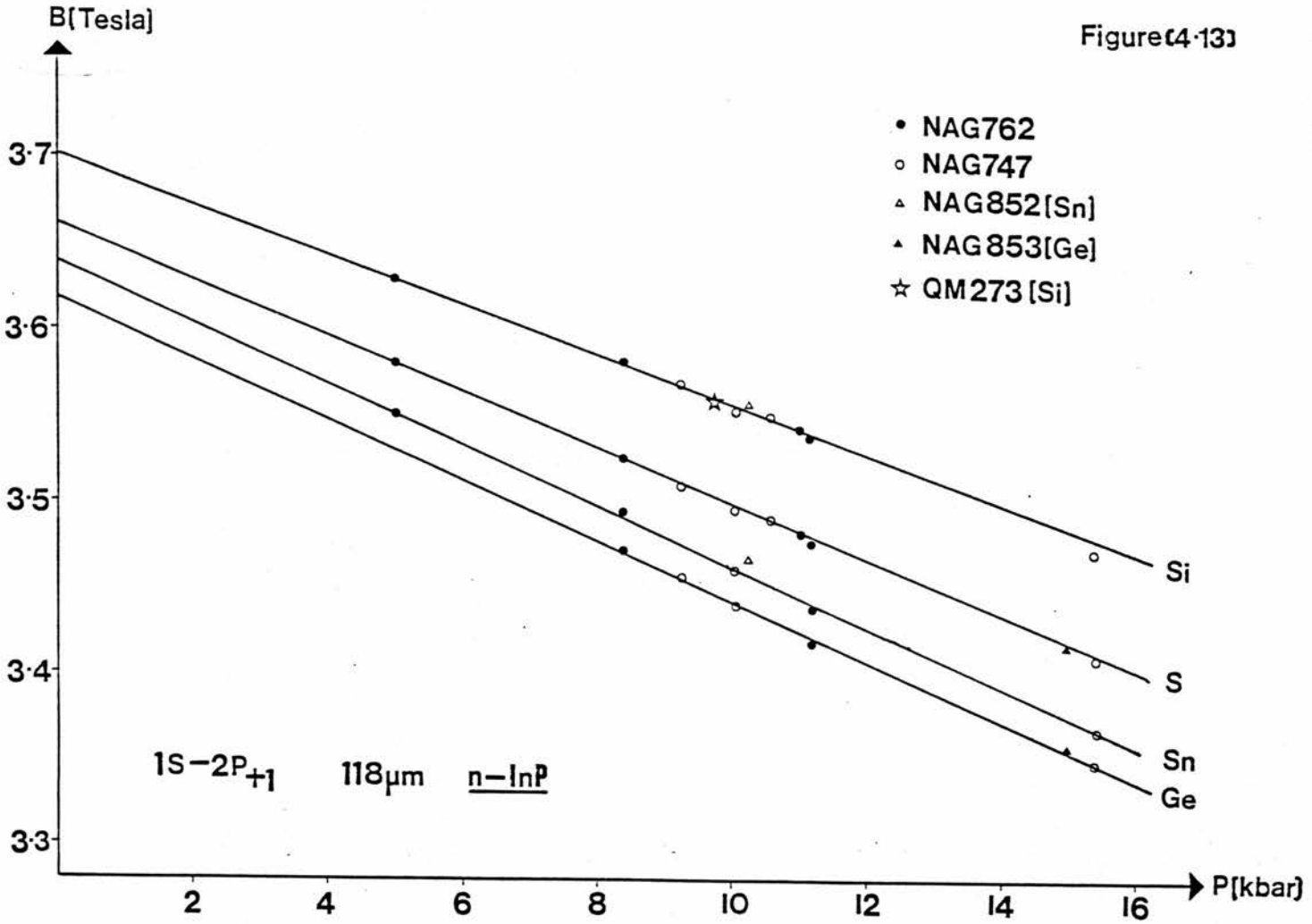

Figure (4.13) Plots pressure P (kbars) against magnetic field B (Tesla) of the $1S-2P_{+1}$ transition at 118μm for various samples of InP.

CONCLUSIONS TO CENTRAL-CELL IDENTIFICATION

The combination of FIR spectroscopy and high magnetic fields is proven to be an extremely powerful, if not unique, method for studying the chemical nature of shallow donor impurities in high quality epitaxial layers. The observation of fine central-cell structure on the 1S-2P Zeeman split transitions provides the only reliable method of identifying the chemical nature of residual contaminants in III-V semiconductors. The study of central-cell components by means of back-doped crystals, has enabled the main central-cell peaks in the photoconductivity response to be provisionally determined. However, it is extremely difficult to introduce a small quantity of specific dopant into the melt, due to line width restrictions. Systematic peak shifts often occur due to asymmetric broadening by ionised impurities. These effects have to be taken into account in the final analysis, since the donor peak does not usually coincide exactly with the peak position in undoped samples. Experiments on additional back-doped crystals are essential for further progress in donor identification. Neutron transmutation doped samples only provide limited information of the chemical identity of certain peaks, because this method is confined to introducing to only two donors for the case of GaAs and one in InP. There is good agreement between the results obtained by NTD and back-doped experiments. Hydrostatic pressure was used as a very useful additional experimental parameter for improving the spectral quality and increasing the central-cell splittings.

FIR experiments are performed on some of the highest purity GaAs grown to date. These methods include LPE, VPE, MOCVD and MBE. The photoconductivity spectra from a range of high purity samples, prepared by several different methods and grown in a variety of

laboratories are compared. Also, the central-cell spectra are compared to spectra published by various groups around the world and show remarkably similar structure. It is found that high purity GaAs always contained the same central-cell 'signature' with samples grown by the same technique, irrespective of the source of samples, but that different growth methods produce a different set of donors. This implies that the residual contaminants are intrinsic to each particular growth system, regardless of the location or starting materials used. Otherwise, 'random' impurity peaks would be expected to appear dependant on contamination from different manufactured source materials, which presumably would have a different set of trace impurities.

Most of the residual donors in GaAs have been provisionally identified using back-doped or NTD samples. Central-cell peaks are observed corresponding to Ge, S, Sn, Si, Se, and Pb/Te , carbon may also be present. Ge (or possibly a Ge associated complex) has been confirmed as responsible for the deepest donor; also the peak position of the Se donor has been positively identified using NTD experiments. There appears to be a trend of increasing electro-negativity with the depth of the donor (with the exception of Si), in accordance with the theory of Hjalmarson et al (1980).

Up to twelve central-cell components have been established in the photoconductivity response of high purity InP. Although, the possibility of peak inversion cannot be ruled out as the cause of some of the structure, it is clear that there are more components than can be accounted for by likely substitutional impurities. Only four donors have been identified; in order of decreasing central-cell shift these are Ge, Sn, S, and Si respectively. The two deepest donors

observed in high quality undoped material are identified for the first time as Ge and Sn using back-doped samples, and the identity of the Sn donor is confirmed by a NTD experiment. Otherwise, most of the residual donors remain unidentified in high purity InP. GaAs and InP appear to have remarkably similar central-cell structure; this consistency is not too surprising considering both crystals are grown by somewhat similar equipment. Thus on electro-negative trends, Pb, Te donors would be expected to be shallow in InP. However, InP samples grown by the same machine can produce additional peaks not reproducible from sample to sample, suggesting contamination from source materials, e.g X_3 and X_6 in the NAG series of InP. Furthermore, the incorporation of impurities appears more irregular in InP, giving rise to inconsistent S/Si profiles from sample to sample grown by the same machine. Thus, it is clear from the FIR data that the growth conditions for InP are far less finely controlled compared to GaAs.

A number of factors determine the capability of achieving high purity GaAs and InP epitaxial layers, which are of course, ultimately dependant on the initial purity of the starting materials. In addition to basic reactor cleanliness and leak integrity, other factors which can influence the incorporation of impurities include, the mole fraction and III/V ratio, the substrate and source temperature, and also the substrate quality and orientation. Most of these above sources of contamination appear to be under control. There is evidence that atmospheric and environmental pollution can introduce impurities, but the main source of contamination appears likely to be from the starting materials. It has not yet been possible to correlate the electrical behaviour of layers of InP with specific impurities in the starting material. Although growth technology for

InP is not as highly developed as for GaAs, it is clear from the limited data available that many of the same considerations apply to both materials. Sulphur contamination appears in all growth systems with both InP and GaAs, and is usually the major donor, except for MOCVD GaAs where X_3/Ge is often the largest component. Silicon commonly appears due to the reaction of H_2 and HCl with the quartz tubing generally used in growth kits, but can be incorporated as either an acceptor or donor, depending on the growth system. Out of ten possible donor candidates, it is obvious that not all the central-cell peaks belong to simple 'hydrogen-like' substitutional impurities. Excluding S and Si, there are only six other likely donor possibilities, since Po does not occur naturally and oxygen is thought to bind much deeper. Thus at most a total of eight central-cell peaks would be expected. Why are there more peaks observed? Peak inversion certainly could explain the occurrence of a few peaks, but it is unlikely that more than two peaks could be attributed to this photoconductivity anomaly. A plausible argument could be that donor complexes form, with a binding energy comparable to a shallow donor. Since the evidence does not necessarily indicate simple substitutional donors, particularly in the tentative observation of the metastability behaviour of X_3/Ge and the Si donor not following the electro-negative trend. However, two additional peaks might be expected to occur in doping experiments, one associated with a donor complex and another with a simple substitutional donor. This has not yet been detected although the two peaks would likely to be of different amplitudes and consequently the second might not be detectable in doping experiments. This would be the case only if the states were accidentally $\sim$5meV below the Γ-minimum. If the complex had a net positive charge it would behave the same as a substitutional donor. NTD experiments of n-InSb by F.Kuchar (1984) produced two additional

peaks, thought to arise from complexing of Sn donors with defects. Also, a pair of peaks appeared in Se and Te doped InSb (Kuchar 1984), which is not expected on the basis of a simple substitutional donor.

The spectral resolution is not limited by the technique itself, but rather by the crystal quality due to broadening from ionised impurities. Several techniques are employed to a varying degree of success to either reduce the effect of the electric fields produced by ionised impurities or by increasing the central-cell splitting. To obtain better data, other possibilities include

i) Since inhomogeneous broadened linewidths are closely related to the total concentration of donors an approach would be to obtain higher purity samples.

ii) larger magnetic fields would be useful by increasing the central-cell splitting.

iii) larger pressures would be beneficial in increasing central-cell shifts and improving spectral quality. Furthermore, non-Γ like donor states could be introduced into the forbidden gap, like X_3 in GaAs. This would largely increase the resolution. Unfortunately, the present technology of the pressure cells limits the pressure to 15kbar. In InP, the problem is even more acute, and much larger pressures are required just to enable the deepest states to cross. Some assistance would be provided by the application of a uniaxial stress along the (111) crystallographic direction in addition to the hydrostatic pressure. This would move a set of L minima further down into the forbidden gap. Strained layered samples can introduce large uniaxial stresses and hence split the L minima, but these samples are

difficult to obtain. Ternary compounds of GaAs and InP could adjust the band structure sufficiently to introduce more states into the gap. However, these materials are of insufficient quality to observe central-cell structure on the Γ-states.

iv) The selective excitation of carriers into impurity states by below band gap dye laser radiation might narrow the lines as it should be possible to reduce the inhomogeneous broadening.

v) The production of a suitable laser wavelengtn to look at the $1S\text{-}2P_{-1}$ transition in InP.

Although a considerable amount of work has gone into establishing the chemical nature of residual impurities and in identifying the source of contamination, there are still many uncertainties in interpreting the results for even the highest quality GaAs. Obviously much more work remains to be done before absolute identification of the donor contaminants can be obtained with certainty , especially for InP. However, significant information has been obtained from the present study and the results and conclusions pose many interesting new problems. In spite of the complications and uncertainties, photothermal ionisation spectroscopy provides one of two methods that can identify the electrically active donor species present in nigh purity epitaxial III-V compound semiconductors.

INTRODUCTION TO D^- STATES

Negatively charged ions make their presence known in many branches of physics. For example, oxygen in the earth's ionosphere is capable of forming negative ions. The continuous emission spectra from the sun and other stars are seriously infuenced by the presence of negative ions in their outer atmospheres. Also, the formation of negative ions in electric discharges can greatly effect the behaviour of the cavity.

In solid-state physics negatively charged impurity defects occur. A neutral donor described by effective mass theory, (D^o), can trap a second electron to form a negatively charged ion (D^- state). Similarly, a neutral acceptor can bind an extra hole to form a A^+ state e.g Ga^+ in Ge. Due to the valence band degeneracy, the Pauli exclusion principle allows a further two holes to bind, giving rise to a triply and quadruply occupied acceptor state e.g Be^+ in Ge and Cu^+ in Ge, respectively (Haller 1983). In addition, 'deep' D^- states e.g O^- in GaP (Jaros 1983), and the existence of interstitial negative ions (Mayer and Spaeth 1984) have been predicted.

The H^- ion has been studied for many years without the effect of a magnetic field, and is now well understood. In this case, the H^- ion is known to have exactly one bound state, a singlet, with a very small binding energy (5.5% of the Rydberg). In a magnetic field, the H^- ion binds additional states, including triplets. However, the behaviour of H^- centres in a magnetic field is much less understood. This particular problem also occurs in astrophysics, where hydrogen ions in the atmosphere of white dwarf stars are subject to intense magnetic

fields i.e 10^5T. D^- states in semiconductors provide a suitable medium in which to study the perturbing effects of a magnetic field on the H^- ion wavefunction. Apart from the above case, an understanding of D^- states is beneficial for several other reasons. The correlation and disorder effects involved in the metal-insulator transition are not yet fully understood. D^- states provide a valuable insight into donor concentration effects that occur around this transition. Also, D^- states have considerable potential of providing an extremely fast infrared detector.

Lampert (1958), first predicted the existence of D^- states in semiconductors. However, experimental evidence identifying D^- states remained elusive for many years until Dean et al (1967) attributed a feature in the photoluminescence of Si, to the existence of a D^- state. Further extensive work by the Japanese (for example, Natori and Kamimura 1978, Taniguchi et al 1978) also attributed very shallow spectral features to D^-. To date, the evidence for D^- states is restricted mainly to the elemental semiconductors, Si and Ge, where mass anisotropy of the degenerate conduction bands complicates the interpretation of the problem. The existence of D^- centres has also been put forward in two single valley semiconductors, CdS (Cohn et al 1971) and CdMnSe (Ichiguchi et al 1983), but little was known about their material properties. Most of the above experiments were performed with samples with unknown compensation ratios, and at zero magnetic field where there is a host of interexcited state transitions with a similar binding energy. All the authors neglected to consider interexcited state transitions as a possible alternative explanation of their results. For example, at zero field the interexcited state n=3-4 transition of the neutral donor occurs at 4.9% of the Rydberg. This transition could easily be mistaken for the D^- to conduction band

transition since both transitions require similar experimental conditions to populate either state , also both transitions are expected to produce fairly broad lines. Furthermore, there is no simultaneous observation of D^{o}, and D^{-} states which would enable each feature to be independently identified. Thus the experimental evidence to date, cannot be taken as demonstrating the existence of D^{-} centres conclusively.

The identification of D^{-} states is reconsidered more carefully, taking into account any possible mis-interpretation and simplifying the problem by only considering semiconductors with a simple conduction band minimum centred at k=0. Hence the D^{-} state will be directly analogous to the H^{-} ion. GaAs and InP are studied as alternatives to Si and Ge for the following reasons.

i) Chemical shifts of the donor states are extremely small, even the 1S ground state of the neutral donor , is typically 1% of the binding energy.

ii) The conduction band is particularly simple as the band edge is located at the centre of the Brillouin zone, non-parabolicity and anisotropy are small. Consequently, the interpretation of the spectra should be straightforward.

iii) The intermediate magnetic field range ($\gamma \sim 1$) can readily be obtained, where the magnetic field has a significant perturbation on the D^{-} wavefunction.

High sensitivity FIRPC techniques are employed in a similar manner to those described in chapter 2, with the exception that much longer wavelengths are required to observe D^{-} states. The optically-pumped laser system provides wavelengths ranging from 300μm to 1.2mm, obtained by using different organic gases in the FIR laser.

Longer wavelengths up to 3mm are produced from solid-state IMPATTS. Magnetic fields were obtained from either a 13T superconducting magnet at St Andrews or for larger fields a 24T Hybrid magnet was available at Grenoble. Spectroscopic transitions are observed as the magnetic field is swept through the various magneto-optical transitions. The experimental conditions required to populate D^- states are very similar to excited state transitions i.e low temperatures and optical pumping.

It is not possible to create a D^- state from an isolated neutral donor by simple photon absorption. Consequently D^- states are metastable. However they can recombine with D^+ states. To populate D^- states, electrons are either thermally or optically excited into the conduction band, where they recombine with neutral donors to form D^- states. Direct photoionisation of one of the D^- electrons into the conduction band is responsible for the change in conductivity, giving rise to the observed D^- structure. This is in contrast to the 2-stage 'photothermal ionisation' mechanism that gives rise to the D^o interexcited state spectra. Also, cyclotron resonance is often observed on the same spectra but is due to the 'cross-modulation' process. Interexcited state transitions, transitions from the ground state of the neutral donor, cyclotron resonance of free carriers and the D^- transition can all be observed simultaneously. However, the D^- state is identified by its characteristic shape and independent behaviour with various experimental parameters. The effect of temperature and electric field bias on the D^- provides a valuable insight into the generation-recombination processes. The D^- to N=0 conduction band transition can be followed to large magnetic fields where the Zeeman splitting is larger than the Coulomb energy i.e $\gamma = \hbar\omega_c / 2R^* > 1$. Hydrostatic pressure is used as an additional

parameter. This thesis describes the first unambiguous spectroscopic identification of D^- states in various uncompensated samples of VPE,LPE and MOCVD GaAs and VPE InP.

CHAPTER 5

THEORY OF D^-

BOUND STATES OF THE D^- ION IN A MAGNETIC FIELD

Consider a neutral donor binding a second electron, giving rise to a D^- state. In GaAs the problem becomes completely analogous to the H^- ion, since the conduction band is at the centre of the Brillouin zone, is isotropic and non-parabolicity is small. The binding energy of the D^- ion is defined as the least amount of energy required to excite an electron into the conduction band without changing the spin configuration. The orbital wavefunctions of the H^- state are either symmetric (singlet state) or anti-symmetric (triplet state) upon exchange. Applying a magnetic field B along the z-direction, the D^- states are labelled by M_L, the component of total orbital angular momentum along z, $M_L=0,-1,-2...$

Only the ground singlet state binds at zero field. In a magnetic field, many more states, including both triplets and additional singlets bind. Two states are of particular interest:

i) $M_L=0$ ground singlet level, this is the only bound state that exists at zero magnetic field.

ii) $M_L=-1$, triplet state, which binds only in a finite magnetic field and is physically very different from the singlet state.

In atomic units, the Hamiltonian for a hydrogen atom in a magnetic field is;

$$H = -\nabla_i^2 - 2/_r + \gamma L_z + (\gamma^2/\rho^2)/4. \qquad (5.1)$$

For the H^- ion in a magnetic field the following Hamiltonian is used,

$$H = H(r_1) + H(r_2) + 2/r_{12} + \gamma M_L \qquad (5.2)$$

where $r_i = (\rho^2 + z^2)^{1/2}$ is the displacement of electron i from the proton.

$$r_{12}=[r_1 - r_2]$$
$$\rho^2=x^2 + y^2$$
$$\gamma=\hbar w_c/2R^*$$
$$w_c=eB/m^*$$
$$R^*=m^* e^4/2\varepsilon^2\hbar^2$$

The binding energy of the D^- ion is given by

$$E_B(S,\gamma) = E_D(\gamma) + \gamma - E_D(S,\gamma) \qquad (5.3)$$

where $E_D(\gamma)$ is the ground state eigenvalues of the neutral donor and $E_D(S,\gamma)$ is the eigenvalue of (5.2). The eigenvalues are obtained using variational techniques which give a higher than true value, hence the binding energies calculated provide a lower bound to the true binding energy.

5.1 SINGLET GROUND STATE (M_L)=0

Various trial wavefunctions describing the ground singlet state in a magnetic field have been proposed with a varying degree of success. Two treatments are described, which probably provide the most successful interpretation of the problem, and give a clear insight into the binding mechanisms.

The Chandrasekhar wavefunction ψ_{CH} (1977) is a simple and reasonably accurate function describing the binding energy of a H^- singlet ground state at zero field. It has the form

$$\psi_{CH} = (1 + Cr_{12})[\, u(r_1)\, U(r_2) + U(r_1)\, u(r_2)\,] \qquad (5.4)$$

where $u(r_i) = \exp(-ar_i)$ is the wavefunction of the inner orbital, and

$U(r_i) = \exp(-br_i)$ is the wavefunction of the outer orbital.

This wavefunction represents approximately an unscreened hydrogen atom plus a very loosely bound outer electron. The electrons are in ground state 'hydrogenic-like' orbitals and are kept apart by the correlation factor

$$(1 + Cr_{12}).$$

Chandrasekhar found that the optimum values are a=1.075, b=0.478 and C=0.312 and these give a binding energy of $0.0518R^*$. This compares with the 'exact' zero field value of $0.0555R^*$ obtained by Vitramo (1976), but his calculations are tedious.

Larsen (1979) generalises equation (5.4), to take into account the influence of a magnetic field. His trial function, analogous to that adopted for a neutral hydrogen atom in a magnetic field, is of the form.

$$\psi^{(k)} = \sum_{n=0}^{k} C_n (\, z_1^{2n} + z_2^{2n}) \exp\, [-\delta (r_1^2 + r_2^2)\,]\psi_{CH}.$$

Thus, the zero-field wavefunction ψ_{CH} is multiplied by a factor producing overall shrinkage $\{\exp\, [-\delta(r_1^2 + r_2^2)]\}$ as well as the factor $C_n(z_1^{2n} + z_2^{2n})$ which describes the compression of the wavefunction in the plane perpendicular to the magnetic field.

The variational energies are calculated by minimising

$$E^{(k)} = \langle \psi^{(k)} | H | \psi^{(k)} \rangle / \langle \psi^{(k)} | \psi^{(k)} \rangle \qquad (5.5).$$

This gives binding energies $E^{(0)}$, $E^{(1)}$, $E^{(2)}$...
An extrapolation procedure allows values of $E^{(k)}$ at effectively infinite k to be calculated (Larsen 1979).

Natori and Kamimura (1977) replace the zero-field functions in equation (5.4), U(r) and U'(r) by the following functions

$$U_B(r) = [(2\pi)^{3/2} a_\perp^2 a_\parallel]^{-1/2} \exp\{-(x^2 + y^2)/ 4a_\perp^2 + z^2/ 4a_\parallel^2)\}$$
$$U'_B(r) = [(2\pi)^{3/2} a'^2_\perp a'_\parallel]^{-1/2} \exp\{-(x^2 + y^2/ 4a'^2_\perp + z^2/ 4a'^2_\parallel)\}$$

$U_B(r)$ and $U'_B(r)$ describe the inner and outer electron respectively under the influence of a magnetic field. The binding energies are again calculated variationally and are plotted together with the spatial extension of the inner and outer D^- wavefunctions. The inner orbital of the D^- ion (corresponding to the two parameters a and a') has almost the same extension as the orbital in a neutral donor ground state, irrespective of the strengtn of the magnetic field. The transverse extension a of the outer orbital which is perpendicular to the magnetic field is almost the same as the cyclotron radius, being independent of the value of γ, while the longitudinal extension a' of the outer orbital is considerably extended by the Coulomb repulsion between the two electrons. The above treatment is not appropriate for weak fields, since at zero magnetic field the trial wavefunction does not give a bound D^- state because a' goes to infinity as γ goes to zero.

In the high field limit, $\gamma >> 1$, the magnetic field dominates both the inner and outer orbital. Equation (5.2) becomes approximately separable and in this limit the trial wavefunction of the form is used.

$$\{ 1 + \mathrm{Ctanh}^2 [E (z_1 - z_2)]\} \{\exp [-K(z_1^2 + \alpha^2)^{1/2} - B(z_2^2 + \alpha^2)^{1/2}] + (1 \leftrightarrow 2)\} \exp \{-1/4\, \gamma' (\rho_1^2 + \rho_2^2)\}.$$

The consideration of correlation is very important for obtaining good energies at $\gamma >> 1$, just as it is at $\gamma = 0$. For $\gamma = 100$, the binding energy is $1.44R^*$; but if C is set equal to zero i.e no correlation, the best binding energy is only $1.14R^*$.

5.2 BOUND STATES INDUCED BY A MAGNETIC FIELD (TRIPLETS)

A neutral donor can bind an extra electron, for $M_L<0$ in a magnetic field. A different approach is required to describe these states which are otherwise unbound at zero field.

Natori and Kamimura (1977) describes the triplet state by the anti-symmetric wavefunction.

$$\Psi^t(r_1,r_2) = (1 + Cr_{12}) \, [u(r_1)U''(r_2) - U''(r_1)u(r_2)].$$

u(r) is the s-like inner orbital of the ground state wavefunction, and

$$U''(r) = [2^{5/2}\pi^{3/2} \, a_\perp'^{\,2} \, a_\parallel' \,]^{-1/2} \rho \exp(-i\phi) \, \{-([\rho^2/4a_\perp'^{\,2}) + (z^2/4a_\parallel'^{\,2})]\}.$$

This function describes the outer p-like wavefunction.
As before, the binding energy is minimised by a variational procedure. Natori and Kamimura predict that the triplet state of a D^- ion becomes bound only above a critical magnetic field. However, this description is expected to be unsuitable especially for the inner orbital at weak fields since the trial functions (5.7) and (5.8) essentially describe high-field orbitals.

Larsen (1979) approaches the problem more carefully in the weak field regime, by considering the polarisation effects induced on the inner neutral donor atom by the outer excited electron of the D^- ion. The outer electron, being only weakly bound, travels in an extended orbital around the central atom. A dipole moment is induced since the outer electron polarises the inner neutral donor. The ground state

wavefunction for a D^o atom polarised by an electron fixed at a large distance r, from the centre of the atom is given by Dalgarno and Lynn (1957);

$$[1 - (r_2^2/2 + r_2)\cos Q_{12} / r_1^2] \exp(-r_2);$$

r_2 being the displacement of the electron in the D^o atom. Larsen uses this function to approximate the ground state wavefunction of the donor atom, polarised by an electron at r_1 and in a weak magnetic field

$$X(r_1,r_2) = [1 + C_1 z_2^2 + P(r_1,r_2)\cos Q_{12}] \exp[-\delta r_2^2 - Kr_2];$$

where $\cos Q_{12} = \underline{r}_1 \cdot \underline{r}_2 / r_1 r_2$ and

$$P(r_1,r_2) = C(1/2\, r_2^2 + r_2) / [(r_1^2 + b)(Br_2^2 + 1)].$$

The parameter C controls the strength of the polarisation, while b cuts off the polarisation at small separations; $\exp(-\delta r_2^2)$ accounts for the compression of the D^o atom by the magnetic field.

The orbital wavefunction for the outer electron is

$$\Phi_{M_L}(r_1) = \exp(iM_L\phi_1)\rho_1^{|M_L|}\exp[-1/4\,\gamma'\rho_1^2 - K(\rho_1^2 + a z^2)^{1/2}];$$

where γ', K, and a are variational parameters, and ϕ_1 is the polar angle of r_1 in circular coordinates. This wavefunction is similar to the lowest Landau level wavefunction.

The trial wavefunction is a combination of the inner and outer wavefunctions i.e

$$\Psi_M(r_1,r_2) = \Phi_M(r_1)\ X(r_1,r_2).$$

The binding energies are obtained by varying the appropriate parameters and then minimising the energy variationally.

The outer electron of the M_L=-1 triplet state of the D^-, even at the lowest fields, is similar to a hydrogen-like atom in a high magnetic field. On the other hand, the inner orbital at low fields is essentially comparable to the low field hydrogen orbital. Thus the variational calculation must be flexible enough to encompass both regimes.

Although, the M_L = -1 level is the stronger of all the states besides M_L=0, singlet states fail to bind at this level.

For M_L < -1

i) both singlet and triplet states bind

ii) the triplet binding energy increases more rapidly than the singlet.

iii) for a given magnetic field, the singlet-triplet splitting is smaller for M_L = -3 than for M_L = -2 and so on.

iv) at constant magnetic field, the binding energy of either state decreases as M_L increases.

In conclusion, Larsen's theory is expected to be most accurate in the small and intermediate magnetic field regime i.e up to γ = ~1, and Kamimura's theory more appropriate in higher fields. In the next chapter, a comparison is made between Larsen's theory and experimental

data on D^- in GaAs.

CHAPTER 6

D^- STATES IN GaAs

6.1 EXCITED STATES

At low temperatures i.e 4.2K, weak lines appear in the photoconductivity spectra by applying FIR radiation with photon energies insufficient to excite electrons from the ground state of the donor impurity i.e λ>300μm. These lines are attributed to transitions originating and terminating on excited states of the shallow donor. At 4.2K, there is a small but significant electron population in excited states. Thus conduction by photothermal ionisation occurs in a similar manner to excitation from the ground state (as described in section 2.2). The study of excited states has certain advantages over measurements involving transitions from the 1S ground state to excited states, for example

i) it becomes possible to observe transitions of states having the same parity as the ground state i.e excited S states, for which the electric-dipole transition from the ground state is parity forbidden.

ii) perturbations due to central-cell effects are small. Even s-like excited states have considerably smaller central-cell shifts than for the 1S ground state.

Possible deviations from EMT include.

i) Chemical shifts are negligible except for excited S-states. Even for the latter they are very small.

ii) Band non-parabolicity principally influences the M_z=+1 states since these are associated with the N=1 Landau level at high fields. Corrections are expected to be negligible at low field and small at high field.

iii) Polaron effects are expected to be small in GaAs, but are more

significant in polar material e.g CdTe.

iv) Stark shifts from neighbouring charged impurity atoms are small but are usually larger compared to the ground state.

Consequently, excited states are generally well described by EMT.

Variational calculations of the magnetic field dependence of excited D^0 states in small steps of field were performed and an interpolation procedure was developed by Makado (1984), so that the exact field position for any transition involving states with principal quantum number's n=2,3,and 4 could be determined. Nearly thirty different interexcited state transitions have been observed and most of them have been positively identified. All of the allowed n=2-2 and 2-3 transitions have been identified within the energy range available, but none of the observed transitions corresponded to the predicted D^- position. The most prominent features in the spectra of the excited states lines are two groups of lines labelled A and B, with A to lower field and B to higher field of the cyclotron resonance (CR). The cyclotron resonance is observed using the 'cross-modulation' process where the absorption of radiation changes the sample mobility and hence the conductivity. Most of these particular transitions originate from n=2 excited state;

$A_1(2S\text{-}2P_{+1})$, $A_2(2P_o\text{-}3D_{+1})$, $A_3(2P_{-1}\text{-}3S)$, $B_1(2P_{-1}\text{-}3D_{-1})$, $B_2(2P_{-1}\text{-}2S)$ and $B_3(2S\text{-}2P_{+1})$.

6.2 D^- STATES IN GaAs

An exhaustive investigation of interexcited state transitions of shallow neutral donors in many different III-V and II-VI compound semiconductors failed to reveal any evidence for the existence of D^- states even though the experimental conditions required to populate either state are very similar (Skolnick et al 1977, Gershenzon et al 1974). This negative result was probably due to residual contaminating acceptors introduced into the semiconductor material during crystal growth, hence suppressing low compensation, which is an important parameter for D^- formation. However, recently a series of high quality VPE GaAs samples was received from P.Colter at the Wright-Patterson Avionics Laboratory. Several of the crystals are exceptionally uncompensated, in particular RR98 (N_A/N_D=0.05), since before growth, the Ga source was pre-baked to eliminate undesirable compensating Zn acceptor impurities. In RR98 an indication of the lack of compensation occurs in a plot of mobility against temperature, where in addition to the expected normal peak at 50K another peak at 10K arises due to the rapid fall in the number of ionised sites as the carriers freeze-out onto donors (Colter et al 1983).

Initially, the study was confined to two extremely high mobility and low compensation VPE GaAs samples, RR98 and S1. S1 has a higher liquid nitrogen mobility (μ=200,000 cm^2/V sec) than RR98 (μ=160,000 cm^2/V sec), but it is thought that the compensation ratio is slightly less in the former. Typical spectra at long wavelength of both samples show very sharp cyclotron lines , together with numerous very narrow interexcited state transitions. Figure (6.1), displays two recordings, the top trace is sample S1, at 742μm and the bottom is

sample RR98, at 944μm. Central-cell structure is observed with optical transitions originating/terminating on the 2S interexcited state, giving an indication of the crystal quality i.e 'B' lines. Also, the intensity of the B lines can be very strong indicating considerable accumulation of carriers in excited states. If intrinsic illumination is applied to the sample, a broad but strong peak appears just below 4T with 742μm radiation (figure 6.1); this feature is attributed to a transition from the D^- state to the lowest Landau level. The recordings give a misleading impression of width in energy because of the strong magnetic field dependence upon wavelengtn. Nevertheless, the total width of the D^- transition at 1.2mm is more than two orders of magnitude greater than the width of the cyclotron resonance. At present, it is not clear if the observed width of the D^- transition is a consequence of the direct photoionisation process or whether it is due to broadening of the D^- states themselves, giving rise to a band. A problem now arises in the analysis of the lineshape, since if the former were correct , the threshold for ionisation would be better described by a half-intensity point or the high-field 'edge' of the observed transition. In contrast, the peak of the observed line in the latter case would give a more accurate comparison with theory. Certainly, broadening is probably a combination of both effects; which one dominates remains to be resolved. Each of the different shallow dopants are expected to contribute to the overall convolution of the observed D^- transition, since no central-cell structure has been observed on any of the D^- spectra. In addition, unresolved interexcited state transitions are expected to also influence the general lineshape of the observed transition. A further complication arises under extreme excitation by electric field bias, strong intrinsic illumination and pumped Helium temperatures i.e 2.0K, the D^- to N=0 landau level develops a

double-humped structure believed to be caused by the formation of complexes of D^- and possibly D^--D^o complexes.

FIR laser wavelengths ranging from 393μm to 1.2mm are used to follow the D^- transition energy as a function of magnetic field. Experiment is compared to theory for the first time in the intermediate magnetic field range, where the Zeeman splitting exceeds the Coulomb binding energy i.e $\gamma=\sim 1$. At zero magnetic field, the binding energy of the D^- is very small and consequently the D^- is expected to be thermally ionised at 4.2K. However, a magnetic field has a large influence on the binding energy of the D^- ground state. At $\gamma=1.0$ the binding energy of D^- has increased by a factor of about 6. The D^- to N=0 Landau level transition is plotted as a function of magnetic field up to $\gamma=1.5$ using the magnetic field facility at St. Andrews. Higher magnetic fields were available at the Max-Plank Institut fur Festkorperforschung Hochfeldmagnetlabor, Grenoble, France, where a 24T hybrid magnet permits the D^- binding energy to be followed up to $\gamma=3.5$ (Figure 6.2) (see Armistead 1985). It is noticed that the experimental points are consistently lower in energy compared to theory. A substantial improvement is obtained if the 'edge' of the transition is taken rather than the peak position suggesting that a photoionisation mechanism is important for the D^- lineshape. However, a discrepancy of a few percent still remains at magnetic field values up to $\gamma\sim 1$. Beyond this value theory and experiment diverge, and the discrepancy becomes more and more pronounced with increasing field. The deviation probably results from an incorrectly chosen variational trial wavefunction.

The effect of the magnetic field on the size of the observed D^- is illustrated in figure (6.3). This figure displays the photoconductive response of sample, RR98, at 2.0K, using a solid-state IMPATT as the source of 88GHz radiation. The cyclotron resonance (CR) and the interexcited state transitions are observed. Peak X lies close to the region of the D^- to N=0 transition and also in the vicinity of the n=3-4 interexcited state transition. At such low magnetic fields, the D^- line is indistinguishable from interexcited state transitions, demonstrating the large effect the magnetic field has on the D^- binding energy. Triplet states are predicted to exist at higher fields with this wavelength of radiation, but no positive identification has yet been made. Perhaps larger magnetic fields are required before this state sufficiently binds so a transition can be observed.

At low magnetic fields ($B < 0.1T$ at 450μm), weaker structure resulting from transitions of the D^- ground state to the five higher Landau levels (N=1 to 5) is apparent (figure 6.4). The top recording is for sample RR98 with 393μm radiation, and the bottom is S1 with 458μm. Both results are taken at 2.0K and with strong optical pumping. The intensity of the D^- to N=1 Landau level transition is comparable to the cyclotron resonance. Interexcited 'A' transitions are also observed on the same spectra. The magnetic field dependence of this structure together with some interexcited state transitions is plotted against energy on a dimensionless diagram (figure 6.5). Variational calculations of the magnetic field dependence of the excited neutral donor, D^o states with principle quantum numbers n=2,3,4 were made by Aldrich and Greene (1977), and Makado (1984). At zero field, n=3-4 transitions have a very similar binding energy to

D^-. With increasing magnetic field, $A_4(3D_o-4P_{+1})$ and $A_1(2S-3P_{+1})$ remain close to the D^- to N=1 Landau level at all fields. $N(3D_{-2}-4F_{-3})$ lies close to the D^- to N=0 transition at fields up to $\gamma\sim0.1$. Transition $I_2(3D_{-2}-4F_{-2})$ (not displayed on this diagram) follows the D^- to N=0 Landau level more closely to higher fields, for example, RR98 at 570μm, I_2 appears on top of the D^- transition (figure 6.6). Under certain experimental conditions, interexcited state transitions can become large features. However, D^- states are distinguishable by their relative width, characteristic lineshape and difference in behaviour with respect to experimental parameters such as temperature, electric field bias and the amount of optical pumping.

The simultaneous detection of D^-, D^o (n=2,3,4) and the cyclotron resonance allows the dependence of the signal strength on the experimental conditions such as temperature, electric field bias and band-gap radiation intensity to be investigated. It is found that the D^- transition is strongly dependant on all of these parameters. Also, a comparison of different GaAs samples with various carrier concentrations, mobilities and compensation ratios is made. Unfortunately, not all the electrical data was available for all the samples at the time of writing, but a reasonable estimate of the sample quality and compensation ratio can be determined by comparison to spectra of samples with know electrical characteristics.

6.3 Comparison of D^- states in GaAs samples grown by different methods

After the initial study, about twelve high purity samples of GaAs were considered. Altogether, D^- states have been observed in seven different GaAs samples, grown by LPE, VPE, and MOCVD kits. This shows that low compensation material can be grown by any of the major growth techniques. Most of the samples have not been purposely grown for low compensation, but rather for high quality. However as a consequence of achieving high purity it is evident that low compensation is also obtained in some.

Figure (6.6) displays FIRPC spectra at 570μm for seven different samples of the RR series of high purity GaAs, with liquid nitrogen mobilities ranging from over 160,000 to below 100,000 (cm^2/VS), carrier concentrations of the order of $10^{14} cm^{-3}$ and compensation ratios as low as $N_A/N_D=0.05$ i.e RR98. Extensive interexcited state transitions are observed on all the spectra, even on the poorest quality sample, RR17, where the B interexcited state lines are almost as strong as the cyclotron resonance. The B lines are usually the most significant interexcited state feature and characteristically appear on all the spectra. The A lines appear below (in field) the cyclotron resonance and are generally small. The D^- to N=1 Landau level transition can appear over these A lines. I_2 ($3D_{-2}$-$4F_{-2}$) is another interexcited state of interest which appears at high magnetic fields in the region of the D^- to N=0 Landau level transition. This transition appears on top of D^- for sample RR98, demonstrating that there can be a significant excited state population, even for the

n=3-4 transitions.

All the spectra displaying D^- in this figure were obtained under similar experimental conditions at 4.2K i.e with strong intrinsic illumination, and with low electric field bias i.e ~ 0.05V/cm, except for RR96 and RR17 where the electric field bias is increased to optimise the size of the D^-, otherwise the magnitude of D^- is very small in these samples. Other samples showed only interexcited state spectra i.e RR136, RR99, and RR125, and did not display D^- structure under any circumstance. Consequently the compensation ratio is expected to be high in these these samples. D^- is clearly observed as the large broad feature at 8T in the spectra of RR98, since this sample is known to have low compensation. RR133 has also a large D^- transition indicating that the Ga source was pre-baked in a similar manner to RR98. The D^- is much less intense in RR96 (N_A/N_D = 0.29), compared to RR98, indicating that the proportion of D^- states formed, falls off with increasing compensation as expected. RR17 (N_A/N_D = 0.16) is the lowest mobility sample studied that showed D^-, and hence has fairly broad lines. It is interesting to note that although the mobility is poorer in RR17, the compensation ratio is significantly lower than RR96. D^- is only just observed under extreme experimental conditions in RR96; even then it is less than the intensity of the cyclotron resonance and B_2. D^- in RR17 under similar experimental conditions is larger than both the cyclotron resonance and the interexcited state transitions. This emphasises the point that low compensation is an important parameter in D^- formation. Also compare D^- spectra in very high quality but higher compensation sample S1 to the spectra of the low compensated sample RR98. However, high quality samples are essential, otherwise the donor-acceptor recombination increases exponentially as tunneling between adjacent states occurs as

exp(-R/a), and hence destroys the formation of D^- states. (R is the distance between each state, and a is the Bohr radius).

Comparing RR98 with RR125, there is little difference in mobility or crystal quality, but there is no D^- line observed in RR125. High quality samples does not necessarily mean low compensation. As a general rule , D^- is most apparent in high quality samples with liquid nitrogen mobilities greater than 100,000 cm^2/V sec and compensation ratios less than 0.1.

Figure (6.7) compares the D^- spectra for three high purity GaAs samples grown by VPE(S1), MOCVD(S2), and LPE(E351) methods, irradiated with 570μm at 4.2K, illuminated with band-gap radiation and similar electric field bias. Interexcited state transitions appear on all the spectra. One of the 'B' lines and the cyclotron resonance provide reference field positions to compare the D^- peak positions. It is clearly noticed from this figure that the peak position of the D^- to N=0 Landau level transition does vary significantly for different growth techniques. The D^- peak position in sample S2 (MOCVD grown GaAs), is consistently at lower magnetic fields with respect to the same transition in LPE (E351) or VPE (S1) samples, using the same laser wavelength. The D^- peak positions align well with samples grown by the same growth technique. This systematic D^- peak shift is explained by the different central-cell 'signatures' obtained by each growth technique. X_3/Ge is the deepest of the shallow donors, and is by far the major contaminant in MOCVD grown GaAs, with shallower donors X_2/S and X_1/Si in much less abundance (see figure 3.9). Thus it is reasonable to expect that D^- states are more likely to form on Ge donors. By comparison, the central-cell spectra of typical VPE and LPE grown GaAs, X_2/S and X_1/Si or even shallower donors are the

dominant residual contaminants (see figure). Although, no central-cell structure has been resolved on the D^- transition, this result suggests that the relative donor concentration significantly distorts the overall D^- lineshape. This is displayed schematically in figure (6.8), where the 'weight' of the deeper donor X_3 in MOCVD grown GaAs 'pulls' the D^- peak position to lower field, compared to the smaller contributions from shallower donors X_1 and X_2. Since the energy of the D^- transition varies slowly as a function of magnetic field , at large magnetic fields i.e ~8T, the central-cell splitting is spread out in energy, in a similar manner to the $1S-2P_{-1}$ transition observed by 302μm radiation (see section 3.2). Thus it may be possible to observe a splitting at sufficiently large magnetic fields. This result is consistent with the long wavelength photoconductivity spectra observed by Taniguchi and Narita (1977). Their experiments consisted of applying uniaxial stress to Sb- and As-doped Ge crystals at very low temperatures i.e 0.38K. Uniaxial stress is applied in order to reduce one of the four Ge conduction band minima with respect to the other three, thus simplifying the analysis to a single valley problem. A chemical shift is observed by comparing the D^- spectra of the two doped samples, and the threshold energies obtained are slightly larger than had been expected by the simple analogy to a free H^- ion. The shift between D^-(Sb) and D^-(As) is much smaller than for the case of neutral donors. This is due to the extended outer orbital of the D^- state, which is approximately four times the radius of a neutral donor at zero field. Consequently at zero magnetic field, the D^- ion in GaAs would be almost unaffected by the local potential of the donor, since the D^0 chemical shifts are of the order of 1% of the binding energy of the neutral donor. At low magnetic field the D^- peak position agrees well with theory i.e chemical shifts are negligible, hence the D^- state behaves almost like

an ideal 'H^-' ion. However, central-cell effects become more important with increasing magnetic field, due to the compression of the D^- wavefunction. This could explain some of the discrepancy between theory and experiment. However, a substantial and increasing deviation still remains at high fields.

6.4 D^- AS A FUNCTION OF ELECTRIC FIELD BIAS

As D^- states, D^o interexcited state transitions and the cyclotron resonance (CR) are all observed simultaneously on the same spectra, this gives an opportunity to study the electron dynamics of the system. D^- is studied as a function of electric field bias and provides a valuable insight into the generation-recombination processes.

Large electric fields can be generated across the sample, entering into the region of 'warm' electron conditions, where the excited electron has an effective temperature T_e, higher than that of the lattice temperature T_l. Ohm's law ceases to be obeyed in the 'warm' electron regime, as the electrons are accelerated by the electric field and are unable to return easily to equilibrium with the lattice. The warm electron coefficient β is defined by the relation

$$\mu = \mu (1 - \beta E^2)$$

where μ is the carrier mobility, and β is proportional to the constant, a, which denotes the degree of electron heating defined according to the formula

$$T_e - T_l = aE^2$$

The density of D^- states is estimated with a knowledge of the generation and recombination mechanisms. Initially, the concentration of electrons in the conduction band , in steady state conditions i.e 4.2K, is typically $10^8 - 10^{10} cm^{-3}$ due to the finite temperature of the system and black-body radiation from warmer parts of the dewar. Carriers are generated by photoionising some of the donors into the conduction band with probability G^o, either by irradiating the sample

with laser radiation (10μm from CO_2) or by applying band-gap illumination provided by the optical pumping unit. Recombination of carriers occurs to excited states of positively charged donors ,D^+, with a capture cross-section σ^+ or are trapped, with capture cross-section σ^o by neutral donors ,D^o, forming D^- centres. Excitation into the conduction band is now possible by applying a suitable laser radiation wavelength. Recombination with D^+ centres, via excited states, creates an additional neutral donor (figure 6.9).

The experimentally determined cross-section is defined as

$$\sigma = 1/(T \langle v \rangle N)$$

where $\langle v \rangle$ is the mean carrier velocity.

T is the carrier lifetime.

N - density of donors.

The density or D^- states without direct neutralisation or band-gap illumination at low temperatures is of the form (where $N_D >> N_A$) (Norton 1976)

$$N_{D-} = N_D/ (2 + \sqrt{g}) - N_A/2$$

N_D - number of donors.

N_A - number of acceptors.

Hence the concentration of N_{D-} is a direct function of g, since N_D and N_A are constant for each particular sample. The importance of low compensation can be seen from this expression. Parameter g is described by

$$g = \sigma^+ G^-/\sigma^o G^o.$$

σ^+ - recombination of the charged donors.

σ^o - recombination of the neutral donors giving D^-.

G^- - generation out of D^-.

G^o - generation out of D^o.

For low electric field bias (D^- in Si) , $\sigma^+ = 6.6\ 10^{-11} cm^{-2}$ (Norton 1976), $\sigma^o = 7\ 10^{-14} cm^2$ (Brown 1970)

G^-/G^o is determined by the photoionisation cross-section of the D^o and D^-. A comparison with the photoionisation cross-section of H^o and H^- is used instead, since no measurement of the D^- photoionisation cross-section has been made. The ratio of generation rates G^-/G^o is found to be 1.2 (Norton 1976). This gives $g \sim 10^3 - 10^4$ for a low electric field bias. This expression predicts very substantial concentrations of D^- centres. However, direct neutralisation by either donor-acceptor or $D^- - D^+$ recombination governs the build up of D^- states.

At higher electric fields, the Coulomb attractive recombination cross-section σ^+ is reduced by several orders of magnitude to $g \sim 10 - 100$, compared to low field. The reduction in σ^+ is explained as follows.

Consider a simple model (neglecting the effect of a magnetic field). At a small electric field bias, an electron excited from a neutral donor into the conduction band is counter-balanced by the creation of a new positive donor ion ,D^+. Recombination occurs either through the excited states (σ^{-+}) or via D^- states (σ^{-o}) (Figure 6.9). Non-equilibrium conditions are necessary otherwise the generation of carriers will equal the recombination and only recombination through the excited states will occur. This condition is satisfied by applying a sufficiently large electric field bias.

The velocity of electrons is directly dependant on the applied electric field bias. If a low bias is applied to the sample, recombination of carriers at positively ionised donor sites is reduced due to the strong electric field dependence of the attractive Coulomb potential. Compared to the neutral donor impurities which are relatively independent of field to first order at capturing high velocity electrons. Furthermore, negatively charged D^- ions will tend to repel any on-coming electrons, consequently the state is relatively stable to impact ionisation. Due to the reduced (D^+) recombination, less neutral donors are formed. At moderate bias, the recombination cross-section (σ^+) compared to (σ^-) is reduced by about two orders of magnitude i.e recombination to excited states is weak, hence the D^- population is enhanced. This process continues with increasing bias until an optimum value is reached.

At higher electric fields, impact ionisation of the D^- centres occurs, creating neutral D^o states, plus an electron excited into the conduction band which will eventually recombine with a D^+ state. Excited state transitions can reappear on the spectra, if the onset of impact ionisation is at larger electric fields than for D^-, i.e if the impact ionisation cross-section is smaller than D^-. This indeed happens, $B_2(2P_{-1} - 2S)$ re-appears on the spectra with very high electric fields, as the magnitude of D^- becomes smaller, but disappears again at the highest bias fields (figure 6.10).

The effect of increasing the electric field bias is demonstrated in figure (6.10). 570μm laser radiation is incident upon the sample, RR98, and the magnetic field is kept stationary at the D^- peak position, while the electric field bias is applied linearly to the

sample. The ratio of the maximum voltage to applied voltage is displayed on the horizontal axis, and the photoconductivity response of the D^- transition is recorded on the vertical scale. A flat response i.e ohmic behaviour, occurs at low electric field bias, indicating that generation and recombination of carriers cancel. Increasing the bias further, a sharp increase in the D^- intensity occurs. A maximum point is reached, corresponding to the onset of impact ionisation, where upon any further bias increase effectively kills D^- formation, since the high velocity electrons impact and destroy the state. A similar picture occurs for interexcited state transition, B_2, but since the cross-section is smaller for this state, impact ionisation happens at higher bias.

Direct comparison of the relative populations of electrons in different states can be misleading. For example, besides the electric field dependence, the magnitude of the D^- transition is further enhanced by the magnetic field with respect to the relative size of the B lines, since the D^- binding energy is a stronger function of magnetic field than D^0. At longer wavelengths, the magnitude of the D^- transition is expected to be smaller since the binding by the magnetic field has a lesser effect and the critical impact ionisation energy moves to lower electric field. Hence, more interexcited state transitions should re-appear after the D^- impact ionises.

The photoconductivity spectra of n-GaAs E351 with 570μm at 4.2K and with strong optical pumping is shown in figure (6.11). This diagram clearly illustrates the change in the electron population between the cyclotron resonance, interexcited states and the D^- transition, as the electric field bias increases. The magnitude of the cyclotron resonance is taken as reference, and is compared to the

relative intensity of the D^- transition ($I(D^-)/I(CR)$). With increasing bias the magnitude of the D^- line grows with respect to the cyclotron resonance, reaches a maximum, then decreases. Also, the interexcited state B lines decrease in intensity, until they almost disappear. At higher bias B_1 disappears completely, but B_2 revives, in accordance with the differing impact-ionisation cross-section.

Figure (6.12) plots the electric field bias, E(V/cm), against the relative D^- to cyclotron resonance intensity $I(D^-)/I(CR)$, for a LPE GaAs sample, E351, irradiated with 570μm laser radiation at 4.2K. With increasing electric field bias, the magnitude of D^- increases, reaches a maximum and decreases, as explained previously. With band-gap illumination the intensity of D^- grows to more than twice that of the cyclotron resonance. Hydrostatic pressure is applied to the LPE sample, and as far as this discussion is concerned, its effect is to further deepen the D^- ground state. D^- grows up to five times the intensity of the cyclotron resonance with the addition of pressure and optical pumping. Order of magnitude differences, in relative intensity between the D^- and cyclotron resonance have been observed at optimum conditions (for example, see figure 6.13).

It was suspected that the FIR laser system and/or the white light optical pumping unit could possibly be providing some additional heating of the carriers. With no filters a small amount of CO_2 radiation (~10μm) is incident upon the sample, in addition to the FIR radiation. The CO_2 radiation should provide additional free carriers in the conduction band, hence the size of the D^- should increase. The magnitude of D^- with respect to the cyclotron resonance increases slightly with CO_2 radiation compared to the case where the CO_2 is filtered out using quartz.

The FIR laser provides output powers in excess of tens of mW on certain lines. An experiment was conducted to see what effect, if any, attenuating the FIR laser power had on the size of D^-. Different thicknesses of PTFE were placed in front of the FIR beam. The attenuated FIR radiation produced an identical spectrum to that with no attenuation except that the signal decreased compared with the back-ground noise level. The experiment was repeated with band-gap illumination present in addition to the FIR attenuated beam, and again no change was observed. It is concluded that laser system and optical pumping unit do not contribute to any significant carrier heating. Any heating effects are simply a direct function of the electric field bias.

6.5 TEMPERATURE DEPENDENCE OF D^- STATES

At very low impurity concentrations, neutral donors (D^o) are far apart from each other. The formation of an isolated D^- state requires an electron to be either thermally or optically excited from the valence band or from a neutral donor into the conduction band, and subsequent trapping by a neutral donor site. Two distinct energy levels arise from the D^o and D^- states, corresponding to the lower and upper Hubbard bands respectively. At larger concentrations the states cannot be regarded as being completely isolated. Interaction of D^- states with themselves or with neighbouring neutral donors are expected to occur as the D^- population increases, giving rise to complex related effects. This situation is achieved by a reduction in the temperature. An estimate of the relative increase of the D^- population produced by reducing the temperature from 4.2K to 2.0K can be obtained. The density of D^- centres, situated at energy E from the bottom of the conduction band, is given by

$$n_{D-} \propto \exp(-E/kT)$$

Consider, a D^- state in a magnetic field of strength γ=1.0. The D^- binding energy is $0.3R^*$ = 1.7meV, giving

$$n_{D-}(2.0K)/n_{D-}(4.2k) = 174/1$$

Thus, by pumping on the liquid helium, the temperature can be reduced from 4.2K to 2.0K, increasing the D^- population by several orders of magnitude.

Consider figure (6.14), an uncompensated GaAs sample, RR98, is subject to 570μm laser radiation, at 2.0K and no optical illumination. The D^- transition appears as a small broad feature at ~7.5T. At lower fields, other broad structure appears. This additional structure is

believed to be caused by complexing of the D^- state with neighbouring states. Also, the size of the D^- to N=1 transition is significantly larger than the cyclotron resonance (CR), indicating considerable excitation into the conduction band. There is little evidence of interexcited state transitions on this spectra. The D^- to N=1 line is approximately four times broader at half width than the cyclotron resonance. Transitions from D^- to higher Landau level states are also clearly observed. Applying intrinsic illumination, both the D^- and complex increase substantially in magnitude with respect to the cyclotron resonance. The overall intensity of the D^- to higher Landau level transition can exceed the size of the cyclotron resonance. Also, the D^- to N=1 transition narrows by almost 50% and decreases in height with respect to the cyclotron resonance. The D^- to N=1 transition can be a large feature compared to the D^- to N=0 transition if the electric field bias is chosen correctly, since this state appears to have a larger impact ionisation cross section compared to D^- to N=0 Landau level. 'A' interexcited state transitions become apparent in the vicinity of the cyclotron resonance. A negative photoconductivity response of the 'B' interexcited states is also observed. The complex peak position moves substantially to higher fields and the overall shape changes slightly with increasing illumination. 'Peak-pulling' is a possible explanation for this effect but it is noticed that the D^- peak remains at the same field position. Hopping conduction between the different complex states could be a more likely explanation, since this mechanism is expected to occur at the onset of D^- band formation. However, this diagram is perhaps misleading, since the electric field bias is reduced with increasing intrinsic illumination.

Figure (6.15), displays the effect of increasing the electric field bias at constant band-gap illumination, for a low compensation MOCVD GaAs sample, S1, irradiated with 570μm laser radiation and at 2.0K. At the smallest electric field bias, a large broad complex (C) is observed on the low field shoulder of the D^- to N=0 Landau level transition. It is also noticed that the D^- to N=1 transition, is of comparable magnitude to the cyclotron resonance. Increasing the electric field bias, the intensity of the complex becomes less and less, until at the highest bias it disappears altogether, leaving the normal D^- lineshape typically observed at 4.2K. In addition, the D^- to N=1 Landau level transition, decreases intensity with respect to the cyclotron resonance. In addition the D^- to higher Landau level transitions, visible at low bias disappear with increasing electric field bias. The additional peak attributed to complex formation (C) disappears with increasing electric field bias, presumably because of a lower impact-ionisation cross-section for the complexes compared to D^-. Thus, referring back to figure (6.14), the complex in this figure probably grows as a combination of two effects, reduced electric field bias and intrinsic illumination. Complexing, also occurs in other GaAs samples with the shape and peak position differing in each case (figure 6.16). Sample S1, shows D^- complex structure, in addition to extensive interexcited state transitions.

It is difficult to speculate exactly what form the complexes take, since there is considerable debate as to how complexes are formed. Furthermore, there is almost no information on complex formation in a magnetic field. This is an important problem in the understanding of the metal-insulator transition, where the effects of correlation and disorder are not yet fully understood. FIRPC in a

large magnetic field provides an ideal opportunity for study of D^- complex formation, which are believed to occur at the onset of the D^- band.

Two possibilities exist for the formation of a complex.

i) A third electron could bind in a magnetic field forming a D^{2-} state. No calculations have been performed as to whether this is a possibility.

ii) A more likely interpretation involves impurity clusters, which are randomly distributed throughout the crystal. The simplest cluster is analogous to the hydrogen molecular ion, where a neutral and a positively ionised donor bind. This type of cluster has been observed by Bajaj et al (1975), in the FIRPC response of compensated GaAs, as a spectral feature at 60% of the Rydberg. Neutral donor clusters, formed by two neutral donors, become important in low compensation materials and it seems reasonable to extend the concept to include a negatively ionised donor - neutral donor cluster i.e $D^o - D^-$, or even a doubly ionised donor cluster i.e $D^- - D^-$. Norton (1980), has extended this idea by suggesting D_n^-, $n>2$ complexes can exist. Furthermore Golka (1980) predicts that three impurity clusters are also important, thus giving rise to the possibility of clusters, formed by different permutations of D^+, D^o, and D^- states. Hopping conduction could easily occur between the different complex states. However, the question of complex formation in a magnetic field remains open.

At larger concentrations, broadening due to interaction with neighbouring impurities causes isolated states to spread out into D^0 and D^- bands. The lower (D^o) Hubbard band is formed principally by the overlap of neutral donor impurity wavefunctions. The upper Hubbard

band is mainly associated with the overlap of D^- states. Impurity conduction arises in the upper Hubbard band due to potential fluctuations from the random distribution of donors and acceptors, given by the equation.

$$\sigma = \sigma_o \exp(-E_2/kT)$$

In resistivity measurements the activation energy E_2, which is related to the energy gap between the D^o and D^- bands, can be measured in uncompensated semiconductors. Norton (1980), describes the formation of complexes by a significant change in the spectra. Similarly, a dramatic change in the FIRPC spectra also occurs when complexing becomes important.

At higher concentrations, broadening causes the overlap of the two bands and the density of states at the Fermi energy, E_F, is non-zero but the states are still localised. The metal-nonmetal transition occurs at even higher concentrations when E_F crosses a 'mobility' edge and into the region of extended states.

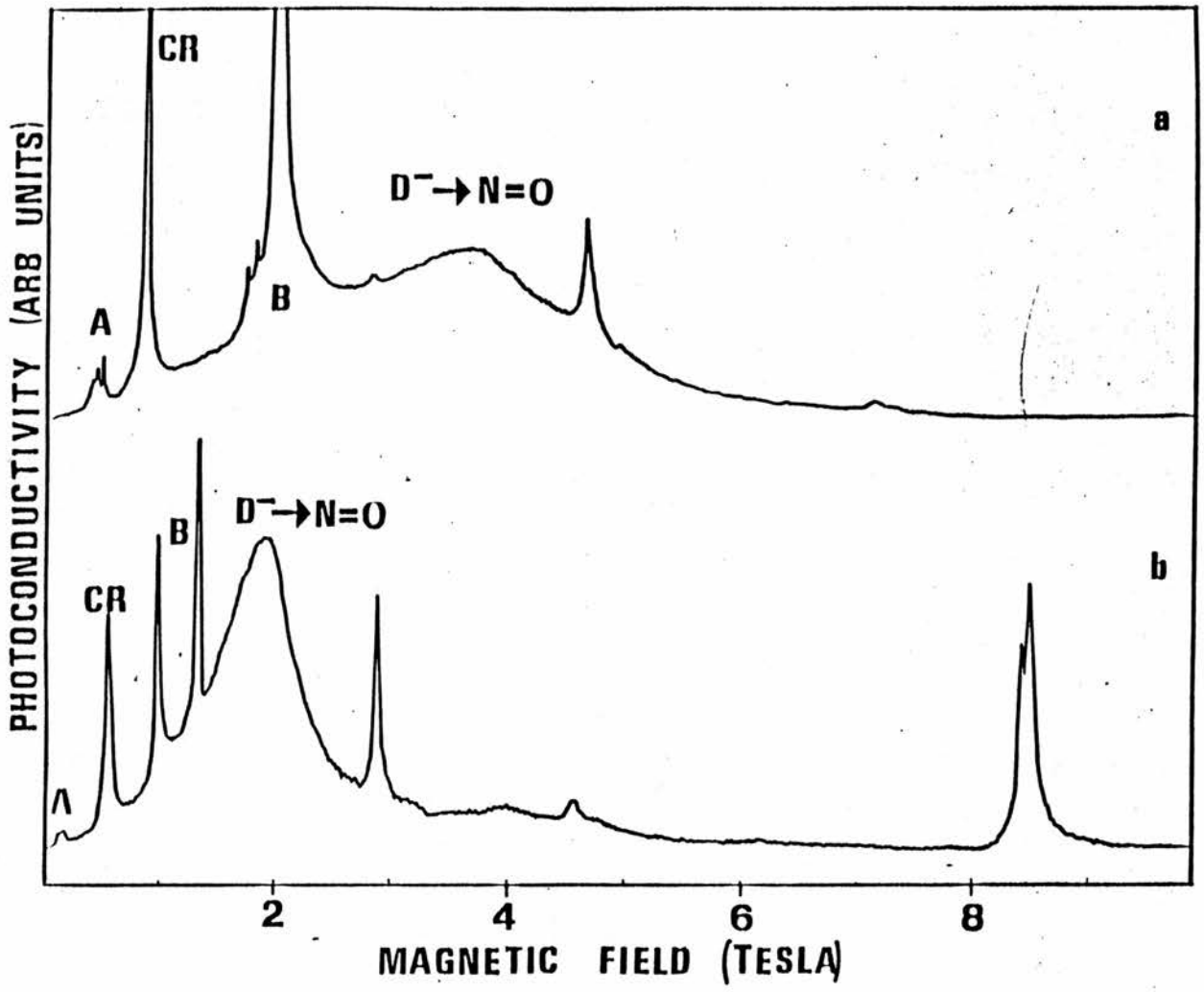

Figure (6.1) Experimental recordings of photoconductivity (in arbitrary units) against magnetic field (in Tesla) for two GaAs samples, RR98 and S1, at 4.2K. The sharp lines are either the cyclotron resonance (CR) or interexcited state transitions. The most prominent groups of the latter are labelled 'A' or 'B'. The 'A' group contains the following lines: $A_1(2S - 2P_{+1})$, $A_2(2P_o - 3D_{+1})$, $A_3(2P_{-1} - 3S)$, $A_4(3D_o - 4P_{+1})$. These lines line close to the N=1 Landau level transition and can be mistaken for the latter, particularly if the A grouping is poorly resolved. The 'B' grouping consists of $B_1(2P_{-1} - 3D_{-1})$, $B_2(2P_{-1} - 2S)$ and $B_3(2S - 2P_{+1})$. The 'I' group of lines which frequently occur close to the high-field 'edge' of the D^- to N=0 Landau level transition may also be misidentified as D^-, $I_1(2P_{-1} - 3D_{-2})$, $I_2(3D_{-2} - 4F_{-2})$ and $I_3(2P_{-1} - 2P_o)$. The upper recording is for sample S1 at 742μm wavelength and with a bias field of 0.03V/cm, the lower recording is for RR98 at 944μm and 0.05V/cm. In both cases intrinsic illumination was used.

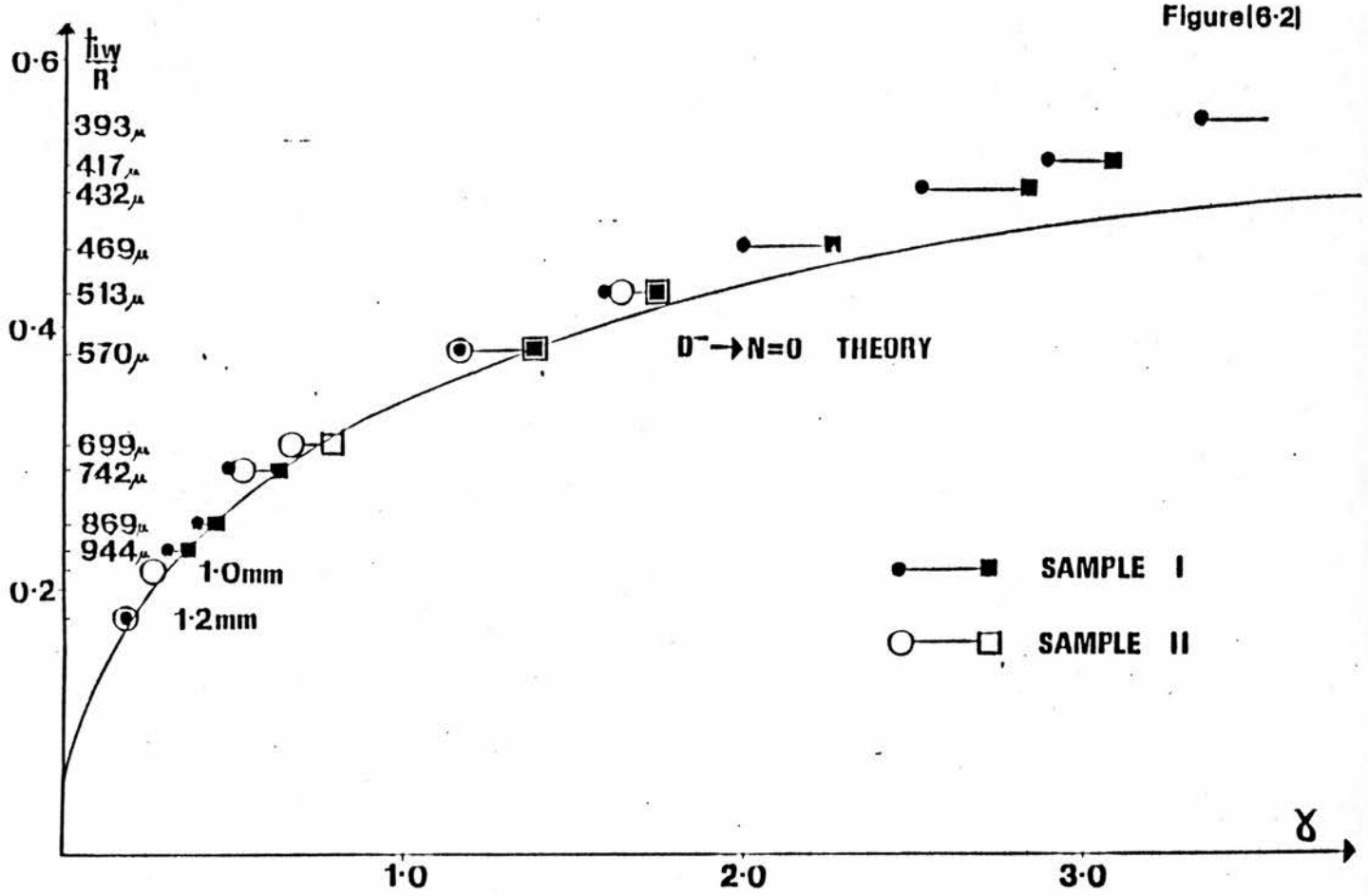

Figure (6.2) is a dimensionless plot of transition energy ($\hbar\omega/R^*$) for the D^- to N=0 transition. The continuous line is the theoretical estimate by Larsen (1979). It is seen that the experimental points diverge substantially from theory above $\gamma=1$. Note - Most of the high field experimental points were obtained by C.J.Armistead (see Armistead 1985).

Figure(6·3)

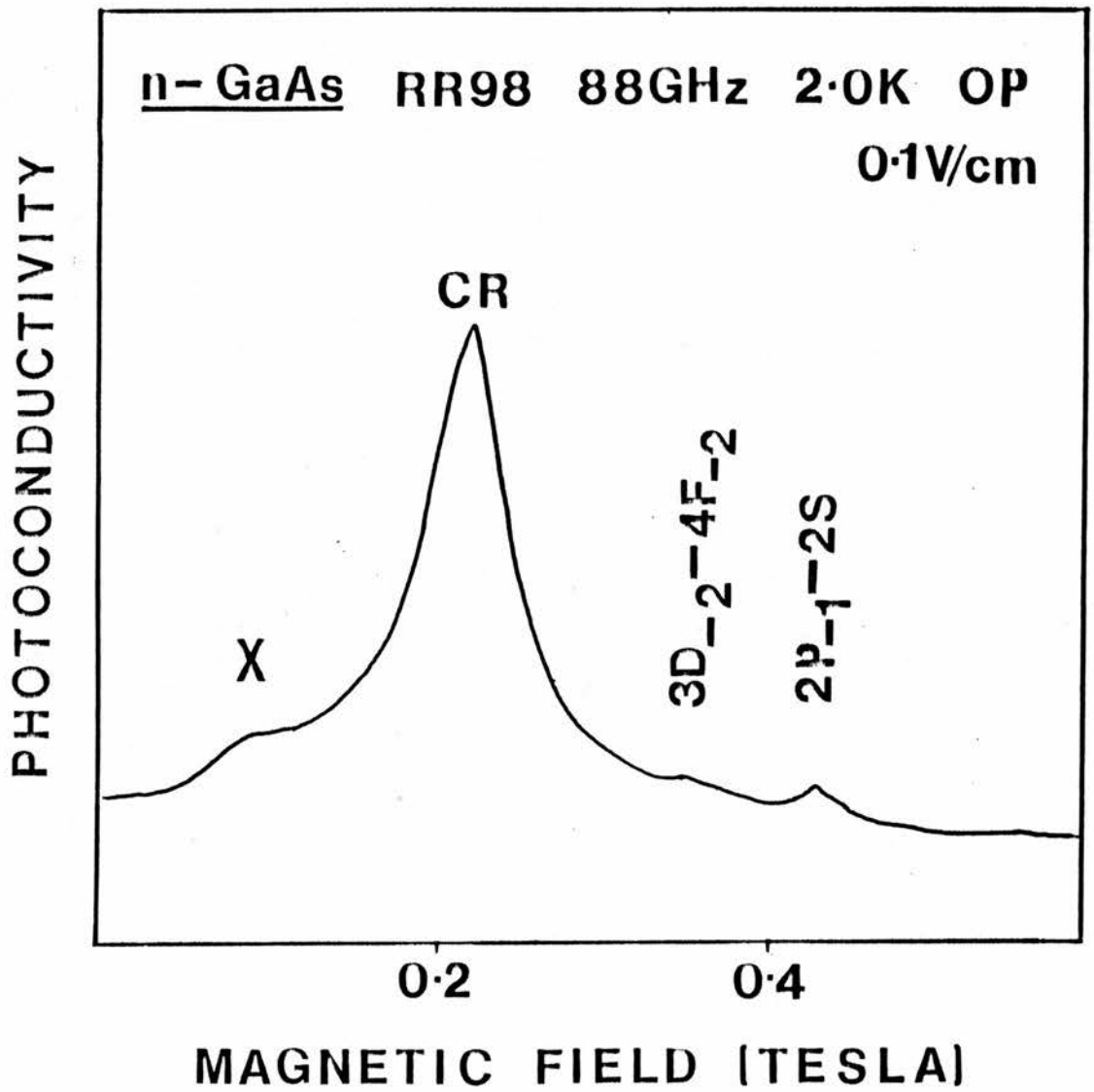

Figure (6.3) Shows magnetic field versus photoconductivity response for an uncompensated GaAs sample, RR98, at 2.0K and subject to optical pumping (OP), using a solid state IMPATT as the source of 88GHz radiation. Peak X is either D^- to N=0 Landau level or a 3-4 interexcited state transition.

Figure(6·4)

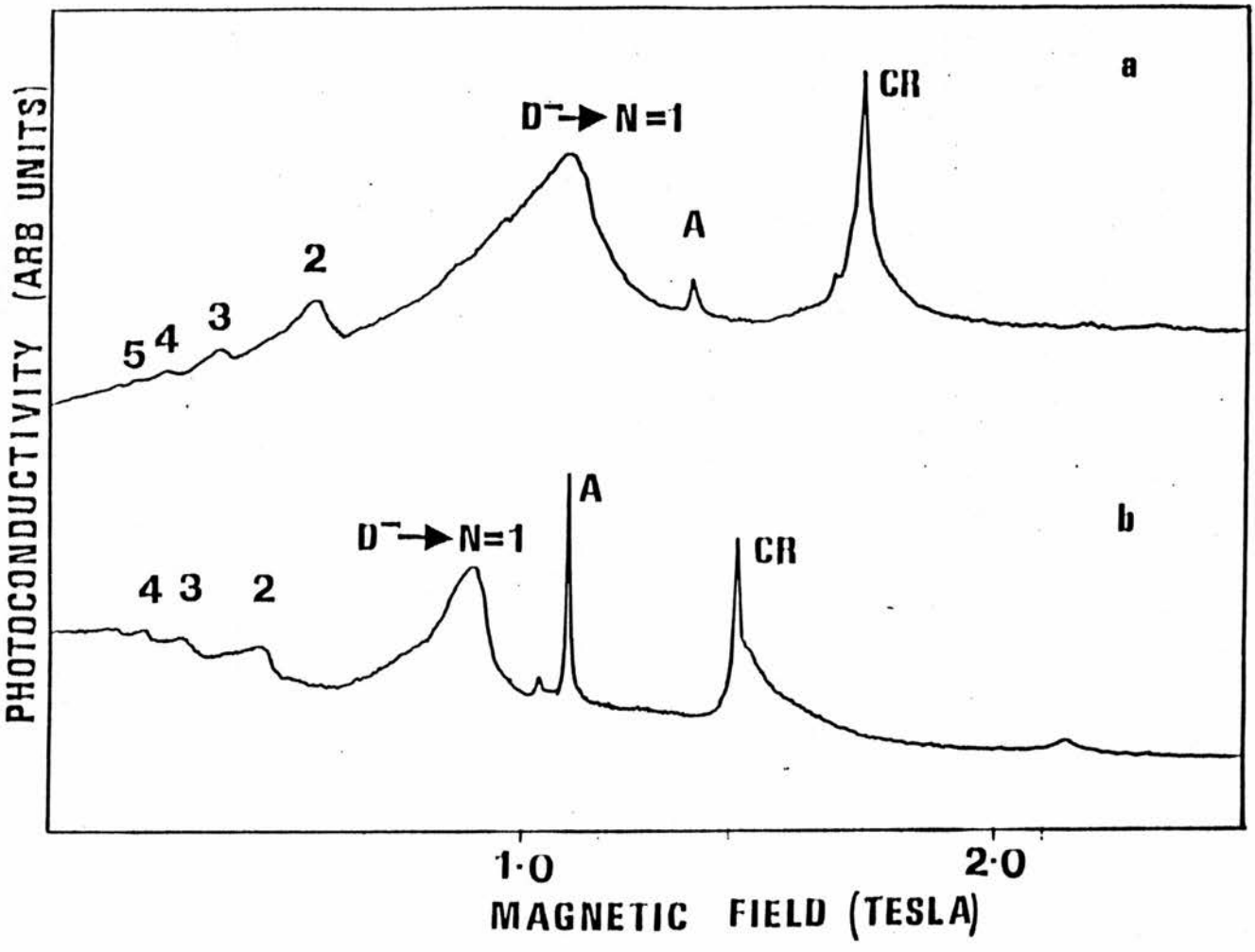

Figure (6.4), displays the photoconductivity (in arbitrary units) against magnetic field (in Tesla's). D^- to higher-order Landau levels (N=1 to 5) are observed as a characteristic 'saw-tooth' line shape. Both recordings are taken at 2K. A reduction in temperature favours the appearance of these higher order D^- transitions compared with the 'A' lines which appear close to the high-field 'edge' of the D^- to N=1 line. The upper curve is n-GaAs RR98 at 393μm wavelength and bias field of 0.08V/cm. The lower recording is for a higher mobility but more compensated sample (S1), taken at 458μm wavelength at a bias field of 0.2V/cm.

Figure(6·5)

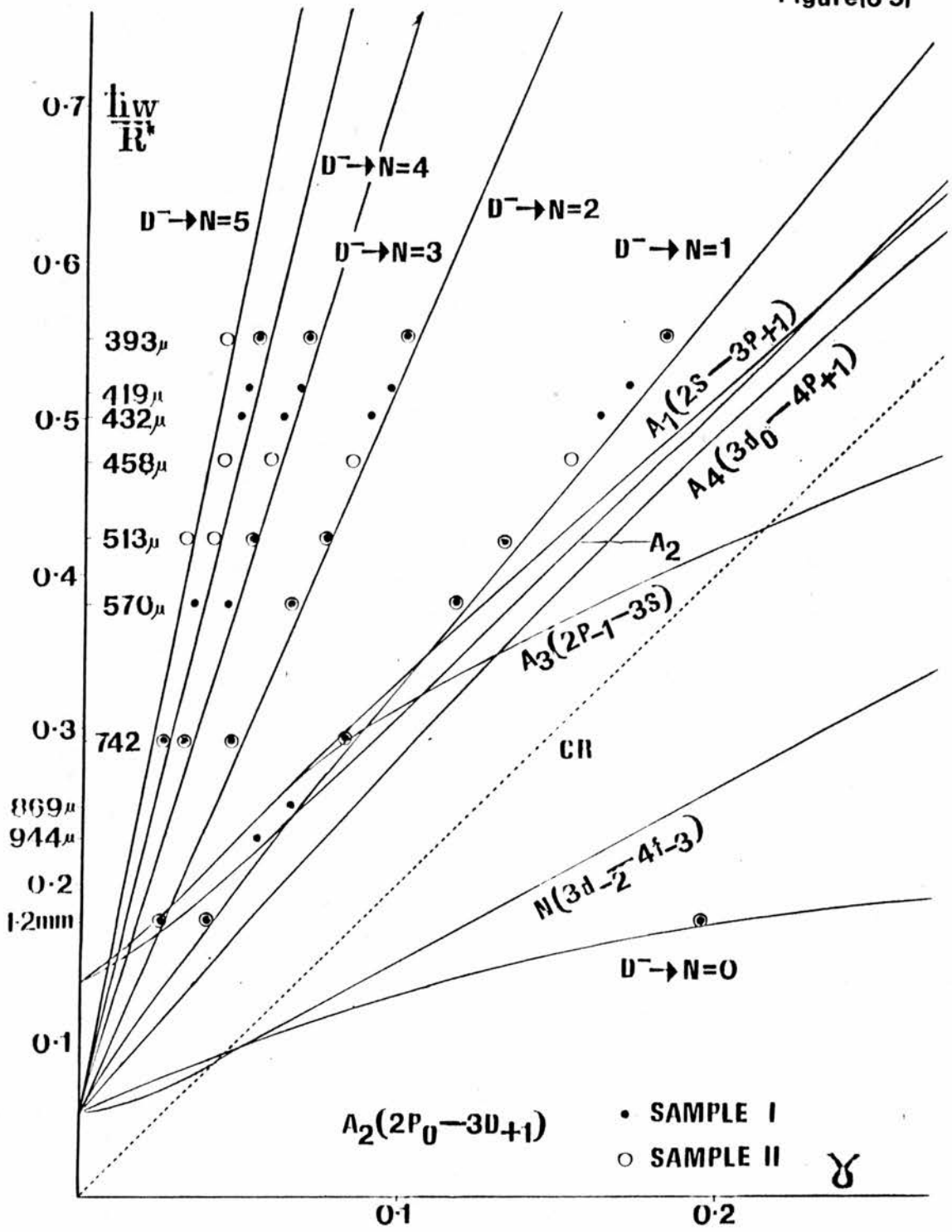

Figure (6.5) is a dimensionless "fan-chart" of possible D^- transition energies against magnetic field and a number of D^o "interexcited state" transitions. The experimental points are the experimental peak positions for the identified D^- to conduction band transitions for two samples (RR98 and S1). It is seen that the experimental points sit consistently to the low field side of the theory (full lines). The points for the high field 'edge' sit on the theoretical lines.

Figure (6·6)

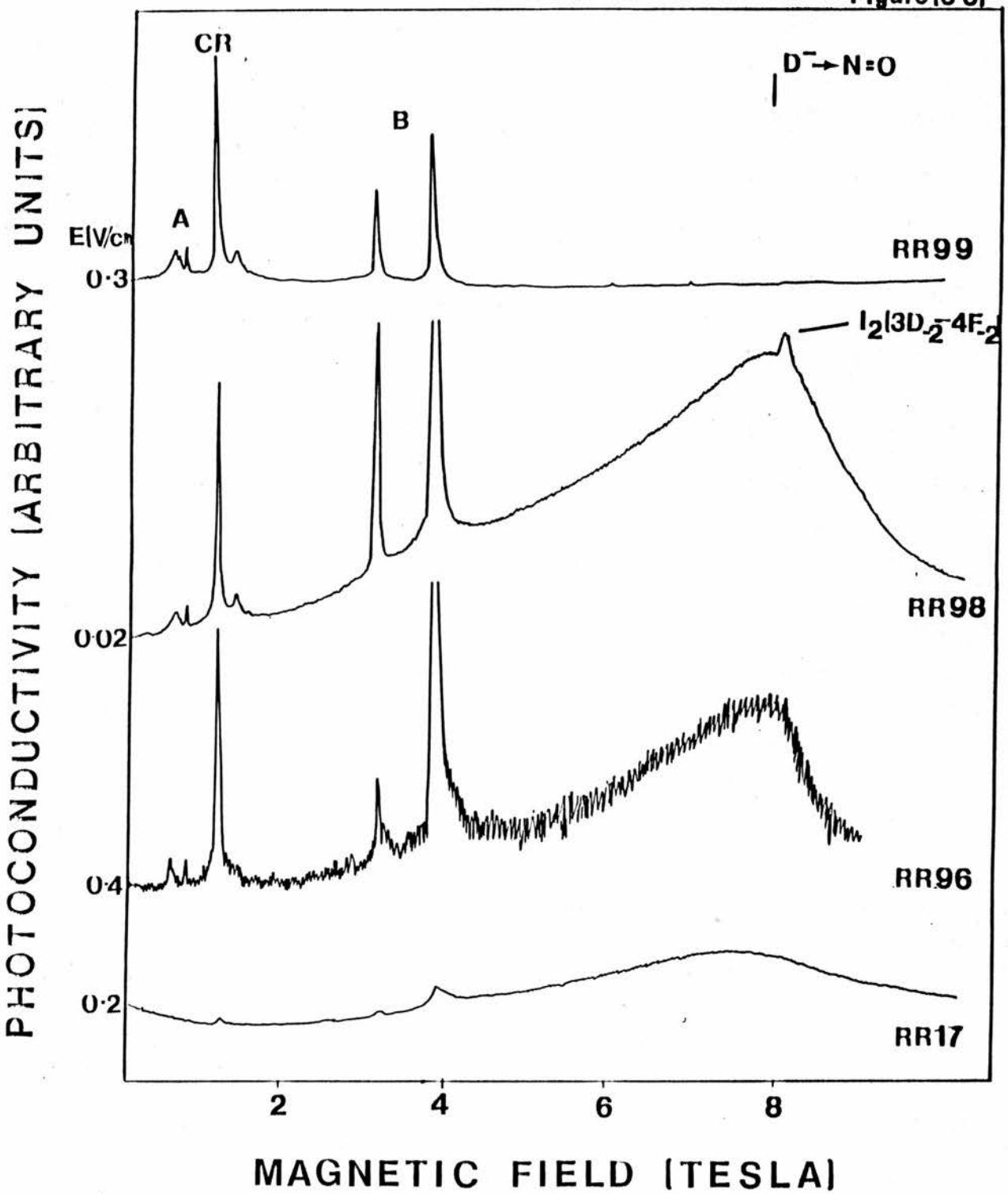

Figure (6.6) Compares the photoconductivity response of a series of high purity GaAs samples grown by P.Colter. A laser wavelength of 570μm, strong optical pumping (OP), and medium electric field bias are applied to the samples. RR133, RR98, RR96 and RR17 have low compensation ratio's and consequently show D^-. RR136 and RR99 have significantly higher compensation ratio's , both display extensive inter-excited state structure, D^- does not appear with these samples under any experimental condition.

Figure(6·6)

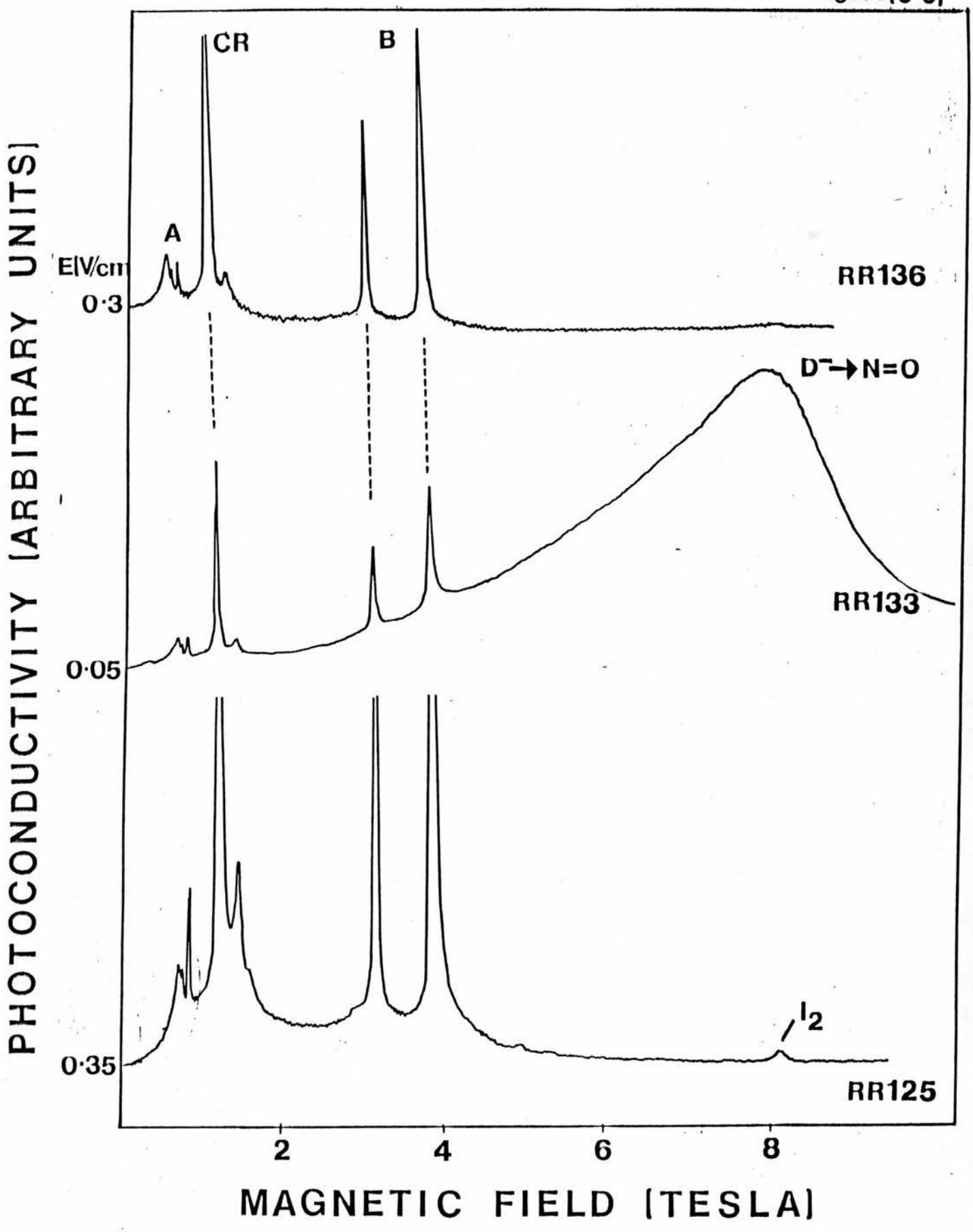
CR
B
A
E(V/cm)
0·3
RR136
D⁻→N=O
RR133
0·05
0·35
I2
RR125
PHOTOCONDUCTIVITY (ARBITRARY UNITS)
2
4
6
8
MAGNETIC FIELD (TESLA)

Figure(6·7)

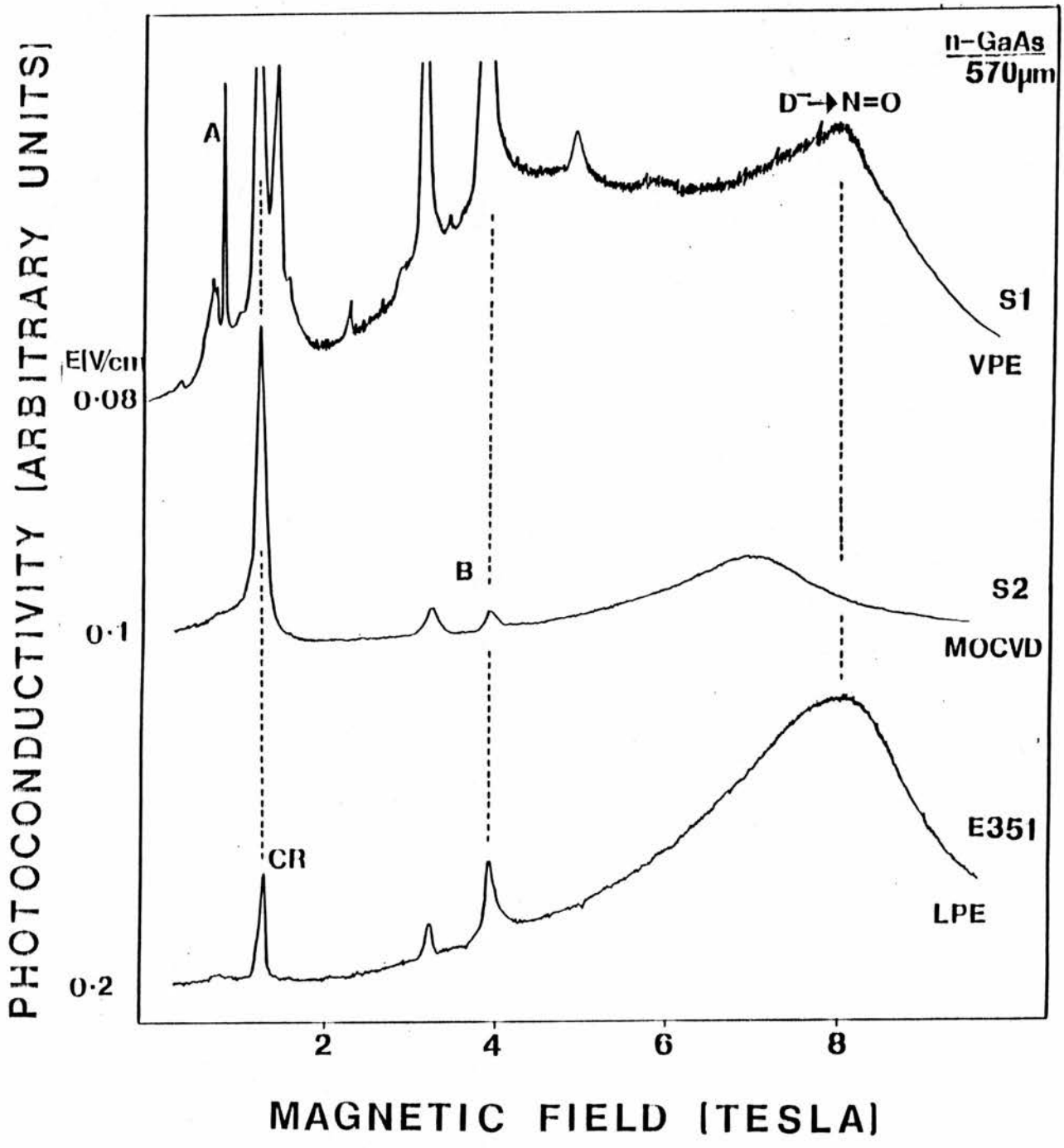

Figure (6.7) Compares the photoconductivity response of three high purity GaAs samples grown by different machines. The D^- peak position of the MOCVD grown sample is at a substantially lower field position compared to the other two growth methods. This reflects the different central-cell 'signature' obtained with MOCVD grown samples.

Figure(6·8)

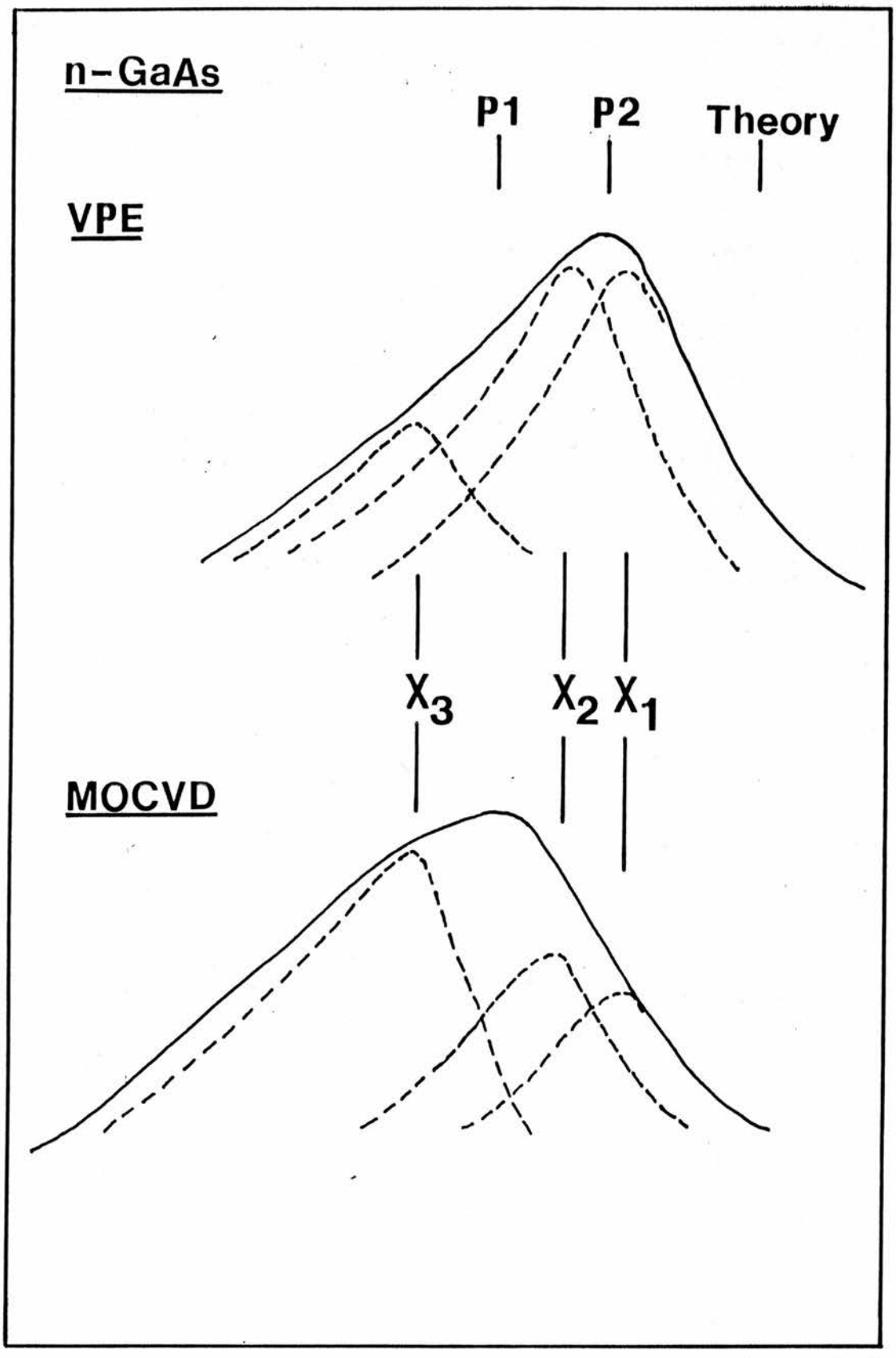

Figure (6.8) Presents a schematic diagram of the D^- lineshape. P1 and P2 are the peak positions for MOCVD and VPE grown material. The energy difference between P1 and P2 and theory predicted by Larsen are approximately to scale. The diagram demonstrates how the 'weight' of central-cell components adjusts the D^- lineshape and peak position.

Figure(6·9)

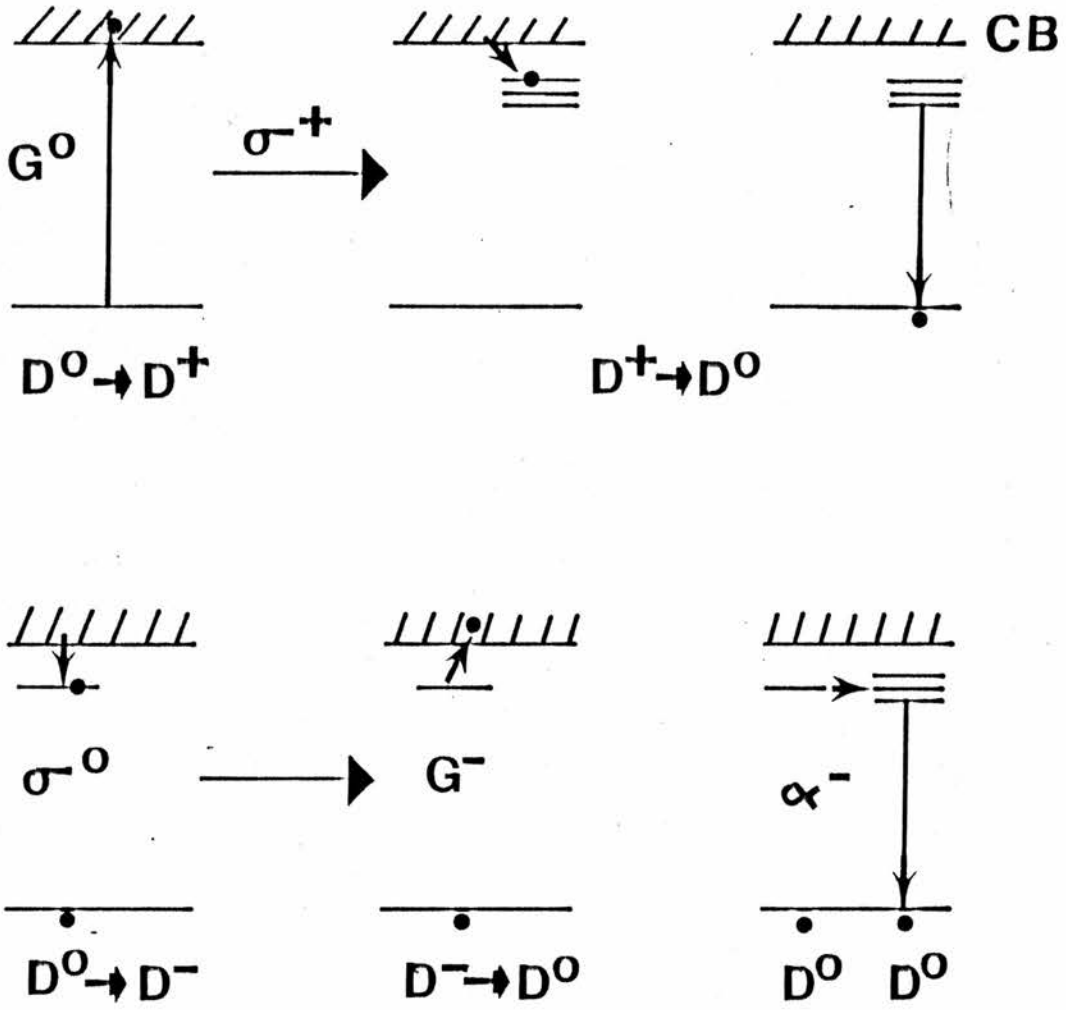

Figure (6.9) Demonstrates the different recombination paths of an electron after excitation into the conduction band.

Figure(6·10)

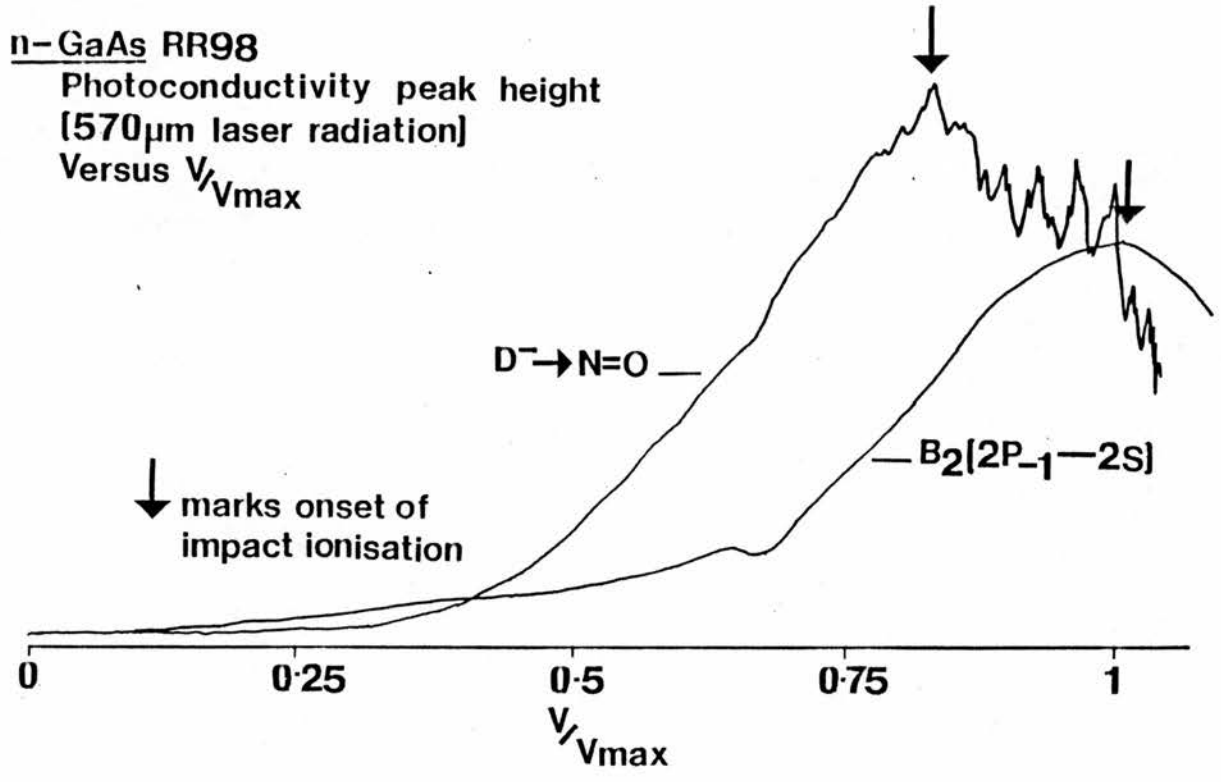

Figure (6.10) Plots the ratio of the applied electric field bias to the maximum voltage against the magnitude of the photoconductivity response of the transition. Impact ionisation occurs at a lower field bias in D^- than for interexcited state transition B_2. (diagram courtesy of C. Trager).

Figure(6·11)

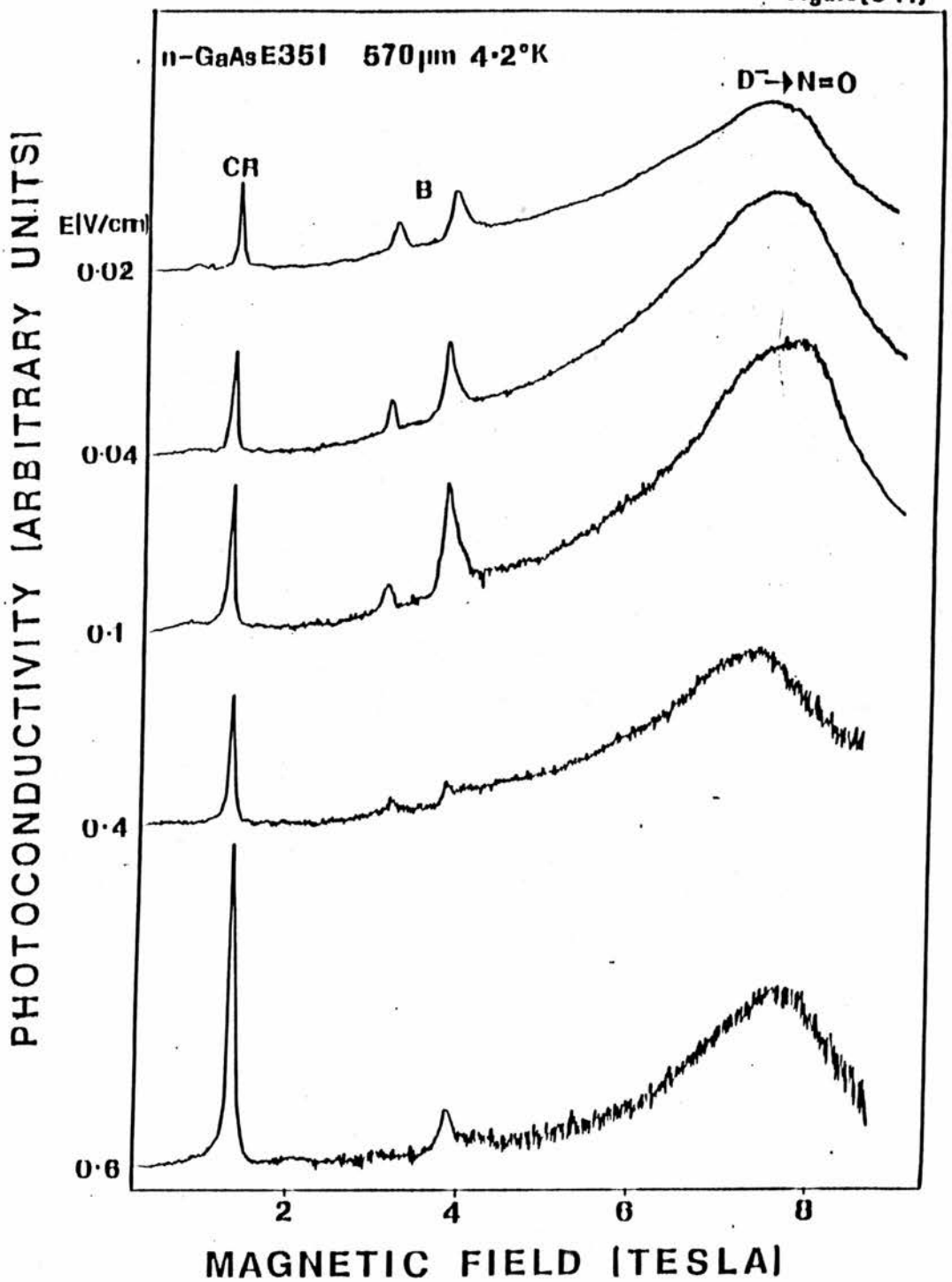

Figure (6.11) Displays a series of recordings with high purity LPE GaAs, sample E351. Photoconductivity against magnetic field is recorded as a function of electric field bias. The temperature is 4.2K and the laser wavelength is 570μm. D^- grows with respect to the cyclotron resonance (CR) with increasing bias, reaches a maximum value then decreases. Interexcited state transition B_2, disappears from the spectra but reappears at higher bias due to the smaller impact ionisation cross-section compared to D^-.

Note - The gain has been adjusted on each recording.

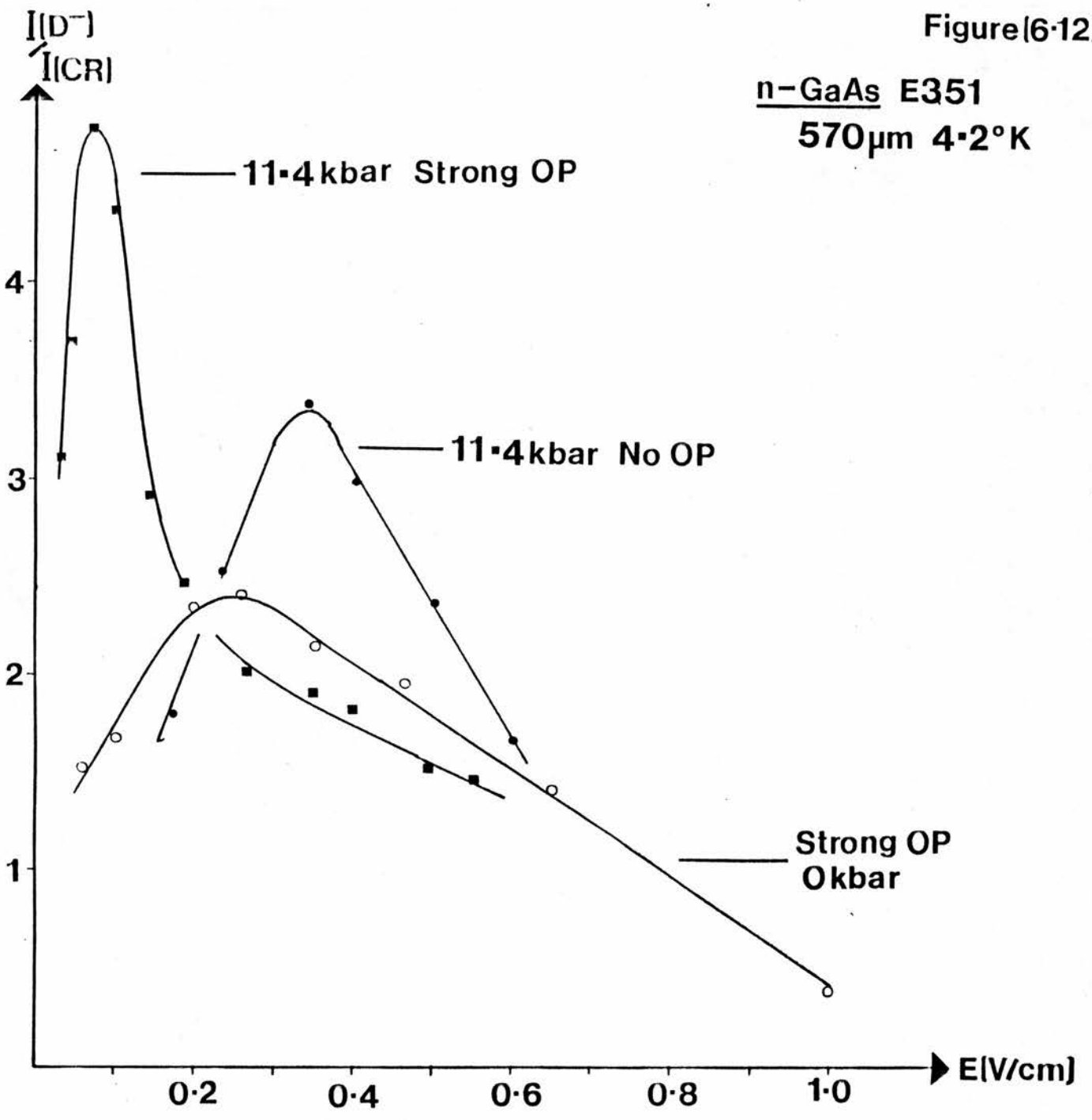

Figure (6.12) Plots the ratio of the magnitude of D^- with respect to the cyclotron resonance (CR) against electric field bias. The increase of D^-/CR with pressure and optical pumping (OP) is observed.

Figure(6·13)

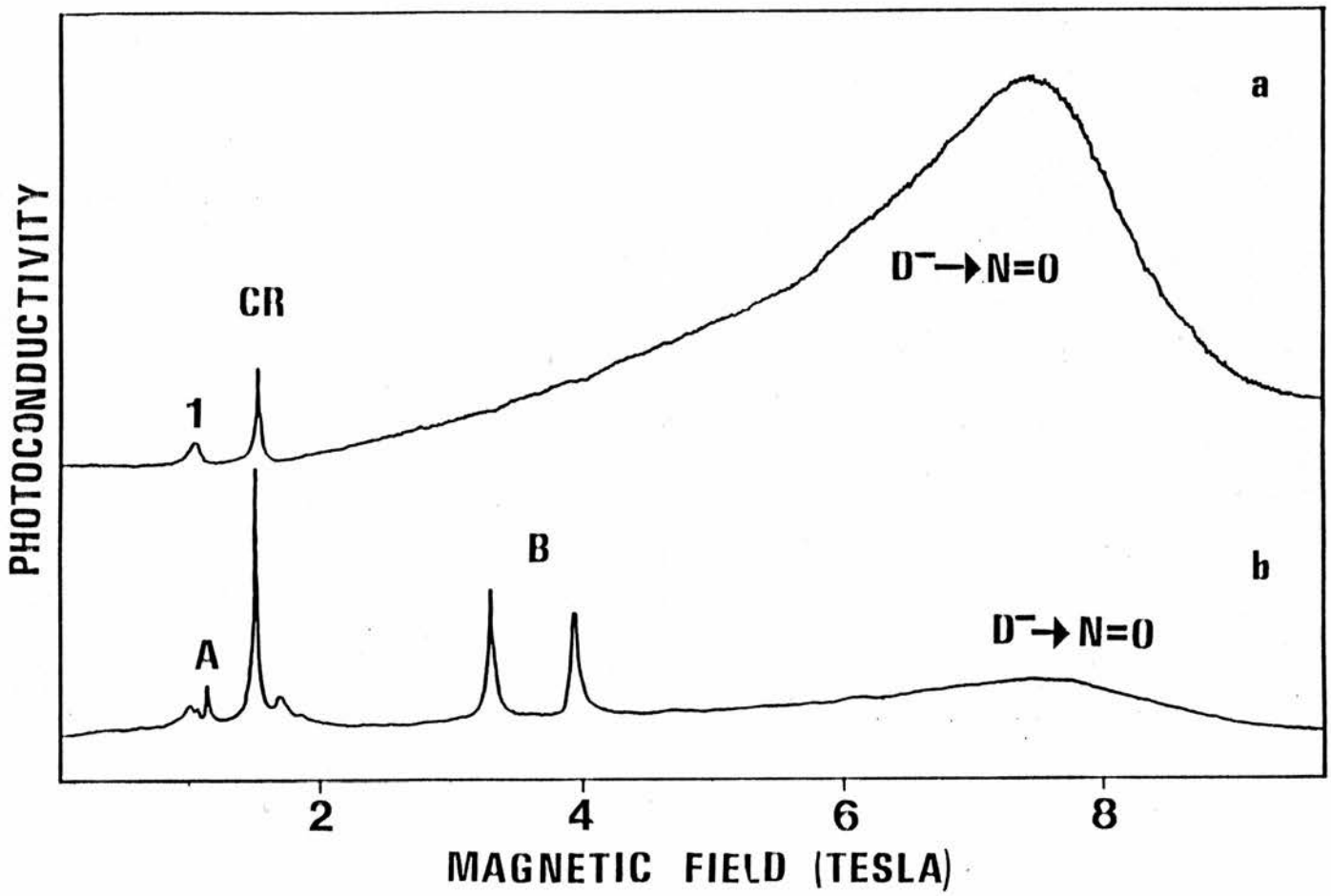

Figure (6.13) Experimental recordings of photoconductivity (arbitrary units) against magnetic field for RR133 (n-GaAs). The experimental conditions for the two recordings are identical (4.2K, 570μm, and intrinsic radiation) except for the electric field bias. The bias field at zero Tesla for the upper recording was 0.4V/cm and that for the lower recording 0.02V/cm. In the lower recording the D^- to N=0 peak is more than a factor of two weaker than the B lines and the D^- to N=1 peak a factor of two weaker than the strongest A line. In the upper recording the A and B lines have disappeared completely.

Figure(6·14)

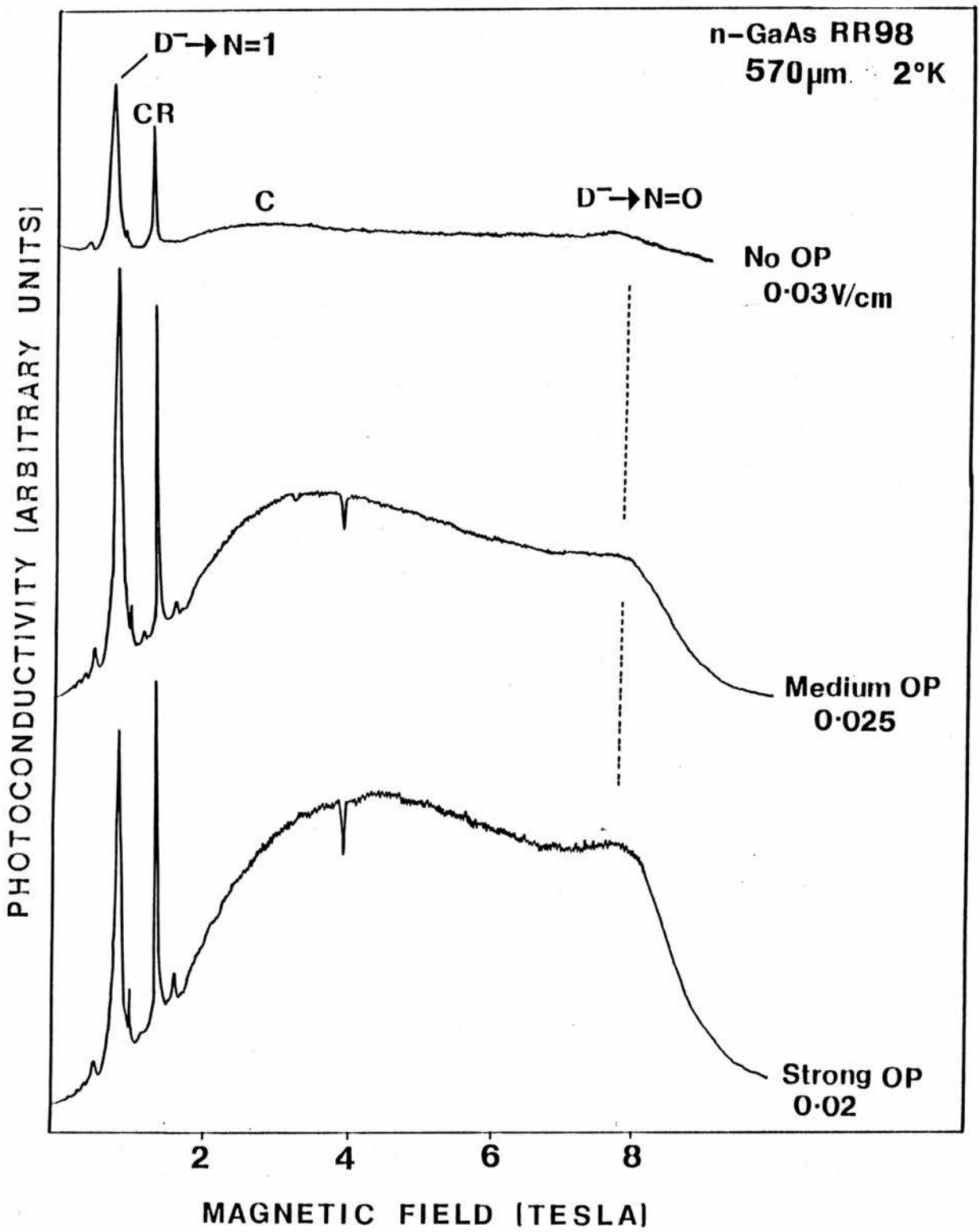

Figure (6.14) Photoconductivity against magnetic field is shown for an uncompensated GaAs sample, RR98, at 570μm and 4.2K. The effect of band-gap illumination is illustrated on this figure. Without optical pumping (OP), the D^- transition is only a small feature on the spectrum. Applying band-gap radiation, the D^- transition and complex (C) both increase with respect to the cyclotron resonance (CR). It is also noticed that the complex peak position moves significantly to higher field with increasing intrinsic illumination.

Figure(6·15)

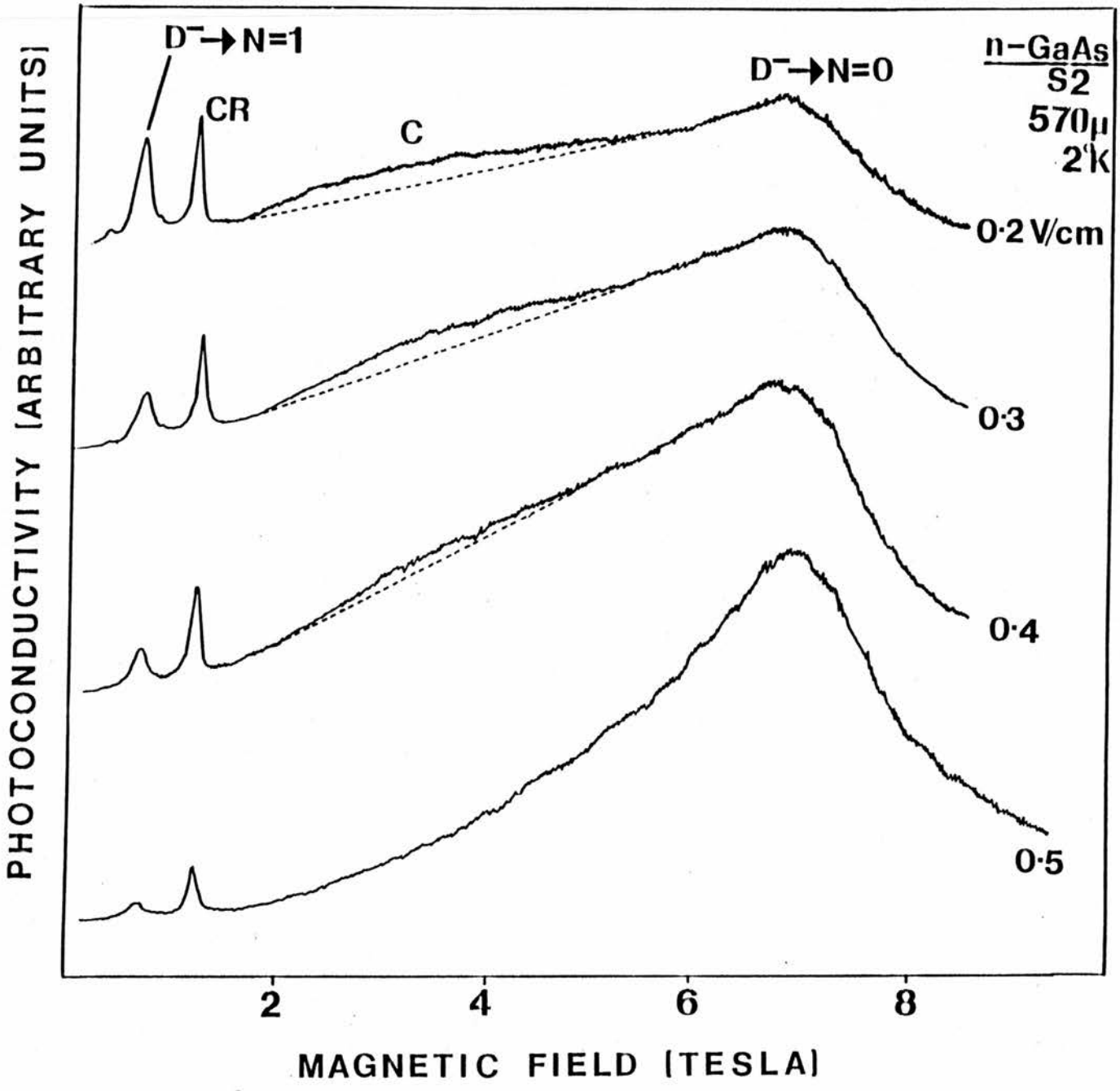

Figure (6.15) Demonstrates the effect of increasing the electric field bias on a MOCVD GaAs sample, S2. The wavelength is 570μm at 2K. The complex (C) is observed to decrease with increasing bias, as the D^- increases with respect to the cyclotron resonance (CR).

Figure(6·16)

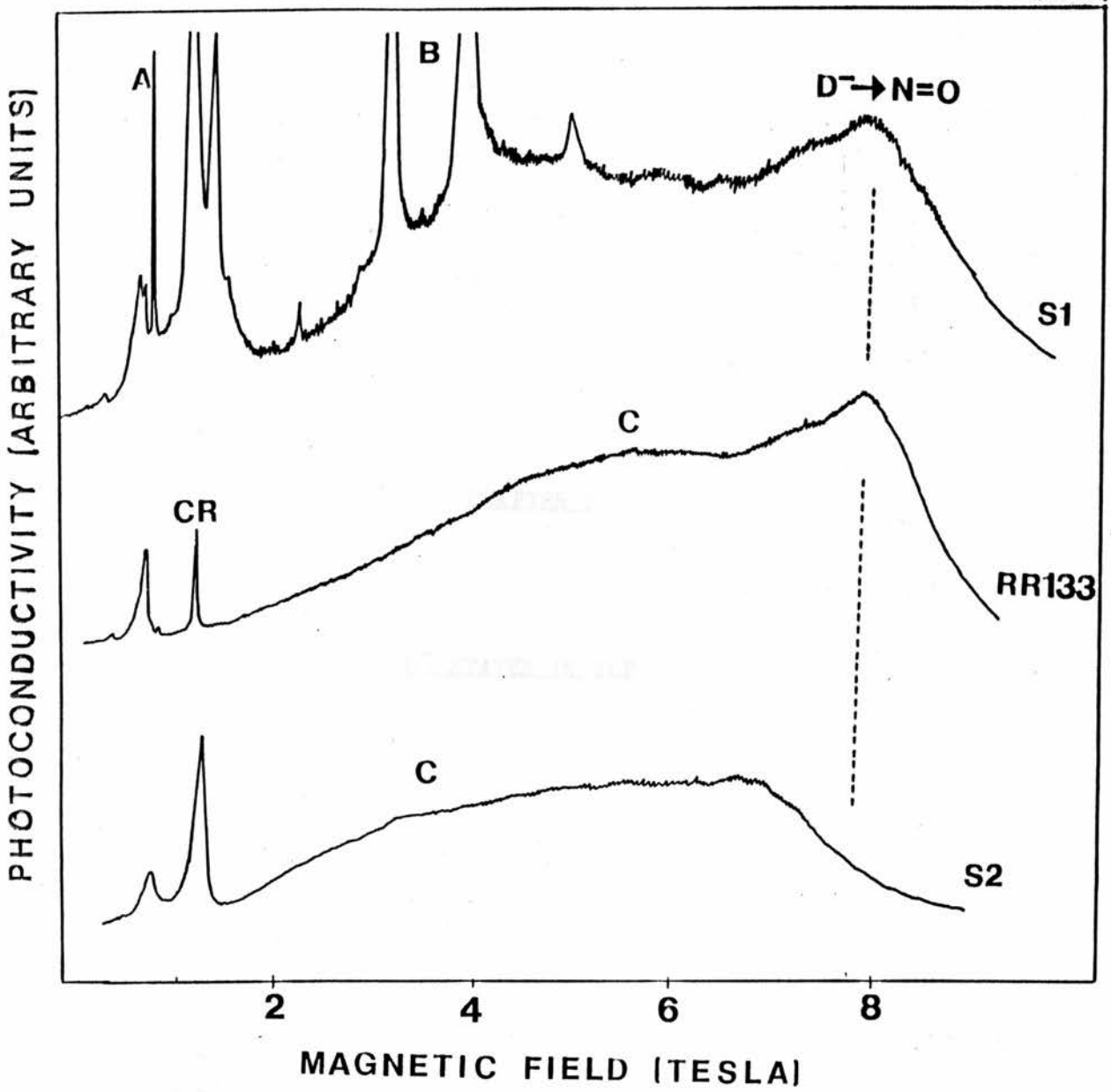

Figure (6.16) A comparison of the photoconductivity structure for three GaAs samples is shown. The top two recordings are with VPE grown samples, the bottom with an MOCVD sample. The D^- peak position is at a substantially lower field compared to VPE material.

7.1 D^- STATES IN InP

The study of D^- states in III-V semiconductors is extended to InP. D^- states are expected to behave very similarly compared to GaAs, since in both cases the conduction band minimum is located at the centre of the Brillouin zone, anisotropy and non-parabolicity are small. Unfortunately, InP growth technology is less advanced than GaAs; consequently crystal quality is inferior and compensation ratios are higher when compared to the best GaAs available. Hence, D^- states are expected to be more difficult to observe in InP. However, two exceptionally pure and uncompensated VPE InP samples were received from RSRE Malvern, where some of the purest InP layers have been grown to date. The two samples employed in the following experiments, NAG747 and NAG762, have carrier concentrations $N_A-N_D=10^{14}cm^{-3}$, liquid nitrogen mobilities in excess of 120,000 cm^2/Vs, together with low compensation ratios (N_A/N_D-0.1). The present work described for InP confirms the previous results and conclusions for GaAs.

The experimental set-up is exactly the same as for GaAs. Similar excited state spectral features are observed with InP as with GaAs. For example consider figure (7.1); a high quality InP sample, NAG747, is irradiated with 570μm laser radiation. Interexcited state transitions and the cyclotron resonance of free carriers are all observed on the same trace. The various interexcited photoconductivity transitions of InP are displaced to slightly higher energy to take into account the larger effective mass, compared to GaAs, hence the magnetic field has a proportionally lesser effect. Interexcited state transitions, labelled A and B in the notation of Skolnick et al (1977) (these are the same interexcited state

transitions which are so prominent in GaAs) are extremely narrow giving an indication of how relatively pure the InP is. Central-cell effects are observed on the interexcited state 'B_2' line. Four other samples of reasonably high quality InP failed to reveal any interexcited state structure at all! Compared to GaAs, the interexcited state transitions are not as extensive (in terms of the number of observed interexcited state transitions) nor as well resolved, illustrating the relative difference in quality between the two materials. The cyclotron resonance is very narrow for InP, as expected from state-of-the-art InP, but again inferior to the best GaAs. The recording displayed in figure (7.1) was taken at low temperatures (2K), high electric field bias and strong intrinsic illumination. These parameters were used previously to optimise the magnitude of D^- in GaAs. Only under the above extreme experimental conditions could D^- be observed, even then the D^- transition is only a very small feature constituting an edge on the photoconductivity spectra. The photoconductivity scale had to be expanded by an order of magnitude, otherwise no D^- structure was apparent.

7.2 D^- STATES AS A FUNCTION OF HYDROSTATIC PRESSURE

NAG762 is subjected to 570μm laser radiation at 4.2K (figure 7.2). With band-gap illumination and at an optimum electric field bias, very broad structure appears at the predicted D^- to N=0 peak position (trace c). This recording is similar to the previous trace of sample NAG747 at 2.0K i.e (figure 7.1). Again the photoconductivity response has to be increased by an order of magnitude to observed D^- structure. Hydrostatic pressure is used as an additional experimental parameter. Applying a large pressure of 10kbar at 4.2K, even with no optical pumping a large increase in the size of D^- occurs. The middle trace displayed on this diagram is taken under the same experimental conditions as above i.e 4.2K, and optical pumping, except a pressure of 10kbar is applied to the sample i.e (trace b). An order of magnitude increase of the D^- absorption with respect to cyclotron resonance is apparent, due to the action of pressure in deepening of the D^- ground state, in a similar manner to magnetic field. If the sample is further cooled to 2K, another dramatic increase in the magnitude of D^- occurs. The top trace shows the photoconductivity response at 2K, under pressure and optimum electric field bias. The interexcited state transitions 'A' and 'B' disappear from the spectrum. Thus the size of the D^- transition increases by several orders of magnitude, by simply increasing the pressure and reducing the temperature. Furthermore, under optimum bias conditions, with high pressure and at 2K, the magnitude of D^- is comparable to the best GaAs spectra at 4.2K and ambient pressure. However, the D^- population in InP was insufficient to induce complex effects, even under extreme experimental conditions.

Similar high pressure experiments were performed with VPE GaAs. However pressure appeared to have little or even the reverse effect, of suppressing the magnitude of D^-. The effect of pressure is explained qualitatively as follows. With increasing pressure, level crossing occurs in GaAs when the deepest shallow donor, X_3, associated with the Γ conduction band minimum, interact with similar donor states associated with the subsidiary minima (see chapter 3.5). The level crossing of the deepest of the shallowest donors present in VPE material, X_3 (believed to be Ge in both InP and GaAs) at pressures above 8.5kbar, is accompanied by a corresponding increase in the effective compensation ratio, due to a reduction of photoexcitable electrons under the Γ minimum. A substantial proportion of electrons which could accumulate on D^- sites cannot, since they are 'trapped out' onto deeper states of subsidiary minima and do not contribute to the observed spectrum. Correspondingly, the D^- signal is reduced in intensity, due to the 'effective' compensation ratio increasing at cross-over.

In addition to this process, a deepening of the D^- ground state occurs due to pressure increasing the effective mass, together with a reduction in width of the upper Hubbard band caused by a compression of D^- wavefunctions. At best in VPE GaAs, the combination of both competing processes, produces no change. However, if there is a reasonably substantial population of X_3 donors, their effect is detrimental to the magnitude of D^- under pressure, due to their influence of the 'effective' compensation ratio. No level crossing of the deepest of the shallow donors has been observed in InP at the available pressures i.e up to 15kbar. Consequently, there is no change in the effective compensation ratio with increasing pressure.

Only the latter process is applicable, enhancing the D^- signal in InP.

There is no indication, in the central-cell structure of LPE GaAs i.e E351, that Ge is incorporated as a residual donor (figure 3.9). This is in comparison to VPE and MOCVD grown material, especially MOCVD where Ge is the major residual dopant. Thus, at high pressure (above 8.5 kbar), there is no change in the effective compensation ratio in either LPE GaAs or InP, since there are no Ge donor electrons to de-populate from the Γ states to subsidiary minima states. The D^- binding energy increases due to the contraction of the D^- wavefunction and the deepening of the D^- state. The enhancement of D^- in LPE GaAs with pressure is shown in figure (6.12).

An indication of the narrowing achieved on the D^- linewidth by the application of hydrostatic pressure is demonstrated in figure (7.3). The sample is LPE GaAs E351, subject to 570μm radiation at 4.2K. The D^- lineshape is compared with (dotted line) and without 11kbar of hydrostatic pressure applied to the sample. Since the pressure moves the D^- peak to lower fields, the D^- lineshapes are brought approximately into coincidence. A narrowing of up to 10% of the D^- linewidth is achieved by the application of pressure. The lineshape narrows on the long low field tail, making the D^- lineshape more symmetrical. It could be anticipated that a large hydrostatic pressure may possibly resolve central-cell structure on the D^- peak. However, no indication of central-cell splitting is apparent, even though hydrostatic pressure would enhance splitting.

Figure (7.4) demonstrates the effect of increasing the electric field bias on the relative size of D^- with respect to the cyclotron resonance $I(D^-)/I(CR)$. The sample is NAG747, subject to 570μm laser radiation at 4.2K, with strong optical pumping, and 11.2kbar of hydrostatic pressure. At the smallest field bias displayed D^- is small compared to the interexcited states 'A' and 'B', and also the cyclotron resonance. Note the appearance of interexcited state transition $I_2(3-4)$ at 6.5T, which has not been resolved at zero pressure in InP. With increasing bias, the intensity of D^- becomes comparable to the 'B' interexcited state lines, but the 'A' lines loose all their intensity. Figure (7.5) displays the relative intensity of D^- with respect to the cyclotron resonance, i.e $I(D^-)/I(CR)$, against the electric field E(V/cm) The enhancement then decrease in the relative size of the D^- is explained in the previous chapter, by the relatively smaller impact ionisation cross-section compared to most of the interexcited states, except B_2. It is clearly observed from this and the previous figure that D^- grows with intrinsic illumination, but hydrostatic pressure has a greater effect, increasing the intensity of D^- by up to an order of magnitude.

The D^- binding energy as a function of magnetic field is plotted on a dimensionless diagram in figure(7.6), for NAG747, subject to different FIR wavelengths. The experimental points lie on the high energy side of Larsen's (1979) theoretical curve, in a similar way to GaAs. However, the D^- peak positions are displaced to even higher energy since hydrostatic pressure is used to enhance the magnitude of D^-, otherwise the D^- transition would be very difficult to observe. Taking into account pressure, experiment and theory align reasonably well i.e to within 5%, in the low magnetic field regime i.e $\gamma < 1$,

but diverge at higher fields, giving in essence the same result as GaAs.

Figure (7.7) shows graphically how the size of D^- increases with magnetic field. With 432μm radiation i.e $\gamma=1$, the intensity of D^- is comparable to that of the cyclotron resonance, with interexcited states 'A' and 'B', appearing much smaller. At 513μm i.e $\gamma=0.7$, the intensity of D^- drops considerably with respect to the cyclotron resonance, and is comparable to the 'B' lines. At lower fields, $\gamma=0.4$, with 742μm radiation, the magnitude of D^- is only a small feature compared to both the 'B' line and cyclotron resonance. Each recording is taken with NAG747 at different FIR wavelengths, and the magnitude of D^- is optimised by the electric field bias and band-gap illumination, otherwise the experimental conditions are similar. It is observed that the size of the D^- increases by almost an order of magnitude with respect to the cyclotron resonance, over a short range of magnetic field, which corresponds to increasing the binding energy by $\sim 0.15R^*$.

It is difficult to compare exactly the relative magnitudes of D^- in InP and GaAs, since the magnetic field has a proportionally lesser effect on the binding energy of D^- in InP. Nevertheless, comparing the result of InP at 432μm ($R^* \sim 0.38$) subject to 11kbar of pressure, to GaAs at 570μm ($R^* \sim 0.38$) at ambient pressure, the ratio of the relative intensity of D^- with respect to the cyclotron resonance $I(D^-)/I(CR)$ of InP under pressure is still up to an order of magnitude less than the optimum intensity ratio in GaAs (see figure (6.6) for example).

The increase in effective mass as a function of pressure is obtained from figure (7.8). The magnetic field peak position (Tesla) of the cyclotron resonance (CR) is plotted against pressure (kbar) for a constant laser wavelength (570μm). At zero pressure, the effective mass is calculated to be within 1% of the value obtained by Skolnick et al (1974). With 10kbar, there is almost a 6% increase in the effective mass.

7.3 D^- STATES IN InSb

The study of D^- states in III-V semiconductors is expanded to include a preliminary study of D^- states in n-InSb, a narrow gap material, with a single conduction band minimum at the centre of the Brillouin zone. InSb is an ideal material to study D^- in the high magnetic field regime i.e $\gamma >> 1$, since the effective mass is so small, $m^* = 0.0139 m_e$ at the band edge at 4.2K. Furthermore, high purity and low compensation samples are available. However, as a consequence of the small direct energy gap, the conduction band is very much more non-parabolic than compared to GaAs and InP. Non-parabolicity is expected to influence the D^- binding energy, especially if D^- broadening due to photoionisation were dominant.

A pressure experiment can be performed on samples of InSb, to give an indication of the degree of compensation of the crystal. Four shallow residual donors commonly appear in the FIRPC spectra of high purity n-InSb (Kuchar et al 1984). A level crossing of the deepest shallow donor (believed to be oxygen), occurs at a pressure at about 7kbar, in a similar manner to GaAs (see section 3.5). If the compensation ratio is sufficiently low, so that the population of shallow donors excluding the deepest shallow states, exceeds the numbers of compensating acceptors, a relatively small change in the sample resistance occurs at cross-over. This is compared to a resistance change of several orders of magnitude if the compensation ratio is high. Sample IS404, was pressure treated in this manner and was found to have a low compensation ratio.

A low compensation, high purity InSb sample IS404, was subject to 110GHz and 88GHz IMPATT radiation at 4.2K. Applying band-gap radiation a large broad structure is apparent at approximately 2T, reminiscent of the D^- lineshape in GaAs and InP, and at higher fields an additional feature is observed (figure 7.9). A dimensionless diagram of magnetic field γ, versus energy E, is plotted in figure (7.10). The theoretical results, calculated by Larsen (1979), of the binding energies of the D^- singlet and triplet states are plotted on this diagram, together with the experimental peak positions of D^- obtained by the GaAs results. The peak position of the structure observed in InSb at the two wavelengths displayed in figure (7.9), are added to this diagram. Unfortunately, there was only limited data available, due to the difficulty of obtaining suitable sources of radiation. However, it is clearly apparent that the structure observed in figure (7.9), could possibly be due to a singlet and triplet D^- state to conduction band transition. Nevertheless, interexcited state transitions cannot be discounted from the analysis, since only the structure attributed to D^- is observed. Also, it is unclear how large central-cell and non-parabolicity effects are (because of the large values of γ central-cell effects in InSb are actually larger than in GaAs at high fields i.e ~10T).

Larsen (1979) suggested that triplet states could be so extended that they could form the basis of a D^- band. This could possibly be the case for low fields, and would explain why no triplet states were observed in GaAs. At larger magnetic fields, the D^- wavefunction is considerably more compressed, perhaps enabling triplets to be resolved. At present the identification is only tentative.

In summary, D^- states are observed unambiguously for the first time in any semiconductor. D^-, D^o(n=2, 3, and 4 interexcited state transitions) and the cyclotron resonance are all observed simultaneously. Extremely low compensation and high purity samples of GaAs and InP are studied, as a function of crystal quality, magnetic field, temperature, electric field bias, optical pumping, and hydrostatic pressure. D^- states have been observed in seven different GaAs samples, grown by three major growth techniques VPE, MOCVD, and LPE; and two VPE n-InP samples. D^- states are generally observed in the highest quality samples with liquid nitrogen mobilities exceeding μ=100,000cm^2/Vs and very low compensation ratios N_A/N_D<0.1. The D^- to N=0 Landau level transition is followed to γ=3.5, where theory and experiment are compared for the first time. A progressive deviation occurs between theory and experiment due to incorrectly chosen variational trial wavefunctions. D^- states to higher Landau levels (N=1 to 5) are also observed. The D^- peak position appears at different field positions depending on the growth technique. This is explained by the different residual donor 'signatures' introduced inadvertently by each growth method. No central-cell structure has been resolved, but the chemical shifts increase with field. The effects of temperature and electric field bias provide a valuable insight into the generation/recombination processes. D^- states can increase by over an order of magnitude with respect to the cyclotron resonance and D^o interexcited state transitions by applying a sufficiently large electric field bias. This is due to the enhanced recombination at D^+ sites and to the relatively small impact ionisation cross-section. D^- complexes are observed in GaAs, but not in InP, if the temperature is reduced from 4.2K to 2.0K. The

complexes are thought to arise from interaction with either neutral or other D^- states. Hydrostatic pressure enhances D^- in InP by deepening the ground state, but suppresses the intensity in VPE GaAs due to an increase in the effective compensation ratio caused by level crossing. D^- state intensity under optimum conditions in InP can be comparable to GaAs at 4.2K, but no complexing has been observed in InP. Triplet states have not yet been positively identified in GaAs, but both triplet and singlet states have been tentatively identified in low compensation n-InSb.

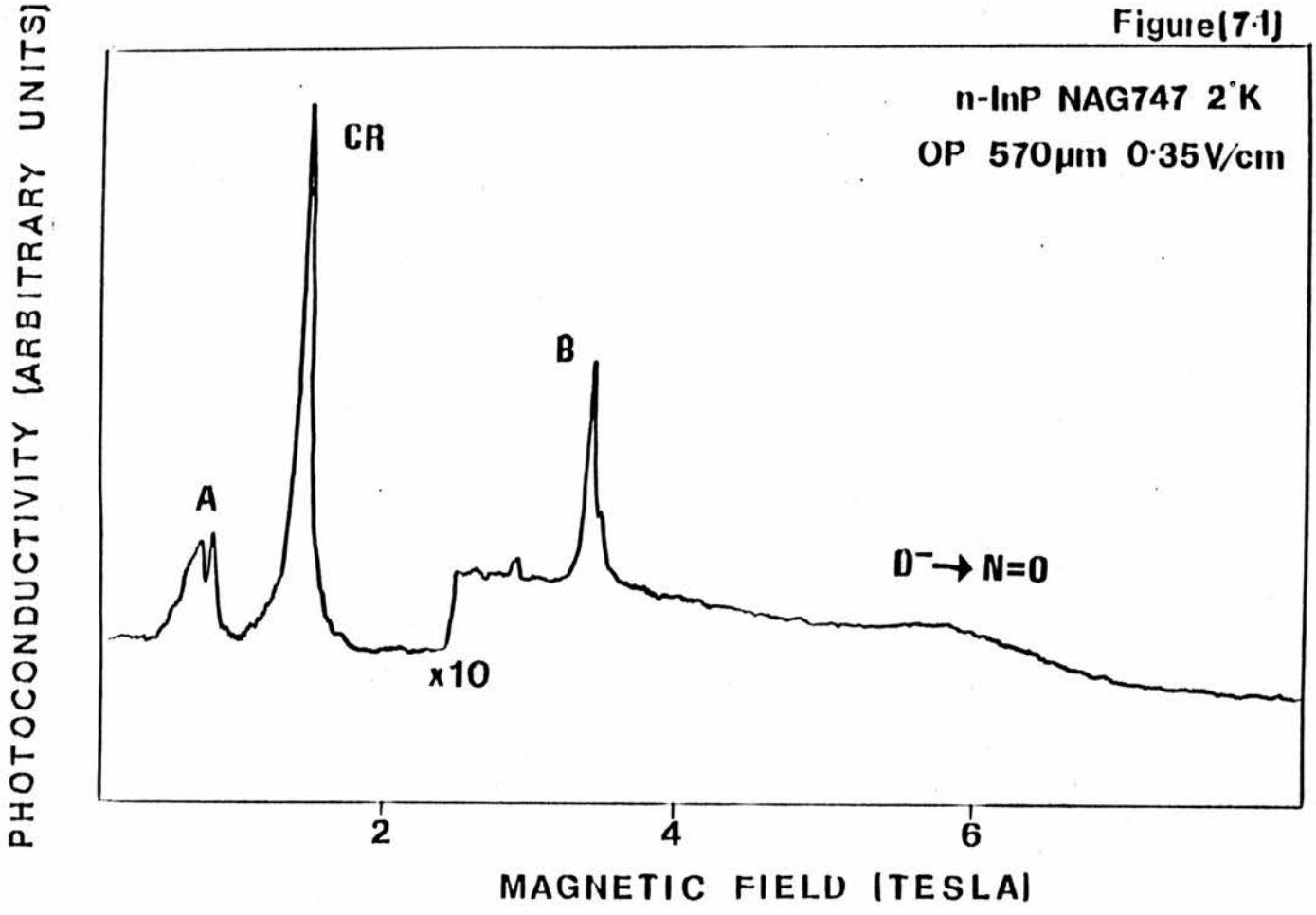

Figure (7.1) Photoconductivity against magnetic field for a high purity n-InP sample, NAG747, subject to 570μm laser radiation at 2K, OP, and optimum electric field bias.

Figure(7·2)

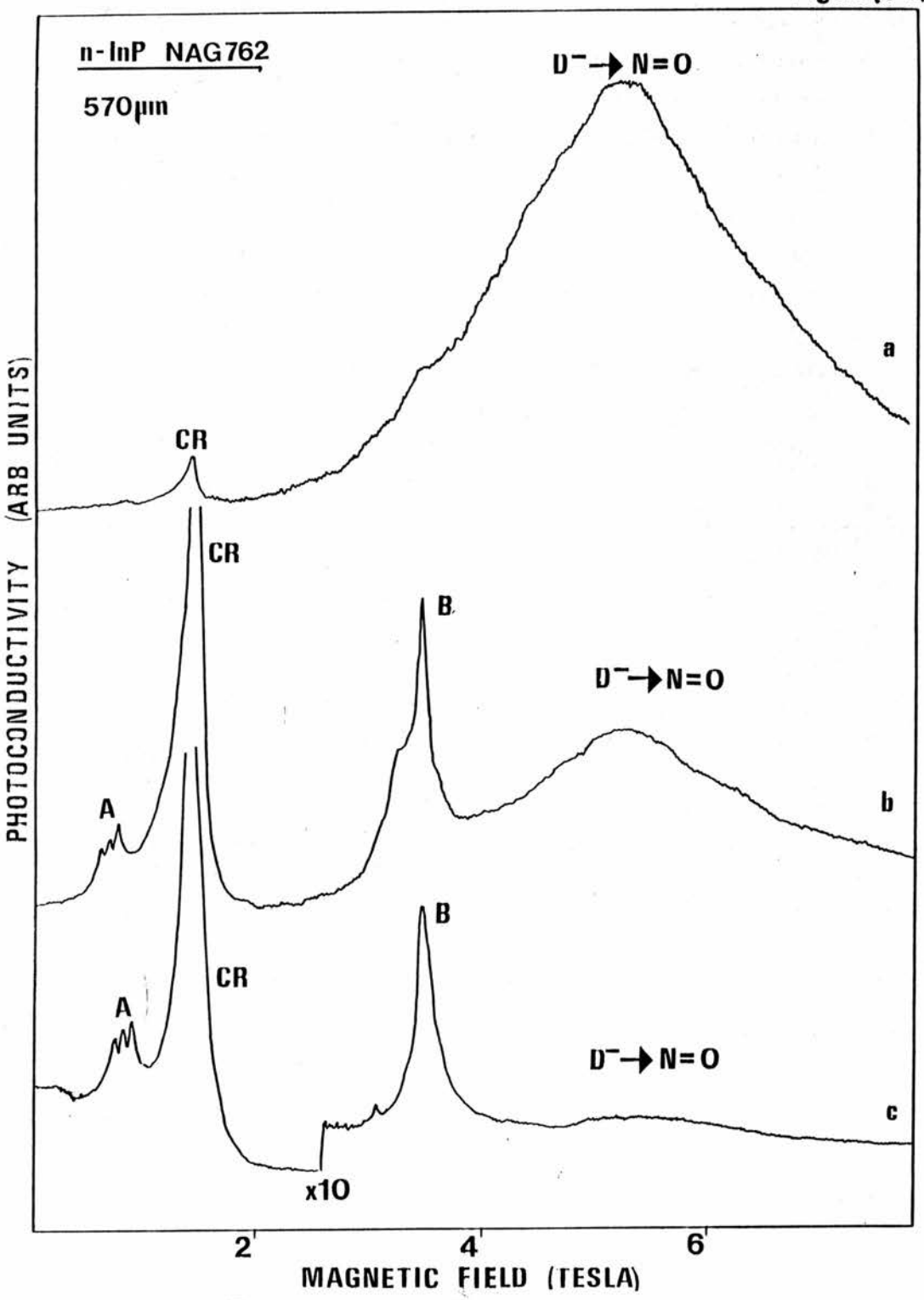

Figure (7.2) Displays the experimental recordings of photoconductivity (arbitrary units) against magnetic field for a high purity sample of n-InP (NAG 762). All the recordings are taken with 570μm laser radiation and with an optimum electric field bias (~0.4V/cm). Trace 'c' has been recorded at 4.2K and with optical pumping (OP). The gain has been increased by a factor of ten at about 3T in order that the weak D^- to N=0 Landau level transition can be observed. At the same experimental conditions, except a hydrostatic pressure of 11kbar is applied to the sample, the D^- intensity increases by an order of magnitude with respect to the cyclotron resonance (CR) (trace b). If the temperature is reduced to 2K, another order of magnitude change in the size of the D^- transition is observed.

Figure(7·3)

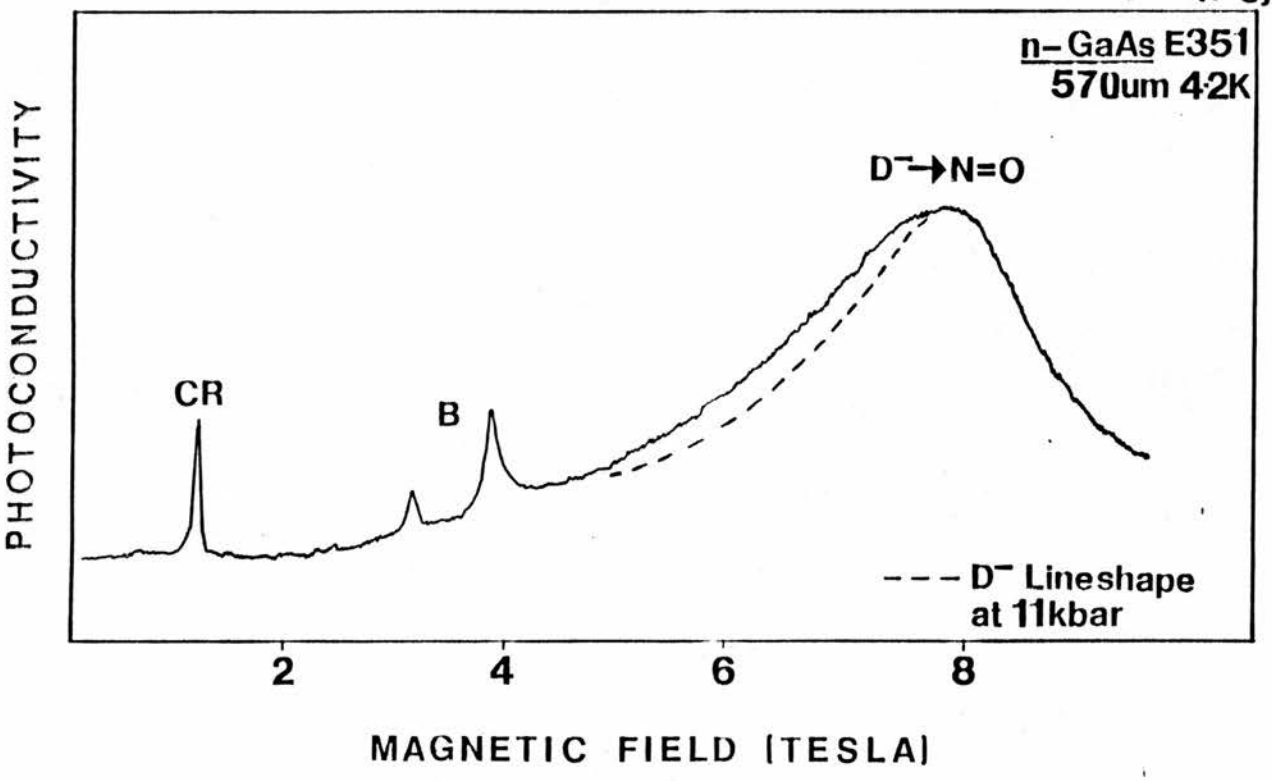

Figure (7.3) Hydrostatic pressure is applied to a LPE GaAs sample. The D^- intensity does not decrease, as with VPE grown material, since donor X_3 is not observed with LPE material. Approximately 10% narrowing of the D^- transition is achieved with the application of pressure.

Figure(7·4)

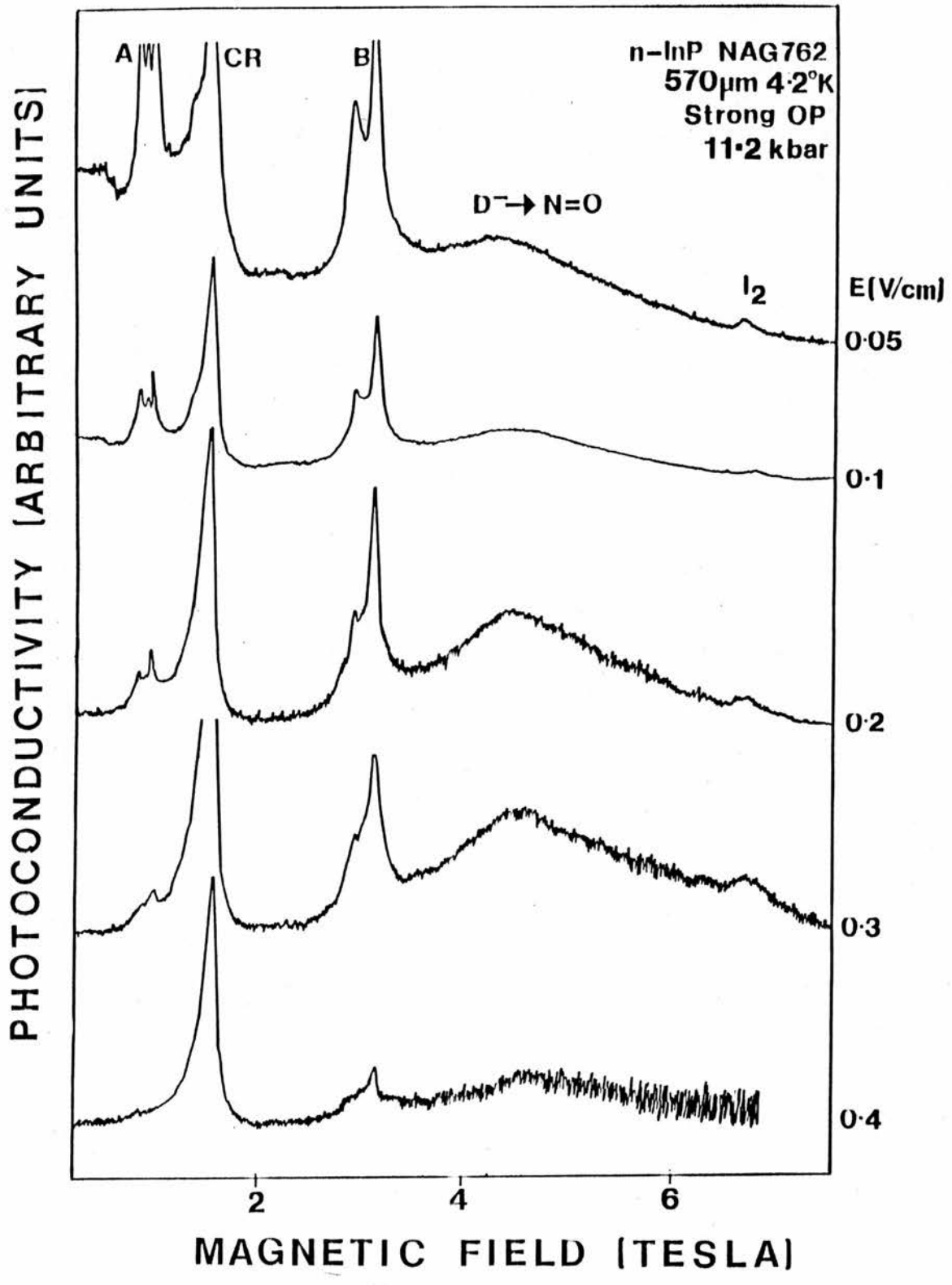

Figures (7.4) Illustrates the effect on the intensity of D^- by increasing the electric field bias. Photoconductivity versus magnetic field is displayed for a laser wavelength of 570μm, at a temperature of 4.2K, with band-gap illumination (OP). Hydrostatic pressure is used as an additional parameter, to increase the magnitude of D^-. D^- increases with electric field bias, reaches a maximum, and then falls off, in a similar manner to GaAs.

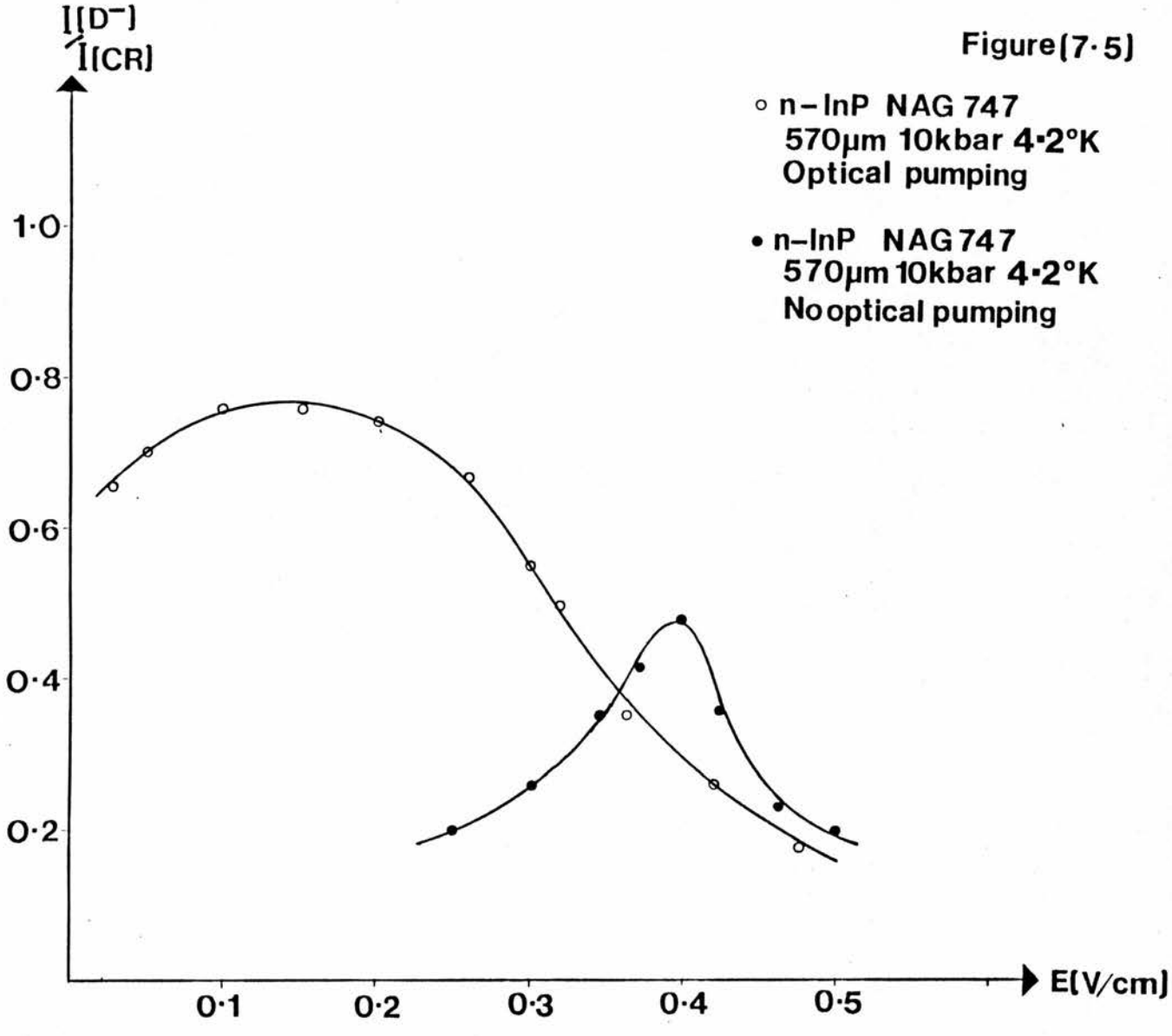

Figure (7.5) The ratio D^-/CR is plotted against electric field bias for NAG747 at 10kbar and 4.2K.

Figure (7·6)

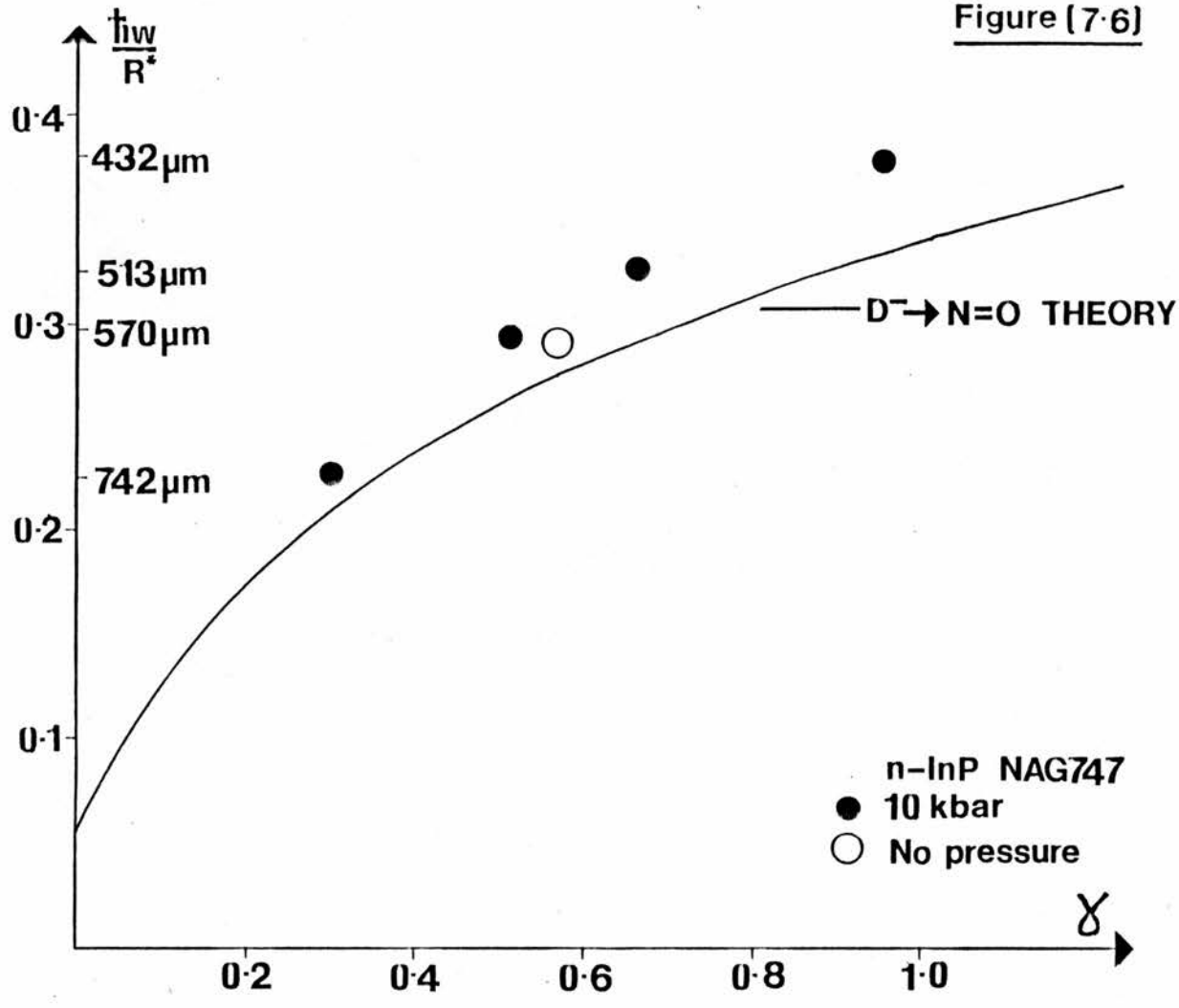

Figure (7.6) Displays a dimensionless plot of energy ($\hbar\omega_c/R^*$) versus $\gamma=\hbar\omega/2R$ for the variation in the D^- peak position as a function of wavelength i.e magnetic field. Hydrostatic pressure is applied on most of the recordings to enhance the D^- signal, otherwise it is insufficiently resolved. Pressure additionally deepens the state, thus moving the D^- peak position to lower field.

Figure(7·7)

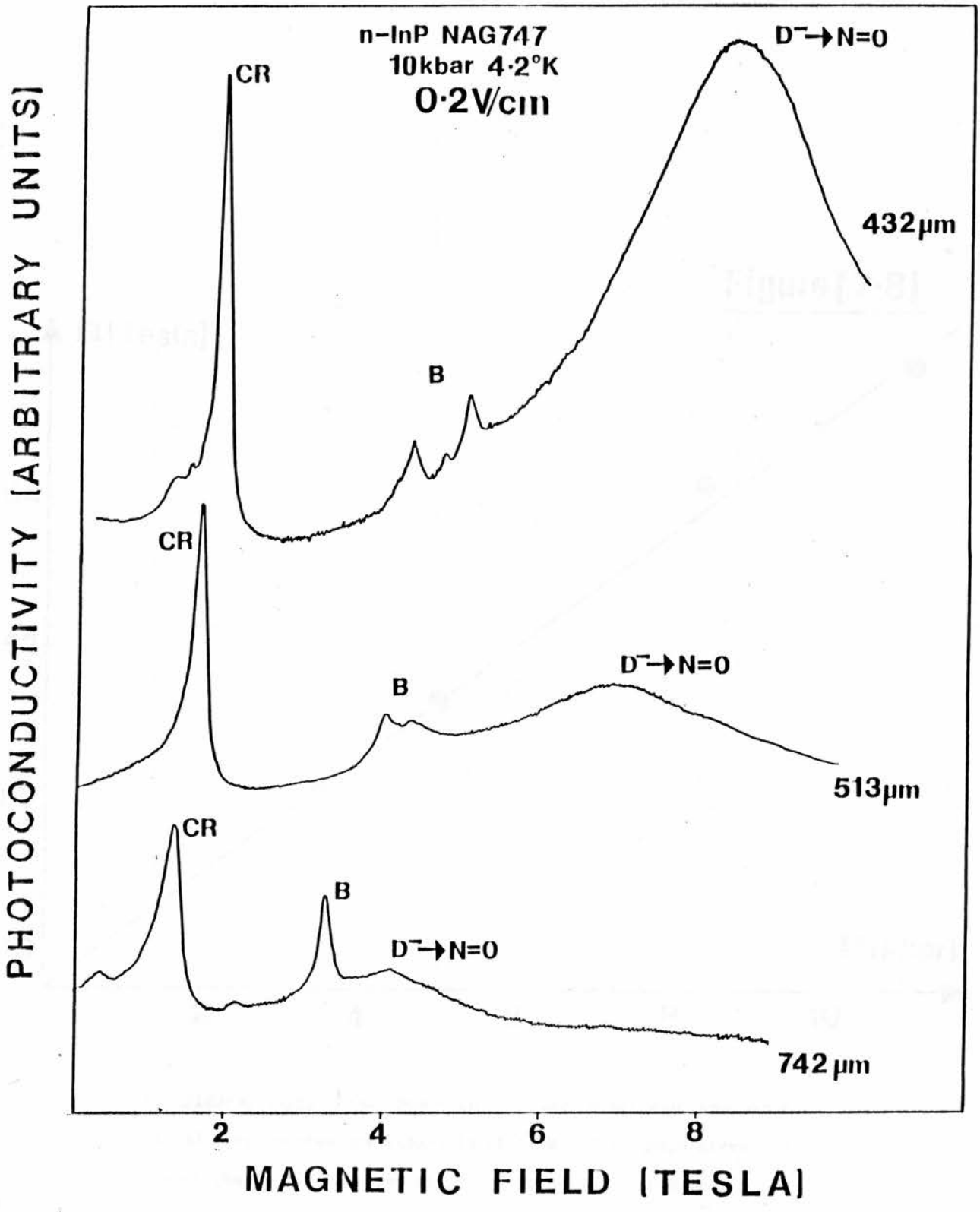

Figure (7.7) D^- is displayed as a function of wavelength for a high purity InP sample, NAG747, under pressure and at 4.2K. This figure demonstrates the increasing binding effect of the magnetic field on the D^- state, since the electric field and intrinsic illumination have been optimised in all the recordings.

Figure[7·9]

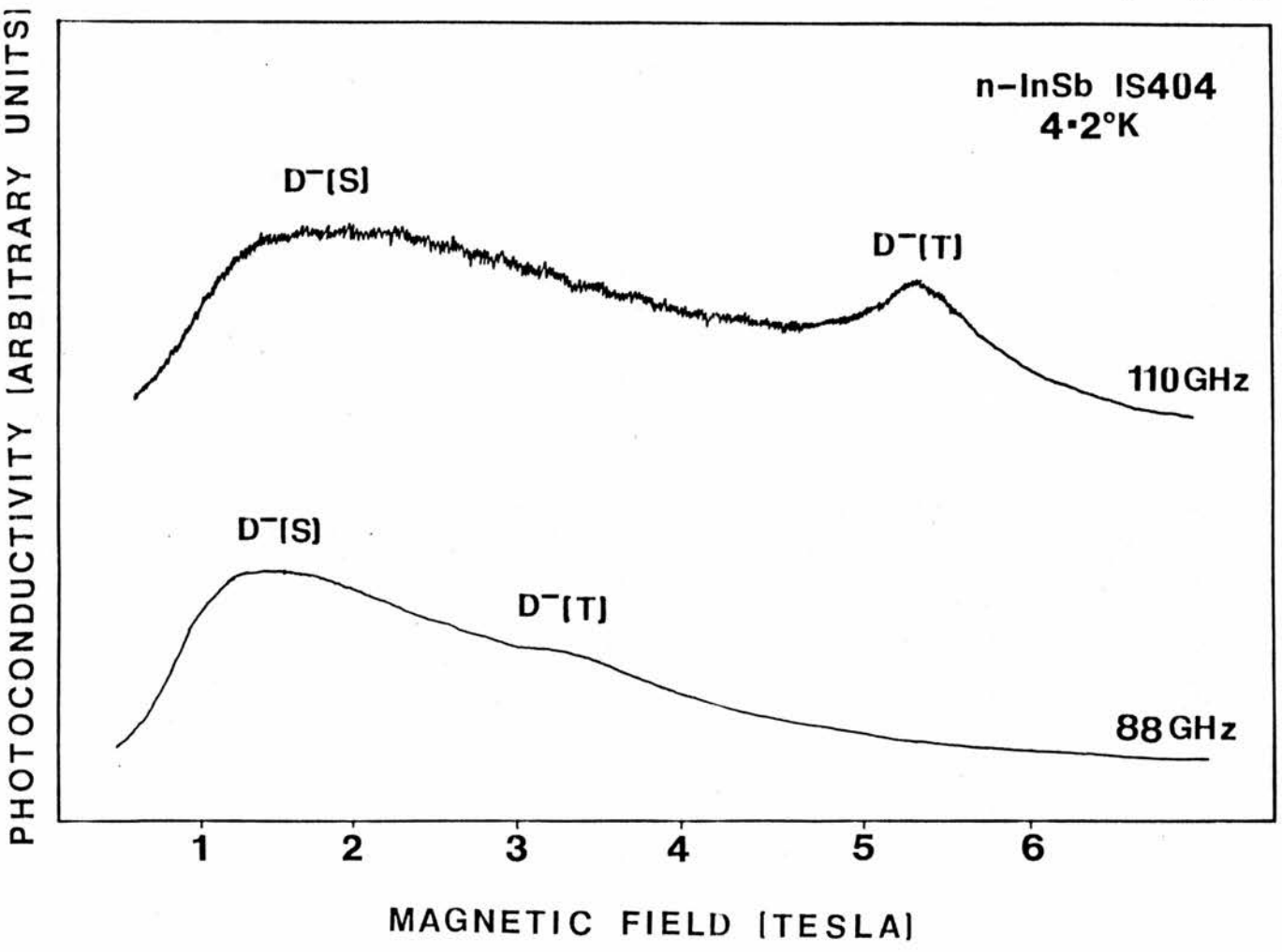

Figure (7.9) Photoconductivity versus magnetic field is shown for an uncompensated n-InSb sample using 110GHz and 88GHz Impatt millimeter wave sources. Two peaks appear which are thought could belong to a D^- singlet and triplet state.

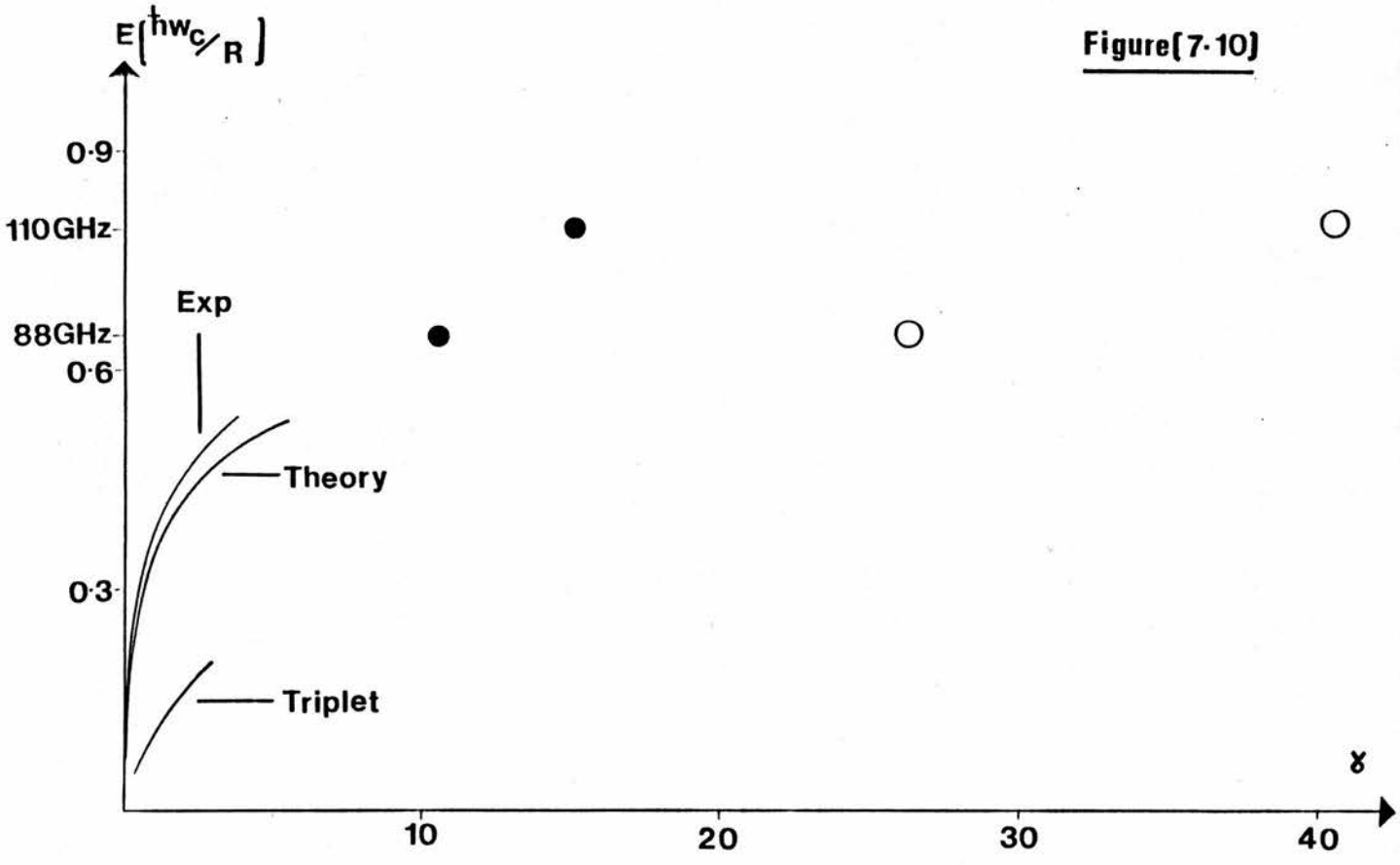

Figure (7.10) A dimensionless diagram of energy against magnetic field is drawn. At low fields ($\varkappa<5$) the experimental results obtained in chapter 6 for GaAs and the theory of Larsen (1979) are compared. At higher fields the peak positions for the InSb spectra displayed in figure (7.9) are plotted.

CONCLUSIONS TO $\bar{D}$

D^o interexcited state transitions have been studied in n-GaAs for more than ten years under similar conditions to the present experiments, without D^- states being detected. Positive identification of D^- states remained elusive until an exceptionally uncompensated GaAs sample became available, illustrating that compensation is an important parameter for D^- formation. Furthermore, the importance of electric field bias was not realised in earlier experiments. A non-equilibrium electron population can assist D^- formation by increasing the recombination rate of electrons on D^0 at the expense of D^+. Such a population can be created by applying a sufficiently large electric field bias to 'heat' the electron system. Under optimum conditions of low temperature, strong magnetic field, moderate electric field bias, optical pumping, and in some cases by using hydrostatic pressure, the D^- intensity can be an order of magnitude larger than D^0 interexcited state transitions and the cyclotron resonance. By optimising the experimental parameters, D^- states have now been observed in a further seven very high purity GaAs samples, some with relatively high compensation as compared to the initial sample e.g S1, E351. Thus, low compensation is important, but not essential for D^- formation. Very high quality samples are also desirable, since donor-acceptor recombination is the ultimate killer of D^- centres when optical pumping is employed. Since, the D^- wavefunction falls as exp(-R/a), so the tunneling probability falls off exponentially. Hence the isolated D^- states have a critical dependence upon concentration and complexing can be observed with quite high purity samples. This set of experiments involving GaAs and InP demonstrates the rather restrictive conditions required to observe D^- states.

Spectral features in the long wavelengtn photoconductivity response in Si and Ge have been attributed to D^- formation and their associated complexes, by various workers (Norton 1976, Taniguchi and Narita 1979). However, none of the spectra published displayed any interexcited state structure or cyclotron resonance from free carriers, nor had any of the author's considered excited states as a possible alternative explanation of their results. By comparing the results and conclusions of D^- states in III-V semiconductors with those in elemental semiconductors, there appears to be reasonable consistency particularly with respect to complexing and magnetic field behaviour, suggesting that D^- states have been probably observed in Si and Ge. Nevertheless, the GaAs and InP results provide a complete and unambiguous identification of D^- states. Detection of D^- states in lesser quality material e.g CdS (Cohn et al 1971) and CdMnSe (Ichiguchi et al 1983) must be treated with a considerable degree of sceptism, since D^- have only been observed in the purest and lowest compensation samples of GaAs and InP where the crystal properties are even more under control. Furthermore, D^- states are only observed in GaAs and InP after optimising a range of experimental parameters.

A particular feature of the use of GaAs and to a lesser extent of InP lies in the ability to observe D^- transitions through the intermediate magnetic field range ($\gamma \sim 1$). The most successful theoretical treatment of the problem of a hydrogen ion in the small or intermediate magnetic field range is described by Larsen. However, there are several points to note.

i) the zero field binding energy is $0.0519R^*$, almost 7% less than the 'exact' zero field binding energy of $0.0555R^*$, this reflects the choice of using a Chandrasekhar basis wavefunction. Larsen simply adds

a constant term of $0.0036R^*$ to all his calculated values in a magnetic field to take into account the initial discrepancy.

ii) Larsen's extrapolation procedure is questionable, especially at higher magnetic fields were it may underestimate the binding energy.

iii) At best, variational calculations will only give the lower bound to the binding energy.

iv) Larsen expects his theory to be inaccurate for $\gamma > 1.5$

v) None of the calculations take into account any central-cell deviations from the 'hydrogen-ion' model.

Theory is compared to experiment for the first time in the intermediate magnetic field range. The comparison is good to within 5% for γ up to 1.5. , beyond this value there becomes an increasingly serious deviation from theory. This is probably due to an incorrectly chosen variational trial wavefunction. The D^- wavefunction becomes increasingly asymmetric with magnetic field. However, the chosen trial wavefunction appears to be rather incompressible in the plane perpendicular to the magnetic field. At very high magnetic fields $\gamma >> 1$, the equation (5.2) becomes approximately separable and a 1-D correlation term is appropriate in this range. A more general wavefunction that is flexible enough to describe the different magnetic field regions is required.

Larsen's theory is calculated for the ideal hydrogen ion and does not take into account the chemical identity of the donors concerned. Central-cell corrections to the effective mass approximation are shown to be significant, especially in the higher field range, since by the nature of the laser experiment, the individual central-cell components are increasingly pulled apart at higher fields. Excited states can also contribute to the overall lineshape, but it is usually clear when

this occurs. These effects can explain the small discrepancy between theory and experiment at low fields, and reduce some of the difference at higher magnetic fields. However, it is difficult to analyse the lineshape properly in the absence of theory.

With optimum electric field bias and strong intrinsic illumination, the D^- peak can be up to a factor of six times bigger than the cyclotron resonance. Reducing the temperature to 1.5K, complexing effects are observed more strongly, suggesting a significant increase in D^- population. If the temperature is further reduced to liquid He^3 temperatures i.e 0.38K, the D^- intensity should increase by several orders of magnitude. An experiment involving a He^3 insert was planned, but unfortunately the system leaked. Even larger D^- effects would of been expected particularly in the weak magnetic field regime, possibly enabling triplets to be resolved in GaAs. Complexing effects should be more pronounced, since the isolated D^- population might be expected to increase as $\exp(-E_D/kT)$, perhaps giving a better indication of their composition. Interexcited state transitions are not expected to be observed at such low temperatures, since there would be an insufficient phonon population to thermally ionise carriers into the conduction band. However, impact ionisation could occur at such low temperatures given a large electric field bias. This situation effectively occurs in Si at an operating temperature of 4.2K With Si photothermal-ionisation is completely ineffective below 10K (see Carter et al 1977).

Because of its low mass and high purity InSb is the best material for studying impurity states in large magnetic fields i.e γ=70 at 10T. Central-cell components are clearly resolved on the D^0 lines and could possibly be resolved on D^- in this material, since the magnetic field

has such a large perturbing effect on the D^- wavefunction. In the tentative identification of D^- states in n-InSb, the D^- lineshapes were very broad, and there was no indication of any central-cell structure. Perhaps the application of hydrostatic pressure would resolve structure. However, an InSb sample without residual oxygen donors would be required, otherwise the D^- intensity would be suppressed in a similar manner to VPE GaAs. Unfortunately, studying InSb in this particular energy region is difficult, since there are few good FIR sources between 1mm and 2mm wavelength.

An attempt was made to increase the strength of D^- lines in GaAs by introducing additional donors by neutron transmutation doping, since this method might be expected to introduce donors without associated shallow acceptors, and hence decrease the compensation ratio. However, the sample becomes high resistance on irradiation due to damage by fast neutrons. On recovering the conductivity by annealing it was found that the D^- spectra had disappeared, almost certainly because of unannealed levels in the mid-gap region. It is believed that D^- states have the potential of providing a very sensitive test for the degree of compensation.

APPENDIX

Ashen D.J, Dean P.J, Hurle D.T.J, Mullin J.B and White A.M J.Phys.Chem.Solids Vol 36, p1041-1053, (1975)

Aspnes D.E and Studna A.A Phys.Rev B7, p4605, (1973)

Aspens D.E Phys.Rev B14, No12, p5331, (1976)

Bajaj K.K, Birch J.R, Eaves L, Hoult R.A, Kirkman R.F, Simmonds P.E, and Stradling R.A J.Phys.C:Solid State Phys 8, p530, (1975)

Berman L.V, Sabanova L.D, and Sidorov V.I Sov.Phys.Semicond 8, p1527, (1975)

Berman L.V and Kalfa A.A Sov.Phys.Semicond 10, p1336, (1976)

Berman L.V and Pomortserva L.I Sov.Phys.Semicond 14, p666, (1980)

Berman L.V Sov.Phys.Semiconductor 17(9), p1004, (1983).

Blackmore G.W, Clegg J.B, Hislop J.S, and Mullin J.B J.Electron Mat. 5, p401-413, (1976).

Brown R.A and Burns M.L Phys.Lett 32A, p513, (1970)

Brust D Solid State Comm, 9, p481-5, (1971)

Cabib D, Fabri E, and Fiorio G Solid State Comm. Vol 9, p1517-1520, (1971)

Camphausen Phys.Rev.Lett 26, p184-8, (1971)

Carter A.C, Carver G.P, Nicholas R.J, Portal J.C, and Stradling R.A Solid State Comm, 24, p55, (1977)

Chandrasekhar S Astrophys J 100, p176 (1944)

Chamberlain J.M, Ergun H.B, Gehring K.A, and Stradling R.A Solid State Comm, 9, p1563-66, (1971)

Chamberlain J.M, Simmonds P.E, Stradling R.A, and Bradley C.C Proc.11th Int.Conf.Phys.Semiconductor, Polish scientific publishers, p1016, Warsaw (1972).

Chamberlain J.M, Simmonds P.E, Stradling R.A and Bradley C.C Solid State Comm Vol 11, p463-468, (1972)

Chelikowsky J.R and Cohen M.L Phys.Rev.B 14, p556, (1976)

Cohn D.R, Lax B, Button K.J and Dreybrodt W Solid State Comm Vol 9, p441-444, (1971)

Colter P.C, Look D.C, and Reynolds A.C Appl.Phys.Lett 43, (3), p282, (1983)

Colter P.C, Look D.C and Reynolds D.C to be published in Appl.Phys.Lett (1984)

Cooke R.A, Hoult R.A, Kirkman R.F, and Stradling R.A J.Phys.D: Appl.Phys Vol 11, p945, (1978).

Dalgrano A and Lynn N Proc.Phys.Soc.London A70, p223, (1957)

Dean P.J, Hayes J.R and Flood W.F Phys.Rev Vol 161, No 3, p711 (1967)

Dean P.J, White A.M, Joyce B.D, Clarke R.C and Taylor L.L Proc.Int.Conf.Phys.of.Semicond. Warsaw (1972), Polish Scientific Publishers, p190-195, (1973).

Dean P.J, Frosch and Henry C.H J.Appl.Phys 39, p5631 (1968).

Dean P.J and Skolnick M.S J.Appl.Phys 54, (1), p346 (1982)

Dean P.J, Skolnick M.S and Talyor L.L J.Appl.Phys 55, p957, (1984)

Dean P.J, Skolnick M.S, Cockayne B, MacEwan W.R, and Iseler G.W J.Crystal Growth 67, p486-494, (1984).

Dunke W.P Phys.Rev B 1, p4668, (1970)

Fedders P.A Phys.Rev.B 25, p3846, (1982)

Fetterman H.R, Larsen D.M, Stillman G.E, Tannenwald P.E and Waldman J Phys.Rev.Lett 26, p975, (1971).

Fetterman H.R, Waldman J, Wolfe C.M, Stillman G.E, and Parker C.D Appl.Phys.Lett Vol 21, No 9, p434, (1972).

Gershenzon E.M, Gol'tsman G.N and Ptitsyna Sov.Phys.Semicond Vol 7, No 10, p1248, (1974)

Gershenson E.M, Gol'tsman G.N and Elant'ev A.I Sov.Phys.JEPT 45, (3), (1977).

Golka.J J.Phys.C: 22, L407, (1974).

Golka J, Trylski J, Skolnick M.S, Stradling R.A and Couder Solid State Comm. Vol 22, p623-626, (1977)

Golka J and Stoll H Solid State Comm Vol 33, p1183-1186, (1980)

Hales and Knight J.Crystal Growth 46, p582, (1979).

Haller E.E, McMurray R.E, Falicov L.M, Haegel N.M and Hansen W.L Phys.Rev.Lett Vol 50, No 8, p612, (1983)

Herring and Vogt Phys.Rev 101, p944 (1956)

Hicks H.G.B and Greene P.D GaAs and related compounds p92-99, (1970).

Hjalmarson H.P, Vogl P, Wolford D.J, and Dow J.D Phys.Rev.Lett Vol 44, No 12, p810, (1980)

Hoult PhD Thesis (unpublished) Oxford (1973)

Ichiguchi T, Drew H.D and Furdyna J.K Phys.Rev.Lett 50, p612, (1983)

Ivanov V.Yu and Lifshits T.M Sov.Phys.Semiconductor 17(11), p1307,

James L.W, Van Dyke J.P, Herman F and Chang D.M Phys.Rev B 1, p3998-4004, (1970)

Jaros M Solid State Comm 51, 6, p411-414, (1983)

Kamimura H J.Non-Cryst.Solids 32, p187-205, (1979)

Kane E.O J.Phys.Chem.Solids, 1, p249, (1957).

Kang C.S and Greene P.D GaAs and related compounds; Conf.Ser.No 7, Institute of Physics, Bristol; p18-21, (1968)

Kirkman R.F, Stradling R.A and Lin-Chung P.J J.Phys.C:Solid State Phys 11, p419, (1978)

Kohn W Phys.Rev 105, 2, p509-16, (1957)

Kogan Sh M and Lifshits T.M Phys.Stat.Sol , 39, p11 (1977)

Knowles P PhD Thesis (unpublished) St Andrews (1982)

Kobayashi M, Sawada S and Narita S J.Phys.Soc.Japan 51, 3, p844-851, (1982)

Kuchar F, Meisels R, Weimann G, and Buckhard H Appl.Phys A33, p83-85, (1984)

Kuchar F, Kaplan R, Wagner R.J, Cooke R.A, Stradling R.A and Vogl

P J.Phys.C:Solid State Phys 17, p6403-6413, (1984)

Lagowski J, Lin D.G, Aoyame T, and Gates H.C Appl.Phys.Lett 44, p336, (1984)

Lampert M.A Phys.Rev.Lett 1, p540, (1958)

Larsen D.M Phys.Rev.B, 8, p535, (1973)

Larsen D.M Phys.Rev.B, 11, p3904, (1975)

Larsen D.M Phys.Rev.B 20, 12, p5217, (1979)

Lifshits T.M and Kogan M Phys.Stat.Sol (a), 39, p11, (1977)

Low T.S, Stillman G.E, Cho A.Y, Morkoc H and Calawa A.R Appl.Phys.Lett 40, 7, p611, (1982)

Low T.S, Stillman G.E, Nakansini T, Udagawa T and Wolfe C.M Appl.Phys.Lett 41, 2, p183, (1982)

Low T.S, Stillman G.E, Collins D.M, Wolfe C.M, Tiwari S, and Eastman L.F Appl.Phys.Lett 40, (12), p1034, (1982)

Lum W.Y and Wielder H.H Appl.Phys.Lett 31, p213-215, (1977)

Makado P PhD Thesis, St Andrews University, (unpublished) (1984)

Meyer B.K and Spaeth J.M J.Phys.C:Solid State Phys 17, p2213-2223, (1984)

Pitt G.D Solid State Comm. 8, p1119, (1970)

Pitt G.D J.Phys.C:Solid State Phys, 6, p1586, (1973)

Pomrenke G.S J.Crystal.Growth, 64, p158-164, (1983)

Pons D and Bourgoin J Phys.Rev.Lett 47, 18, p1293 (1981)

Rochen P and Fortin E Phys.Rev B, 12, p5803, (1975)

Schairer W, Bimberg D, Kottler W, Cho K, and Schmidt M Phys.Rev.B, 13, p3452, (1976)

Schiff E.A Phil.Mag B 45, 1, p69-93, (1982)

Simmonds P.E PhD Thesis (unpublished) Oxford (1973)

Simmonds P.E, Chamberlain J.M, Hoult R.A, Stradling R.A and Bradley C.C J.Phys.C:Solid State Phys 7, p4164, (1974)

Skolnick M.S, Eaves L, Stradling R.A, Portal J.C, and Askenazy S, Solid State Comm, 15, p1403, (1974).

Skolnick M.S, Carter A.C, Couder Y and Stradling R.A J.Opt.Soc.Am 67, 7, (1977)

Skolnick M.S, Dean P.J, Groves S.H and Kupal E Appl.Phys.Lett 45, 9, p962, (1984)

Skolnick M.S, Dean P.J, Taylor L.L, Anderson D.A, Najda S.P, Armistead

C.J and Stradling R.A Appl.Phys.Lett 44, (9), p881 (1984)

Stillman G.E, Larsen D.M, Wolfe C.M, and Brandt R.C Solid State Comm 9, p2245-2249, (1971)

Stillman G.E Proc 11th Int.Conf.Semiconductor, p863, Warsaw (1972).

Stillman G.E and Wolfe C.M in Semimetals and semiconductors ed by Willardson and Beer A.C (Academic Press, New York, 1977) 12, p169-200, (1977)

Stillman G.E, Low T.S, Nakanisi T, Udagawa T and Wolfe C.M Appl.Phys.Lett, 41(2), p183, (1982)

Stillman G.E, Low T.S and Lee B to be published Solid State Comm. (1985)

Stoelinga J.H.M, Larsen D.M, Walukiewicz W and Bolzer J J.Phys.Chem.Solids 10, p871-877, (1978)

Stradling R.A, Eaves L, Hoult R.A, Miura N, Simmonds P.E and Bradley C.C GaAs and related compounds 1972; Conf.Ser.No 17 Inst.Phys, Bristol p65-74 (1972)

Taniguchi M and Nartia S J.Phys.Soc.Japan 43, 4, p1262, (1977)

Taniguchi M, Narita S, Hasegawa N and Kobayashi M J.Phys.Soc.Japan 45, 2, p545, (1978)

Taniguchi M and Narita S J.Phys.Soc.Jpn 47, 5, p1503, (1979)

Thomas G.A, Kawabata A, Ootuka Y, Katsumoto S, and Sasaki W Phys.Rev.B 24, p4886, (1981)

Townsend P J.Phys.C: Solid State Physics 11, p1481, (1978)

Vitramo J J.Phys.B 9, p751, (1976)

Walukiewicz W, Lagowski J and Gatos H.C Appl.Phys.Lett 43, 1, p112 (1983)

Wasilewski Z, Stradling R.A, Baj M, Brunel L.C, Huant S, Trzeciakowski W and Porowski S Proc. 17th. Int. Conf. Semicond (San Fransico), Springer:Berlin (1984)

White A.M, Dean P.J, Joyce B.D, Clarke R.C and Taylor L.L Proc.Int.Conf on Phys.Semicond (Warsaw) 1972; Polish scientific publishers p190-195, (1973).

Wolfe C.M, Korn D.M and Stillman G.E Appl.Phys.Lett 24, 2, (1972)

Wolfe C.M, Stillman G.E, and Korn D.M GaAs and related compounds Conf.Ser.No 33b, p120-128, St Louis (1976).

Wolfe C.M, Stillman G.E and Korn D.M GaAs and related compounds (St Louis); Inst.Phys.Conf. Ser.no 33b, p120-128, (1977).

Yafet Y, Keyes R.W, and Adams E.N, J.Phys.Chem.Solids, 1, p137-142, (1956).

Table 1 Electrical characteristics of the GaAs samples described in the thesis.

Sample	Source	N_D-N_A (77K) cm^{-3}	Mobility(77K)cm^2/VS.
3LE32	STL (LPE)	-	150,000
3LE165(Sn)	STL (LPE)	$5\ 10^{14}$	105,000
7LE45	STL (LPE)	$3\ 10^{13}$	170,000
E351	Max-Plank (LPE)	-	150,000
R137	Max-Plank (LPE)	$1\ 10^{13}$	150,000
MBV20	Philips (MBE)	$7\ 10^{14}$	49,600
MBV380	Philips (MBE)	$3\ 10^{14}$	55,000
RR17	Wright-Patterson	-	90,800
RR39	Wright-Patterson	$5.6\ 10^{14}$	90,290
RR96	Wright-Patterson	-	122,000
RR97	Wright-Patterson	-	-
RR98	Wright-Patterson	$2\ 10^{14}$	163,000
RR99	Wright-Patterson	$3\ 10^{14}$	-
RR125	Wright-patterson	$3\ 10^{14}$	150,000
RR133	Wright-Patterson	-	120,000
RR136	Wright-Patterson	-	120,000
SN26R6(Ge)	RSRE (VPE)	$1\ 10^{15}$	55,000
S1	Motorola (VPE)	$5\ 10^{13}$	160,000
S11	-	-	-

Table 2 Electrical characteristics of InP samples

MOCVD Samples	(N_D-N_A) 77K cm^{-3}	Mobility at 77K cm^2/Vs.
806A RSRE	$1.8\ 10^{15}$	55,000
807A RSRE	$2.0\ 10^{15}$	49,000
T127 Thomson-CSF	-	-
Bulk InP Samples		
L816 RSRE	$3.0\ 10^{15}$	39,000
L1PC F81 MCP	$5.0\ 10^{15}$	25,000
V1PC 611 MCP	$2.8\ 10^{15}$	26,000
LIPC F/70 MCP	$2.8\ 10^{15}$	39,000
VPE Samples (RSRE) (PCl_3)		
KV354(Si)	$4.0\ 10^{13}$	44,000
KV468	$1.6\ 10^{14}$	92,000
KV469	$4.0\ 10^{14}$	83,000
NAG618	$4.0\ 10^{14}$	53,000
NAG634	$1.1\ 10^{15}$	58,230
NAG681	$3.7\ 10^{14}$	86,000
NAG686	$4.0\ 10^{14}$	99,000
NAG688	$2.3\ 10^{14}$	74,150
NAG747	$2.0\ 10^{14}$	120,000
NAG762	$6.0\ 10^{13}$	130,000
NAG775	-	-
NAG780	$1.0\ 10^{14}$	100,000
NAG852(Sn)	$3.0\ 10^{15}$	37,000
NAG853(Ge)	$4.0\ 10^{15}$	26,000

VPE Samples (Plessey) (PCl_3)

R56	-	-
CR276	$6.0\ 10^{14}$	64,000
QM272(S)	$8.7\ 10^{14}$	61,100
QM273(Si)	$2.0\ 10^{15}$	41,000
QM274	$5.0\ 10^{14}$	90,000